TABLE OF CONTENTS

TABLE OF CONTENTS (Continued)

LIST OF TABLES

LIST OF FIGURES

LIST OF FIGURES (Continued)

LIST OF FIGURES (Continued)

RN 03-017

LIST OF FIGURES (Continued)

LIST OF EFFECTIVE PAGES (LEP)

The following list delineates pages to Chapter 4 of the Virgil C. Summer Nuclear Station Final Safety Analysis Report which are current through December 2015. The latest changes to pages and figures are indicated below by Revision Number (RN) in the Amendment column along with the Revision Number and date for each page and figure included in the Final Safety Analysis Report.

Page/Fig. No.	Amend. No.	Date
Page 4-i	Reset	December 2015
4-ii	Reset	December 2015
4-iii	Reset	December 2015
4-iv	Reset	December 2015
4-v	Reset	December 2015
4-vi	Reset	December 2015
4-vii	Reset	December 2015
4-viii	Reset	December 2015
4-ix	Reset	December 2015
4-x	Reset	December 2015
4-xi	Reset	December 2015
Page 4.1-1	RN11-013	November 2011
4.1-2	RN11-013	November 2011
4.1-3	RN96-043	November 1997
4.1-4	RN11-013	November 2011
4.1-5	RN01-113	December 2001
4.1-6	02-01	May 2002
4.1-7	RN11-013	November 2011
4.1-8	RN01-113	December 2001
4.1-9	RN01-113	December 2001
4.1-10	02-01	May 2002
4.1-11	RN01-113	December 2001
4.1-12	02-01	May 2002
Page 4.2-1	00-01	December 2000
4-2.2	RN96-043	November 1997
4.2-3	RN14-005 RN14-036	January 2015 January 2015
4.2-4	RN09-022	November 2011
4.2-5	RN09-022	November 2011
4-2.6	RN01-113	December 2001
4.2-7	RN96-043	November 1997
4.2-8	RN96-043	November 1997
4.2-9	RN96-043	November 1997
Page 4.2-10	RN09-022 RN11-013	November 2011 November 2011
4.2-11	RN14-036	January 2015
4.2-12	RN14-036	January 2015
4.2-13	RN14-036	January 2015
4.2-14	RN14-005	January 2015
4.2-15	RN14-005	January 2015
4.2-16	RN14-036	January 2015
4.2-17	RN96-043	November 1997
4.2-18	RN09-022	November 2011
4.2-19	RN09-022	November 2011
4.2-20	RN95-022	July 1996
4.2-21	00-01	December 2000
4.2-22	RN14-036	January 2015
4.2-23	00-01	December 2000
4.2-24	00-01	December 2000
4.2-25	00-01	December 2000
4.2-26	RN09-022	November 2011
4.2-27	00-01	December 2000
4.2-28	00-01	December 2000
4.2-29	RN15-023	December 2015
4.2-30	00-01	December 2000
4.2-31	00-01	December 2000
4.2-32	00-01	December 2000
4.2-33	00-01	December 2000
4.2-34	00-01	December 2000
4.2-35	RN95-022	July 1996
4.2-36	RN99-134	March 2000
4.2-37	00-01	December 2000
4.2-38	RN96-043	November 1997
4.2-39	00-01	December 2000
4.2-40	RN99-141	January 2000
4.2-41	00-01	December 2000

Page/Fig. No.		Amend. No.	Date
Page	4.2-42	00-01	December 2000
	4.2-43	00-01	December 2000
	4.2-44	00-01	December 2000
	4.2-45	00-01	December 2000
	4.2-46	00-01	December 2000
	4.2-47	00-01	December 2000
	4.2-48	00-01	December 2000
	4.2-49	RN95-022	July 1996
	4.2-50	RN95-022	July 1996
	4.2-51	0-01	December 2000
	4.2-52	RN95-022	July 1996
	4.2-53	00-01	December 2000
	4.2-54	00-01	December 2000
	4.2-55	00-01	December 2000
	4.2-56	RN95-022	July 1996
	4.2-57	00-01	December 2000
	4.2-58	00-01	December 20007
	4.2-59	00-01	December 2000
	4.2-60	RN14-036	January 2015
	4.2-61	RN14-005 RN14-036	January 2015 January 2015
	4.2-62	RN15-023	December 2015
	4.2-63	RN01-113	December 2001
Fig.	4.2-1	96-02	July 1996
	4.2-2	98-01	April 1998
	4.2-3	98-01	April 1998
	4.2-4	96-02	July 1996
	4.2-5	96-02	July 1996
	4.2-6	96-02	July 1996
	4.2-7	96-02	July 1996
	4.2-8	0	August 1984
	4.2-9	0	August 1984
	4.2-10	RN09-022	November 2011
	4-2.11	0	August 1984
	4.2-12	0	August 1984
	4-2.13	0	August 1984
	4.2-14	0	August 1984
Fig.	4-2.15	0	August 1984
	4-2.17	6	August 1990
	4.2-18	6	August 1990
	4.2-18a	6	August 1990
	4-2.19	0	August 1984
	4.2-20	6	August 1990
	4-2.21	6	August 1990
	4.2-22	0	August 1984
	4-2.23	0	August 1984
	4-2.26	0	August 1984
	4.2-27	0	August 1984
	4.2-28	0	August 1984
Page	4.3-1	00-01	December 2000
	4.3-2	00-01	December 2000
	4.3-3	RN95-022	July 1996
	4.3-4	00-01	December 2000
	4.3-5	00-01	December 2000
	4.3-6	00-01	December 2000
	4.3-7	RN11-013	November 2011
	4.3-8	00-01	December 2000
	4.3-9	RN96-043	November 1997
	4.3-10	00-01	December 2000
	4.3-11	00-01	December 2000
	4.3-12	RN96-043	November 1997
	4.3-13	00-01	December 2000
	4.3-14	00-01	December 2000
	4.3-15	00-01	December 2000
	4.3-16	RN95-022	July 1996
	4.3-17	RN00-011	June 2001
	4.3-18	00-01	December 2000
	4.3-19	RN01-113	December 2001
	4.3-20	RN95-022	July 1996
	4.3-21	00-01	December 2000
	4.3-22	00-01	December 2000
	4.3-23	00-01	December 2000
	4.3-24	RN95-022	July 1996
	4.3-25	00-01	December 2000

Page/Fig. No.		Amend. No.	Date
Page	4.3-26	00-01	December 2000
	4.3-27	RN95-022	July 1996
	4.3-28	00-01	December 2000
	4.3-29	00-01	December 2000
	4.3-30	00-01	December 2000
	4.3-31	00-01	December 2000
	4.3-32	RN14-006	March 2014
	4.3-33	RN03-017	December 2003
	4.3-34	RN03-017	December 2003
	4.3-35	RN03-017	December 2003
	4.3-36	RN95-022	July 1996
	4.3-37	00-01	December 2000
	4.3-38	00-01	December 2000
	4.3-39	00-01	December 2000
	4.3-40	00-01	December 2000
	4.3-41	RN95-022	July 1996
	4.3-42	RN95-022	July 1996
	4.3-43	RN95-022	July 1996
	4.3-44	RN95-022	July 1996
	4.3-45	00-01	December 2000
	4.3-46	00-01	December 2000
	4.3-47	00-01	December 2000
	4.3-48	RN12-027	December 2012
	4.3-49	Blank	
	4.3-50	RN11-013	November 2011
	4.3-51	00-01	December 2000
	4.3-52	00-01	December 2000
	4.3-53	02-01	May 2002
	4.3-54	RN03-017	December 2003
	4.3-55	RN01-113	December 2001
	4.3-56	RN01-113	December 2001
	4.3-57	RN01-113	December 2001
	4.3-58	RN01-113	December 2001
	4.3-59	02-01	May 2002
	4.3-60	RN01-113	December 2001
	4.3-61	RN01-113	December 2001
	4.3-1	6	August 1990
Fig.	4.3-2	0	August 1984
	4.3-3	96-02	July 1996
	4.3-4(Sh 1)	96-02	July 1996
	4.3-4(Sh 2)	96-02	July 1996
	4.3-5	6	August 1990
	4.3-6	6	August 1990
	4.3-7	6	August 1990
	4.3-8	6	August 1990
	4.3-9	6	August 1990
	4.3-10	6	August 1990
	4.3-11	96-02	July 1996
	4.3-12	96-02	July 1996
	4.3-13	96-02	July 1996
	4.3-14	96-02	July 1996
	4.3-15	96-02	July 1996
	4.3-16	6	August 1990
	4.3-17	6	August 1990
	4.3-18	96-02	July 1996
	4.3-19	96-02	July 1996
	4.3-20	96-02	July 1996
	4.3-22	6	August 1990
	4.3-23	6	August 1990
	4.3-24	6	August 1990
	4.3-25	6	August 1990
	4.3-26	6	August 1990
	4.3-27	6	August 1990
	4.3-28	6	August 1990
	4.3-29	6	August 1990
	4.3-30	6	August 1990
	4.3-31	6	August 1990
	4.3-32	6	August 1990
	4.3-33	6	August 1990
	4.3-34	6	August 1990
	4.3-35	6	August 1990
	4.3-36	6	August 1990
	4.3-37	96-02	July 1996
	4.3-38	6	August 1990

Page/Fig. No.		Amend. No.	Date
Fig.	4.3-39	6	August 1990
	4.3-40	6	August 1990
	4.3-41	6	August 1990
	4.3-42	6	August 1990
	4.3-43	6	August 1990
	4.3-44	RN03-017	December 2003
	4.3-46	6	August 1990
	4.3-47	6	August 1990
	4.3-48	6	August 1990
	4.3-49	6	August 1990
	4.3-50	6	August 1990
	4.3-51	6	August 1990
Page	4.4-1	RN95-022	July 1996
	4.4-2	RN96-043	November 1997
	4.4-3	RN95-022	July 1996
	4.4-4	RN14-036	January 2015
	4.4-5	RN14-036	January 2015
	4.4-6	RN14-036	January 2015
	4.4-7	RN95-022	July 1996
	4.4-8	RN95-022	July 1996
	4.4-9	02-01	May 2002
	4.4-10	RN95-022	July 1996
	4.4-11	RN01-113	December 2001
	4.4-12	RN14-023	May 2014
	4.4-13	02-01	May 2002
	4.4-14	02-01	May 2002
	4.4-15	02-01	May 2002
	4.4-16	02-01	May 2002
	4.4-17	02-01	May 2002
	4.4-18	02-01	May 2002
	4.4-19	RN95-022	July 1996
	4.4-20	RN01-113	December 2001
	4.4-21	02-01	May 2002
	4.4-22	02-01	May 2002
	4.4-23	RN95-022	July 1996
	4.4-24	RN95-022	July 1996
	4.4-25	RN01-113	December 2001
Page	4.4-26	RN95-022	July 1996
	4.4-27	RN95-022	July 1996
	4.4-28	02-01	May 2002
	4.4-29	02-01	May 2002
	4.4-30	RN95-022	July 1996
	4.4-31	RN95-022	July 1996
	4.4-32	RN95-022	July 1996
	4.4-33	RN00-023	March 2001
	4.4-34	RN00-011	June 2001
	4.4-35	02-01	May 2002
	4.4-36	RN01-113	December 2001
	4.4-37	02-01	May 2002
	4.4-38	02-01	May 2002
	4.4-39	02-01	May 2002
	4.4-40	02-01	May 2002
	4.4-41	RN14-036	January 2015
	4.4-42	02-01	May 2002
	4.4-43	02-01	May 2002
	4.4-44	02-01	May 2002
	4.4-45	RN95-022	July 1996
	4.4-46	RN00-011	June 2001
	4.4-47	RN09-022	November 2011
	4.4-48	RN09-022	November 2011
	4.4-49	RN01-113	December 2001
Fig.	4.4-3	0	August 1984
	4.4-6	6	August 1990
	4.4-8	0	August 1984
	4.4-9	0	August 1984
	4.4-10	0	August 1984
	4.4-11	0	August 1984
	4.4-12	0	August 1984
	4.4-19	0	August 1984

4.0 REACTOR

4.1 SUMMARY DESCRIPTION

This chapter describes the mechanical components of the reactor and reactor core including the fuel rods and fuel assemblies, reactor internals, and the control rod drive mechanisms (CRDM's); the nuclear design; and the thermal - hydraulic design.

The reactor core is comprised of VANTAGE + fuel assemblies arranged in a checkered, low-leakage core loading pattern. 98-01

The VANTAGE + fuel system design is based upon the Westinghouse VANTAGE 5 fuel designs as described in WCAP-10444-P-A, "Reference Core Report, VANTAGE 5 Fuel Assembly," (Reference [1]).

VANTAGE + is a modification of the NRC-approved VANTAGE 5 fuel assembly design; it includes the following VANTAGE 5 product features:

- Reconstitutable Top Nozzle (RTN)
- Intermediate Flow Mixing (IFM) Grids
- Axial Blankets
- Integral Fuel Burnable Absorbers (IFBA)

A detailed description and evaluation of these features is provided in Reference [1]. NRC approval for the above VANTAGE 5 features and assembly fuel system design was received in a July 1985 SER.

VANTAGE + also includes the following: 98-01

- ZIRLO®/Optimized ZIRLO™ Fuel Rod Clad
- ZIRLO® Guide Thimbles
- Plenum Fuel Stack Variable Pitch Coil Spring
- Annular Axial Blanket Pellets
- Modified Assembly Skeleton Dimensions

RN 11-013

A detailed description and evaluation of the above features is provided in Reference [4]. RN 11-013

This Page Intentionally Left Blank

Recent Vantage + fuel assemblies contain Performance + features. The additional features include: 98-01

Additional reduced fuel rod to bottom nozzle gap
Extended burnup bottom grid design
ZIRLO® mid-grids and Intermediate Flow Mixer grids
Mid enriched annular pellets in axial blankets

RN 11-013

The V. C. Summer VANTAGE + fuel assembly will continue to use the Debris Filter Bottom Nozzle (DFBN) which is present in V. C. Summer VANTAGE 5 fuel assemblies.

The core is cooled and moderated by light water at a normal operating pressure of 2250 psia in the reactor coolant system. The moderator coolant contains boron as a neutron absorber. The concentration of boron in the coolant is varied as required to control relatively slow reactivity changes including the effects of fuel burnup. Additional boron, in the form of IFBA or burnable absorber rods, may be employed in the core to establish the desired initial reactivity.

Two hundred and sixty-four fuel rods are mechanically joined in a square array to form a fuel assembly. The fuel rods are supported in intervals along their length by grid assemblies which maintain the lateral spacing between the rods throughout the design life of the assembly. The grid assembly consists of an "egg-crate" arrangement of interlocked straps. The straps contain spring fingers and dimples for fuel rod support as well as coolant mixing vanes. The fuel rods consist of uranium dioxide ceramic cylindrical pellets contained in slightly cold worked zirconium alloy tubing which is plugged and seal welded at the ends to encapsulate the fuel. All fuel rods are pressurized with helium during fabrication to reduce stresses and strains in order to increase fatigue life. 98-01

The center position in the assembly is reserved for the incore instrumentation, while the remaining 24 positions in the array are equipped with guide thimbles joined to the grids and the top and bottom nozzles. Depending upon the position of the assembly in the core, the guide thimbles are used as core locations for rod cluster control assemblies (RCCA's), neutron source assemblies, and burnable absorber rods (if used). Otherwise, the guide thimbles may be fitted with plugging devices to further limit bypass flow. Starting with the Cycle 5 core, the use of plugging devices is optional.

The bottom nozzle is a box-like structure which serves as a bottom structural element of the fuel assembly and directs the coolant flow distribution to the assembly.

The top nozzle assembly functions as the upper structural element of the fuel assembly in addition to providing a partial protective housing for the RCCA or other components.

The RCCA's each consist of a group of individual absorber rods fastened at the top end to a common hub or spider assembly. These assemblies contain absorber material to control the reactivity of the core under operating conditions.

The CRDM's are of the magnetic jack type. Control rods are positioned by electro-mechanical (solenoid) action utilizing gripper latches, which engage grooved drive rods which in turn are coupled to the RCCA's. The CRDM's are so designed that upon a loss of electrical power to the coils, the RCCA is released and falls by gravity to shutdown the reactor.

The components of the reactor internals are divided into three parts consisting of the lower core support structure (including the entire core barrel and neutron shield pad assembly), the upper core support structure and the incore instrumentation support structure. The reactor internals support the core, maintain fuel alignment, limit fuel assembly movement, maintain alignment between fuel assemblies and CRDM's, direct coolant flow past the fuel elements and to the pressure vessel head, provide gamma and neutron shielding, and provide guides for the incore instrumentation.

The nuclear design analyses and evaluation establish physical locations for control rods, burnable absorber assemblies and physical parameters such as fuel enrichments and boron concentration in the coolant. The nuclear design evaluation established that the reactor core has inherent characteristics which together with corrective actions of the reactor control and protective systems provide adequate reactivity control even if the highest reactivity worth RCCA is stuck in the fully withdrawn position.

The design also provides for inherent stability against diametral and azimuthal power oscillations and for control of induced axial power oscillations.

The thermal-hydraulic design analyses and evaluation establish coolant flow parameters which assure that adequate heat transfer is provided between the fuel clad and the reactor coolant. The thermal design takes into account local variations in dimensions, power generation, flow distribution and mixing. The mixing vanes incorporated in the fuel assembly spacer grid design, and the IFM grids induce additional flow mixing between the various flow channels within a fuel assembly as well as between adjacent assemblies. 98-01

Instrumentation is provided in and out of the core to monitor the nuclear, thermal-hydraulic and mechanical performance of the reactor, and to provide inputs to automatic control functions.

Table 4.1-1 presents the principal nuclear, thermal-hydraulic, and mechanical reactor design parameters. 98-01

The effects of fuel densification were evaluated with the methods described in Reference [2].

The analysis techniques employed in the core design are tabulated in Table 4.1-2. The loading conditions considered in general for the core internals and components are tabulated in Table 4.1-3. Specific or limiting loads considered for design purposes of the various components are listed as follows: fuel assemblies in Section 4.2.1.1.2; reactor internals in Section 4.2.2.3 and Table 5.2-2; neutron absorber rods, burnable absorber rods, neutron source rods, and thimble plug assemblies in Section 4.2.3.1.3; and CRDM's in Section 4.2.3.1.4. The dynamic analyses, input forcing functions, and response loadings are presented in Section 3.9.

4.1.1 REFERENCES

1. Davidson, S. L. (Ed.), "Reference Core Report - VANTAGE 5 Fuel Assembly," WCAP-10444-P-A, September, 1985.

2. Hellman, J. M. (Ed.), "Fuel Densification Experimental Results and Model for Reactor Application," WCAP-8218-P-A (Proprietary) and WCAP-8219-A (Non-Proprietary), March, 1975.

3. Davidson, S.L. and Nuhfer, D.L., "VANTAGE + Fuel Assembly Reference Core Report," WCAP-12610, June 1990.

4. Letter from R. W. Kerr (Westinghouse) to W. Herwig (SCE&G), "South Carolina Electric & Gas Company, V. C. Summer Nuclear Station, Transmittal of 'SER Compliance of WCAP-12610-P-A & CENPD-404-P-A Addendum 1-A, Optimized ZIRLO™' (Proprietary)," NF-CG-10-58, July 29, 2010.

RN 11-013

TABLE 4.1-1

REACTOR DESIGN PARAMETERS

	Thermal and Hydraulic Design Parameters	Current RTP and Engineered Safeguards Design Rating	
1.	Reactor Core Heat Output, MWt	2900	02-01
2.	Reactor Core Heat Output, 10^6 Btu/hr	9898	
3.	Heat Generated in Fuel, %	97.4	
4.	System Pressure, Nominal, psia	2250	
5.	System Pressure, Minimum Steady-State, psia	2200	
6.	Minimum Departure from Nucleate Boiling Ratio for Design Transients (Design Limit)	1.23 (Typical Flow Channel) 1.23 (Thimble Flow Channel)	
6a.	DNB Correlation Used	WRB-2	02-01
	COOLANT FLOW		
7.	Total Thermal Design Flow Rate (TDF), 10^6 lbm/hr	104.0	
7a.	Minimum Measured Flow Rate, 10^6 lbm/hr	106.1	
8.	Effective Flow Rate for Heat Transfer, 10^6 lb/hr	94.74	
9.	Effective Flow Area for Heat Transfer, ft^2	44.0	
10.	Average Velocity Along Fuel Rods, ft/sec	13.7	
11.	Average Mass Velocity, 10^6 lbm/hr-ft^2	2.15	02-01

TABLE 4.1-1 (Continued)

REACTOR DESIGN PARAMETERS

	Thermal and Hydraulic Design Parameters	Current RTP and Engineered Safeguards Design Rating
	COOLANT TEMPERATURE, °F (BASED ON TDF)	
12.	Nominal Inlet	552.9
13.	Average Rise in Vessel	69.0
14.	Average Rise in core	74.8
15.	Average in core	592.8
16.	Average in Vessel	587.4
	HEAT TRANSFER	
17.	Active Heat Transfer, Surface Area, ft^2	46,780
18.	Average Heat Flux, BTU/hr-ft^2	206,100
19.	Maximum Heat Flux for Normal Operation, Btu/hr-ft^2	504,900
20.	Average Thermal Output, kW/ft	5.69
21.	Maximum Thermal Output for Normal Operation, kW/ft	13.9(3)
22.	Peak Linear Power for Determination of Protection Setpoints, kW/ft	<22.6(1)
23.	Heat Flux Hot Channel Factor, F_Q	2.45(2)
24.	Peak Fuel Central Temperature at Maximum Thermal Output for Maximum Overpower Trip Point, °F	<4700

TABLE 4.1-1 (Continued)

REACTOR DESIGN PARAMETERS

	Core Mechanical Design Parameters	VANTAGE+ Fuel Assembly	
	FUEL ASSEMBLIES		
25.	Design	RCC Canless	
26.	Number of Fuel Assemblies	157	
27.	UO_2 Rods per Assembly	264	
28.	Rod Pitch, in.	0.496	
29.	Overall Dimensions, in.	8.426 x 8.426	
30.	Fuel Weight (as UO_2), lb	174,894	
31.	Clad Weight, lb	35,244	
32.	Number of Grids per Assembly	2 - Type R (Inconel End) 6 - Zircaloy (Internal) 1 - Protective	98-01
33.	Number of IFMs per Assembly	3	
34.	Loading Technique	multi-region nonuniform-checkered	
	FUEL RODS		
35.	Number	41,448	
36.	Outside Diameter, in.	0.360	
37.	Diametral Gap, in.	0.0062	
38.	Clad Thickness, in.	0.0225	
39.	Clad Material	ZIRLO®/Optimized ZIRLO™	RN 11-013

TABLE 4.1-1 (Continued)

REACTOR DESIGN PARAMETERS

	Core Mechanical Design Parameters	VANTAGE+ Fuel Assembly	
	FUEL PELLETS		
40.	Material	UO_2 Sintered	
41.	Density (% of Theoretical)	95	
42.	Diameters, in. OD/ID	0.3088/-(Enriched) 0.3088/0.155 (Unenriched/Midenriched)	98-01
43.	Length, in.	0.370 (Enriched) 0.458 (Unenriched/Midenriched)	98-01
	ROD CLUSTER CONTROL ASSEMBLIES		02-01
44.	Neutron Absorber	Ag-In-Cd	
45.	Cladding Material	Type 304 SS-Cold Worked	
46.	Clad Thickness, in.	0.0185	02-01
47.	Number of Clusters	48	
48.	Number of Absorber Rods per Cluster	24	
	CORE STRUCTURE		
49.	Core Barrel, I.D./O.D., in.	133.85/137.875	
50.	Thermal Shield, I.D./O.D., in.	Neutron Pad Design	02-01

TABLE 4.1-1 (Continued) 02-01

REACTOR DESIGN PARAMETERS

	Core Mechanical Design Parameters	VANTAGE+ Fuel Assembly
	STRUCTURE CHARACTERISTICS	
51.	Core Diameter, in. (Equivalent)	119.7
52.	Core Height, in. (Active Fuel)	144
	REFLECTOR THICKNESS AND COMPOSITION	
53.	Top - Water plus Steel, in.	~ 10
54.	Bottom - Water plus Steel, in.	~ 10
55.	Side - Water plus Steel, in.	~ 15
56.	H_2O/U Molecular Ratio core, Lattice (Cold)	2.73

(1) See Section 4.3.2.2.6

(2) This is the value of F_Q for normal operation

(3) This limit associated with an F_Q = 2.45

TABLE 4.1-2

ANALYTIC TECHNIQUES IN CORE DESIGN

Analysis	Technique	Computer Code	Section Referenced
Mechanical Design of Core Internals			
Loads, Deflections, and Stress Analysis	Static and dynamic modeling	Blowdown code, FORCE, finite element structural analysis code, and others	3.7.2.1 3.9.1 3.9.3
Fuel Rod Design			
Fuel Performance Characteristics (temperature, internal pressure, clad stress, etc.)	Semi-empirical thermal model of fuel rod with consideration of fuel density changes, heat transfer, fission gas release, etc.	Westinghouse fuel rod design model	4.2.1.3.1 4.3.3.1 4.4.2.2 4.4.3.4.2
Nuclear Design			
1. Cross Sections and Group Constants	Microscopic data; Macroscopic constants for homogenized core regions	PHOENIX	4.3.3.2 4.3.3.2
	Group constants for control rods with self-shielding	PHOENIX	4.3.3.2
2. X-Y-Z Power Distributions, Fuel Depletion, Critical Boron Concentrations, x-y Xenon Distributions, Reactivity Coefficients	3-D, Advanced Nodal Theory	ANC	4.3.3.3

TABLE 4.1-2(Continued)

ANALYTIC TECHNIQUES IN CORE DESIGN

Analysis	Technique	Computer Code	Section Referenced	
3. Axial Power Distributions, Control Rod Worths, and Axial Xenon Distribution	1-D, 2-Group Diffusion Theory	APOLLO	4.3.3.3	
4. Fuel Rod Power	Integral Transport Theory	LASER	4.3.3.1	
Effective Resonance Temperature	Monte Carlo Weighting Function	REPAD		
Thermal-Hydraulic Design				02-01
1. Steady-State	Subchannel analysis of local fluid conditions in rod bundles, including inertial and crossflow resistance terms, solution progresses from core-wide to hot assembly to hot channel	THINC-IV	4.4.3.4.1	02-01
2. Transient Departure from Nucleate Boiling Analysis	Subchannel analysis of local fluid conditions in rod bundles during transients by including accumulation terms in conservation equations	THINC-I (THINC-III)	4.4.3.4.1	

TABLE 4.1-3

DESIGN LOADING CONDITIONS FOR REACTOR CORE COMPONENTS

1. Fuel Assembly Weight
2. Fuel Assembly Spring Forces
3. Internals Weight
4. Control Rod Trip (equivalent static load)
5. Differential Pressure
6. Spring Preloads
7. Coolant Flow Forces (static)
8. Temperature Gradients
9. Differences in Thermal Expansion
    a. Due to temperature differences
    b. Due to expansion of different materials
10. Interference Between Components
11. Vibration (mechanically or hydraulically induced)
12. One or More Loops Out of Service
13. All Operational Transients Listed in Table 5.2-2
14. Pump Overspeed
15. Seismic Loads (operating basis earthquake and safe shutdown earthquake)
16. Blowdown Forces (due to cold and hot leg break)

4.2 MECHANICAL DESIGN

The plant conditions for design are divided into 4 categories in accordance with their anticipated frequency of occurrence and risk to the public: Condition I - Normal Operation; Condition II - Incidents of Moderate Frequency; Condition III - Infrequent Incidents; Condition IV - Limiting Faults.

The reactor is designed so that its components meet the following performance and safety criteria:

1. The mechanical design of the reactor core components and their physical arrangement, together with corrective actions of the reactor control, protection and emergency cooling systems (when applicable) assure that:

    a. Fuel damage (1) is not expected during Condition I and Condition II events. It is not possible, however, to preclude a very small number of rod failures. These are within the capability of the plant cleanup system and are consistent with plant design bases.

    b. The reactor can be brought to a safe state following a Condition III event with only a small fraction of fuel rods damaged [1] although sufficient fuel damage might occur to preclude resumption of operation without considerable outage time.

    c. The reactor can be brought to a safe state and the core can be kept subcritical with acceptable heat transfer geometry following transients arising from Condition IV events.

2. The fuel assemblies are designed to accommodate expected conditions for handling during assembly inspection, refueling operations and shipping loads.

3. The fuel assemblies are designed to accept control rod insertions in order to provide the required reactivity control for power operations and reactivity shutdown conditions.

4. All fuel assemblies have provisions for the insertion of incore instrumentation necessary for plant operation.

(1) Fuel damage as used here is defined as penetration of the fission product barrier (i.e., the fuel rod clad).

5. The reactor internals, in conjunction with the fuel assemblies, direct reactor coolant through the core to achieve acceptable flow distribution and to restrict bypass flow so that the heat transfer performance requirements can be met for all modes of operation. In addition, the internals provide core support and distribute coolant flow to the pressure vessel head so that the temperature differences between the vessel flange and head do not result in leakage from the flange during the Condition I and II modes of operation. Required inservice inspection can be carried out as the internals are removable and provide access to the inside of the pressure vessel.

4.2.1 FUEL

4.2.1.1 Design Bases

The fuel rod and fuel assembly design bases are established to satisfy the general performance and safety criteria presented in Section 4.2 and specific criteria noted below.

RN 95-022 96-043

4.2.1.1.1 Fuel Rods

The integrity of the fuel rods is ensured by designing to prevent excessive fuel temperatures, excessive internal rod gas pressures due to fission gas releases, and excessive cladding stresses and strains. This is achieved by designing the fuel rods so that the following conservative design bases are satisfied during Condition I and Condition II events over the fuel lifetime:

1. Fuel Pellet Temperatures - The center temperature of the hottest pellet is to be below the melting temperature of the UO_2 (melting point of 5080°F [1] unirradiated and decreasing by 58°F per 10,000 MWD/MTU). While a limited amount of center melting can be tolerated, the design conservatively precludes center melting. A calculated fuel centerline temperature of 4700°F has been selected as an overpower limit to assure no fuel melting. This provides sufficient margin for uncertainties as described in Sections 4.4.1.2 and 4.4.2.10.1.

2. Internal Gas Pressure - The internal pressure of the lead rod in the reactor will be limited to a value below that which could cause: 1) the diametral gap to increase due to outward cladding creep during steady state operation, and 2) extensive DNB propagation to occur. Reference [20] shows that the DNB propagation criteria is satisfied.

3. Clad Stress - The clad stresses are less than the clad yield stress, with due consideration for temperature and irradiation effects. While the clad has some capability for accommodating plastic strain, the yield stress has been accepted as a conservative design basis.

RN 95-022

An alternative criterion has been developed to evaluate cladding stress in Reference [23]. Per the revised stress criterion, maximum cladding stress intensities excluding pellet clad interaction (PCI) induced stress will be evaluated using ASME pressure vessel guidelines. Cladding corrosion is accounted for as a loss of load carrying material. Stresses are combined to calculate a maximum stress intensity which is then compared to criteria based on the ASME code (Addendum 1-A of Reference [23]). RN 14-005

4. Clad Tensile Strain - The clad tensile strain is less than 1%. This limit is consistent with proven practice.

5. Strain Fatigue - The cumulative strain fatigue cycles are less than the design strain fatigue life. This basis is consistent with proven practice.

The preceding fuel rod design bases and other supplementary fuel design criteria/limits are given in Section 2 of Reference [23], Section 2 of Reference [27], Section A of Reference [7], and Appendix B of Reference [27]. The detailed fuel rod design establishes such parameters as pellet size and density, clad-pellet diametral gap, gas plenum size, and helium pre-pressure. The design also considers effects such as fuel density changes, fission gas release, clad creep, and other physical properties which vary with burnup. RN 95-022 14-036

An extensive irradiation testing and fuel surveillance operational experience program has been, and continues to be, conducted to verify the adequacy of the fuel performance and design bases. This program is discussed in Section 4.2.1.3.3. Fuel surveillance and testing results, as they become available, are used to improve fuel rod design and manufacturing processes and assure that the design bases and safety criteria are satisfied. RN 95-022

4.2.1.1.2 Fuel Assembly Structure

Structural integrity of the fuel assemblies is assured by setting limits on stresses and deformations due to various loads and by determining that the assemblies do not interfere with the functioning of other components. Three (3) types of loads are considered.

1. Nonoperational loads such as those due to shipping and handling.

2. Normal and abnormal loads which are defined for Conditions I and II.

3. Abnormal loads which are defined for Conditions III and IV.

These criteria are applied to the design and evaluation of the top and bottom nozzles, the guide thimbles, grids and thimble joints.

The design bases for evaluating the structural integrity of the fuel assemblies are:

1. Nonoperational (e.g., shipping) - 4 g axial loading and 6 g lateral loading with dimensional stability.

2. For the normal operating and upset conditions, the fuel assembly component structural design criteria are classified into 2 material categories, namely austenitic steels and zirconium alloys. The stress categories and strength theory presented in the ASME Boiler and Pressure Vessel Code, Section III, are used as a general guide. The maximum shear-theory (Tresca criterion) for combined stresses is used to determine the stress intensities for the austenitic steel components. The stress intensity is defined as the numerically largest difference between the various principal stresses in a 3 dimensional field. The allowable stress intensity value for austenitic steels, such as nickel-chromium-iron alloys, is given by the lowest of the following: RN 96-043

    a. 1/3 of the specified minimum tensile strength or 2/3 of the specified minimum yield strength at room temperature;

    b. 1/3 of the tensile strength or 90% of the yield strength at temperature but not to exceed 2/3 of the specified minimum yield strength at room temperature.

The stress limits for the austenitic steel components are given below. All stress nomenclature is per the ASME Boiler and Pressure Vessel Code, Section III.

Stress Intensity Limits

Categories	Limit
General Primary Membrane Stress Intensity	Sm
Local Primary Membrane Stress Intensity	1.5 Sm
Primary Membrane plus Bending Stress Intensity	1.5 Sm
Total Primary plus Secondary Stress Intensity	3.0 Sm

The zirconium alloy structural components which consist of guide thimble and fuel tubes are in turn subdivided into 2 categories because of material differences and functional requirements. The fuel tube design criteria are covered separately in Section 4.2.1.1.1. The maximum shear theory is used to evaluate the guide thimble design. For conservative purposes, the zirconium alloy unirradiated properties are used to define the stress limits. RN 95-022 96-043 09-022

3. Abnormal loads during Conditions III or IV - worst cases represented by combined seismic and blowdown loads.

    a. Deflections or failures of components cannot interfere with the reactor shutdown or emergency cooling of the fuel rods.

b. The fuel assembly structural component stresses under faulted conditions are evaluated using primarily the methods outlined in Appendix F of the ASME Boiler and Pressure Vessel Code, Section III. Since the current analytical methods utilize elastic analysis, the stress allowables are defined as the smaller value of 2.4 Sm or 0.70 Su for primary membrane and 3.6 Sm or 1.05 Su for primary membrane plus primary bending. For the austenitic steel fuel assembly components, the stress intensity is defined in accordance with the rules described in the previous section for normal operating conditions. For the zirconium alloy components, the stress intensity limits are set at 2/3 of the material yield strength, Sy, at reactor operating temperature. This results in stress limits being the smaller of 1.6 Sy or 0.70 Su for primary membrane and 2.4 Sy or 1.05 Su for primary membrane plus bending. For conservative purposes, the zirconium alloy unirradiated properties are used to define the stress limits. RN 95-022 96-043

The grid component strength criteria are based on experimental tests. For grids, the limit is established based on the 95% confidence level on the true mean of the test data (experimental collapse load) at operating temperature. RN 96-043 09-022

4.2.1.2 Design Description

Fuel assembly and fuel rod design data are given in Table 4.1-1. NRC approval of the VANTAGE+ design was given in Reference [29]. RN 95-022 96-043

Two hundred sixty four (264) fuel rods, or variations of fuel rods and filler rods (with respect to fuel assembly reconstitution, Reference [30]), 24 guide thimble tubes and 1 instrumentation thimble tube are arranged within a supporting structure to form a fuel assembly. The instrumentation thimble is located in the center position and provides a channel for insertion of an incore neutron detector, if the fuel assembly is located in an instrumented core position. The guide thimbles provide channels for insertion of either a rod cluster control assembly, a neutron source assembly, a burnable absorber assembly or a plugging device (if used), depending on the position of the particular fuel assembly in the core. Figure 4.2-1 shows a cross-section of the fuel assembly array, and Figure 4.2-2 shows fuel assembly full length view. The fuel rods are loaded into the fuel assembly structure so that there is clearance between the fuel rod ends and the top and bottom nozzles. RN 95-022 RN 96-043

Since the VANTAGE+ fuel is intended to replace either the Westinghouse LOPAR, Optimized, or VANTAGE 5 fuel designs, the VANTAGE+ exterior assembly envelope is equivalent to those of previous Westinghouse fuel designs. Also, the VANTAGE+ fuel assembly is designed to be mechanically and hydraulically compatible with the LOPAR, Optimized and VANTAGE 5 designs in full or transition cores, and the same functional requirements and design criteria as previously established for the Westinghouse VANTAGE 5 fuel assembly remain valid for the VANTAGE+ fuel assembly, Reference [29]. The VANTAGE+ fuel assembly design is provided in Table 4.1-1. Figure 4.2-2 compares the VANTAGE 5 and VANTAGE+ fuel assembly designs. RN 95-022 96-043

Each fuel assembly is installed vertically in the reactor vessel and stands upright on the lower core plate, which is fitted with alignment pins to locate and orient the assembly. After all fuel assemblies are set in place, the upper support structure is installed. Alignment pins, built into the upper core plate, engage and locate the upper ends of the fuel assemblies. The upper core plate then bears downward against the fuel assembly top nozzle via the holddown springs to hold the fuel assemblies in place.

4.2.1.2.1 Fuel Rods

The fuel rods consist of uranium dioxide ceramic pellets contained in slightly cold worked zirconium alloy tubing which is plugged and seal welded at the ends to encapsulate the fuel. A schematic of the fuel rods is shown in Figure 4.2-3. The fuel pellets are right circular cylinders consisting of uranium dioxide powder which has been compacted by cold pressing and then sintered to the required density. The fuel rods also contain, annular Axial Blanket pellets, and an Integral Fuel Burnable Absorber (IFBA) coating on some of the enriched fuel pellets. RN 95-022 96-043

The bottom end plug has an internal grip feature to facilitate rod loading and provides appropriate lead-in for the removable top nozzle reconstitution feature. RN 95-022 96-043 01-113

A chamfered pellet design is used with the objective of improving manufacturability while maintaining or improving performance (e.g., improved pellet chip resistance during manufacturing/handling).

The axial blankets are a nominal 6 inches of fuel pellets at each end of the fuel rod pellet stack. VANTAGE+ fuel uses unenriched annular axial blanket pellets. VANTAGE+ fuel with Performance+ features uses mid-enriched annular axial blanket pellets. Axial blankets reduce neutron leakage and improve fuel utilization. The axial blankets utilize chamfered pellets physically different than the pellets, which help to prevent accidental mixing during manufacturing. The physical difference includes a longer pellet length than the pellet (see Table 4.1-1). RN 95-022 96-043 01-113

The IFBA coated fuel pellets are identical to the enriched uranium dioxide pellets except for the addition of a thin boride coating on the pellet cylindrical surface. Coated pellets occupy the central portion of the fuel column. The number and pattern of IFBA rods within an assembly may vary depending on specific application. The ends of the enriched coated pellets and enriched uncoated pellets are dished to allow for greater axial expansion at the pellet centerline and void volume for fission gas release. An evaluation and test program for the IFBA design features are given in Section 2.5 in Reference [24].

To avoid overstressing of the clad or seal welds, void volume and clearances are provided within the rods to accommodate fission gases released from the fuel, differential thermal expansion between the clad and the fuel, and fuel density changes during burnup. Shifting of the fuel within the clad during handling or shipping prior to core loading is prevented by a stainless steel helical spring which bears on top of the fuel. At assembly the pellets are stacked in the clad to the required fuel height, the spring is then inserted into the top end of the fuel tube and the end plugs pressed into the ends of the tube and welded. All fuel rods are internally pressurized with helium during the welding process in order to minimize compressive clad stresses and creep due to coolant operating pressures.

The fuel rods are presently being pre-pressurized and designed so that the internal gas pressure design basis (Section 4.2.1.1.1) is satisfied and clad flattening will not occur during the fuel core life as determined by the methods in Reference [3].

4.2.1.2.2 Fuel Assembly Structure

The fuel assembly structure consists of a bottom nozzle, top nozzle, guide thimbles, and grids, as shown in Figure 4.2-2.

RN 95-022

4.2.1.2.2.1 Bottom Nozzle

The bottom nozzle is a box-like structure which serves as a bottom structural element of the fuel assembly and directs the coolant flow distribution to the assembly. The VANTAGE+ with Performance + features includes a 2 piece composite bottom nozzle design incorporating a highly machined stainless steel adaptor plate welded to a low cobalt investment casting as shown in Figure 4.2-2. The plate itself acts to prevent a downward ejection of the fuel rods from their fuel assembly. The bottom nozzle is fastened to the fuel assembly guide tubes by weld-locked screws which penetrate through the nozzle and mate with an inside fitting in each guide tube.

RN 95-022 96-043

The debris filter bottom nozzle (DFBN) is used to reduce the possibility of fuel rod damage due to debris-induced fretting. The relatively large flow holes in a conventional bottom nozzle are replaced with a new pattern of smaller flow holes for the DFBN. The holes are sized to minimize passage of debris particles large enough to cause damage while providing sufficient flow area, comparable pressure drop, and continued structural integrity of the nozzle. Tests to measure pressure drop and demonstrate structural integrity have been performed to verify that the DFBN is totally compatible with the current design.

RN 96-043

Coolant flow through the fuel assembly is directed from the plenum in the bottom nozzle upward through the penetrations in the plate to the channels between the fuel rods. The penetrations in the plate are positioned between the rows of the fuel rods.

RN 95-022

Axial loads (holddown) imposed on the fuel assembly and the weight of the fuel assembly are transmitted through the bottom nozzle to the lower core plate. Indexing and positioning of the fuel assembly is controlled by alignment holes in 2 diagonally opposite bearing plates which mate with locating pins in the lower core plate. Any lateral loads on the fuel assembly are transmitted to the lower core plate through the locating pins.

4.2.1.2.2.2 Top Nozzle

The top nozzle assembly functions as the upper structural element of the fuel assembly in addition to providing a partial protective housing for the rod cluster control assembly or other components. It consists of an adapter plate, enclosure, top plate, and pads. The integral welded assembly has holddown springs mounted on the assembly as shown in Figure 4.2-2. The springs and bolts are made of Inconel-718 and Inconel-600, respectively, whereas other components are made of Type 304 stainless steel. RN 95-022

The square adapter plate is provided with round penetrations and semicircular ended slots to permit the flow of coolant upward through the top nozzle. Other round holes are provided to accept sleeves which are welded to the adapter plate and mechanically attached to the thimble tubes. The ligaments in the plate cover the tops of the fuel rods and prevent their upward ejection from the fuel assembly. The enclosure is a box-like structure which sets the distance between the adapter plate and the top plate. The top plate has a large square hole in the center to permit access for the control rods and the control rod spiders. Holddown springs are mounted on the top plate and are fastened in place by bolts and clamps located at 2 diagonally opposite corners. On the other 2 corners integral pads are positioned which contain alignment holes for locating the upper end of the fuel assembly.

To remove the top nozzle, a tool is first inserted through a lock tube and expanded radially to engage the bottom edge of the tube. An axial force is then exerted on the tool which overrides local lock tube deformations and withdraws the lock tube from the insert. After the lock tubes have been withdrawn, the nozzle is removed by raising it off the upper slotted ends of the nozzle inserts which deflect inwardly under the axial lift load. With the top nozzle removed, direct access is provided for fuel rod examinations or replacement. Reconstitution is completed by the remounting of the nozzle and the insertion of lock tubes. Additional details of this design feature, the design bases and evaluation of the reconstitutable top nozzle are given in Section 2.3.2 in Reference [24]. RN 95-022 96-043

4.2.1.2.2.3 Guide and Instrument Thimbles

The guide thimbles are structural members which also provide channels for the neutron absorber rods, burnable absorber rods, thimble plugs, or neutron source assemblies. Each one is fabricated from zirconium alloy tubing having 2 different diameters. The larger diameter at the top provides a relatively large annular area to permit rapid insertion of the control rods during a reactor trip as well as to accommodate the flow of coolant during normal operation. Four (4) holes are provided on the thimble tube above the dashpot to reduce the rod drop time. The lower portion of each guide thimble has a RN 95-022 96-043

reduced diameter to produce a dashpot action near the end of the control rod travel during normal operation and to accommodate the outflow of water from the dashpot during a reactor trip. The dashpot is closed at the bottom by means of an end plug which is provided with a small flow port to avoid fluid stagnation in the dashpot volume during normal operation. The top end of the guide thimble is fastened to a tabular insert by 3 expansion swages. The insert engages into the top nozzle and is secured into position by a lock tube. The lower end of the guide thimble is fitted with an end plug which is then fastened into the bottom nozzle by a weld locked screw. RN 95-022

Each grid is fastened to the guide thimble assemblies to create an integrated structure. Westinghouse has chosen one 4 lobe bulge at each thimble and instrumentation tube location for the fastening technique as depicted in Figures 4.2-4 and 4.2-5 for all but the top and bottom grids. RN 95-022 96-043

An expanding tool is inserted into the inner diameter of the thimble tube to the elevation of the sleeves that have been welded to the middle grid assemblies. The 4 lobed tool forces the thimble and sleeve outward to a predetermined diameter, thus joining the 2 components. RN 95-022 96-043

For the VANTAGE+ assembly, the top grid to nozzle attachment is shown in Figure 4.2-6. The thimbles are fastened to the top nozzle inserts by expanding the members as shown in Figures 4.2-4 and 4.2-5. The inserts then engage the top nozzle and are secured into position by the insertion of lock tubes. RN 95-022 96-043

The bottom grid assembly is not mechanically fastened as described above, but rather is joined to the assembly as shown in Figure 4.2-7. The stainless steel insert is spotwelded to the bottom grid and later captured between the guide thimble end plug and the bottom nozzle by means of a stainless steel thimble screw.

The central instrumentation thimble of each fuel assembly is not attached to either the top or bottom nozzles, but the thimble is constrained by its seating in counterbores of each nozzle. This thimble's internal diameter does not vary, and incore neutron detectors pass through the bottom nozzle's large counterbore into the center thimble. This thimble is expanded at the top and mid grids in the same manner as the previously discussed expansion of the guide thimbles to the grids. RN 96-043

The guide thimble tube ID provides an adequate nominal diametral clearance for the control rods. The thimble tube ID also provides sufficient diametral clearance for burnable absorber rods, source rods, and dually compatible thimble plugs (see Figures 4.2-20 and 4.2-2). RN 95-022 96-043

The instrumentation tube also has a sufficient diametral clearance for the flux thimble to traverse the tube without binding. RN 95-022 96-043

The IFM grids employ a single bulge connection to the sleeve and thimble just as is used in the intermediate grids.

RN 95-022 96-043

4.2.1.2.2.4 Grid Assemblies

The fuel rods, as shown in Figure 4.2-2, are supported laterally at intervals along their length by grid assemblies which maintain the lateral spacing between the rods throughout the design life of the assembly. Each fuel rod is afforded lateral support within each grid by the combination of support dimples and springs. The grid assembly consists of individual slotted straps interlocked and welded in an “egg-crate" arrangement to join the straps permanently at their points of intersection. The straps contain spring fingers, support dimples and mixing vanes.

RN 95-022

RN 95-022

The grid material is zirconium alloy (mid-grids) and Inconel 718 (end grids) for VANTAGE+ assemblies. Inconel 718 was chosen for its corrosion resistance assembly and high strength properties. Zirconium Alloy was chosen for the VANTAGE+ assembly mid-grids due to its corrosion resistance, low neutron cross-section, and adequate strength properties. The magnitude of the grid restraining force on the fuel rod is set high enough to minimize possible fretting, without overstressing the cladding at the points of contact between the grids and fuel rods. The grid assemblies also allow axial thermal expansion of the fuel rods without imposing restraint sufficient to develop buckling or distortion of the fuel rods.

RN 95-022 96-043 11-013

RN 95-022

For VANTAGE+ fuel with Performance + features, 4 types of grid assemblies are used. The top and bottom Inconel (non-mixing vane) grids of the VANTAGE+ fuel assemblies are used. Six (6) intermediate (mixing vane) structural grids are used. They are made of Zirconium Alloy material. The third grid type for the VANTAGE+ assembly is an Intermediate Flow Mixer, also made of Zirconium Alloy. These Intermediate Flow Mixer (IFM) grids shown in Figure 4.2-2 are located in the 3 uppermost spans between the Zirconium Alloy mixing vane structural grids and incorporate a similar mixing vane array. Their prime function is mid-span flow mixing in the hottest fuel assembly spans. Each IFM grid cell contains 4 dimples which are designed to prevent mid-span channel closure in the spans containing IFMs and fuel rod contact with the mixing vanes. This simplified cell arrangement allows short grid cells so that the IFM grid can accomplish its flow mixing objective with minimal pressure drop.

RN 95-022 96-043 11-013

The VANTAGE+ IFM grids are not intended to be structural members. The outer strap configuration is designed to preclude grid hang-up and damage during fuel handling. Additionally, the grid envelope is smaller which further minimizes the potential for damage and reduces calculated forces during seismic/LOCA events.

RN 95-022 09-022 11-013

A fourth type of grid used in VANTAGE+ fuel with Performance + features is a Robust Protective Grid (RPG). The grid is an Inconel 718 grid that is mounted below the bottom grid (on top of the bottom nozzle) and acts to strain out foreign materials before they can flow up the fuel assembly, be trapped by the other grids and cause damage to the fuel rods.

RN 96-043 11-013

4.2.1.3 Design Evaluation

4.2.1.3.1 Fuel Rods

The fuel rods are designed to assure the design bases are satisfied for Condition I and II events. This assures that the fuel performance and safety criteria (Section 4.2) are satisfied.

4.2.1.3.1.1 Materials - Fuel Cladding

The desired fuel rod clad is a material which has a superior combination of neutron economy (low absorption cross section), high strength (to resist deformation due to differential pressures and mechanical interaction between fuel and clad), high corrosion resistance (to coolant, fuel and fission products), and high reliability. ZIRLO®/Optimized ZIRLO™ has this desired combination of clad properties. As shown in Reference [4], there is considerable PWR operating experience on the capability of Zircaloy and ZIRLO® as a clad material. Optimized ZIRLO™ has the same chemical composition as ZIRLO® with the exception of a lower tin content for improved corrosion resistance, Reference [16]. Clad hydriding has not been a significant cause of clad perforation since current controls on levels of fuel contained moisture were instituted, Reference [4]. RN 95-022 96-043 11-013 14-036

Metallographic examinations of irradiated commercial fuel rods have shown occurrences of fuel/clad chemical interaction. Reaction layers of < 1 mil in thickness have been observed between fuel and clad at limited points around the circumference. Westinghouse metallographic data indicates that this interface layer remains very thin even at high burnup. Thus, there is no indication of propagation of the layer and eventual clad penetration. RN 11-013

Stress corrosion cracking is another postulated phenomenon related to fuel/clad chemical interaction. Reaction tests have shown that in the presence of high clad tensile stresses, large concentrations of iodine can chemically attack the Zirconium-based alloy tubing and can lead to eventual clad cracking. Westinghouse has no in reactor evidence that this mechanism is operative in commercial fuel. RN 95-022 11-013

4.2.1.3.1.2 Materials - Fuel Pellets

Sintered, high density uranium dioxide fuel reacts only slightly with the clad, at core operating temperatures and pressures. In the event of clad defects, the high resistance of uranium dioxide to attack by water protects against fuel deterioration although limited fuel erosion can occur. As has been shown by operating experience and extensive experimental work, the thermal design parameters conservatively account for changes in the thermal performance of the fuel elements due to pellet fracture which may occur during power operation. The consequences of defects in the clad are greatly reduced by the ability of uranium dioxide to retain fission products including those which are gaseous or highly volatile. Observations from several operating Westinghouse PWRs

(References [2] and [4]) have shown that fuel pellets can densify under irradiation to a density higher than the manufactured values. Fuel densification and subsequent incomplete settling of the fuel pellets results in local and distributed gaps in the fuel rods.

Fuel densification has been minimized by improvements in the fuel manufacturing process and by specifying a nominal initial fuel density of 95%.

The effects of fuel densification have been taken into account in the nuclear and thermal hydraulic design of the reactor described in Sections 4.3 and 4.4, respectively.

4.2.1.3.1.3 Materials - Strength Considerations

One of the most important limiting factors in fuel element duty is the mechanical interaction of fuel and clad. This fuel/clad interaction produces cyclic stresses and strains in the clad, and these in turn consume clad fatigue life. The reduction of fuel/clad interaction is therefore a principal goal of design. In order to achieve this goal and to enhance the cyclic operational capability of the fuel rod, the technology for using pre-pressurized fuel rods in Westinghouse PWR's has been developed.

Initially the gap between the fuel and clad is sufficient to prevent hard contact between the two. However, during power operation a gradual compressive creep of the clad onto the fuel pellet occurs due to the external pressure exerted on the rod by the coolant. Clad compressive creep eventually results in the hard fuel/clad contact. During this period of fuel/clad contact, changes in power level could result in significant changes in clad stresses and strains. By using pre-pressurized fuel rods to partially offset the effect of the coolant external pressure, the rate of clad creep toward the surface of the fuel is reduced. Fuel rod pre-pressurization delays the time at which substantial fuel/clad interaction and hard contact occur and hence significantly reduces the number and extent of cyclic stresses and strains experienced by the clad both before and after fuel/clad contact. These factors result in an increase in the fatigue life margin of the clad and lead to greater clad reliability. If gaps should form in the fuel stacks, clad flattening will be prevented by the rod pre-pressurization so that the flattening time will be greater than the fuel core life.

RN
14-036

4.2.1.3.1.4 Steady-State Performance Evaluation

In the calculation of the steady-state performance of a nuclear fuel rod, the following interacting factors must be considered:

1. Clad creep and elastic deflection,

2. Pellet density changes, thermal expansion, gas release, and thermal properties as a function of temperature and fuel burnup,

3. Internal pressure as a function of fission gas release, rod geometry, and temperature distribution.

These effects are evaluated using an overall fuel rod design model, per References [5, 6, 7, 17, 20, and 28] which include appropriate models for time dependent fuel densification. With these interacting factors considered, the model determines the fuel rod performance characteristics for a given rod geometry, power history, and axial power shape. In particular, internal gas pressure, fuel and clad temperatures, and clad deflections are calculated. The fuel rod is divided lengthwise into several sections and radially into a number of annular zones. Fuel density changes, clad stresses, strains and deformations, and fission gas releases are calculated separately for each segment. The effects are integrated to obtain the internal rod pressure.

RN 95-022 14-036

The initial rod internal pressure is selected to delay fuel/clad mechanical interaction and to avoid the potential for flattened rod formation. It is limited, however, by the rod internal pressure design basis given in Section 4.2.1.1.1.

The gap conductance between the pellet surface and the clad inner diameter is calculated as a function of the composition, temperature, and pressure of the gas mixture, and the gap size or contact pressure between clad and pellet. After computing the fuel temperature for each pellet annular zone, the fractional fission gas release is assessed using an empirical model derived from experimental data in References [5, 17, and 28]. The total amount of gas released is based on the average fractional release within each axial and radial zone and the gas generation rate which in turn is a function of burnup. Finally, the gas released is summed over all zones and the pressure is calculated.

RN 95-022 14-036

The model shows good agreement in fit for a variety of published and proprietary data on fission gas release, fuel temperatures and clad deflections, References [5, 17, and 28]. Included in this spectrum are variations in power, time, fuel density, and geometry. The in-pile fuel temperature measurement comparisons used are shown in References [5, 17, and 28].

RN 95-022 14-036

Typical fuel clad inner diameter and the fuel pellet outer diameter as a function of exposure are presented in Figure 4.2-8. The cycle to cycle changes in the pellet outer diameter represent the effects of power changes as the fuel is moved into different positions as a result of refueling. The gap size at any time is merely the difference between clad inner diameter and pellet outer diameter. Total clad-pellet surface contact occurs near the end of Cycle 2. The figure represents hot fuel dimensions for a fuel rod operating at the power level shown in Figure 4.2-9. Figure 4.2-9 illustrates representative fuel rod internal gas pressure and linear power for the lead burnup rod versus irradiation time. In addition, it outlines the typical operating range of internal gas pressures which is applicable to the total fuel rod population within a region. The "best estimate" fission gas release model was used in determining the internal gas pressures as a function of irradiation time. The plenum height of the fuel rod has been designed to ensure that the maximum internal pressure of the fuel rod will not exceed the design pressure of the reactor coolant.

The clad stresses at a constant local fuel rod power are low. Compressive stresses are created by the pressure differential between the coolant pressure and the rod internal gas pressure. Because of the pre-pressurization with helium, the volume average effective stresses are less than 13,500 psi at the pressurization level used in this fuel rod design. Stresses due to the temperature gradient are not included in this average effective stress because thermal stresses are, in general, negative at the clad inside diameter and positive at the clad outside diameter and their contribution to the clad volume average stress is small. Furthermore, the thermal stress decreases with time during steady-state operation due to stress relaxation. The stress due to pressure differential is highest in the minimum power rod at the beginning of life (due to low internal gas pressure). The thermal stress is highest in the maximum power rod (due to steep temperature gradient). RN 95-022

Tensile stresses could be created once the clad has come in contact with the pellet. These stresses would be induced by the fuel pellet swelling during irradiation. As shown in Figure 4.2-8, there is very limited clad pushout after pellet-clad contact. Fuel swelling can result in small clad strains (< 1%) for expected discharge burnups but the associated clad stresses are very low because of clad creep (thermal and irradiation-induced creep). Furthermore, the 1% strain criterion is extremely conservative for fuel-swelling driven clad strain because the strain rate associated with solid fission products swelling is very slow (-5 x 10^{-7} hr-1). In-pile experiments in Reference [8] have shown that Zircaloy tubing exhibits "superplasticity" at slow strain rates during neutron irradiation. Uniform clad strains of greater than 10% have been achieved under these conditions with no sign of plastic instability.

4.2.1.3.1.5 Transient Evaluation Method

Pellet thermal expansion due to power increases is considered the only mechanism by which significant stresses and strains can be imposed on the clad. Power increases in commercial reactors can result from fuel shuffling (e.g., Region 3 positioned near the center of the core for Cycle 2 operation after operating near the periphery during Cycle 1), reactor power escalation following extended reduced power operation, and control rod movement. In the mechanical design model, lead rods are depleted using best estimate power histories as determined by core physics calculations. During the depletion, the amount of diametral gap closure is evaluated based upon the pellet expansion-cracking model, clad creep model, and fuel swelling model. At various times during depletion the rod power is assumed to increase locally up to the burnup dependent attainable power density as determined by core physics calculations. Historically, the radial, tangential, and axial clad stresses resulting from the power increase are combined into a volume average effective clad stress. RN 14-005

The Von Mises criterion is used to evaluate whether the clad yield stress has been exceeded. This criterion states that an isotropic material in multi-axial stress will begin to yield plastically when the effective stress exceeds the yield stress as determined by a uniaxial tensile test. The yield stress is correlated for irradiated cladding since fuel/clad interaction occurs at high burnup. Furthermore, the effective stress is increased by an allowance which accounts for stress concentrations in the clad adjacent to radial cracks

in the pellet prior to the comparison with the yield stress. This allowance was evaluated using a 2-dimensional (r,θ) finite element model.

According to the revised stress criterion documented in Reference [23], the transient clad stress limit was designed to protect the cladding during pellet clad interaction (PCI). This is one of the four criteria which were imposed to protect the cladding from PCI during Condition I and II operation. The other three remaining criteria are transient strain less than 1%, no centerline fuel melt, and cladding total strain less than 1%. The later three criteria are sufficient to protect the cladding from PCI. The transient stress criterion is redundant and does not represent industry practice and the following describes the criterion for fuel rod clad stress per Addendum 1-A of Reference [23]: Maximum cladding stress intensities excluding PCI induced stress will be evaluated using ASME pressure vessel guidelines. Cladding corrosion is accounted for as a loss of load carrying material. Stresses are combined to calculate a maximum stress intensity which is then compared to criteria based on the ASME code. RN 14-005

Slow transient power increases can result in large clad strains because of clad creep and stress, therefore, a criterion on allowable clad positive strain is necessary. Based upon high strain rate burst and tensile test data on irradiated tubing, 1% strain was determined to be the lower limit on irradiated clad ductility and thus adopted as a design criterion. RN 14-005

In addition to the mechanical design models and design criteria, Westinghouse relies on performance data accumulated through transient power test programs in experimental and commercial reactors, and through normal operation in commercial reactors.

It is recognized that a possible limitation to the satisfactory behavior of the fuel rods in a reactor which is subjected to daily load follow is the failure of the clad by low cycle strain fatigue. During their normal residence time in reactor, the fuel rods may be subjected to 1,000 or more cycles with typical changes in power level from 50 to 100% of their steady-state values. RN 95-022

The assessment of the fatigue life of the fuel rod clad is subjected to a considerable uncertainty due to the difficulty of evaluating the strain range which results from the cyclic interaction of the fuel pellets and clad. This difficulty arises from such highly unpredictable phenomena as pellet cracking, fragmentation, and relocation. Nevertheless, since early 1968, Westinghouse has been investigating this particular phenomenon both analytically and experimentally. Strain fatigue tests on irradiated and nonirradiated hydrided Zircaloy-4 claddings were performed which permitted a definition of a conservative fatigue life limit and recommendation of a methodology to treat the strain fatigue evaluation of the Westinghouse reference fuel rod designs.

However, Westinghouse is convinced that the final proof of the adequacy of a given fuel rod design to meet the load follow requirements can only come from incore experiments performed on actual reactors. The Westinghouse experience in load follow operation dates back to early 1970 with the load follow operation of the Saxton reactor.

Successful load follow operation has been performed on reactor A (300 load follow cycles) and reactor B (150 load follow cycles). In both cases, there was no significant coolant activity increase that could be associated with the load follow mode of operation.

The following paragraphs present briefly the Westinghouse analytical approach to strain fatigue.

A comprehensive review of the available strain-fatigue models was conducted by Westinghouse as early as 1968. This included the Langer-O'Donnel model Reference [9], the Yao-Munse model, and the Manson-Halford model. Upon completion of this review and using the results of the Westinghouse experimental programs discussed below, it was concluded that the approach defined by Langer-O'Donnel would be retained and the empirical factors of their correlation modified in order to conservatively bound the results of the Westinghouse testing program.

RN 14-036

The Langer-O'Donnel empirical correlation has the following form:

$$S_a = \frac{E}{4(N_f)^{0.5}} \ln\left(\frac{100}{100 - RA}\right) + S_e$$

Where:

S_a = 1/2 E $\Delta\varepsilon_t$ = pseudo-stress amplitude which causes failure in N_f cycles (lb/in^2)

$\Delta\varepsilon_t$ = total strain range (in/in)

E = Young's Modulus (lb/in^2)

N_f = number of cycles to failure

RA = reduction in area at fracture in a uniaxial tensile test (%)

S_e = endurance limit (lb/in^2)

Both RA and S_e are empirical constants which depend on the type of material, the temperature and irradiation. The Westinghouse testing program was subdivided in the following subprograms:

1. A rotating bend fatigue experiment on unirradiated Zircaloy-4 specimens at room temperature and at 725°F. Both hydrided and nonhydrided Zircaloy-4 cladding were tested.

2. A biaxial fatigue experiment in gas autoclave on unirradiated Zircaloy-4 cladding both hydrided and nonhydrided.

3. A fatigue test program on irradiated cladding from the CVTR and Yankee Core V conducted at Battelle Memorial Institute.

The results of these test programs provided information on different cladding conditions including the effect of irradiation, hydrogen level, and temperature.

The Westinghouse design equations followed the concept for the fatigue design criterion according to the ASME Boiler and Pressure Vessel Code, Section III, namely:

1. The calculated pseudo-stress amplitude (S_a) has to be multiplied by a factor of 2 in order to obtain the allowable number of cycles (N_f).

2. The allowable cycles for a given S_a is 5% of N_f, or a safety factor of 20 on cycles.

The lesser of the 2 allowable number of cycles is selected. The cumulative fatigue life fraction is then computed as:

$$\sum_{1}^{k} \frac{n_k}{N_{fk}} \leq 1$$

RN 96-043

Where:

n_k = number of diurnal cycles of mode k.

The potential effects of operation with waterlogged fuel are discussed in Section 4.4.3.6. Waterlogging is not considered to be a concern during operational transients.

4.2.1.3.1.6 Rod Bowing

Reference [10] presents the model used for evaluation of fuel rod bowing.

4.2.1.3.2 Fuel Assembly Structure

4.2.1.3.2.1 Stresses and Deflections

The fuel assembly component stress levels are limited by the design. For example, stresses in the fuel rod due to thermal expansion and cladding irradiation growth are limited by the relative motion of the rod as it slips over the grid spring and dimple surfaces. Clearances between the fuel rod ends and nozzles are provided so that cladding irradiation growth will not result in rod end interferences. Stresses in the fuel assembly caused by tripping of the rod cluster control assembly have little influence on fatigue because of the small number of events during the life of an assembly. Assembly components and prototype fuel assemblies made from production parts have been subjected to structural tests to verify that the design bases requirements are met. RN 95-022 96-043

The fuel assembly response resulting from the most limiting pipe break was analyzed using time-history numerical techniques. Since the resulting vessel motion induces primarily lateral loads on the reactor core, a finite element model similar to the seismic model described in Reference [31] was used to assess the fuel assembly deflections and impact forces. RN 95-022 09-022

The reactor core finite element model which simulates the fuel assembly interaction during lateral excitation consists of fuel assemblies arranged in a planer array with inter assembly gaps. For the Virgil C. Summer Nuclear Station the fuel assembly rows 15, 13, 11, 9, 7, and 3 were analyzed. The fuel assemblies and the reactor baffle supports are represented by single beam elements. Figure 4.2-28 shows this single beam schematic for row 15, the maximum number of assemblies across the core diameter. The time-history motion for the upper and lower core plates and the barrel at the upper core plate elevation are simultaneously applied to the simulated reactor core model as illustrated in Figure 4.2-28. The 3 time-history motions were obtained from the time-history analysis of the reactor vessel and internals finite element model. RN 09-022

An evaluation of fuel assembly structural integrity considered the lateral effects of a LOCA accident with an upflow conversion determined that the seismic analysis of record remains applicable to the VC Summer Upflow conversion. The grid impact loads resulting from seismic and LOCA accidents were combined by SRSS (Square root sum of square) method. The safe shutdown earthquake and LOCA analyses indicated that the flow mixers will share some grid load among the structural grids. The analysis results confirmed that the calculated grid loads are less than the allowable limit except 3 fuel assembly (FA) row. According to Reference [32], the core coolable geometry is maintained when the crushed grids occur at 3 FA row. RN 96-043 09-022

Because the Virgil C. Summer Nuclear Station is not bounded by the LOCA/Seismic loads considered in Reference [25] and Reference [24], additional analyses have been performed to demonstrate fuel assembly structural integrity. The evaluation of the VANTAGE 5 fuel assembly, in accordance with NRC requirements as given in SRP 4.2, Appendix A, shows that the VANTAGE 5 fuel is structurally acceptable for an all VANTAGE 5 core; the grids will not buckle due to combined impact forces of a seismic/LOCA event except in the 3 fuel assembly row. Since the 3 fuel assembly row is located at a low powered region, the core coolable geometry is maintained based on Reference [32]. The stresses in the fuel assembly components resulting from seismic and LOCA loads are well within acceptable limits ensuring that the reactor can be safely shutdown under the combined faulted condition loads.

RN 95-022 09-022

Since the VANTAGE+ assembly is structurally identical to that of VANTAGE 5, the evaluations discussed above are also applicable to VANTAGE+.

RN 95-022 96-043

The fuel assembly design loads for shipping have been established at 6 g lateral and 4 g axial. Accelerometers are permanently placed into the shipping cask to monitor and detect fuel assembly accelerations that would exceed the criteria. Past history and experience has indicated that loads which exceed the allowable limits rarely occur. Exceeding the limits requires reinspection of the fuel assembly for damage. Tests on various fuel assembly components such as the grid assembly, sleeves, inserts and structure joints have been performed to assure that the shipping design limits do not result in impairment of fuel assembly function.

4.2.1.3.2.2 Dimensional Stability

The VANTAGE 5 Mechanical Test Program description and results are given in Appendix A of Reference [24] and are considered to be applicable to VANTAGE+ as the 2 assemblies are essentially identical from a structural standpoint.

RN 95-022

The coolant flow channels are established and maintained by the structure composed of grids and guide thimbles. The lateral spacing between fuel rods is provided and controlled by the support dimples of adjacent grid cells. Contact of the fuel rods on the dimples is maintained through the clamping force of the grid springs. Lateral motion of the fuel rods is opposed by the spring force and the internal moments generated between the spring and the support dimples.

No interference with control rod insertion into thimble tubes will occur during a postulated loss of coolant accident transient due to fuel rod swelling, thermal expansion, or bowing. In the early phase of the transient following the coolant break, the high axial loads, which potentially could be generated by the difference in thermal expansion between fuel clad and thimbles, are relieved by slippage of the fuel rods through the grids. The relatively low drag force restraint on the fuel rods will induce only minor thermal bowing, which is insufficient to close the fuel rod-to-thimble tube gap. This rod-to-grid slip mechanism occurs simultaneously with control rod drop. Subsequent to the control rod insertion the transient temperature increase of the fuel rod clad can result in swelling sufficient to contact the thimbles.

4.2.1.3.2.3 Vibration and Wear

Fuel rod vibrations are flow induced. The effect of the vibration on the fuel assembly and individual fuel rods is minimal. The cyclic stress range associated with deflections of such small magnitude is insignificant and has no effect on the structural integrity of the fuel rod.

The reaction force on the grid supports due to rod vibration is small and is much less than the spring preload. Firm contact is maintained. No significant wear of the clad or grid supports is expected during the life of the fuel assembly.

Clad fretting and fuel rod vibration has been experimentally investigated as discussed in Reference [24] for VANTAGE 5 fuel and is applicable directly to VANTAGE+ fuel design.

RN 95-022

4.2.1.3.3 Operational Experience

A discussion of fuel operating experience is given in Reference [4].

4.2.1.4 Tests and Inspections

4.2.1.4.1 Quality Assurance Program

The Quality Assurance Program Plan of the Westinghouse Commercial Nuclear Fuel Division is summarized in Reference [13].

The program provides for control over all activities affecting product quality, commencing with design and development, and continuing through procurement, materials handling, fabrication, testing and inspection, storage, and transportation. The program also provides for the indoctrination and training of personnel and for the auditing of activities affecting product quality through a formal auditing program.

Westinghouse drawings and product, process, and material specifications identify the inspection to be performed.

4.2.1.4.2 Quality Control

Quality control philosophy is generally based on the following inspections being performed to a 95% confidence that at least 95% of the product meets specification, unless otherwise noted.

1. Fuel System Components and Parts

   The characteristics inspected depends upon the component parts and includes dimensional, visual, check audits of test reports, material certification and nondestructive examination such as X-Ray and ultrasonic.

   All material used in this core is verified and released by Quality control.

2. Pellets

   Inspection is performed for dimensional characteristics such as diameter, density, length and squareness of ends. Additional visual inspections are performed for cracks, chips and surface conditions according to approved standards.

   Density is determined in terms of weight per unit length and is plotted on zone charts used in controlling the process. Chemical analyses are taken on a specified sample basis through pellet production.

3. Rod Inspection

   Fuel rod, control rodlet, burnable poison and source rod inspection consists of the following nondestructive examination techniques and methods, as applicable.

   a. Leak Testing

      Each rod is tested using a calibrated mass spectrometer with helium being the detectable gas.

   b. Enclosure Welds

      Rod welds are inspected by ultrasonic test or X-ray in accordance with a qualified technique and Westinghouse specifications.

   c. Dimensional

      All rods are dimensionally inspected prior to final release. The requirements include such items as length, camber, and visual appearance.

d. Plenum Dimensions

100% of the fuel rods are inspected by gamma scanning or other approved methods to ensure proper plenum dimensions.

e. Pellet-to-Pellet Gaps

100% of the fuel rods are inspected by gamma scanning or other methods to ensure that no significant gaps exist between pellets.

f. Pellet Enrichment

RN 14-036

100% of the fuel rods are active gamma scanned to verify enrichment control prior to acceptance for assembly loading.

g. Traceability

Traceability of rods and associated rod components is established by Quality Control.

4. Assemblies

Each fuel, control rod, burnable absorber and source rod assembly is inspected for drawing and/or specification requirements. Other incore control component inspection and specification requirements are given in Section 4.2.3.4.

5. Other Inspections

The following inspections are performed as part of the routine inspection operation:

a. Tool and gage inspection and control including standardization to primary and/or secondary working standards. Tool inspection is performed at prescribed intervals on all serialized tools. Complete records are kept of calibration and conditions of tools.

b. Audits are performed of inspection activities and records to assure that prescribed methods are followed and that records are correct and properly maintained.

c. Surveillance inspection where appropriate, and audits of outside contractors are performed to ensure conformance with specified requirements.

6. Process Control

To prevent the possibility of mixing enrichments during fuel manufacture and assembly, strict enrichment segregation and other process controls are exercised.

The UO_2 powder is kept in sealed containers or is processed in a closed system. The containers are either fully identified both by descriptive tagging and preselected color coding or, for the closed system, the material is monitored by a computer data management information system. For the sealed container system, a Westinghouse identification tag completely describing the contents is affixed to the containers before transfer to powder storage. Isotopic content is confirmed by analysis.

Powder withdrawal from storage can be made by only one authorized group, which directs the powder to the correct pellet production line. All pellet production lines are physically separated from each other and pellets of only a single nominal enrichment and density are produced in a given production line.

Finished pellets are placed on trays and transferred to segregated storage racks within the confines of the pelleting area. Samples from each pellet lot are tested for physical and chemical properties including isotopic content and impurity levels prior to acceptance by Quality Control. Physical barriers prevent mixing of pellets of different nominal designs and enrichment in this storage area. Unused powder and substandard pellets are returned to storage for disposition.

Loading of pellets into the clad is performed in isolated production lines and again only one density and enrichment is loaded on a line at a time.

A serialized traceability code is placed on each fuel tube which identifies the enrichment. The end plugs are inserted and then inert welded to seal the tube. The fuel tube remains coded and traceability identified until just prior to installation in the fuel assembly.

At the time of installation into an assembly, the traceability codes are removed and a matrix is generated to identify each rod in its position within a given assembly. After the fuel rods are installed, an inspector verifies that all fuel rods in an assembly carry the correct identification character describing the fuel enrichment and density for the core region being fabricated. The top nozzle is inscribed with a permanent identification number providing traceability to the fuel contained in the assembly.

Similar traceability is provided for burnable absorber, source rods and control rodlets as required.

4.2.1.4.3 Onsite Inspection

Onsite inspection programs for fuel, control rods, and internals are based on the NSSS supplier's detailed procedures. In the event reloads or other components are supplied by other suppliers, additional programs will be developed based on that supplier's procedures.

Loaded fuel containers, when received onsite, are externally inspected to ensure that labels and markings are intact and seals are unbroken. After the containers are opened, the shock indicators attached to the suspended internals are inspected to determine if movement during transit exceeded design limitations.

Following removal of the fuel assembly from the container in accordance with detailed procedures from the fuel fabricator the polyethylene wrapper is then removed and a visual inspection of the entire bundle is performed.

Control rod assemblies are shipped in fuel assemblies and are inspected. The control rod assembly is withdrawn a few inches from the fuel assembly using the fuel handling tool to ensure free and unrestricted movement. The exposed section is then visibly inspected for mechanical integrity, replaced in the fuel assembly and stored with the fuel assembly.

Reactor internals are visually inspected and manually checked for tightness upon receipt at the site. Clearance measurements performed during assembly and installation in accordance with the manufacturer's detailed procedures, also serve to verify the mechanical integrity of the internals.

Surveillance of fuel and reactor performance is routinely conducted by operating personnel. Coolant activity and chemistry are followed to permit early detection of any fuel clad defects.

Visual fuel inspection utilizing binoculars is routinely conducted during refueling. This type of inspection is capable of identifying gross anomalies such as broken fuel rods or torn grid straps. No less than 10% of the fuel permanently removed from the core will be examined routinely. Additional fuel inspections are dependent on the results of the operational monitoring and visual inspection.

Extensive examination, such as using television for fuel inspection, is not performed in the Virgil C. Summer Nuclear Station since performance verification has been demonstrated on other Westinghouse plants with similar fuel design.

4.2.2 REACTOR VESSEL INTERNALS

4.2.2.1 Design Bases

The design bases for the mechanical design of the reactor vessel internals components are as follows:

1. The reactor internals in conjunction with the fuel assemblies shall direct reactor coolant through the core to achieve acceptable flow distribution and to restrict bypass flow so that the heat transfer performance requirements are met for all modes of operation. In addition, required cooling for the pressure vessel head shall be provided so that the temperature differences between the vessel flange and head do not result in leakage from the flange during reactor operation.

2. In addition to neutron shielding provided by the reactor coolant, the reactor internals are designed to limit the exposure of the pressure vessel in order to maintain the required ductility of the material for all modes of operation.

3. Provisions shall be made for installing incore instrumentation useful for the plant operation and vessel material test specimens required for a pressure vessel irradiation surveillance program.

4. The core internals are designed to withstand mechanical loads arising from operating basis earthquake, safe shutdown earthquake and pipe ruptures and meet the requirement of item 5 below.

5. The reactor shall have mechanical provisions which are sufficient to adequately support the core and internals and to assure that the core is intact with acceptable heat transfer geometry following transients arising from abnormal operating conditions.

6. Following the design basis accident, the plant shall be capable of being shutdown and cooled in an orderly fashion so that fuel cladding temperature is kept within specified limits. This implies that the deformation of certain critical reactor internals must be kept sufficiently small to allow core cooling.

The functional limitations for the core structures during the design basis accident are shown in Table 4.2-1. To ensure no column loading of rod cluster control guide tubes, the upper core plate deflection is limited to not exceed the value shown in Table 4.2-1. Details of the dynamic analyses, input forcing functions, and response loadings are presented in Section 3.9.

4.2.2.2 Description and Drawings

The reactor vessel internals are described as follows:

The components of the reactor internals are divided into 3 parts consisting of the lower core support structure (including the entire core barrel and neutron shield pad assembly), the upper core support structure and the incore instrumentation support structure. The reactor internals support the core, maintain fuel alignment, limit fuel assembly movement, maintain alignment between fuel assemblies and control rod drive mechanisms, direct coolant flow past the fuel elements, direct coolant flow to the pressure vessel head, provide gamma and neutron shielding, and guides for the incore instrumentation. The coolant flows from the vessel inlet nozzles down the annulus between the core barrel and the vessel wall and then into a plenum at the bottom of the vessel. It then reverses and flows up through the core support and through the lower core plate. The lower core plate is sized to provide the desired inlet flow distribution to the core. After passing through the core, the coolant enters the region of the upper support structure and then flows radially to the core barrel outlet nozzles and directly through the vessel outlet nozzles. A small portion of the coolant flows between the baffle plates and the core barrel to provide additional cooling of the barrel. Beginning with Cycle 19, the direction of coolant flow between the baffle plates and core barrel was changed from a downflow configuration to an upflow configuration to reduce baffle jetting - related fuel failures. Similarly, a small amount of the entering flow is directed into the vessel head plenum and exits through the vessel outlet nozzles.

RN 09-022

All the major material for the reactor internals is Type 304 stainless steel. Parts not fabricated from Type 304 stainless steel include bolts and dowel pins which are fabricated from Type 316 stainless steel and radial support key bolts which are fabricated of Inconel-750. These materials are listed in Table 5.2-12. There are no other materials used in the reactor internals or core support structures which are not otherwise included in ASME Code, Section III, Appendix I.

The discussions provided in Sections 5.2.3 and 5.2.5 are applicable to the welding of reactor internals and core support components.

The discussions provided in Sections 5.2.5.1, 5.2.5.2, 5.2.5.3, 5.2.5.4, 5.2.5.5, and 5.2.5.6 are applicable to the degree of conformance of reactor internals and core support structures with Regulatory Guide 1.44.

The discussion provided in Section 5.2.5.7 addresses Regulatory Guide 1.31 with respect to reactor internals and core support structures.

Appendix 3A addresses Regulatory Guides 1.66 and 1.71 with respect to reactor internals and core support structures.

Austenitic stainless steel is used for the majority of reactor internals structures, and this material is not subject to brittle fracture. The core hold down spring, however, is made of Type 403 stainless steel. Significant crack growth has been found to be impossible for this component considering the stress state and possible flaw size. The core hold down spring is the only stainless steel material in the reactor core support structure with a yield strength greater than 90,000 psi and is acceptable based upon Code Case 1337.

All reactor internals are removable from the vessel for the purpose of their inspection as well as the inspection of the vessel internal surface.

4.2.2.2.1 Lower Core Support Structure

The major containment and support member of the reactor internals is the lower core support structure, shown in Figure 4.2-10. This support structure assembly consists of the core barrel, the core baffle, the lower core plate and support columns, the neutron shield pads, and the core support which is welded to the core barrel. All the major material for this structure is Type 304 stainless steel. The lower core support structure is supported at its upper flange from a ledge in the reactor vessel head flange and its lower end is restrained in its transverse movement by a radial support system attached to the vessel wall. Within the core barrel are in axial baffle and a lower core plate, both of which are attached to the core barrel wall and form the enclosure periphery of the assembled core. The lower core support structure and principally the core barrel serve to provide passageways and control for the coolant flow. The lower core plate is positioned at the bottom level of the core below the baffle plates and provides support and orientation for the fuel assemblies.

The lower core plate is a member through which the necessary flow distribution holes for each fuel assembly are machined. Fuel assembly locating pins (2 for each assembly) are also inserted into this plate. Columns are placed between this plate and the core support of the core barrel in order to provide stiffness and to transmit the core load to the core support. Adequate coolant distribution is obtained through the use of the lower core plate and core support.

The neutron shield pad assembly consists of 4 pads that are bolted and pinned to the outside of the core barrel. These pads are constructed of Type 304 stainless steel and are approximately 48 inches wide by 148 inches long by 2.8 inches thick. The pads are located azimuthally to provide the required degree of vessel protection. Specimen guides in which material surveillance samples can be inserted and irradiated during reactor operation are attached to the pads. The samples are held in the guides by a preloaded spring device at the top and bottom to prevent sample movement. Additional details of the neutron shield pads and irradiation specimen holders are given in Reference [14].

Vertically downward loads from weight, fuel assembly preload, control rod dynamic loading, hydraulic loads and earthquake acceleration are carried by the lower core plate partially into the lower core plate support flange on the core barrel shell and partially through the lower support columns to the core support and thence through the core barrel shell to the core barrel flange supported by the vessel head flange. Transverse loads from earthquake acceleration, coolant cross flow, and vibration are carried by the core barrel shell and distributed between the lower radial support to the vessel wall, and to the vessel flange. Transverse loads of the fuel assemblies are transmitted to the core barrel shell by direct connection of the lower core plate to the barrel wall and by upper core plate alignment pins which are welded onto the core barrel.

The main radial support system of the lower end of the core barrel is accomplished by "key" and "keyway" joints to the reactor vessel wall. At equally spaced points around the circumference, an Inconel clevis block is welded to the vessel inner diameter. Another Inconel insert block is bolted to each of these blocks and has a "keyway" geometry. Opposite each of these is a "key" which is attached to the internals. At assembly, as the internals are lowered into the vessel, the keys engage the keyways in the axial direction. With this design, the internals are provided with a support at the furthest extremity, and may be viewed as a beam fixed at the top and simply supported at the bottom.

Radial and axial expansions of the core barrel are accommodated but transverse movement of the core barrel is restricted by this design. With this system, cyclic stresses in the internal structures are within the ASME Section III limits. In the event of an abnormal downward vertical displacement of the internals following a hypothetical failure, energy absorbing devices limit the displacement after contacting the vessel bottom head. The load is then transferred through the energy absorbing devices of the internals to the vessel.

The energy absorbers, cylindrical in shape, are contoured on their bottom surface to the reactor vessel bottom head geometry. Assuming a downward vertical displacement the potential energy of the system is absorbed mostly by the strain energy of the energy absorbing devices.

4.2.2.2.2 Upper Core Support Assembly

The upper core support assembly, shown in Figures 4.2-11 and 4.2-12 consists of the upper support plate assembly and the upper core plate between which are contained support columns and guide tube assemblies. The support columns establish the spacing between the upper support plate assembly and the upper core plate and are fastened at top and bottom to these plates. The support columns transmit the mechanical loadings between the 2 plates and serve the supplementary function of supporting thermocouple guide tubes. The guide tube assemblies, sheath and guide the control rod drive shafts and control rods. They are fastened to the top support plate and are restrained by pins in the upper core plate for proper orientation and support.

Additional guidance for the control rod drive shafts is provided by the upper guide tube which is attached to the upper support plate and guide tube.

The upper core support assembly is positioned in its proper orientation with respect to the lower support structure by flat-sided pins pressed into the core barrel which in turn engage in slots in the upper core plate. At an elevation in the core barrel where the upper core plate is positioned, the flat-sided pins are located at angular positions of 90° from each other. Four (4) slots are milled into the core plate at the same positions. As the upper support structure is lowered into the main internals, the slots in the plate engage the flat-sided pins in the axial direction. Lateral displacement of the plate and of the upper support assembly is restricted by this design. Fuel assembly locating pins protrude from the bottom of the upper core plate and engage the fuel assemblies as the upper assembly is lowered into place. Proper alignment of the lower core support structure, the upper core support assembly, the fuel assemblies and control rods are thereby assured by this system of locating pins and guidance arrangement. The upper core support assembly is restrained from any axial movements by a large circumferential spring which rests between the upper barrel flange and the upper core support assembly and is compressed by the reactor vessel head flange.

Vertical loads from weight, earthquake acceleration, hydraulic loads and fuel assembly preload are transmitted through the upper core plate via the support columns to the top support plate assembly and then the reactor vessel head. Transverse loads from coolant cross flow, earthquake acceleration, and possible vibrations are distributed by the support columns to the top support plate and upper core plate. The top support plate is particularly stiff to minimize deflection. During RF-20 and RF-21, repairs were performed to mitigate Primary Water Stress Corrosion Cracking (PWSCC) in the CRDM nozzle J-groove welds in the Reactor Vessel Upper Head enclosure (per ECR-50846). The J-groove weld repairs follow WCAP-15987-P, Rev. 2-P-A, “Technical Basis for the Embedded Flaw Process for Repair of Reactor Vessel Head Penetrations,” which has been approved by the NRC on April 30, 2014, under Relief Request RR-4-05, “Alternative Weld Repair for Reactor Vessel Upper Head Penetrations.” This repair required the permanent removal of the Part-Length (P/L) Mechanism drive rod located in penetration #19 during RF-20. Additional P/L CRDM drive rods were cut in penetrations #1 and 18 in RF-21 to facilitate the thermal sleeve degradation inspections. To retain the flow characteristics through the upper internals, flow restrictors were mechanically clamped into the Upper Internals assembly guide tubes which sit under RV Head penetration #1, 18 and 19.

RN
12-042
14-024
15-023

4.2.2.2.3 Incore Instrumentation Support Structures

The incore instrumentation support structures consist of an upper system to convey and support thermocouples penetrating the vessel through the head and a lower system to convey and support flux thimbles penetrating the vessel through the bottom (Figure 7.7-9 shows the basic flux-mapping system).

The upper system utilizes the reactor vessel head penetrations. Instrumentation port columns are slip-connected to inline columns that are in turn fastened to the upper support plate. These port columns protrude through the head penetrations. The thermocouples are carried through these port columns and the upper support plate at positions above their readout locations. The thermocouple conduits are supported from the columns of the upper core support system. The thermocouple conduits are sealed stainless steel tubes.

In addition to the upper incore instrumentation, there are reactor vessel bottom port columns which carry the retractable, cold worked stainless steel flux thimbles that are pushed upward into the reactor core. Conduits extend from the bottom of the reactor vessel down through the concrete shield area and up to a thimble seal line. The minimum bend radii are about 144 inches and the trailing ends of the thimbles (at the seal line) are extracted approximately 15 feet during refueling of the reactor in order to avoid interference within the core. The thimbles are closed at the leading ends and serve as the pressure barrier between the reactor pressurized water and the containment atmosphere.

Mechanical seals between the retractable thimbles and conduits are provided at the seal line. During normal operation, the retractable thimbles are stationary and move only during refueling or for maintenance, at which time a space of approximately 15 feet above the seal line is cleared for the retraction operation.

The incore instrumentation support structure is designed for adequate support of instrumentation during reactor operation and is designed to resist damage or distortion under the conditions imposed by handling during the refueling sequence. These are the only conditions which affect the incore instrumentation support structure. Reactor vessel surveillance specimen capsules are covered in Section 5.4.3.6.

4.2.2.3 Design Loading Conditions

The design loading conditions that provide the basis for the design of the reactor internals are:

1. Fuel Assembly Weight
2. Fuel Assembly Spring Forces
3. Internals Weight
4. Control Rod Trip (equivalent static load)
5. Differential Pressure
6. Spring Preloads

7. Coolant Flow Forces (static)

8. Temperature Gradients

9. Differences in thermal expansion

    a. Due to temperature differences

    b. Due to expansion of different materials.

10. Interference between components

11. Vibration (mechanically or hydraulically induced)

12. One (1) or more loops out of service

13. All operational transients listed in Table 5.2-2

14. Pump overspeed

15. Seismic loads (operating basis earthquake and safe shutdown earthquake)

16. Blowdown forces (due to cold and hot leg break)

The main objective of the design analysis is to satisfy allowable stress limits, to assure an adequate design margin, and to establish deformation limits which are concerned primarily with the functioning of the components. The stress limits are established not only to assure that peak stresses will not reach unacceptable values, but also limit the amplitude of the oscillatory stress component in consideration of fatigue characteristics of the materials. Both low and high cycle fatigue stresses are considered when the allowable amplitude of oscillation is established. Dynamic analysis on the reactor internals are provided in Section 3.9.

As part of the evaluation of design loading conditions, extensive testing and inspections are performed from the initial selection of raw materials up to and including component installation and plant operation. Among these tests and inspections are those performed during component fabrication, plant construction, startup and checkout, and during plant operation.

4.2.2.4 Design Loading Categories

The combination of design loadings fit into either the normal, upset, emergency or faulted conditions as defined in the ASME Code, Section III.

Loads and deflections imposed on components due to shock and vibration are determined analytically and experimentally in both scaled models and operating reactors. The cyclic stresses due to these dynamic loads and deflections are combined with the stresses imposed by loads from component weights, hydraulic forces and thermal gradients for the determination of the total stresses of the internals.

The reactor internals are designed to withstand stresses originating from various operating conditions as summarized in Table 5.2-2.

The scope of the stress analysis problem is very large requiring many different techniques and methods, both static and dynamic. The analysis performed depends on the mode of operation under consideration.

For normal operating conditions, downward vertical deflection of the lower core support plate is negligible.

For the loss of coolant accident plus the safe shutdown earthquake condition, the deflection criteria of critical internal structures are the limiting values given in Table 4.2-1. The corresponding no loss of function limits are included in Table 4.2-1 for comparison purposes with the allowed criteria.

The criteria for the core drop accident is based upon analyses which have to determine the total downward displacement of the internal structures following a hypothesized core drop resulting from loss of the normal core barrel supports. The initial clearance between the secondary core support structures and the reactor vessel lower head in the hot condition is approximately 1/2 inch. An additional displacement of approximately 3/4 inch would occur due to strain of the energy absorbing devices of the secondary core support; thus the total drop distance is about 1-1/4 inches which is insufficient to permit the tips of the rod cluster control assembly to come out of the guide thimble in the fuel assemblies.

Specifically, the secondary core support is a device which is never expected to be used, except during a hypothetical accident of the core support (core barrel, barrel flange, etc.). There are 4 supports in each reactor. This device limits the fall of the core and absorbs the energy of the fall which otherwise would be imparted to the vessel. The energy of the fall is calculated assuming a complete and instantaneous failure of the primary core support and is absorbed during the plastic deformation of the controlled volume of stainless steel, loaded in tension. The maximum deformation of this austenitic stainless piece is limited to approximately 15%, after which a positive stop is provided to ensure support.

For additional information on design loading categories see Section 3.9.

4.2.2.5 Design Criteria Basis

For normal operating conditions Section III of the ASME Nuclear Power Plant Components Code is used as a basis for evaluating acceptability of calculated stresses. Both static and alternating stress intensities are considered. It should be noted that the allowable stresses in Section III of the ASME Code are based on unirradiated material properties. In view of the fact that irradiation increases the strength of the Type 304 stainless steel used for the internals, although decreasing its elongation, it is considered that use of the allowable stresses in Section III is appropriate and conservative for irradiated internal structures.

The allowable stress limits during the design basis accident used for the core support structures are based on the January 1971 draft of the ASME Code for Core Support Structures, Subsection NG, and the Criteria for Faulted Conditions.

4.2.3 REACTIVITY CONTROL SYSTEM

4.2.3.1 Design Bases

Bases for temperature, stress on structural members, and material compatibility are imposed on the design of the reactivity control components.

4.2.3.1.1 Design Stresses

The reactivity control system is designed to withstand stresses originating from various operating conditions as summarized in Table 5.2-2.

1. Allowable Stresses

   For normal operating conditions Section III of the ASME Boiler and Pressure Vessel Code is used. All pressure boundary components are analyzed as Class 1 components under Article NB-3000.

2. Dynamic Analysis

   The cyclic stresses due to dynamic loads and deflections are combined with the stresses imposed by loads from component weights, hydraulic forces and thermal gradients for the determination of the total stresses of the reactivity control system.

4.2.3.1.2 Material Compatibility

Materials are selected for compatibility in a PWR environment, for adequate mechanical properties at room and operating temperature, for resistance to adverse property changes in a radioactive environment, and for compatibility with interfacing components.

4.2.3.1.3 Reactivity Control Components

The reactivity control components are subdivided into 2 categories:

1. Permanent devices used to control or monitor the core and,

2. Optional devices used to control or monitor the core.

The permanent type components are the rod cluster control assemblies (contain absorber rods), control rod drive mechanisms and neutron source assemblies. The optional type components are the IFBA, burnable absorber assembly, and thimble plug assembly. Although the thimble plug assembly does not directly contribute to the reactivity control of the reactor, it is presented as a reactivity control system component in this document because it may be used to restrict bypass flow through those thimbles not occupied by absorber, source or burnable absorber rods. The design bases for each of the mentioned components, except the IFBA rods, are in the following paragraphs. The IFBA rods are discussed in the Fuel Section 4.2.1.

4.2.3.1.3.1 Absorber Rods

The following are considered design conditions under Article NB-3000 of the ASME Boiler and Pressure Vessel Code, Section III.

1. The external pressure equal to the reactor coolant system operating pressure.

2. The wear allowance equivalent to 1,000 reactor trips.

3. Bending of the rod due to a misalignment in the guide tube.

4. Forces imposed on the rods during rod drop.

5. Loads caused by accelerations imposed by the control rod drive mechanism.

6. Radiation exposure for maximum core life.

The control rod which is cold rolled Type 304 stainless steel is the only noncode material used in the control rod assembly. The stress intensity limit Sm for this material is defined at 2/3 of the 0.2% offset yield stress.

The absorber material temperature shall not exceed its melting temperature of 1470°F for silver-indium-cadmium alloy absorber material[15].

4.2.3.1.3.2 Burnable Absorber Rods

The burnable absorber rods may be of the design containing borosilicate glass or the Wet Annular Burnable Absorber (WABA) design containing Al_2O_3-B_4C absorber material.

The burnable absorber rod clad (304 SS for the borosilicate design and Zircaloy 4 for the WABA design) is designed using the requirements of a Class 1 component under Article NB-3000 of the ASME Boiler and Pressure Vessel Code, Section III, 1973 for Conditions I and II as a guide. For abnormal loads during Conditions III and IV, code stresses are not considered limiting. Failures of the burnable absorber rods during these conditions must not interfere with reactor shutdown or cooling of the fuel rods.

The burnable poison absorber material is nonstructural. The structural elements of the burnable absorber rod are designed to maintain the absorber geometry even if the absorber material is fractured. The rods are designed so that the borosilicate absorber material is below its softening temperature (1492°F [1] for reference 12.5 w/o boron rods), and the Al_2O_3-B_4C material is below 1200°F during normal operation or overpower transients.

4.2.3.1.3.3 Neutron Source Rods

The neutron source rods are designed to withstand the following:

1. The external pressure equal to the reactor coolant system operating pressure and

2. An internal pressure equal to the pressure generated by released gases over the source rod life.

4.2.3.1.3.4 Thimble Plug Assembly (if used)
The thimble plug assemblies satisfy the following:

RN 95-022

1. Accommodate the differential thermal expansion between the fuel assembly and the core internals.

2. Maintain positive contact with the fuel assembly and the core internals.

3. Be inserted into the fuel assembly by a force not exceeding 40 pounds.

4.2.3.1.4 Control Rod Drive Mechanisms

The control rod drive mechanisms (CRDMs) pressure housings are Class 1 components designed to meet the stress requirements for normal operating conditions of Section III of the ASME Boiler and Pressure Vessel Code. Both static and alternating stress intensities are considered. The stresses originating from the required design transients are included in the analysis.

---

[1] Borosilicate glass is accepted for use in burnable absorber rods if the softening temperature is 1510 ±18°F. The softening temperature is defined in ASTM C 338.

A dynamic seismic analysis is required on the CRDMs when a seismic disturbance has been postulated to confirm the ability of the pressure housing to meet ASME Code, Section III allowable stresses and to confirm its ability to trip when subjected to the seismic disturbance.

4.2.3.1.4.1 Control Rod Drive Mechanism Operation Requirements

The basic operational requirements for the CRDMs are:

1. 5/8 inch step,

2. 144 inch travel,

3. 360 pound maximum load (includes drive rod weight), RN 99-134

4. Step in or out at 5 to 45 inches/minute (8 to 72 steps/minute),

5. Electrical power interruption shall initiate release of drive rod assembly,

6. Trip delay time of less than 150 milliseconds - Free fall of drive rod assembly shall begin less than 150 milliseconds after power interruption no matter what holding or stepping action is being executed with any load and coolant temperature of 100°F to 550°F.

7. 40 year design life with normal refurbishment.

4.2.3.2 Design Description

Reactivity control is provided by IFBA pins, burnable absorber rods, and a soluble chemical neutron absorber (boric acid). The boric acid concentration is varied to control long term reactivity changes such as:

1. Fuel depletion and fission product buildup.

2. Cold to hot, zero power reactivity change.

3. Reactivity change produced by intermediate term fission products such as xenon and samarium.

4. Burnable absorber depletion.

Chemical and volume control is covered in Section 9.3.4.

The rod cluster control assemblies provide reactivity control for:

1. Shutdown.

2. Reactivity changes due to coolant temperature changes in the power range.

3. Reactivity changes associated with the power coefficient or reactivity.

4. Reactivity changes due to void formation.

The neutron source assemblies provide a means of monitoring the core during periods of low neutron activity.

The most effective reactivity control components are the rod cluster control assemblies and their CRDMs which are the only kinetic parts in the reactor. Figure 4.2-13 identifies the full length rod cluster control and CRDM assembly, in addition to the arrangement of these components in the reactor relative to the interfacing fuel assembly and guide tubes. In the following paragraphs, each reactivity control component is described in detail.

The guidance system for the control rod cluster is provided by the guide tube as shown in Figure 4.2-13. The guide tube provides 2 sections of guidance: 1) In the lower section a continuous guidance system provides support immediately above the core. The system protects the rod against excessive deformation and wear due to hydraulic loading. 2) The region above the continuous section provides support and guidance at uniformly spaced intervals.

The envelope of support is determined by the pattern of the control rod cluster as shown in Figure 4.2-14. The guide tube assures alignment and support of the control rods, spider body, and drive rod while maintaining trip times at or below required limits.

4.2.3.2.1 Reactivity Control Components

4.2.3.2.1.1 Rod Cluster Control Assembly

The rod cluster control assemblies are divided into 2 categories: control and shutdown. The control groups compensate for reactivity changes due to variations in operating conditions of the reactor; i.e., power and temperature variations. Two (2) criteria have been employed for selection of the control group. First the total reactivity worth must be adequate to meet the nuclear requirements of the reactor. Second, in view of the fact that these rods may be partially inserted at power operation, the total power peaking factor should be low enough to ensure that the power capability is met. The control and shutdown group provides adequate shutdown margin which is defined as the amount by which the core would be subcritical at hot shutdown if all rod cluster control assemblies are tripped assuming that the highest worth assembly remains fully withdrawn and assuming no changes in xenon or boron concentration.

A rod cluster control assembly comprises a group of individual neutron absorber rods fastened at the top end to a common spider assembly, as illustrated in Figure 4.2-14.

The absorber material used in the control rods is silver-indium-cadmium alloy which is essentially "black" to thermal neutrons and has sufficient additional resonance absorption to significantly increase its worth. The alloy is in the form of extruded rods which are sealed in stainless steel tubes to prevent the rods from coming in direct contact with the coolant. In construction, the silver-indium-cadmium rods are inserted into cold-worked stainless steel tubing which is then sealed at the bottom and the top by welded end plugs as shown in Figure 4.2-15. Sufficient diametral and end clearance is provided to accommodate relative thermal expansions. A thin layer of chrome electroplate is applied to the stainless steel cladding.

RN 96-043

The bottom plugs are made bullet-nosed to reduce the hydraulic drag during reactor trip and to aid smooth entry into the dashpot section of the fuel assembly guide thimbles. The upper plug is threaded for assembly to the spider and has a reduced end section to make the joint more flexible.

The material used in the absorber rod end plugs is Type 308 stainless steel. The design stresses used for the Type 308 material are the same as those defined in the ASME Code, Section III, for Type 304 stainless steel. At room temperature the yield and ultimate stresses per ASTM-580 are exactly the same for the 2 alloys. In view of the similarity of the alloy composition, the temperature dependence of strength for the 2 materials is also assumed to be the same.

The allowable stresses used as a function of temperature are listed in Table 1-1.2 of Section III of the ASME Boiler and Pressure Vessel Code. The fatigue strength for the Type 308 material is based on the S-N curve for austenitic stainless steels in Figure 1-9.2 of Section III. There are no other applications of stressed wrought Type 308 stainless steel in the control rod assembly.

The spider assembly is in the form of a central hub with radial vanes containing cylindrical fingers from which the absorber rods are suspended. Handling detents and detents for connection to the drive rod assembly are machined into the upper end of the hub. A coil spring inside the spider body absorbs the impact energy at the end of a trip insertion. The radial vanes are joined to the hub by tack welds and brazing while the fingers are joined to the vanes by brazing alone. A centerpost which holds the spring and its retainer is threaded into the hub within the skirt and welded to prevent loosening in service. All components of the spider assembly are made from Types 304 and 308 stainless steel except for the retainer which is of 17-4 PH material and the springs which are Inconel-718 alloy or oil tempered carbon steel where the springs do not contact the coolant.

The absorber rods are fastened securely to the spider to assure trouble free service. The rods are first threaded into the spider fingers and then pinned to maintain joint

tightness, after which the pins are welded in place. The end plug below the pin position is designed with a reduced section to permit flexing of the rods to correct for small operating or assembly misalignments.

The overall length is such that when the assembly is withdrawn through its full travel the tips of the absorber rods remain engaged in the guide thimbles so that alignment between rods and thimbles is always maintained. Since the rods are long and slender, they are relatively free to conform to any small misalignments with the guide thimble.

4.2.3.2.1.2 Burnable Absorber Assembly

Each burnable absorber assembly consists of borosilicate or wet annular burnable absorber rods attached to a hold down assembly. Conceptual burnable absorber assemblies (containing borosilicate) are shown in Figure 4.2-17. WABA rods may be used in place of the borosilicate rods.

The borosilicate absorber rods consist of borosilicate glass tubes contained within Type 304 stainless steel tubular cladding which is plugged and seal welded at the ends to encapsulate the glass. The glass is also supported along the length of its inside diameter by a thin wall tubular inner liner. The top end of the liner is open to permit the diffused helium to pass into the void volume and the liner overhangs the glass. The liner has an outward flange at the bottom end to maintain the position of the liner with the glass. A typical borosilicate burnable absorber rod is shown in longitudinal and transverse cross-sections in Figure 4.2-18.

A WABA rod (Figure 4.2-18a) consists of annular pellets of alumina-boron carbide (Al_2O_3-B_4C) burnable absorber material contained within 2 concentric Zircaloy tubes. These Zircaloy tubes, which form the inner and outer clad for the WABA rod, are plugged and welded at each end to encapsulate the annular stack of absorber material. The assembled rod is then internally pre-pressurized to 650 psig and seal welded. The absorber stack lengths are positioned axially within the WABA rods by the use of Zircaloy bottom-end spacers. An annular plenum is provided within the rod to accommodate the helium gas released from absorber material depletion during irradiation. The reactor coolant flows inside the inner tube and outside the outer tube of the annular rod. Further design details are given in Section 3.0 of Reference [26].

The burnable absorber rods are statically suspended and positioned in selected guide thimbles within the fuel assemblies. The absorber rods in each assembly are attached together at the top end of the rods to a hold down assembly by a flat, perforated retaining plate which fits within the fuel assembly top nozzle and rests on the adaptor plate. The absorber rod assembly is held down and restrained against vertical motion through a spring pack which is attached to the plate and is compressed by the upper core plate when the reactor upper internals assembly is lowered into the reactor. This arrangement ensures that the absorber rods cannot be ejected from the core by flow forces. Each rod is permanently attached to the base plate by a nut which is locked into place.

The borosilicate rod clad is slightly cold worked Type 304 stainless steel, and the WABA rod clad is Zircaloy 4. All other structural materials are Types 304 or 308 stainless steel except for the springs which are Inconel-718. The absorber rods and IFBAs provide sufficient boron content to meet the criteria discussed in Section 4.3.1.

4.2.3.2.1.3 Neutron Source Assembly

The purpose of the neutron source assembly is to provide a base neutron level to ensure that the detectors are operational and responding to core multiplication neutrons. Since there is very little neutron activity during loading, refueling, shutdown, and approach to criticality, a neutron source may be placed in the reactor to provide a positive neutron count of at least 2 counts per second on the source range detectors attributable to core neutrons. The detectors, called source range detectors, are used primarily when the core is subcritical and during special subcritical modes of operations. RN 99-141

The source assembly also permits detection of changes in the core multiplication factor during core loading refueling, and approach to criticality. This can be done since the multiplication factor is related to an inverse function of the detector count rate. Therefore a change in the multiplication factor can be detected during addition of fuel assemblies while loading the core, a change in control rod positions, and changes in boron concentration.

Both primary and secondary neutron source rods are used. The primary source rod, containing a radioactive material, spontaneously emits neutrons during initial core loading and reactor startup. After the primary source rod decays beyond the desired neutron flux level, neutrons are then supplied by the secondary source rod. The secondary source rod contains a stable material, which must be activated by neutron bombardment during reactor operation. The activation results in the subsequent release of neutrons. This becomes a source of neutrons during periods of low neutron flux, such as during refueling and the subsequent startups.

The reactor core may employ 2 secondary source assemblies. Each secondary source assembly contains a symmetrical grouping of 4 secondary source rods. Locations not filled with a source or burnable absorber rod contain a thimble plug. Conceptual source assemblies are shown in Figures 4.2-19 and 4.2-20. RN 95-022 99-141

Neutron source assemblies are employed at opposite sides of the core. The assemblies are inserted into the rod cluster control guide thimbles in fuel assemblies at selected unrodded locations.

The source assemblies contain a hold down assembly identical to that of the burnable absorber assembly.

The primary and secondary source rods both utilize slightly coldworked 304 SS cladding material. The secondary source rods contain 500 grams of stacked antimony-beryllium pellets and the rod is internally pre-pressurized to 650 psig. The primary source rods contain capsules of Californium source material and alumina spacer rods to position the

source material within the cladding. The rods in each assembly are permanently fastened at the top end to a hold down assembly, which is identical to that of the burnable absorber assemblies.

The other structural members are fabricated from Type 304 and 308 stainless steel except for the springs exposed to the reactor coolant. They are wound from an age hardened nickel base alloy for corrosion resistance and high strength.

4.2.3.2.1.4 Thimble Plug Assembly

If it is desired to further limit bypass flow through the rod cluster control guide thimbles in fuel assemblies which do not contain either control rods, source rods, or burnable absorber rods, the fuel assemblies at those locations may be fitted with thimble plug assemblies.

The thimble plug assemblies as shown in Figure 4.2-21 consist of a flat base plate with short rods suspended from the bottom surface and a spring pack assembly. The 24 short rods, called thimble plugs, project into the upper ends of the guide thimbles to reduce the bypass flow. Similar short rods are also used on the source assemblies and burnable absorber assemblies to plug the ends of all vacant fuel assembly guide thimbles. At installation in the core, the thimble plug assemblies interface with both the upper core plate and with the fuel assembly top nozzles by resting on the adaptor plate. The spring pack is compressed by the upper core plate when the upper internals assembly is lowered into place. Each thimble plug is permanently attached to the base plate by a nut which is locked to the threaded end of the plug.

All components in the thimble plug assembly, except for the springs, are fabricated from Type 304 and 308 stainless steel. The springs are wound from an age hardened nickel base alloy for corrosion resistance and high strength.

4.2.3.2.2 Control Rod Drive Mechanism

All parts exposed to reactor coolant are fabricated of metals which resist the corrosive action of the primary coolant. Three (3) types of metals are used exclusively: stainless steels, nickel-chrome-iron alloys and cobalt based alloys. In the case of stainless steels, only austenitic and martensitic stainless steels are used.

The discussions (Sections 5.2.5, 5.2.5.1, 5.2.5.2, 5.2.5.3, 5.2.5.4, 5.2.5.5, and 5.2.5.6) concerning the processes, inspections and tests on austenitic stainless steel components to assure freedom from increased susceptibility to intergranular corrosion caused by sensitization, and the discussions (Sections 5.2.5.5 and 5.2.5.7) on the control of welding of austenitic stainless steels, especially control of delta ferrite, are applicable to the austenitic stainless steel pressure retaining components of the control rod drive mechanisms.

Wherever magnetic flux is induced on parts exposed to the main coolant, 400 series stainless steel is used. Cobalt based alloys are used for the pins and latch tips.

Nickel-chrome-iron alloy is used for the springs of both latch assemblies and Type 304 stainless steel is used for all pressure containing parts as listed in Table 5.2-9.

Hard chrome plating provides wear surfaces on the sliding parts and prevents galling between mating parts.

Position indicator assemblies slide over the control rod drive mechanism rod travel housings. Each assembly detects the drive rod position by means of 42 discrete coils that magnetically sense the entry and presence of the rod drive line through its center line over the normal length of the drive rod travel.

Control rod drive mechanisms are located on the dome of the reactor vessel. They are coupled to rod control clusters which have absorber material over the entire length of the control rods. The full length control rod drive mechanism is shown in Figure 4.2-22 and schematically in Figure 4.2-23.

The primary function of the control rod drive mechanism is to insert or withdraw a rod cluster control assembly within the core to control average core temperature and to shutdown the reactor.

The control rod drive mechanism is a magnetically operated jack. A magnetic jack is an arrangement of 3 electromagnets which are energized in a controlled sequence by a power cycler to insert or withdraw a rod cluster control assembly in the reactor core in discrete steps. Rapid insertion of the rod cluster control assembly occurs where electrical power is interrupted.

The control rod drive mechanism consists of 4 separate subassemblies. They are the pressure vessel, coil stack assembly, latch assembly, and the drive rod assembly.

1. The pressure vessel includes a latch housing and a rod travel housing which are connected by a threaded, seal welded, maintenance joint which facilitates replacement of the latch assembly. The closure at the top of the rod travel housing is a threaded plug with a canopy seal weld for pressure integrity. This closure contains a threaded plug used for venting.

   The latch housing is the lower portion of the vessel and contains the latch assembly. The rod travel housing is the upper portion of the vessel and provides space for the drive rod during its upward movement as the control rods are withdrawn from the core.

2. The coil stack assembly includes the coil housings, an electrical conduit and connector, and 3 operating coils; 1) the stationary gripper coil, 2) the moveable gripper coil, and 3) the lift coil.

The coil stack assembly is a separate unit which is installed on the drive mechanism by sliding it over the outside of the latch housing. It rests on the base of the latch housing without mechanical attachment.

Energizing the operating coils causes movement of the pole pieces and latches in the latch assembly.

3. The latch assembly includes the guide tube, stationary pole pieces, moveable pole pieces, and the 2 sets of latches; 1) the moveable gripper latches and 2) the stationary gripper latches.

   The latches engage grooves in the drive rod assembly. The moveable gripper latches are moved up or down in 5/8 inch steps by the lift pole to raise or lower the drive rod. The stationary gripper latches hold the drive rod assembly while the moveable gripper latches are repositioned for the next 5/8 inch step.

4. The drive rod assembly includes a flexible coupling, a drive rod, a disconnect button, a disconnect rod, and a locking button.

   The drive rod has 5/8 inch grooves which receive the latches during holding or moving of the drive rod. The flexible coupling is attached to the drive rod and provides the means for coupling to the rod cluster control assembly.

   The disconnect button, disconnect rod, and locking button provide positive locking of the coupling to the rod cluster control assembly and permits remote disconnection of the drive rod.

The control rod drive mechanism is a trip design. Tripping can occur during any part of the power cycler sequencing if electrical power to the coils is interrupted.

The control rod drive mechanism is threaded and seal welded on an adaptor on top of the reactor vessel and is coupled to the rod cluster control assembly directly below.

The mechanism is capable of raising or lowering a 360 pound load, (which includes the drive rod weight) at a rate of 45 inches/minute. Withdrawal of the rod cluster control assembly is accomplished by magnetic forces while insertion is by gravity.

The mechanism internals are designed to operate in 650°F reactor coolant. The pressure vessel is designed to contain reactor coolant at 650°F and 2500 psia. The 3 operating coils are designed to operate at 392°F with forced air cooling required to maintain that temperature.

The full length control rod drive mechanism, shown schematically in Figure 4.2-23, withdraws and inserts a rod cluster control assembly, as shaped electrical pulses are received by the operating coils. An ON or OFF sequence, repeated by silicon controlled rectifiers in the power programmer, causes either withdrawal or insertion of the control

rod. Position of the control rod is measured by 42 discrete coils mounted on the position indicator assembly surrounding the rod travel housing. Each coil magnetically senses the entry and presence of the top of the ferromagnetic drive rod assembly as it moves through the coil center line.

During plant operation the stationary gripper coil of the drive mechanism holds the rod cluster control assembly in a static position until a stepping sequence is initiated at which time the moveable gripper coil and lift coil is energized sequentially.

1. Rod Cluster Control Assembly Withdrawal

   The rod cluster control assembly is withdrawn by repetition of the following sequence of events (refer to Figure 4.2-23):

   a. Movable Gripper Coil (B) – ON

      The latch locking plunger raises and swings the movable gripper latches into the drive rod assembly groove. A 1/16 inch axial clearance exists between the latch teeth and the drive rod.

   b. Stationary Gripper Coil (A) – OFF

      The force of gravity, acting upon the drive rod assembly and attached control rod, causes the stationary gripper latches and plunger to move downward 1/16 inch until the load of the drive rod assembly and attached control rod is transferred to the movable gripper latches. The plunger continues to move downward and swings the stationary gripper latches out of the drive rod assembly groove.

   c. Lift Coil (C) – ON

      The 5/8 inch gap between the movable gripper pole and the lift pole closes, and the drive rod assembly raises 1 step length (5/8 inch).

   d. Stationary Gripper Coil (A) – ON

      The plunger raises and closes the gap below the stationary gripper pole. The 3 links, pinned to the plunger, swing the stationary gripper latches into a drive rod assembly groove. The latches contact the drive rod assembly and lift it (and the attached control rod) 1/16 inch. The 1/16 inch vertical drive rod assembly movement transfers the drive rod assembly load from the movable gripper latches to the stationary gripper latches.

e. Movable Gripper Coil (B) – OFF

The latch locking plunger separates from the movable gripper pole under the force of a spring and gravity. Three (3) links, pinned to the plunger, swing the 3 movable gripper latches out of the drive rod assembly groove.

f. Lift Coil (C) – OFF

The gap between the movable gripper pole and lift pole opens. The movable gripper latches drop 5/8 inch to a position adjacent to a drive rod assembly groove.

g. Repeat Step a

The sequence described above (Items a through f) is termed as 1 step or 1 cycle. The rod cluster control assembly moves 5/8 inch for each step or cycle. The sequence is repeated at a rate of up to 72 steps per minute and the drive rod assembly (which has a 5/8 inch groove pitch) is raised 72 grooves per minute. The rod cluster control assembly is thus withdrawn at a rate up to 45 inches per minute.

2. Rod Cluster Control Assembly Insertion

The sequence for rod cluster control assembly insertion is similar to that for control rod withdrawal, except the timing of lift coil (C) ON and OFF is changed to permit lowering the control assembly.

a. Lift Coil (C) – ON

The 5/8 inch gap between the movable gripper and lift pole closes. The movable gripper latches are raised to a position adjacent to a drive rod assembly groove.

b. Movable Gripper Coil (B) – ON

The latch locking plunger raises and swings the movable gripper latches into a drive rod assembly groove. A 1/16 inch axial clearance exists between the latch teeth and the drive rod assembly.

c. Stationary Gripper Coil (A) – OFF

The force of gravity, acting upon the drive rod assembly and attached rod cluster control assembly, causes the stationary gripper latches and plunger to move downward 1/16 inch until the load of the drive rod assembly and attached rod cluster control assembly is transferred to the movable gripper

latches. The plunger continues to move downward and swings the stationary gripper latches out of the drive rod assembly groove.

d. Lift Coil (C) – OFF

The force of gravity and spring force separate the movable gripper pole from the lift pole and the drive rod assembly and attached rod cluster control drop down 5/8 inch.

e. Stationary Griper (A) – ON

The plunger raises and closes the gap below the stationary gripper pole. The 3 links, pinned to the plunger, swing the 3 stationary gripper latches into a drive rod assembly groove. The latches contact the drive rod assembly and lift it (and the attached control rod) 1/16 inch. The 1/16 inch vertical drive rod assembly movement transfers the drive rod assembly load from the movable gripper latches to the stationary gripper latches.

f. Movable Gripper Coil (B) – OFF

The latch locking plunger separates from the movable gripper pole under the force of a spring and gravity. Three (3) links, pinned to the plunger, swing the 3 movable gripper latches out of the drive rod assembly groove.

g. Repeat Step a

The sequence is repeated, as for rod cluster control assembly withdrawal, up to 72 times per minute which gives an insertion rate of 45 inches per minute.

3. Holding and Tripping of the Control Rods

During most of the plant operating time, the control rod drive mechanisms hold the rod cluster control assemblies withdrawn from the core in a static position. In the holding mode, only 1 coil, the stationary gripper coil (A), is energized on each mechanism. The drive rod assembly and attached rod cluster control assemblies hang suspended from the 3 latches.

If power to the stationary gripper coil is cut off, the combined weight of the drive rod assembly and the rod cluster control assembly plus the stationary gripper return spring is sufficient to move latches out of the drive rod assembly groove. The control rod falls by gravity into the core. The trip occurs as the magnetic field, holding the stationary gripper plunger half against the stationary gripper pole, collapses and the stationary gripper plunger half is forced down by the stationary gripper return spring and the weight acting upon the latches. After the rod cluster control assembly is released by the mechanism, it falls freely until the control rods enter the dashpot section of the thimble tubes in the fuel assembly.

4.2.3.3 Design Evaluation

4.2.3.3.1 Reactivity Control Components

The components are analyzed for loads corresponding to normal, upset, emergency and faulted conditions. The analysis performed depends on the mode of operation under consideration.

The scope of the analysis requires many different techniques and methods, both static and dynamic.

Some of the loads that are considered on each component where applicable are as follows:

1. Control Rod Trip (equivalent static load)
2. Differential Pressure
3. Spring Preloads
4. Coolant Flow Forces (static)
5. Temperature Gradients
6. Differences in thermal expansion
    a. Due to temperature differences
    b. Due to expansion of different materials
7. Interference between components
8. Vibration (mechanically or hydraulically induced)
9. All operational transients listed in Table 5.2-2
10. Pump Overspeed
11. Seismic Loads (operating basis earthquake and safe shutdown earthquake)
12. Blowdown Forces (due to cold and hot leg break)

The main objectives of the analysis are to satisfy allowable stress limits, assure an adequate design margin, and establish deformation limits which are concerned primarily with the functioning of the components. The stress limits are established not only to assure that peak stresses will not reach unacceptable values, but also to limit the

amplitude of the oscillatory stress component in consideration of fatigue characteristics of the materials. Standard methods of strength of materials are used to establish the stresses and deflections of these components. The dynamic behavior of the reactivity control components has been studied using experimental test data and experience from operating reactors.

The design of reactivity component rods provides a sufficient cold void volume within the burnable absorber and source rods to limit the internal pressures to a value which satisfies the criteria in Section 4.2.3.1. The void volume for the helium in the borosilicate glass burnable absorber rods is obtained through the use of glass in tubular form which provides a central void along the length of the rods. For the WABA rods, an annular void volume is provided between the 2 tubes at the top, and along the length of each WABA rod (Figure 4.2-18a). Helium gas is not released by the neutron absorber rod material, thus the absorber rod only sustains an external pressure during operating conditions. The internal pressure of source rods continues to increase from ambient until end of life at which time the internal pressure never exceeds that allowed by the criteria in Section 4.2.3.1. Except for WABA rods, the stress analysis of reactivity component rods assumes 100% gas release to the rod void volume, considers the initial pressure within the rod, and assumes the pressure external to the component rod is zero. Stress analysis for the WABA rods assumed a maximum 30% gas released, consistent with Reference [26].

Based on available data for properties of the borosilicate glass and on nuclear and thermal calculations for these burnable absorber rods, gross swelling or cracking of the glass tubing is not expected during operation. Some minor creep of the glass at the hot spot on the inner surface of the tube could occur but would continue only until the glass came in contact with the inner liner. The wall thickness of the inner liner is sized to provide adequate support in the event of slumping and to collapse locally before rupture of the exterior cladding if unexpected large volume changes due to swelling or cracking should occur. The top of the inner liner is open to allow communication to the central void by the helium which diffuses out of the glass.

An evaluation of the WABA rod design is given in Reference [26].

Sufficient diametral and end clearances have been provided in the neutron absorber, burnable absorber and source rods to accommodate the relative thermal expansions between the enclosed material and the surrounding clad and end plugs. There is no bending or warping induced in the rods although the clearance offered by the guide thimble would permit a postulated warpage to occur without restraint on the rods. Bending, therefore, is not considered in the analysis of the rods. The radial and axial temperature profiles have been determined by considering gap conductance, thermal expansion, and neutron and/or gamma heating of the contained material as well as gamma heating of the clad. The maximum neutron absorber material temperature was found to be less than 850°F which occurs axially at only the highest flux region. The maximum borosilicate glass temperature was calculated to be about 1200°F and takes place following the initial rise to power. The glass temperature then decreases rapidly

for the following reasons: 1) reduction in power generation due to B_{10} depletion; 2) better gap conductance as the helium produced diffuses to the gap; and 3) external gap reduction due to borosilicate glass creep. Rod, guide thimble, and dashpot flow analysis performed indicates that the flow is sufficient to prevent coolant boiling and maintain clad temperatures at which the clad material has adequate strength to resist coolant operating pressures and rod internal pressures.

Temperatures for thimbles at the bottom of the fuel assemblies range from approximately 530°F to 553°F. Mid-assembly temperatures reach a high of about 593°F while the maximum temperatures at the top of the assemblies are about 641°F.

Analysis on the rod cluster control spider indicates the spider is structurally adequate to withstand the various operating loads including the higher loads which occur during the drive mechanism stepping action and rod drop. Experimental verification of the spider structural capability has been completed (see Section 1.5).

The materials selected are considered to be the best available from the standpoint of resistance to irradiation damage and compatibility to the reactor environment. The materials selected partially dictate the reactor environment (e.g., Cl^- control in the coolant). The current design type reactivity controls have been in service for many years with no unanticipated degradation of construction materials.

With regard to the materials of construction exhibiting satisfactory resistance to adverse property changes in a radioactive environment, it should be noted that work on breeder reactors in current design, similar materials are being applied. At high fluences the austenitic materials increase in strength with a corresponding decreased ductility (as measured by tensile tests) but energy absorption (as measured by impact tests) remain quite high. Corrosion of the materials exposed to the coolant is quite low and proper control of Cl^- and O_2 in the coolant will prevent the occurrence of stress corrosion. All of the austenitic stainless steel base materials used are processed and fabricated to preclude sensitization. Although the control rod spiders are fabricated by furnace brazing, the procedure used requires that the pieces be rapidly cooled so that the time-at-temperature is minimized. The time that is spent by the control rod spiders in the sensitization range, 800 - 1500°F, is not more than 0.2 hour, as a maximum, during fabrication to preclude sensitization. The 17-4 PH parts are all aged at the highest standard aging temperature of 1100°F to avoid stress corrosion problems exhibited by aging at lower temperatures.

RN 95-022

Analysis of the rod cluster control assemblies show that if the drive mechanism housing ruptures, the rod cluster control assembly will be ejected from the core by the pressure differential of the operating pressure and ambient pressure across the drive rod assembly. The ejection is also predicated on the failure of the drive mechanism to retain the drive rod/rod cluster control assembly position. It should be pointed out that a drive mechanism housing rupture will cause the ejection of only 1 rod cluster control assembly with the other assemblies remaining in the core. Analysis also showed that pressure drop in excess of 4000 psi must occur across a two-fingered vane to break the

vane/spider body joint causing ejection of 2 neutron absorber rods from the core. Since the greatest pressure drop in the system is only 2250 psi, a pressure drop in excess of 4000 psi is incredible. Thus, the ejection of the neutron absorber rods is not possible.

Ejection of a burnable absorber or thimble plug assembly is conceivable based on the postulation that the holddown bar fails and that the base plate and burnable absorber rods are severely deformed. In the unlikely event that failure of the holddown bar occurs, the upward displacement of the burnable absorber assembly only permits the base plate to contact the upper core plate. Since this displacement is small, the major portion of the borosilicate glass tubing remains positioned within the core. In the case of the thimble plug assembly, the thimble plugs will partially remain in the fuel assembly guide thimbles thus maintaining a majority of the desired flow impedance. Further displacement or complete ejection would necessitate the square base and burnable absorber rods be forced, thus plastically deformed, to fit up through a smaller diameter hole. It is expected that this condition requires a substantially higher force or pressure drop than that of the holddown bar failure.

RN 95-022

Experience with control rods, burnable absorber rods, and source rods are discussed in Reference [4].

The mechanical design of the reactivity control components provides for the protection of the active elements to prevent the loss of control capability and functional failure of critical components. The components have been reviewed for potential failure and consequences of a functional failure of critical parts. The results of the review are summarized below.

4.2.3.3.1.1 Rod Cluster Control Assembly

1. The basic absorbing material is sealed from contact with the primary coolant, the fuel assembly and guidance surfaces by a high quality stainless steel clad. Potential loss of absorber mass or reduction in reactivity control material due to mechanical or chemical erosion or wear is therefore reliably prevented.

2. A breach of the cladding for any postulated reason does not result in serious consequences. The silver-indium-cadmium absorber material is relatively inert and would still remain remote from high coolant velocity regions. Rapid loss of material resulting in significant loss of reactivity control material would not occur.

3. The individually clad absorber rods are doubly secured to the retaining spider vane by a threaded joint and a welded lock pin. This joint has been qualified by functional testing and actual service in operating plants.

   It should also be noted that in several instances of control rod jamming caused by foreign particles, the individual rods at the site of the jam have borne the full capacity of the control rod drive mechanism and higher impact loads to dislodge the jam without failure. The conclusion to be drawn from this experience is that this joint is extremely insensitive to potential mechanical damage. A failure of the

joint would result in the insertion of the individual rod into the core resulting in reduced reactivity.

4. The spider finger braze joint by which the individual rods are fastened to the vanes has also experienced the service described above and been subjected to the same jam freeing procedures also without failure. A failure of this joint would also result in insertion of the individual rod into the core.

5. The radial vanes are attached to the spider body, again by a brazed joint. The joints are designed to a theoretical strength in excess of that of the components joined.

   It is a feature of the design that the guidance of the rod cluster control is accomplished by the inner fingers of these vanes. They are therefore the most susceptible to mechanical damage. Since these vanes carry 2 rods, failure of the vane-to-hub joint such as the isolated incidents at Connecticut-Yankee does not prevent the free insertion of the rod pair. Neither does such a failure interfere with the continuous free operation of the drive line, also as experienced at Connecticut-Yankee.

   Failure of the vane-to-hub joint of a single rod vane could potentially result in failure of the separated vane and rod to insert. This could occur only at withdrawal elevations where the spider is above the continuous guidance section of the guide tube (in the upper internals). A rotation of the disconnected vane could cause it to hang on one of the guide cards in the intermediate guide tube. Such an occurrence would be evident from the failure of the rod cluster control to insert below a certain elevation but with free motion above this point.

   This possibility is considered extremely remote because the single rod vanes are subjected to only vertical loads and very light lateral reactions from the rods. The consequences of such a failure are not considered critical since only 1 drive line of the reactivity control system would be involved. This condition is readily observed and can be corrected at shutdown.

6. The spider hub being of single unit cylindrical construction is very rugged and of extremely low potential for damage. It is difficult to postulate any condition to cause failure. Should some unforeseen event cause fracture of the hub above the vanes, the lower portion with the vanes and rods attached would insert by gravity into the core causing a reactivity decrease. The rod could then not be removed by the drive line. Fracture below the vanes cannot be postulated since all loads, including scram impact, are taken above the vane elevation.

7. The rod cluster control rods are provided a clear channel for insertion by the guide thimbles of the fuel assemblies. All fuel rod failures are protected against by providing this physical barrier between the fuel rod and the intended insertion channel. Distortion of the fuel rods by bending cannot apply sufficient force to

damage or significantly distort the guide thimble. Fuel rod distortion by swelling, though precluded by design, would be terminated by fracture before contact with the guide thimble occurs. If such were not the case, it would be expected that a force reaction at the point of contact would cause a slight deflection of the guide thimble. The radius of curvature of the deflected shape of the guide thimbles would be sufficiently large to have a negligible influence on rod cluster control insertion.

4.2.3.3.1.2 Burnable Absorber Assemblies

The burnable absorber assemblies are static temporary reactivity control elements. The axial position is assured by the holddown assembly which bears against the upper core plate. Their lateral position is maintained by the guide thimbles of the fuel assemblies.

The individual rods are shouldered against the underside of the retainer plate and securely fastened at the top by a threaded nut which is then locked in place. The square dimension of the retainer plate is larger than the diameter of the flow holes through the core plate. Failure of the holddown bar or spring pack therefore does not result in ejection of the burnable absorber rods from the core.

The only incident that could potentially result in ejection of the burnable absorber rods is a multiple fracture of the retainer plate. This is not considered credible because of the light loads borne by this component. During normal operation the loads borne by the plate are approximately 5 pounds/rod or a total of 100 pounds distributed at the points of attachment. Even a multiple fracture of the retainer plate would result in jamming of the plate segments against the upper core plate, again preventing ejection. Excessive reactivity increase due to burnable absorber rod ejection is therefore prevented.

Burnable absorber rods are clad with either stainless steel or Zircaloy 4. The burnable absorber is either a borosilicate glass tube which is maintained in position by a central hollow stainless steel tube or Al_2O_3-B_4C annular pellets contained within 2 concentric Zircaloy tubes. Burnable absorber rods are placed in static assemblies and are not subjected to motion which might damage the rods. Further, the guide thimble tubes of the fuel assembly afford additional protection from damage.

During the accumulated thousands of years of burnable absorber rodlet operating experience, only 1 instance of penetration of the stainless steel burnable absorber cladding has been observed. The consequences of clad breach are also small. It is anticipated that upon clad breach, the B_4C or borosilicate glass would be leached by the coolant water and that localized power peaking of a few percent would occur; no design criteria would be violated. Additional information on the consequences of postulated WABA rod failures is presented in Reference [26].

RN 95-022

4.2.3.3.1.3 Drive Rod Assemblies

All postulated failures of the drive rod assemblies either by fracture or uncoupling lead to a decrease in reactivity. If the drive rod assembly fractures at any elevation, that portion remaining coupled falls with, and is guided by the rod cluster control assembly. This always results in reactivity decrease for control rods.

4.2.3.3.2 Control Rod Drive Mechanism

4.2.3.3.2.1 Material Selection

All pressure containing materials comply with Section III of the ASME Boiler and Pressure Vessel Code, and are fabricated from austenitic (Type 304) stainless steel.

Magnetic pole pieces are fabricated from Type 410 stainless steel. All nonmagnetic parts, except pins and springs, are fabricated from Type 302 stainless steel. Haynes 25 is used to fabricate link pins. Springs are made from nickel-chrome-iron alloy. Latch arm tips are clad with Stellite-6 to provide improved wearability. Hard chrome plate and Stellite-6 are used selectively for bearing and wear surfaces.

At the start of the development program, a survey was made to determine whether a material better than Type 410 stainless steel was available for the magnetic pole pieces. Ideal material requirements are as follows:

1. High magnetic saturation value.
2. High permeability.
3. Low coercive force.
4. High resistivity.
5. High curie temperature.
6. Corrosion resistance.
7. High impact strength.
8. Nonoriented.
9. High machinability.
10. Low susceptibility to radiation damage.

After a comprehensive material study was made it was decided that the Type 410 stainless steel was satisfactory for this application.

The cast coil housings require a magnetic material. Both low carbon cast steel and ductile iron have been successfully tested for this application. The choice, made on the basis of cost, indicates that ductile iron will be specified on the control rod drive mechanism. The finished housings are zinc plated or flame sprayed to provide corrosion resistance.

Coils are wound on bobbins of molded Dow Corning 302 material, with double glass insulated copper wire. Coils are then vacuum impregnated with silicon varnish. A wrapping of mica sheet is secured to the coil outside diameter. The result is a well insulated coil capable of sustained operation at 200° centigrade.

The drive rod assembly utilizes a Type 410 stainless steel drive rod. The coupling is machined from Type 403 stainless steel. Other parts are Type 304 stainless steel with the exception of the springs which are nickel-chrome-iron alloy and the locking button which is Haynes 25.

4.2.3.3.2.2 Radiation Damage

As required by the equipment specification, the control rod drive mechanisms are designed to meet a radiation requirement of 10 rads/hour. Materials have been selected to meet this requirement. The above radiation level which amounts to 1.753×10^6 rads in 20 years will not limit control rod drive mechanism life. Control rod drive mechanisms at Yankee Rowe which have been in operation since 1960 have not experienced problems due to radiation.

4.2.3.3.2.3 Positioning Requirements

The control rod drive mechanism has a step length of 5/8 inch which determines its positioning capabilities. Positioning requirements are determined by reactor physics.

4.2.3.3.2.4 Evaluation of Material's Adequacy

The ability of the pressure housing components to perform throughout the design lifetime as defined in the equipment specification is confirmed by the stress analysis report required by the ASME Boiler and Pressure Vessel Code, Section III. Internal components subjected to wear will withstand a minimum of 3,000,000 steps without refurbishment as confirmed by life tests. Latch assembly inspection is recommended after 2.5×10^6 steps have been accumulated on a single control rod drive mechanism.

4.2.3.3.2.5 Results of Dimensional and Tolerance Analysis

With respect to the control rod drive mechanism system as a whole, critical clearances are present in the following areas:

1. Latch assembly (Diametral clearances).

2. Latch arm-drive rod clearances.

3. Coil stack assembly-thermal clearances.

4. Coil fit in coil housing.

The following write-up defines clearances that are designed to provide reliable operation in the control rod drive mechanism in these 4 critical areas. These clearances have been proven by life tests and actual field performance at operating plants.

4.2.3.3.2.6 Latch Assembly - Thermal Clearances

The magnetic jack has several clearances where parts made of Type 410 stainless steel fit over parts made from Type 304 stainless steel. Differential thermal expansion is therefore important. Minimum clearances of these parts at 68°F is 0.011 inch. At the maximum design temperature of 650°F minimum clearance is 0.0045 inch and at the maximum expected operating temperatures of 550°F is 0.0057 inch.

4.2.3.3.2.7 Latch Arm - Drive Rod Clearances

The control rod drive mechanism incorporates a load transfer action. The movable or stationary gripper latch are not under load during engagement, as previously explained, due to load transfer action.

Figure 4.2-26 shows latch clearance variation with the drive rod as a result of minimum and maximum temperatures. Figure 4.2-27 shows clearance variations over the design temperature range.

4.2.3.3.2.8 Coil Stack Assembly - Thermal Clearances

The assembly clearance of the coil stack assembly over the latch housing was selected so that the assembly could be removed under all anticipated conditions of thermal expansion.

At 70°F the inside diameter of the coil stack is 7.308/7.298 inches. The outside diameter of the latch housing is 7.260/7.270 inches.

Thermal expansion of the mechanism due to operating temperature of the control rod drive mechanism results in the minimum inside diameter of the coil stack being 7.310 inches at 222°F and the maximum latch housing diameter being 7.302 inches at 532°F.

Under the extreme tolerance conditions listed above, it is necessary to allow time for a 70°F coil housing to heat during a replacement operation.

Four (4) coil stack assemblies were removed from 4 hot control rod drive mechanisms mounted on 11.035 inch centers on a 550°F test loop, allowed to cool, and then replaced without incident as a test to prove the preceding.

4.2.3.3.2.9 Coil Fit in Coil Housing

Control rod drive mechanism and coil housing clearances are selected so that coil heat up results in a close to tight fit. This is done to facilitate thermal transfer and coil cooling in a hot control rod drive mechanism.

4.2.3.3.2.10 Protection from Pipe Rupture and Missiles

The control rod drive mechanisms are protected from postulated pipe ruptures and missiles as discussed in Sections 3.6 and 3.5, respectively.

4.2.3.4 Tests, Verification and Inspections

4.2.3.4.1 Reactivity Control Components

Tests and inspections are performed on each reactivity control component to verify the mechanical characteristics. In the case of the rod cluster control assembly, prototype testing has been conducted and both manufacturing test/inspections and functional testing at the plant site are performed.

During the component manufacturing phase, the following requirements apply to the reactivity control components to assure the proper functioning during reactor operation:

1. All materials are procured to specifications to attain the desired standard of quality.

2. A spider from each braze lot is proof tested by applying a 5000 pound load to the spider body, so that approximately 310 pounds is applied to each vane. This proof load provides a bending moment at the spider body approximately equivalent to 1.4 times the load caused by the acceleration imposed by the control rod drive mechanism.

3. All clad/end plug welds are checked for integrity by visual inspection, X-ray, and are helium leak checked. All the seal welds in the neutron absorber rods, burnable absorber rods and source rods are checked in this manner.

RN 95-022

4. To assure proper fit with the fuel assembly, the rod cluster control, burnable absorber and source assemblies are installed in the fuel assembly without restriction or binding in the dry condition. Also a straightness of 0.01 in/ft is required on the entire inserted length of each rod assembly.

   The rod cluster control assemblies are functionally tested, following core loading but prior to criticality to demonstrate reliable operation of the assemblies.

In order to demonstrate continuous free movement of the rod cluster control assemblies, and to ensure acceptable core power distributions during operations, partial movement checks are performed on the rod cluster control assemblies as required by the Technical Specifications. In addition, periodic drop tests of the rod cluster control assemblies are performed at each refueling shutdown to demonstrate continued ability to meet trip time requirements. During these tests the acceptable drop time of each assembly is not greater than 2.7 seconds, at full flow and operating temperatures, from the beginning of motion to dashpot entry.

If a rod cluster control assembly cannot be moved by its mechanism, adjustments in the boron concentration ensure that adequate shutdown margin would be achieved following a trip. Thus, inability to move 1 rod cluster control assembly can be tolerated. More than 1 inoperable rod cluster control assembly could be tolerated, but would impose additional demands on the plant operator. Therefore, the number of inoperable rod cluster control assemblies has been limited to 1.

4.2.3.4.2 Control Rod Drive Mechanisms

Quality assurance procedures during production of control rod drive mechanisms include material selection, process control, mechanism component tests and inspections during production and hydrotests.

After all manufacturing procedures had been developed, several prototype control rod drive mechanisms and drive rod assemblies were life tested with the entire drive line under environmental conditions of temperature, pressure and flow. All acceptance tests confirm the 3×10^6 step unrefurbished life capability of the control rod drive mechanism and drive rod assembly. 98-01

These tests include verification that the trip time achieved by the control rod drive mechanisms meet the original design requirement of 2.7 seconds from start of rod cluster control assembly motion to dashpot entry. This trip time requirement will be confirmed for each control rod drive mechanism prior to initial reactor operation and at periodic intervals after initial reactor operation. In addition, a Technical Specification has been set to ensure that the trip time requirement is met. 98-01

It is expected that all control rod drive mechanisms will meet specified operating requirements for the duration of plant life with normal refurbishment. However, a Technical Specification pertaining to an inoperable rod cluster control assembly has been set. 98-01

To confirm the mechanical adequacy of the fuel assembly, the control rod drive mechanism, and rod cluster control assembly, functional test programs have been conducted on a full scale 12 foot control rod. The 12 foot prototype assembly was tested under simulated conditions of reactor temperature, pressure, and flow for approximately 1000 hours. The prototype mechanism accumulated about 3,000,000 steps and 600 trips. At the end of the test the control rod drive mechanism was still operating satisfactorily. A correlation was developed to predict the amplitude of flow excited vibration of individual fuel rods and fuel assemblies. Inspection of the drive line components did not reveal significant fretting.

There are no significant differences between the prototype control rod drive mechanisms and the production units. Design materials, tolerances and fabrication techniques (Section 4.2.3.3.2) are the same.

Actual experience in many operating Westinghouse plants, indicates excellent performance of these control rod drive mechanisms.

All units are production tested prior to shipment to confirm ability of the control rod drive mechanism to meet design specification operational requirements.

Each control rod drive mechanism undergoes a production test as listed below:

Test	Acceptance Criteria
Cold (ambient) hydrostatic	ASME Section III
Confirm step length and load transfer (stationary gripper to movable gripper or movable gripper to stationary gripper)	Step Length 5/8 $\pm$0.015 inch axial movement Load Transfer 0.047 inch nominal axial movement
Cold (ambient) performance Test at design load - 5 full travel excursions	Operating Speed 45 inches/minute Trip Delay Free fall of drive rod to begin within 150 MS

4.2.3.5 Instrumentation Applications

Instrumentation for determining reactor coolant average temperature (T_{avg}) is provided to create demand signals for moving groups of rod cluster control assemblies to provide load follow (determined as a function of first stage turbine pressure) during normal operation and to counteract operational transients. The hot and cold leg resistance temperature detectors (RTDs) are described in Section 7.2 in the reactor coolant bypass loops. The location of the RTDs in each loop is shown on the flow diagrams in Chapter 5.0. The reactor control system which controls the reactor coolant average temperature by regulation of control rod bank position is described in Section 7.3.

Rod position indication instrumentation is provided to sense the actual position of each control rod so that the actual position of the individual rod may be displayed to the operator. Signals are also supplied by this system as input to the rod deviation comparator. The rod position indication system is described in Chapter 7.0.

The reactor makeup control system whose functions are to permit adjustment of the reactor coolant boron concentration for reactivity control (as well as to maintain the desired operating fluid inventory in the volume control tank), consists of a group of instruments arranged to provide a manually preselected makeup composition that is borated or diluted as required to the charging pump suction header or the volume control tank. This system, as well as other systems including boron sampling provisions that are part of the chemical and volume control system, are described in Section 9.3.

Monitoring of the neutron flux for various phases of reactor power operation as well as of core loading, shutdown, startup, and refueling is by means of the nuclear instrumentation system. The monitoring functions, readout and indication characteristics for the following means of monitoring reactivity during these phases are included in the discussion on safety-related display instrumentation in Section 7.5:

1. Nuclear Instrumentation System

2. Temperature Indicators

    a. T average (Measured)

    b. ΔT (Measured)

    c. Auctioneered T average

    d. T reference

3. Demand Position of Rod Cluster Control Assembly Group

4. Actual Rod Position Indicator.

4.2.4 REFERENCES

1. Christensen, J. A., Alio, R. J., and Biancheria, A., "Melting Point of Irradiated UO_2," WCAP-6065, February 1965.

2. Eggleston, F. T., "Safety-Related Research and Development for Westinghouse Pressurized Water Reactors, Program Summaries, Spring, 1976," WCAP-8768, June 1976.

3. Eng, G. H., George, R. A., Lee, and V. C., "Revised Clad Flattening Model," WCAP-8377 (Proprietary) and WCAP-8381 (Non-Proprietary), July 1974.

4. Slagle, W. H., "Operational Experience with Westinghouse Cores Through December 31, 1994," WCAP-8183, Revision 23, January 1996. RN 95-022 96-043

5. Miller, J. V. (Ed.), "Improved Analytical Models Used in Westinghouse Fuel Rod Design Computations," WCAP-8720 (Proprietary) and WCAP-8785 (non-Proprietary), October 1976.

6. Hellman, J. M., (Ed.), "Fuel Densification Experimental Results and Model for Reactor Application," WCAP-8218-P-A (Proprietary) and WCAP-8219-A (Non-Proprietary), March 1975.

7. Lenahan, R., "Westinghouse Clad Corrosion Model for *ZIRLO* and *Optimized ZIRLO*," WCAP-12610-P-A & CENPD-404-P-A Addendum 2-A (Proprietary) and WCAP-14342-A & CENPD-404-NP-A Addendum 2-A (Non-Proprietary), October 2013. RN 14-036

8. Wood, D. S., "High Deformation Creep Behavior of 0.6 Inch Diameter Zirconium Alloy Tubes Under Irradiation," ASTM-STP-551, American Society for Testing and Materials, 1973.

9. O'Donnel, W. J. and Longer, B. F., "Fatigue Design for Zircaloy Components," Nuclear Science and Engineering, 20, 1-12, 1964.

10. Skaritka, J. (Ed.), "Fuel Rod Bow Evaluations," WCAP-8691, Revision 1 (Proprietary), July 1979.

11. Gesinski, L., Chiang, D., and Nakazato, S., "Safety Analysis of the 17 x 17 Fuel Assembly for Combined Seismic and Loss of Coolant Accident," WCAP-8236 (Proprietary), December, 1973 and WCAP-8288 (Non-Proprietary), January 1974.

12. DeMario, E. E., "Hydraulic Flow Test of the 17 x 17 Fuel Assembly," WCAP-8278 (Proprietary) and WCAP-8279 (Non-Proprietary), February 1974.

13. Dollard, W. J., "Nuclear Fuel Division Quality Assurance Program Plan," WCAP-7800, Revision 7-A, December 1988. RN 95-022

14. Kraus, S., "Neutron Shielding Pads," WCAP-7870, May 1972.

15. Cohen, J., "Development and Properties of Silver Base Alloys as Control Rod Materials for Pressurized Water Reactors," WAPD-214, December 1959.

16. Shah, H., "Optimized ZIRLO™," WCAP-12610-P-A & CENPD-404-P-A Addendum 1-A (Proprietary) and WCAP-14342-A & CENPD-404-NP-A Addendum 1-A (Non-Proprietary), June 2006. RN 14-036

17. Sidener, S., et. al., “Westinghouse Improved Performance Analysis and Design Model (PAD 4.0),” WCAP-15063-P-A Revision 1, with Errata (Proprietary) and WCAP-15064-NP-A Revision 1, with Errata (Non-Proprietary), July 2000. RN 14-036

18. Deleted

19. Deleted

20. Risher, D. H., et al., "Safety Analysis for the Revised Fuel Rod Internal Pressure Design Basis," WCAP-8963 (Proprietary) and WCAP-8964 (Non-Proprietary), June 1977.

21. Deleted

22. Deleted

23. Davidson, S. L. (Ed.), et al., "Extended Burnup Evaluation of Westinghouse Fuel," WCAP-10125-P-A (Proprietary), December 1985 and Bahr, K. E., “Extended Burnup Evaluation of Westinghouse Fuel, Revision to Design Criteria,” WCAP-10125-P-A, Addendum 1-A, Revision 1-A, May 2005. RN 14-005

24. Davidson, S. L. (Ed.), "Reference Core Report - VANTAGE 5 Fuel Assembly," WCAP-10444-P-A, September 1985.

25. Davidson, S. L., et al., (Ed.), "Verification Testing and Analysis of the 17 x 17 Optimized Fuel Assembly," WCAP-9401-P-A, August 1981.

26. Skaritka, J., "Westinghouse Wet Annular Burnable Absorber Evaluation Report," WCAP-10021-P-A, Revision 1, October 1983.

27. Davidson, S.L., and Nuhfer, D.L., "VANTAGE+ Fuel Assembly Reference Core Report," WCAP-12610 (Proprietary), June 1990.

28. Weiner, R.A., et al., "Improved Fuel Performance Models for Westinghouse Fuel Rod Design and Safety Evaluations," WCAP-10851-P-A (Proprietary) and WCAP-11873-A (Non Proprietary), August 1988.

29. Thadani, A.C., "Acceptance For Referencing of Topical Report", WCAP-12610 "VANTAGE+ Fuel Assembly Reference Core Report," (TAC No. 77258), July 1, 1991. RN 95-022

30. Slagle, W.H. (Ed.), “Westinghouse Fuel Assembly Reconstitution Evaluation Methodology," WCAP-13060-P, September 1991.

31. Davidson, S. L. (Ed), "Reference Core Report - VANTAGE 5 Fuel Assembly," WCAP-10444-P-A, September 1985.

32. Gergos, B. W., WCAP-16980, "Reactor Internals Upflow Conversion Program Engineering Report V. C. Summer Nuclear Plant," December 2008. RN 09-022

33. Bamford, W. H., et al, “Technical Basis for the Embedded Flaw Process for Repair of Reactor Vessel Head Penetrations,” WCAP-15987-P Revision 2-P-A (Proprietary), December 2003.

34. Letter from Chief Robert J. Pascarelli (NRC) to Mr. Thomas D. Gatlin, “Virgil C. Summer Nuclear Station, Unit 1 – Alternative Request Weld Repair for Reactor Vessel Upper Head Penetrations (TAC NO. MF3546),” April 30, 2014.

RN 15-023

TABLE 4.2-1

MAXIMUM DEFLECTIONS ALLOWED FOR
REACTOR INTERNAL SUPPORT STRUCTURES

Component	Allowable Deflections (in.)	No-Loss-of Function Deflections (in.)
Upper Barrel		
radial inward	4.1	8.2
radial outward	1.0	1.0
Upper Package (1)	0.10	0.15
Rod Cluster Guide Tubes	1.00	1.75

RN 01-113

(1) The vertical motion of the upper core plate relative to the upper support plate shall not cause buckling of the guide tubes.

This Page Intentionally Left Blank

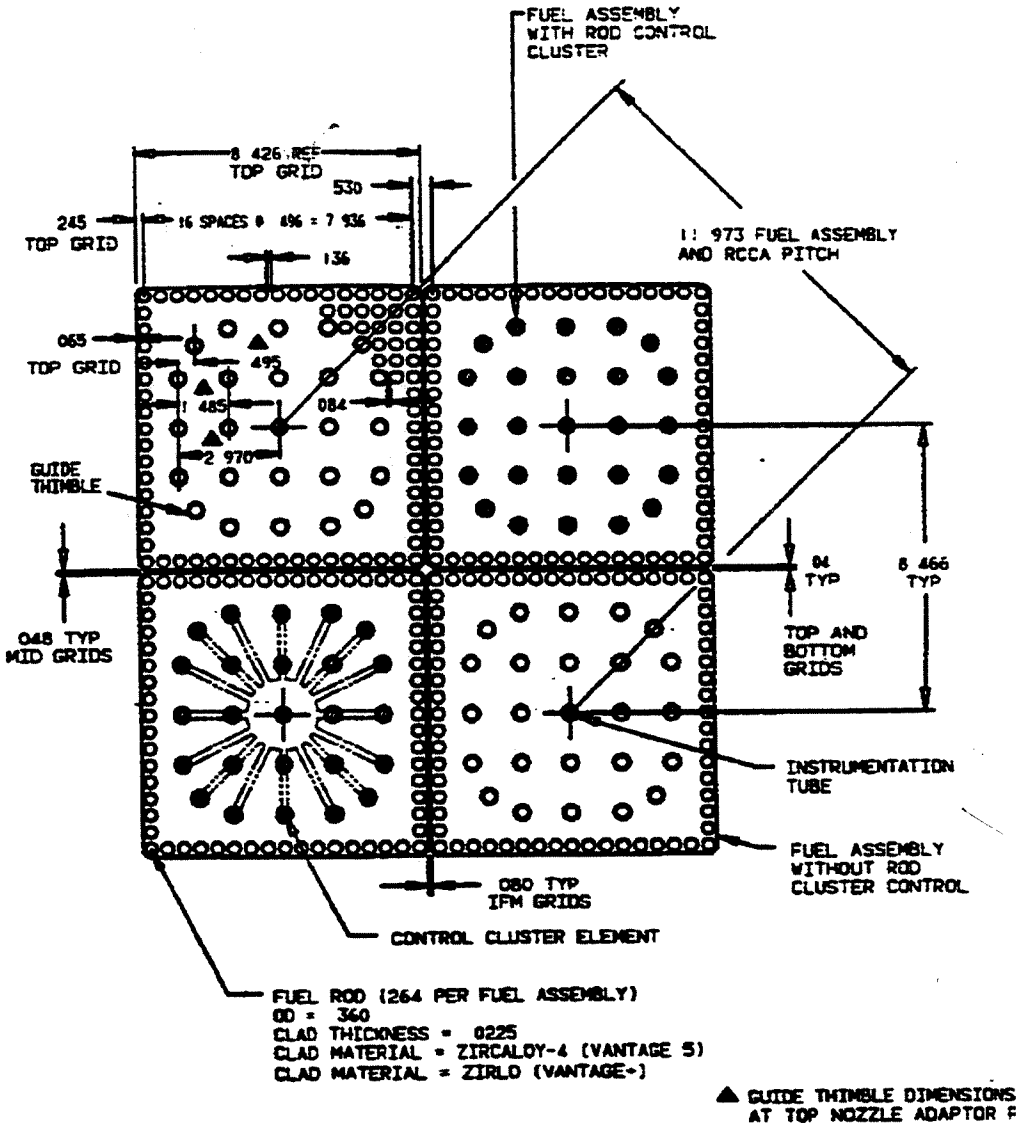

DIMENSIONS ARE IN INCHES (NOMINAL)

SOUTH CAROLINA ELECTRIC & GAS CO. VIRGIL C. SUMMER NUCLEAR STATION
Fuel Assembly Cross Section 17x17 Figure 4.2-1

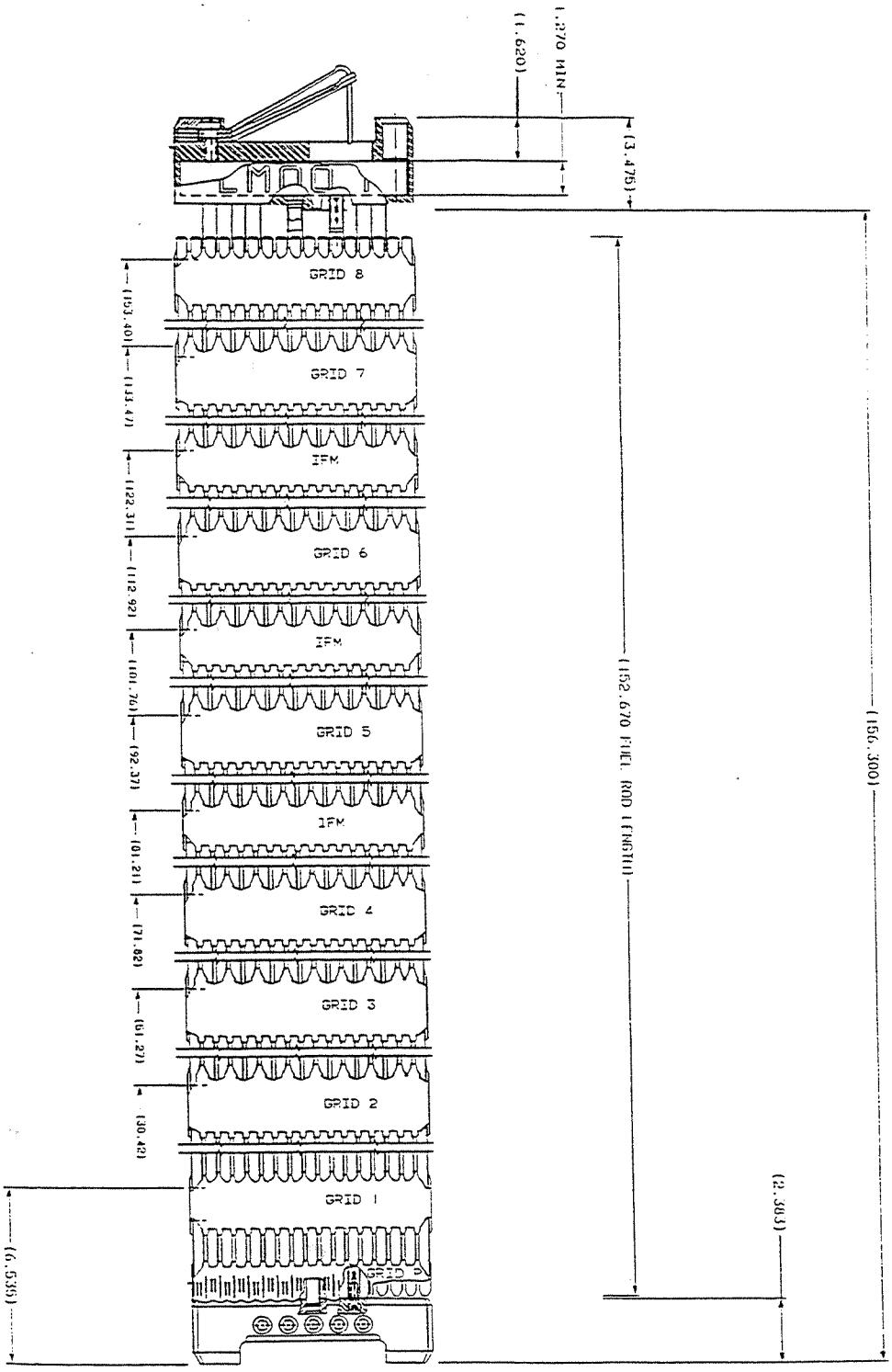

Amendment 98-01
April 1998

SOUTH CAROLINA ELECTRIC & GAS CO. VIRGIL C. SUMMER NUCLEAR STATION
17 x 17 Vantage + with Performance + Fuel Assembly Figure 4.2-2

Amendment 98-01 Aug 1998

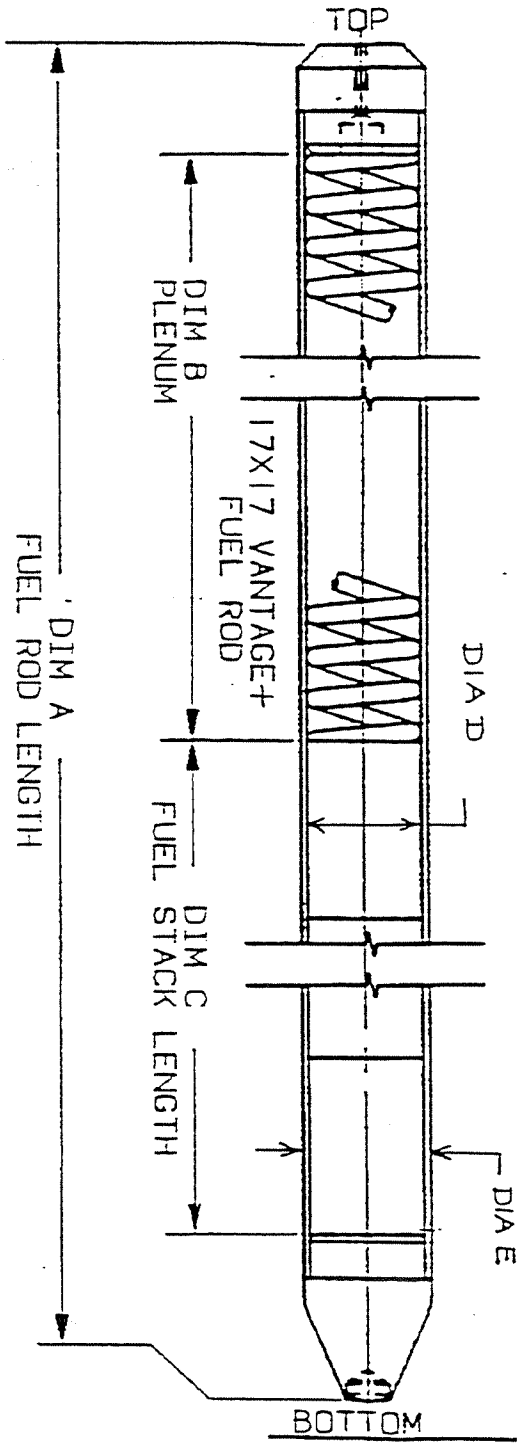

DIM	V+ with P+ Features
A	152.670 in
B	7.410 in
C	144.00 in
DIA D	0.315 in
DIA E	0.360 in

SOUTH CAROLINA ELECTRIC & GAS CO.
VIRGIL C. SUMMER NUCLEAR STATION

17 x 17 Vantage + with Performance +

Fuel Rod

Figure 4.2-3

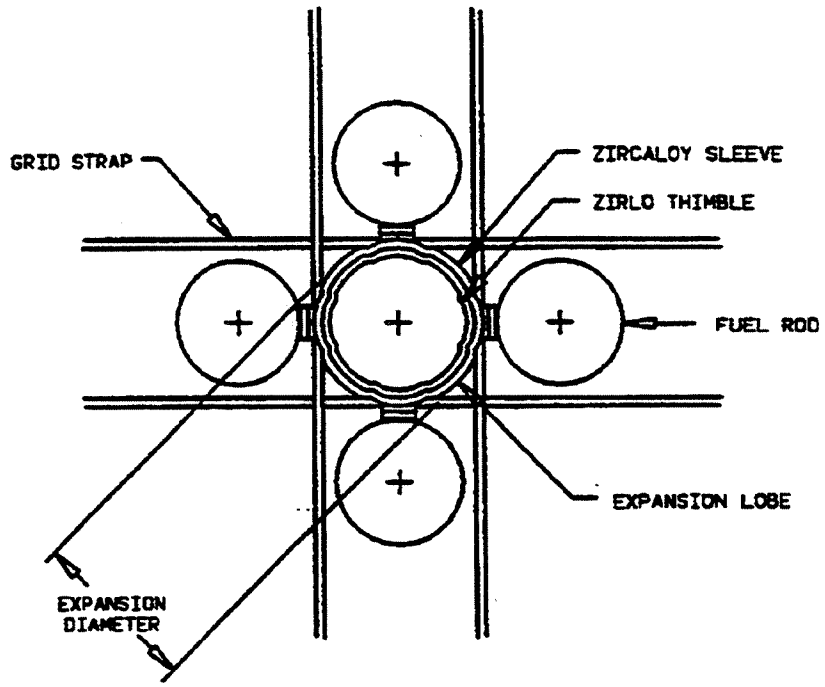

MID GRID EXPANSION JOINT DESIGN

SOUTH CAROLINA ELECTRIC & GAS CO. VIRGIL C. SUMMER NUCLEAR STATION
Vantage+ Fuel Plan View
Figure 4.2-4

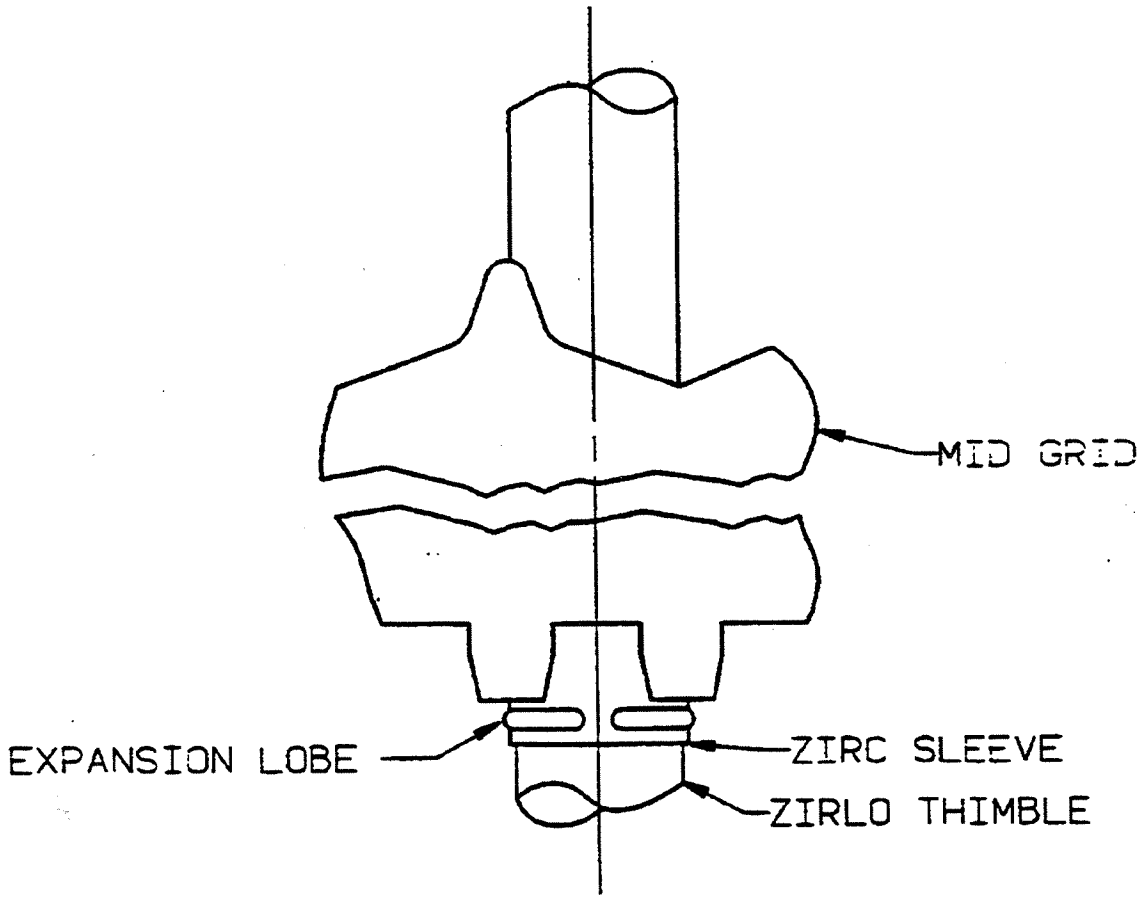

SOUTH CAROLINA ELECTRIC & GAS CO. VIRGIL C. SUMMER NUCLEAR STATION
Elevation View - Vantage+ Fuel
Figure 4.2-5

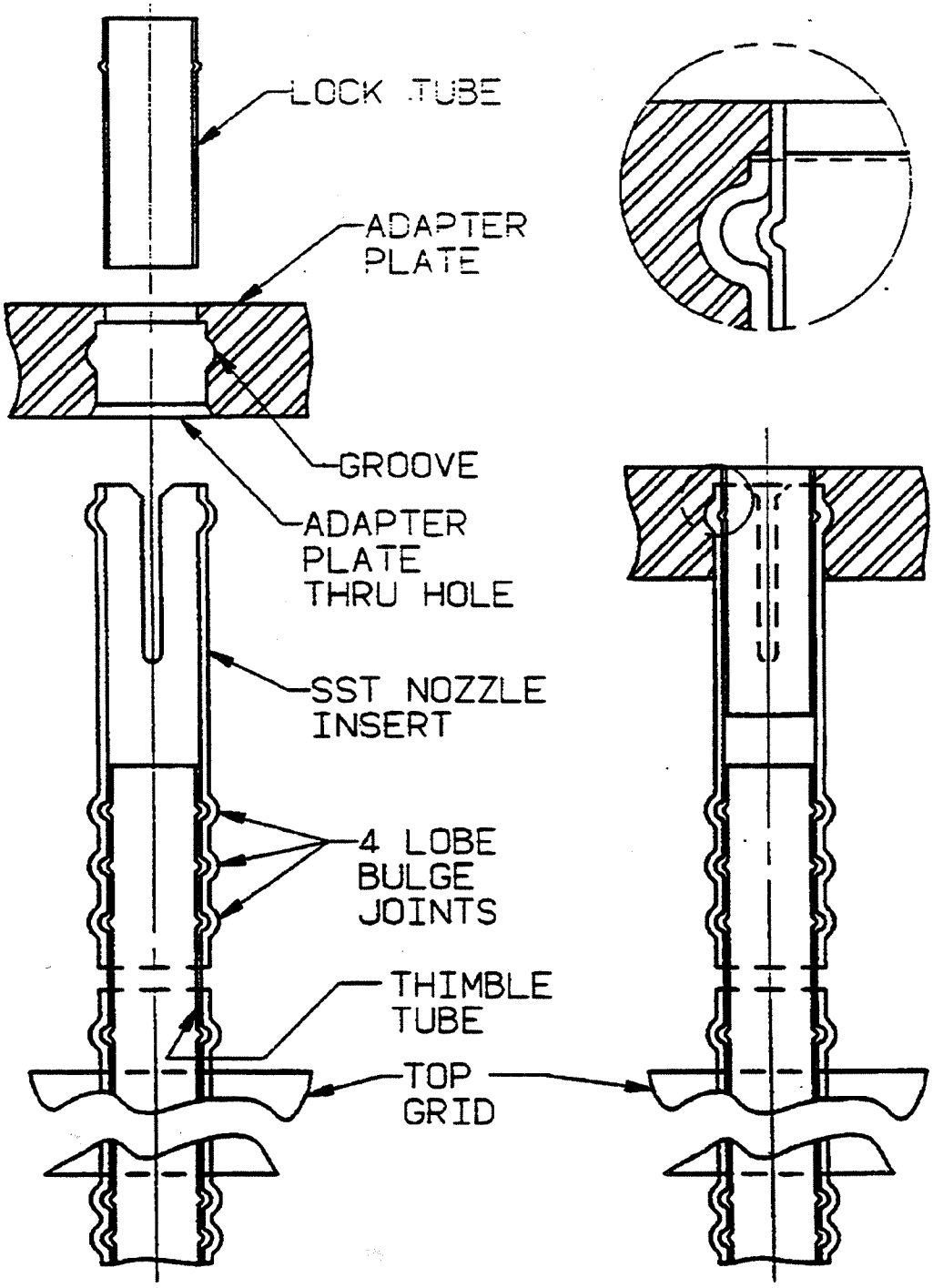

SOUTH CAROLINA ELECTRIC & GAS CO.
VIRGIL C. SUMMER NUCLEAR STATION

Vantage+ Fuel Top Grid To Nozzel Attachment

Figure 4.2-6

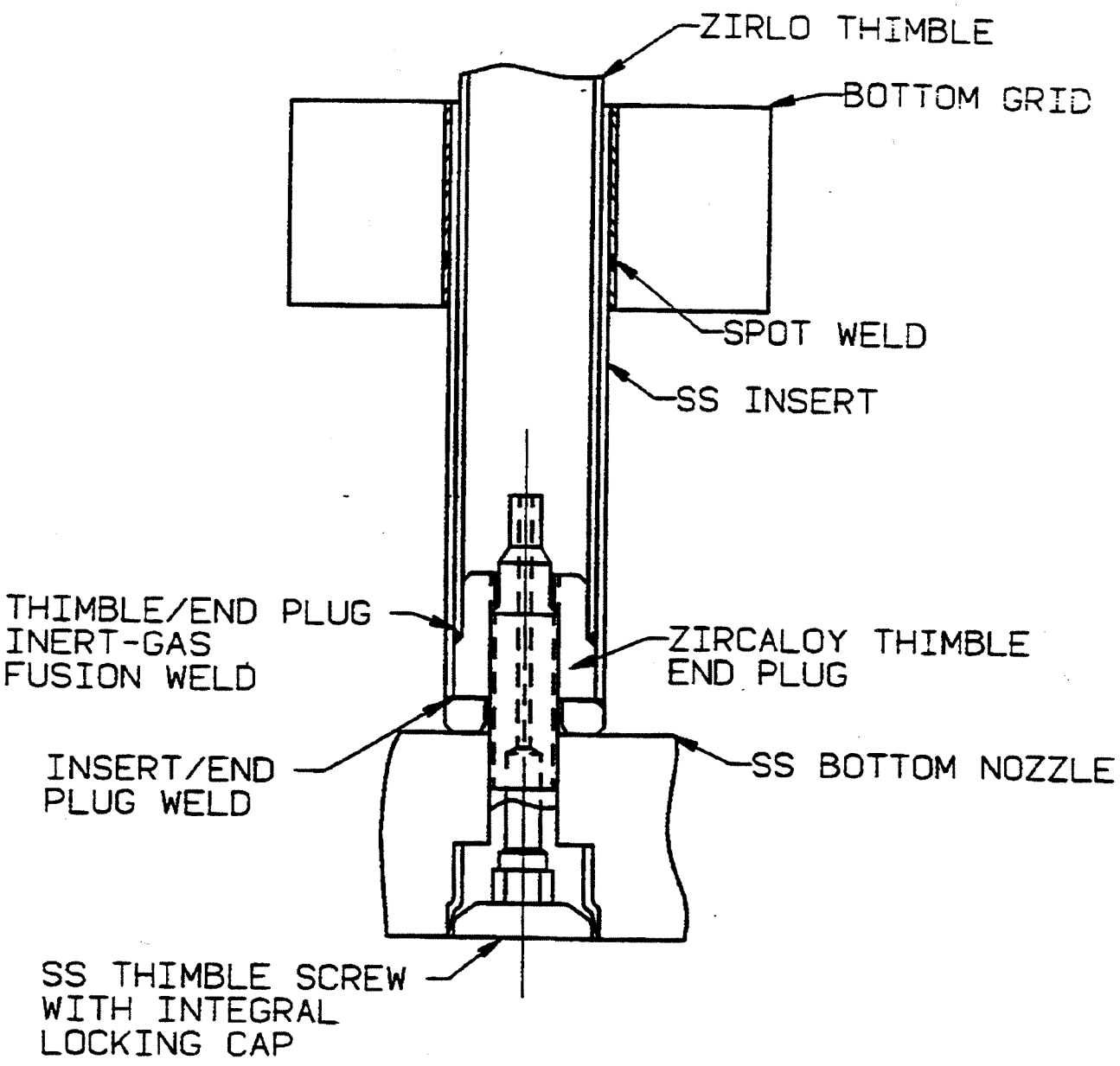

SOUTH CAROLINA ELECTRIC & GAS CO. VIRGIL C. SUMMER NUCLEAR STATION
Vantage+ Fuel Guide Thimble To Bottom Nozzle Joint Figure 4.2-7

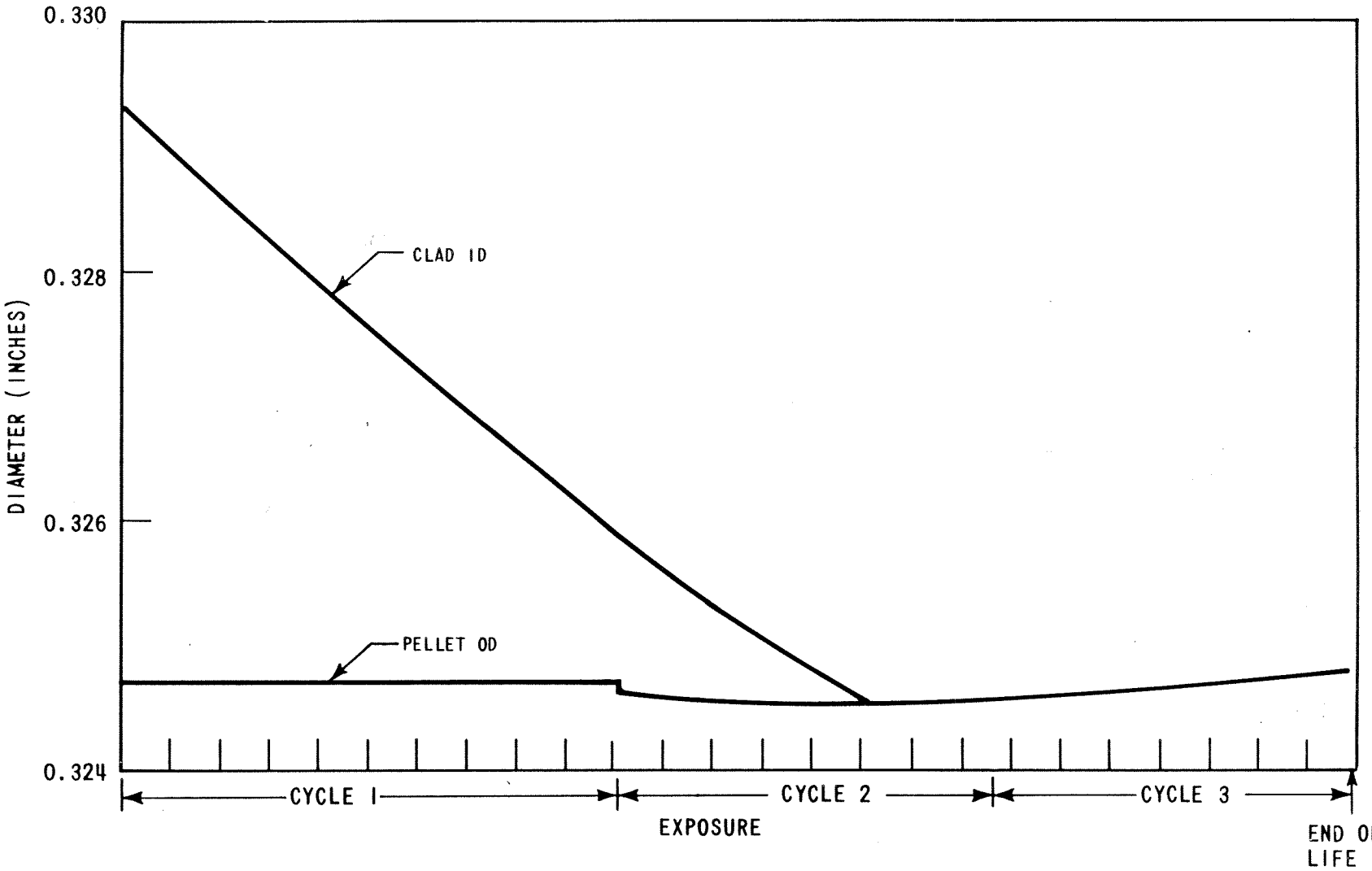

SOUTH CAROLINA ELECTRIC & GAS CO.
VIRGIL C. SUMMER NUCLEAR STATION

Typical Clad and Pellet Dimensions as a Function of Exposure

Figure 4.2-8

Amendment 0
August 1984

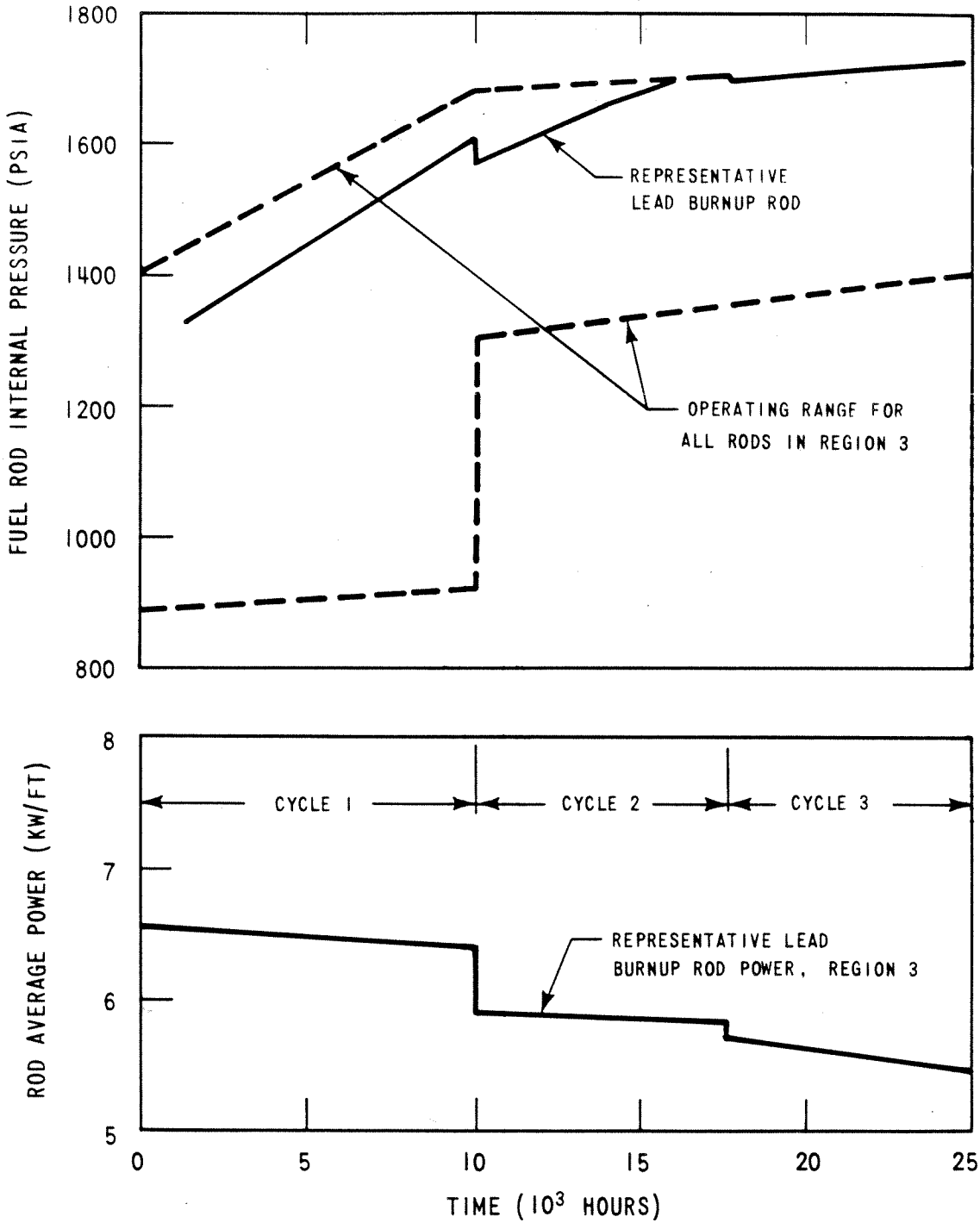

Amendment 0
August 1984

SOUTH CAROLINA ELECTRIC & GAS CO.
VIRGIL C. SUMMER NUCLEAR STATION

Representive Fuel Rod Internal Pressure and Linear Power Density for the Lead Burnup Rod as a Function of Time

Figure 4.2-9

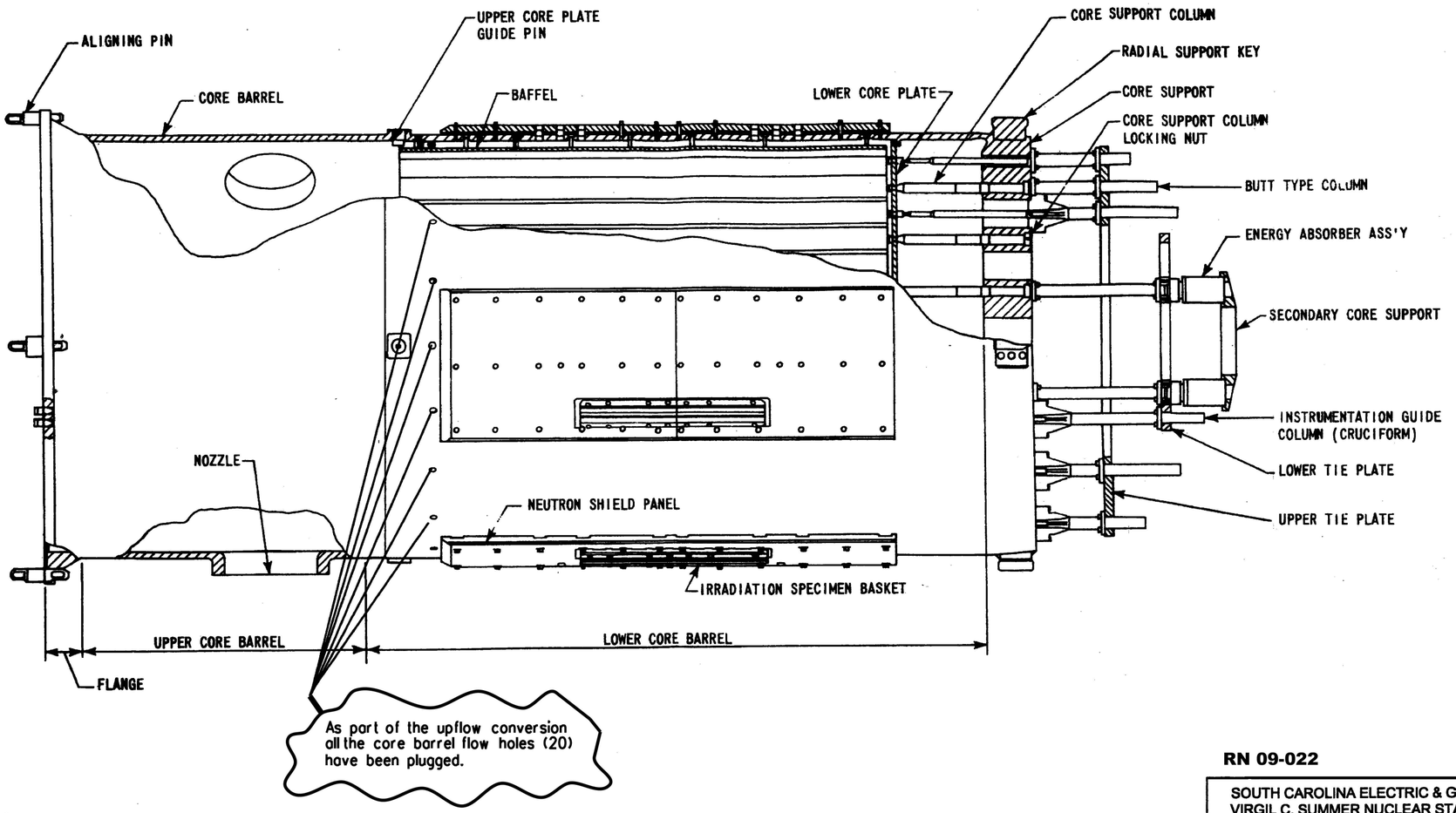

RN 09-022

SOUTH CAROLINA ELECTRIC & GAS CO.
VIRGIL C. SUMMER NUCLEAR STATION

Lower Core Support Assembly
(Core Barrel Assembly)

Figure 4.2-10 Rev. 1

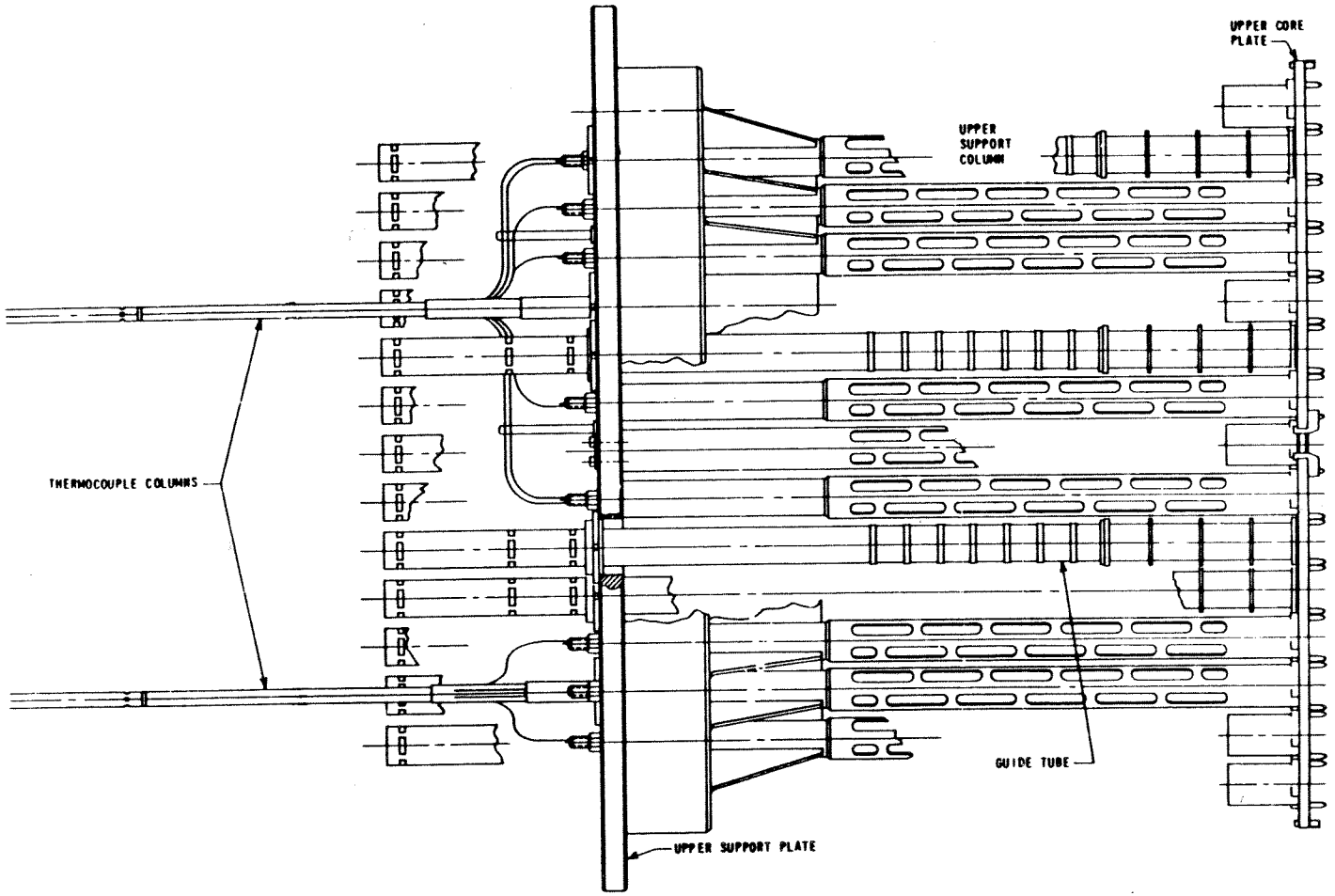

Amendment 0
August 1984

SOUTH CAROLINA ELECTRIC & GAS CO.
VIRGIL C. SUMMER NUCLEAR STATION

Upper Core Support Assembly

Figure 4.2-11

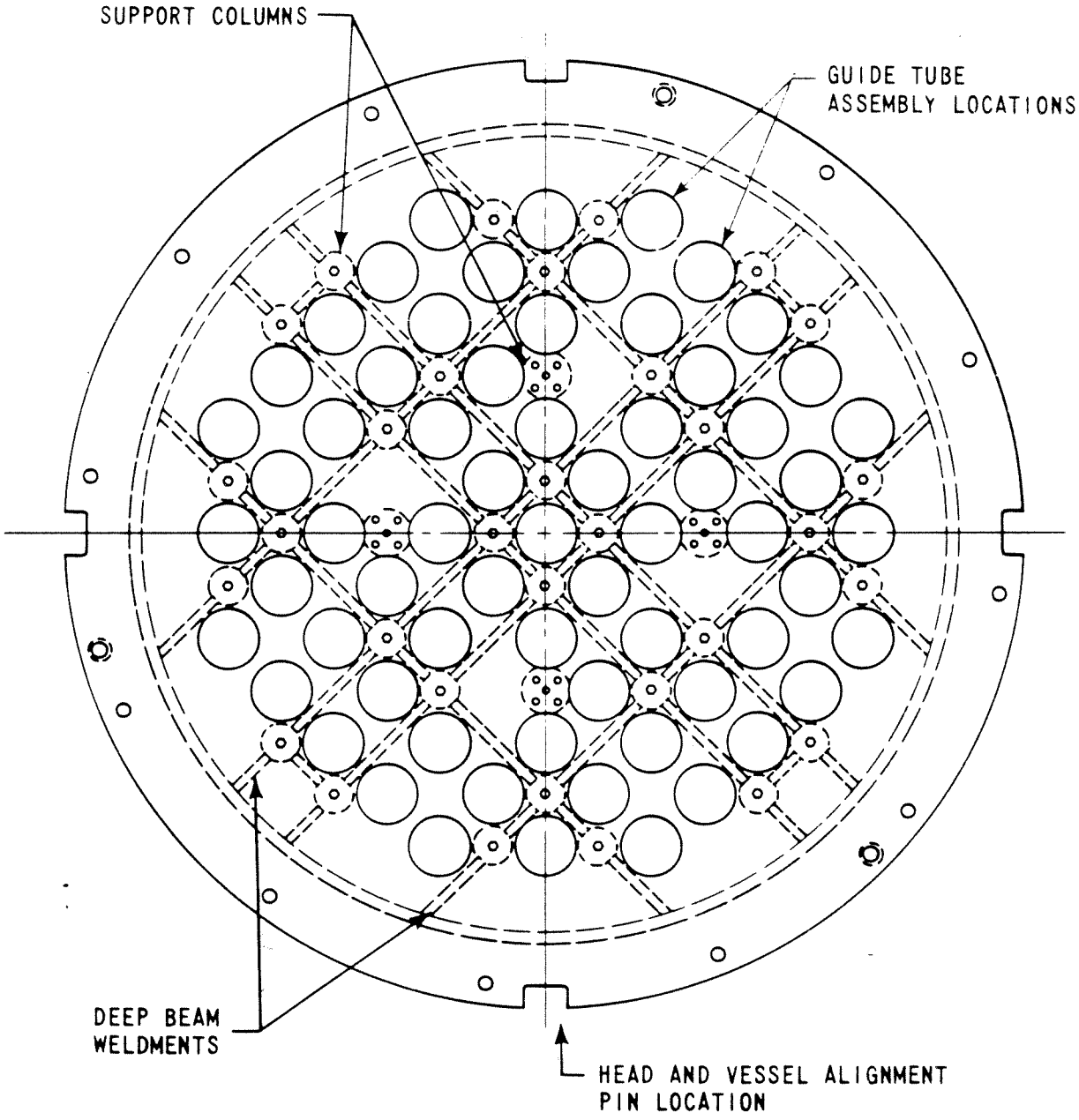

Amendment 0
August 1984

SOUTH CAROLINA ELECTRIC & GAS CO. VIRGIL C. SUMMER NUCLEAR STATION
Plan View of Upper Core Support Structure Figure 4.2-12

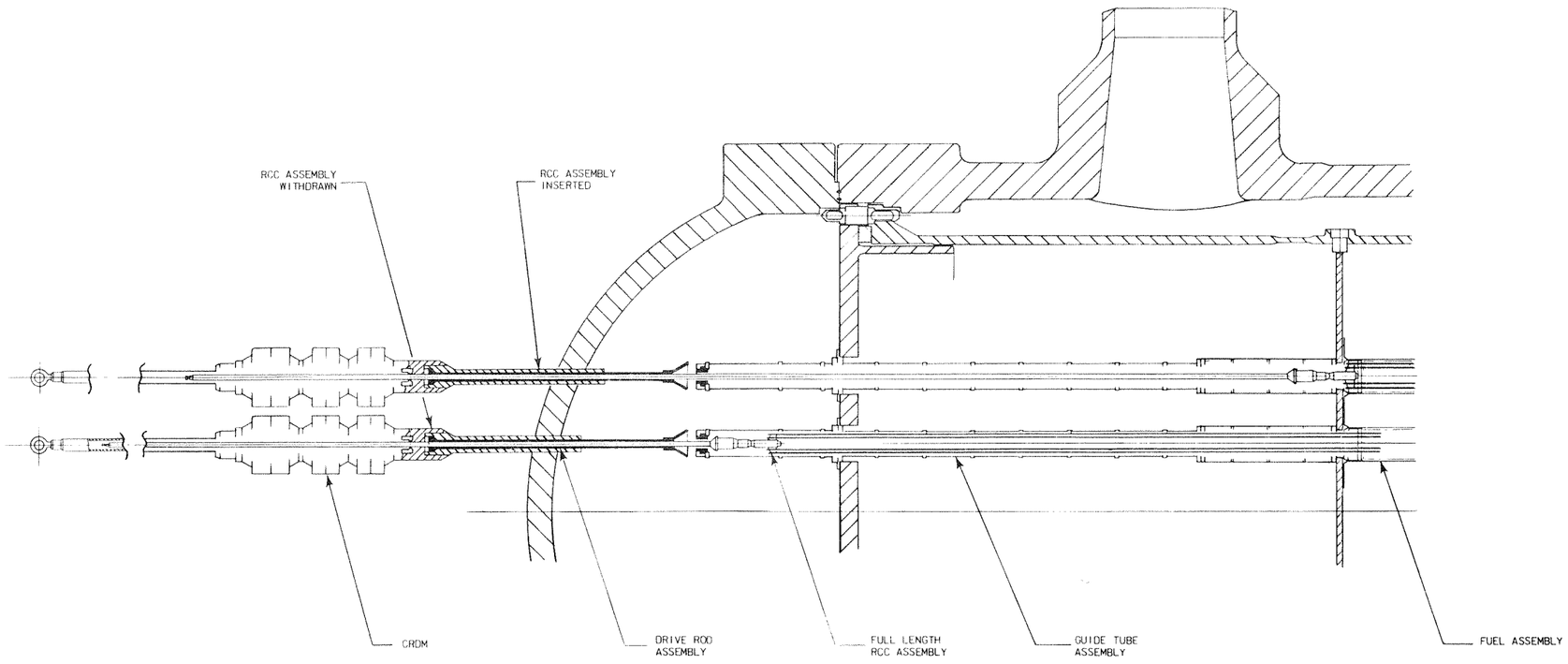

Amendment 0
August 1984

SOUTH CAROLINA ELECTRIC & GAS CO.
VIRGIL C. SUMMER NUCLEAR STATION

Full Length Rod Cluster Control and Drive Rod Assembly with Interfacing Components

Figure 4.2-13

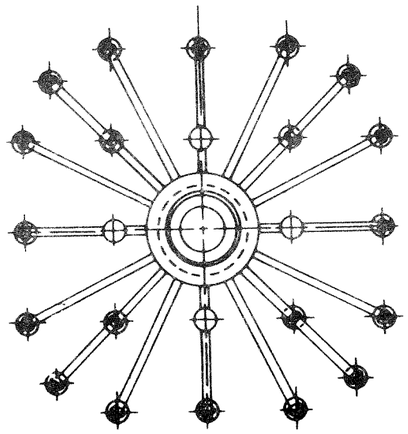

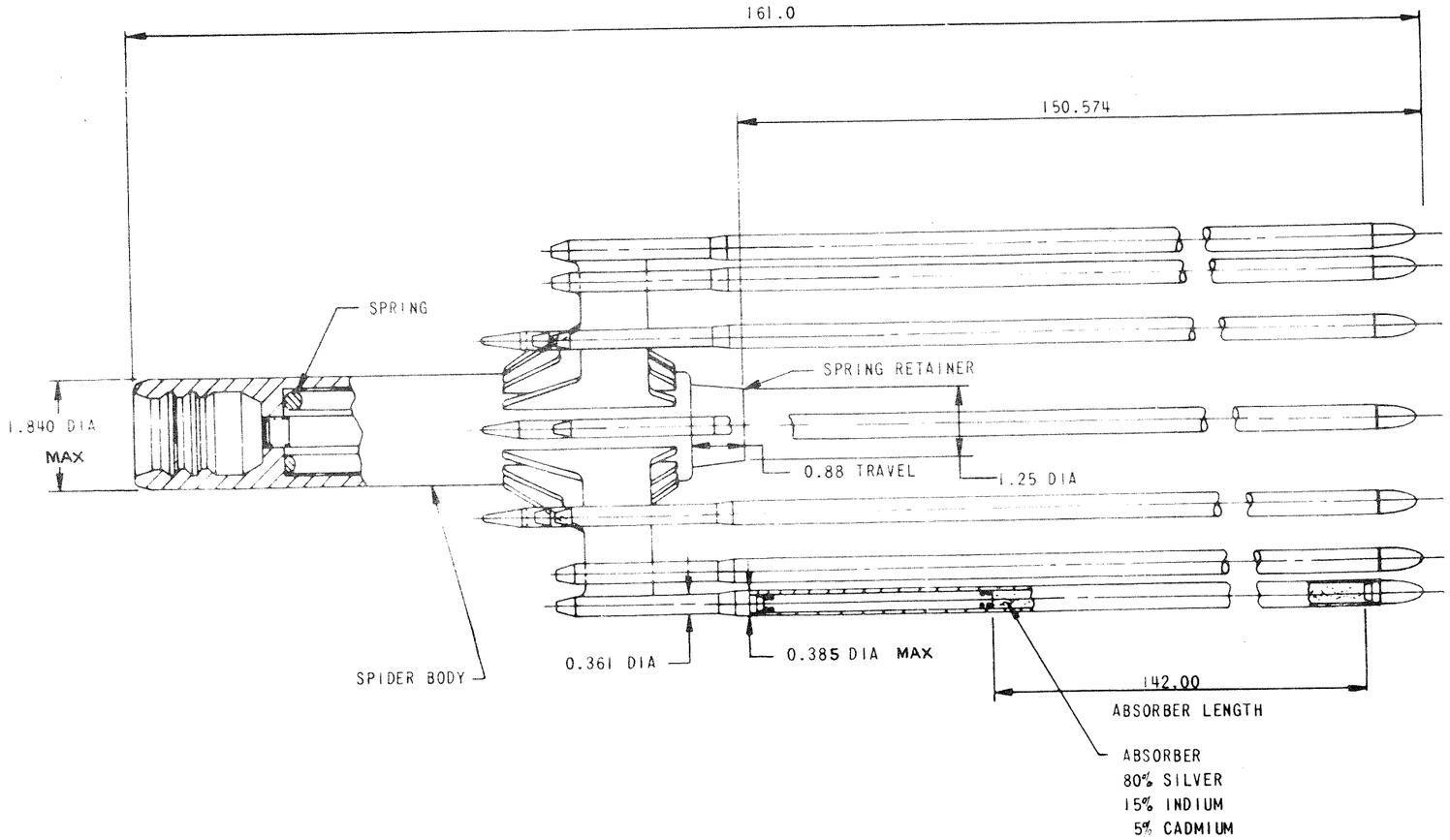

Amendment 0
August 1984

SOUTH CAROLINA ELECTRIC & GAS CO.
VIRGIL C. SUMMER NUCLEAR STATION

Full Length Rod Cluster Control Assembly Outline

Figure 4.2-14

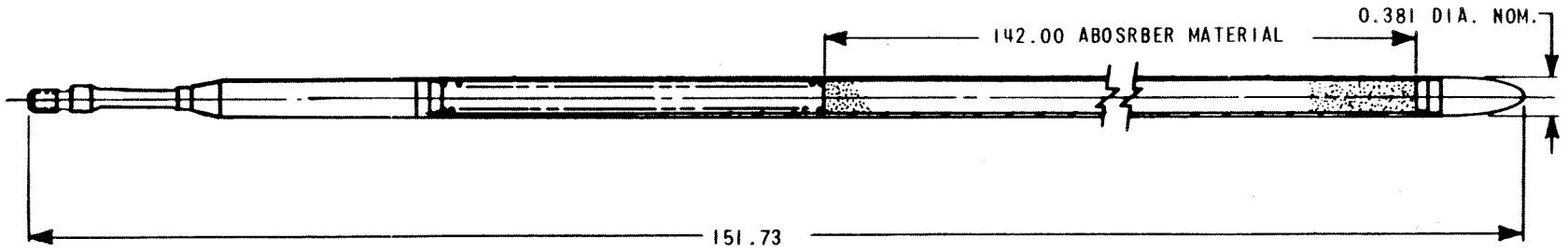

Amendment 0
August 1984

SOUTH CAROLINA ELECTRIC & GAS CO.
VIRGIL C. SUMMER NUCLEAR STATION

Full Length Absorber
Rod

Figure 4.2-15

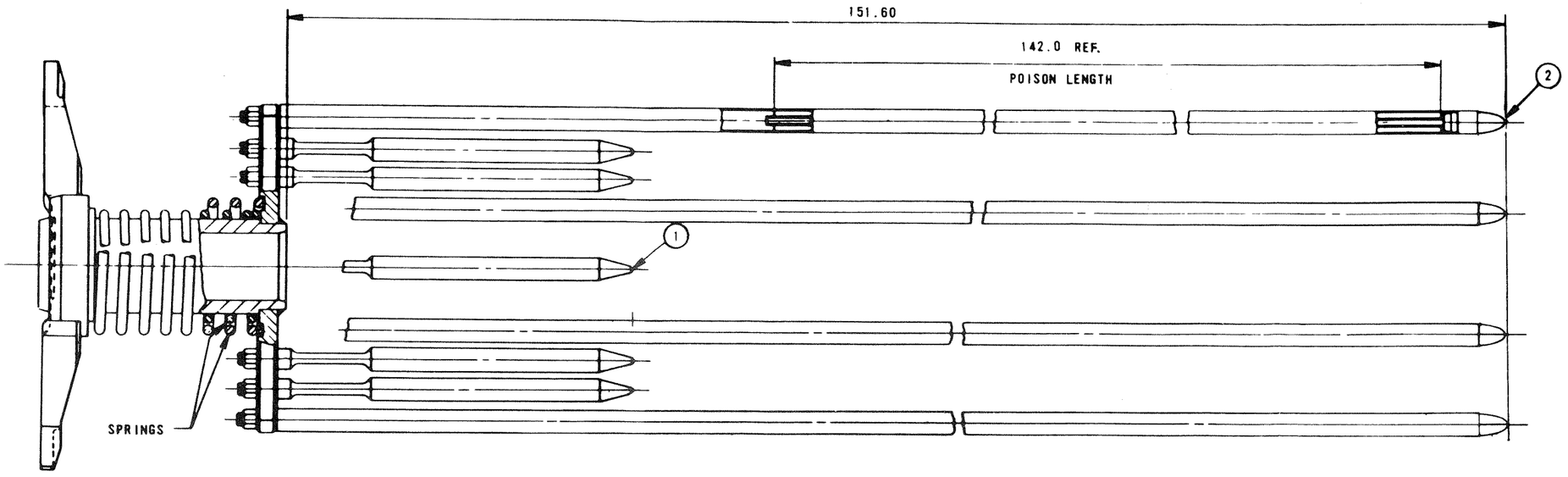

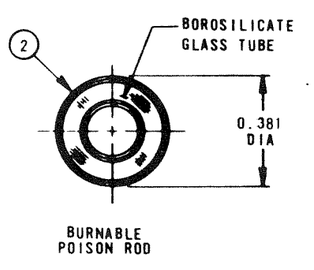

BURNABLE
POISON ROD

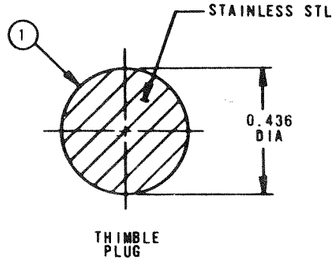

THIMBLE
PLUG

AMENDMENT 6
AUGUST, 1990

SOUTH CAROLINA ELECTRIC & GAS CO.
VIRGIL C. SUMMER NUCLEAR STATION

Borosilicate Absorber Assembly

Figure 4.2-17

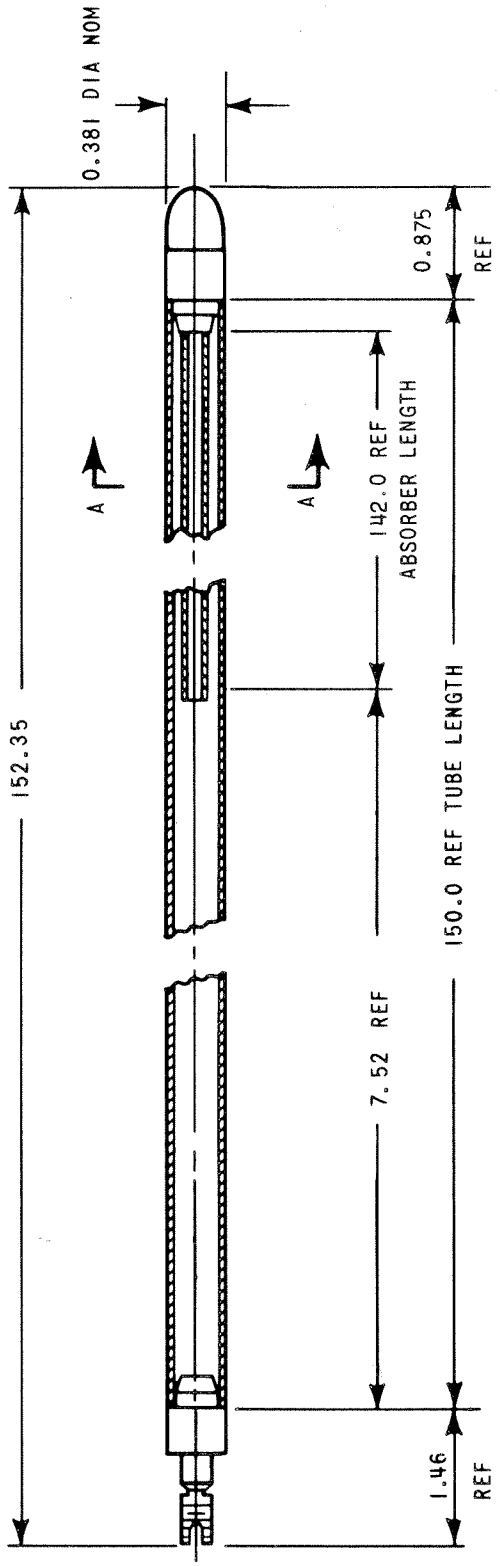

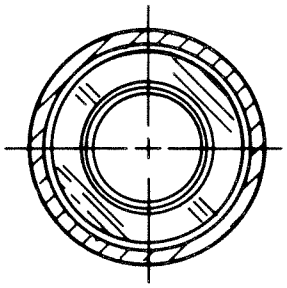

AMENDMENT 6
AUGUST, 1990

SOUTH CAROLINA ELECTRIC & GAS CO.
VIRGIL C. SUMMER NUCLEAR STATION

Borosilicate Absorber Rod Cross Section

Figure 4.2-18

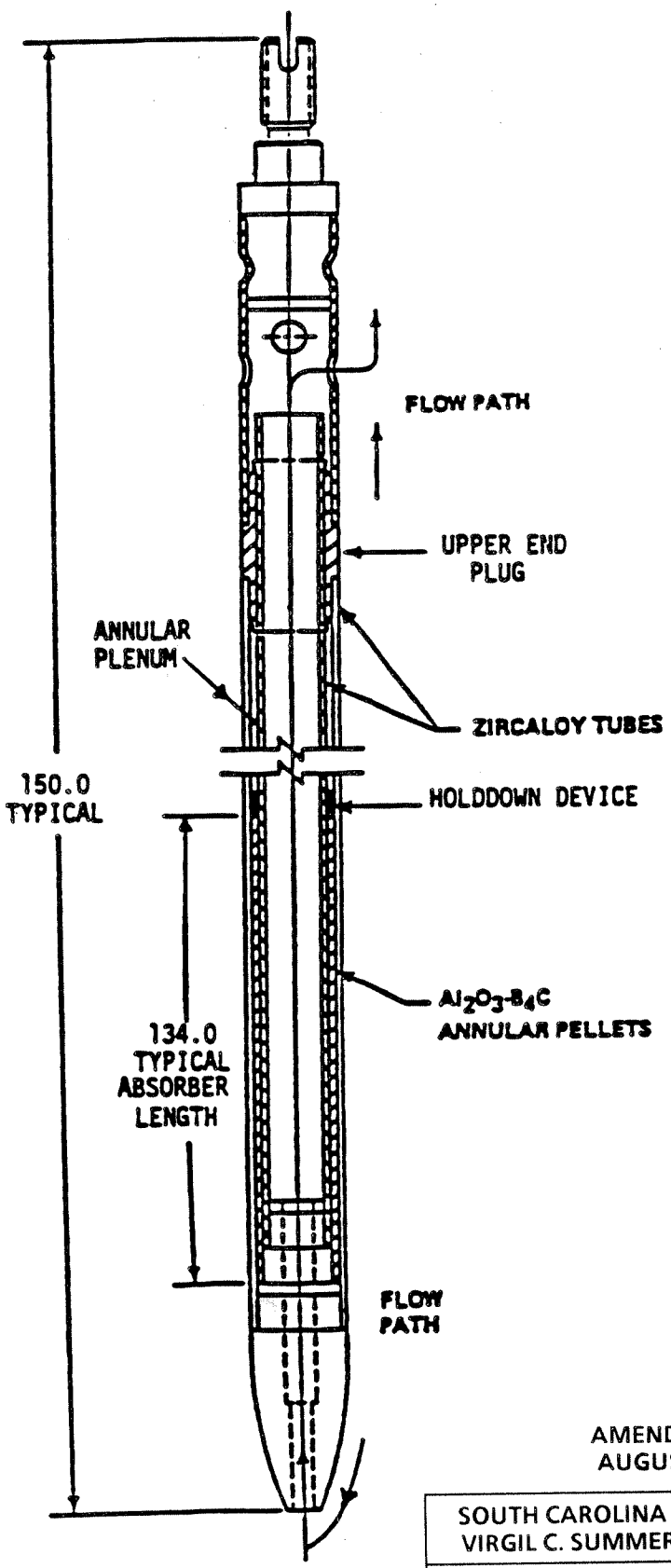

AMENDMENT 6
AUGUST, 1990

SOUTH CAROLINA ELECTRIC & GAS CO.
VIRGIL C. SUMMER NUCLEAR STATION

Wet Annular Burnable Absorber Rod

Figure 4.2-18a

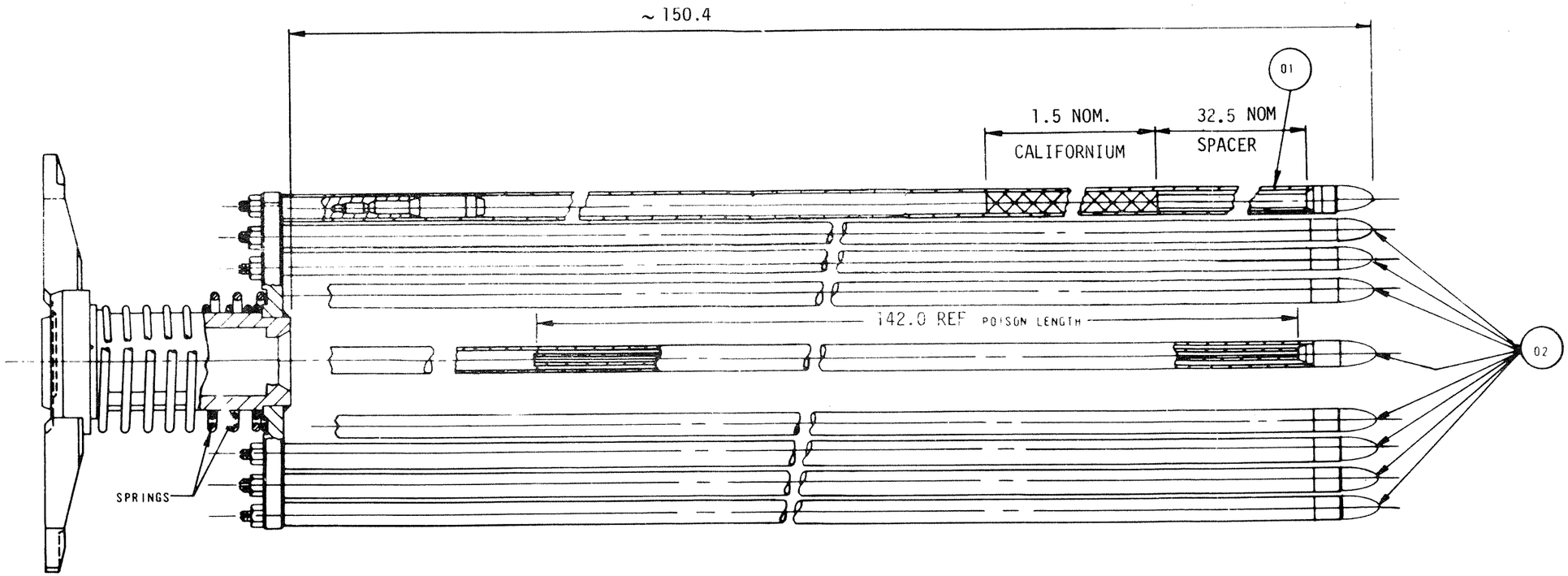

NOTE: ALL DIMENSIONS ARE IN INCHES

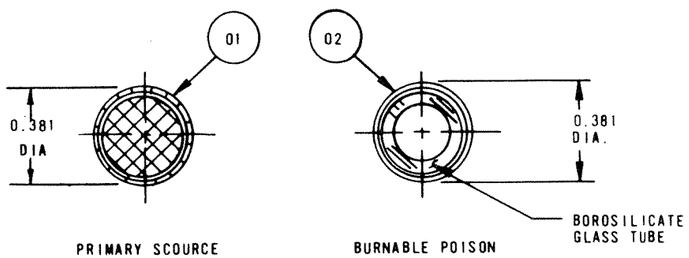

Amendment 0
August 1984

SOUTH CAROLINA ELECTRIC & GAS CO. VIRGIL C. SUMMER NUCLEAR STATION
Primary Source Assembly Figure 4.2-19

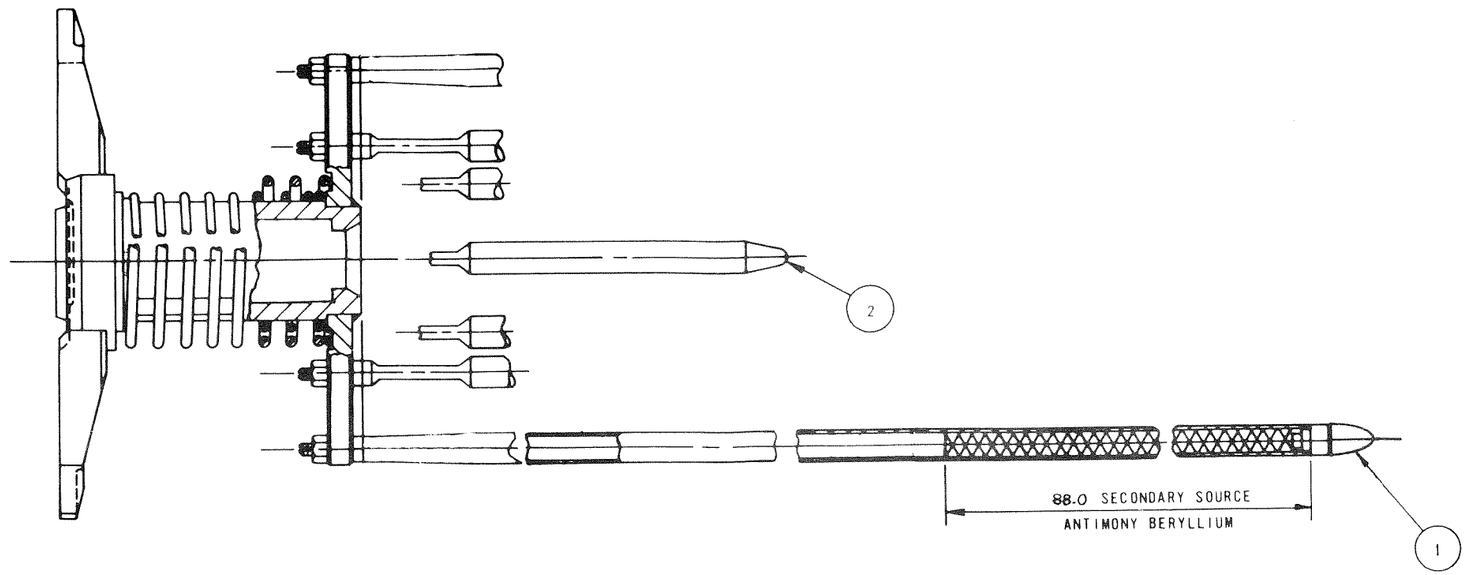

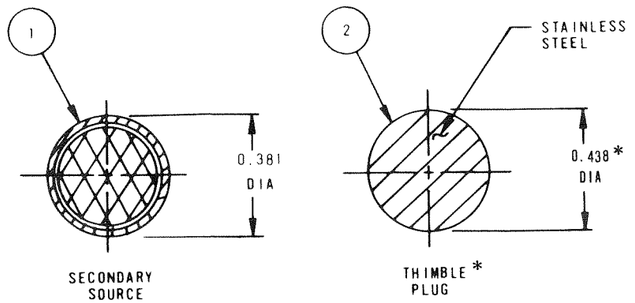

* FITS ONLY LOPAR ASSEMBLY THIMBLE TUBES. TO FIT INTO VANTAGE 5 THIMBLE TUBES, MUST USE DUALLY COMPATIBLE PLUG DESIGN WITH 0.424 INCH DIAMETER.

NOTE ALL DIMENSIONS ARE IN INCHES

AMENDMENT 6
AUGUST, 1990

SOUTH CAROLINA ELECTRIC & GAS CO.
VIRGIL C. SUMMER NUCLEAR STATION

Secondary Source Assembly

Figure 4.2-20

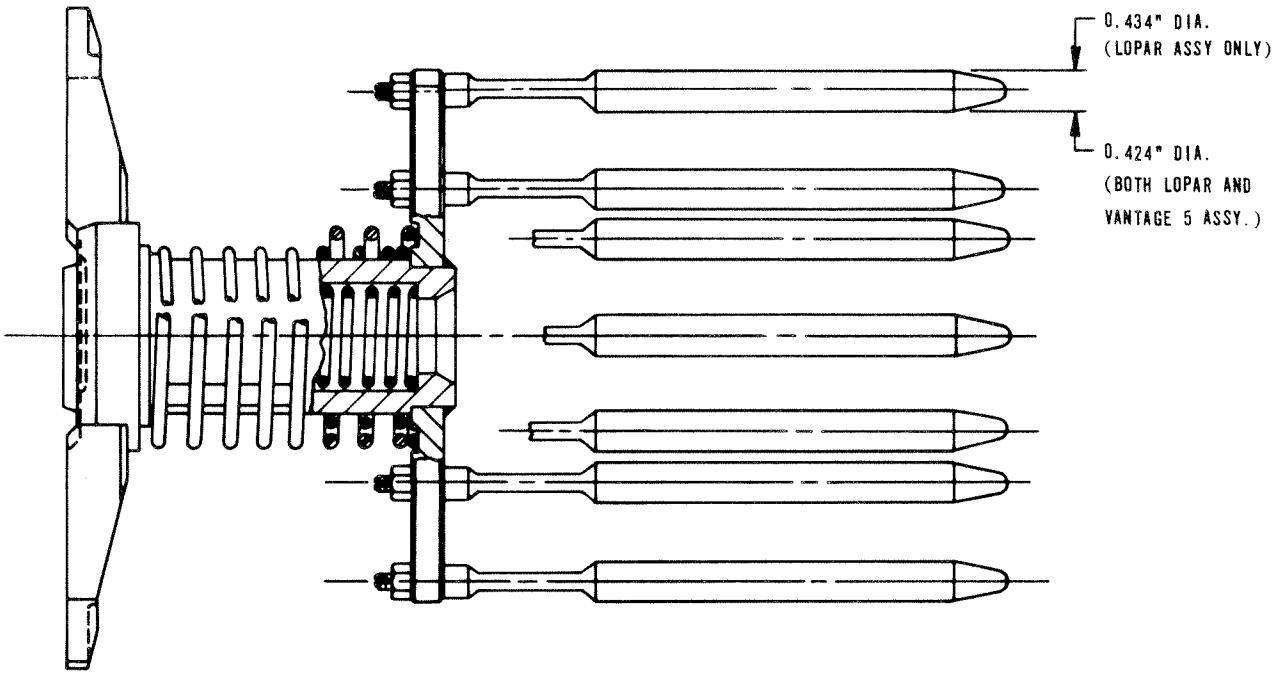

AMENDMENT 6
AUGUST, 1990

SOUTH CAROLINA ELECTRIC & GAS CO.
VIRGIL C. SUMMER NUCLEAR STATION

Thimble Plug Assembly

Figure 4.2-21

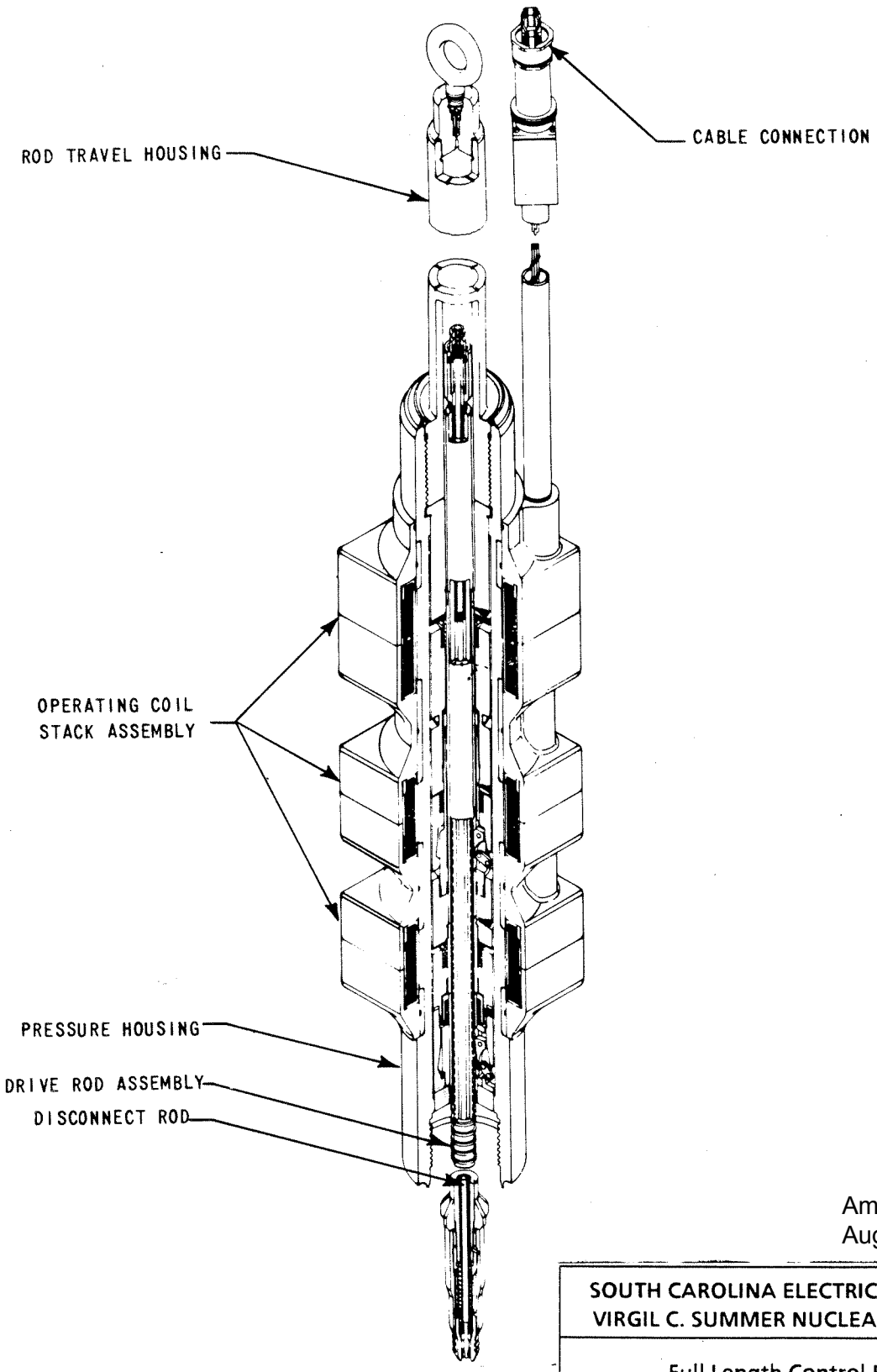

Amendment 0
August 1984

SOUTH CAROLINA ELECTRIC & GAS CO.
VIRGIL C. SUMMER NUCLEAR STATION

Full Length Control Rod
Drive Mechanism

Figure 4.2-22

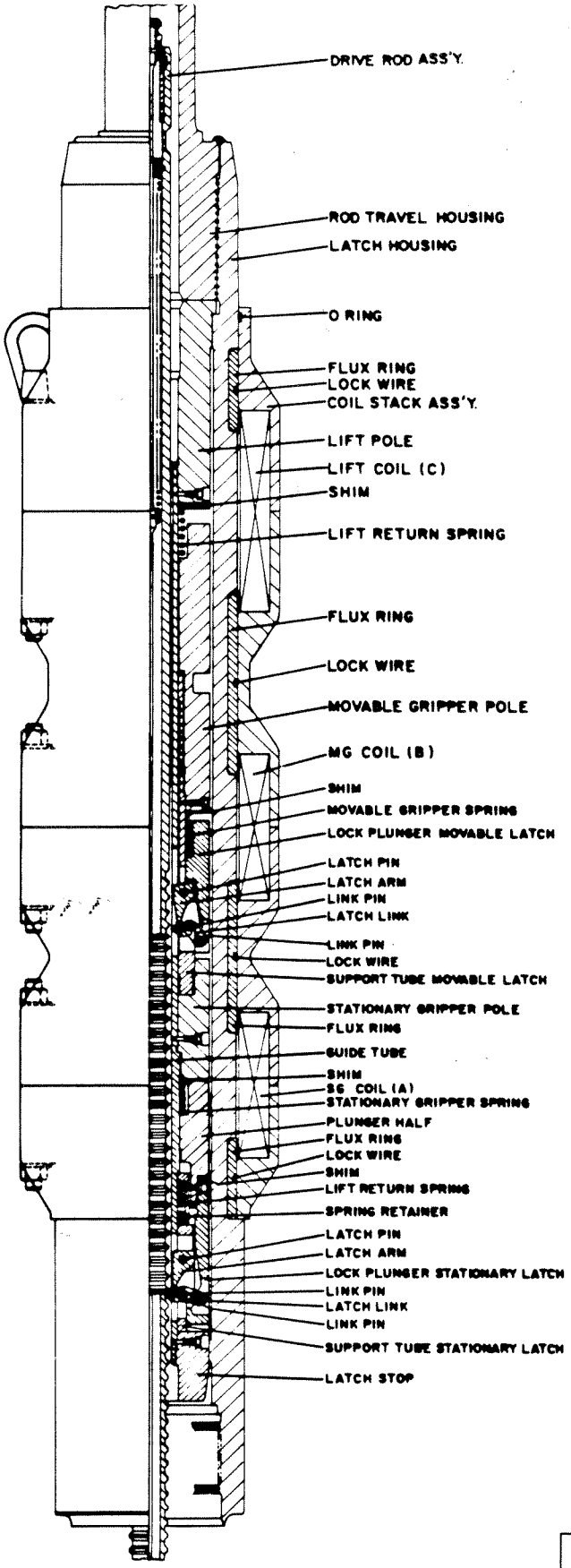

Amendment 0
August 1984

SOUTH CAROLINA ELECTRIC & GAS CO.
VIRGIL C. SUMMER NUCLEAR STATION

Full Length Control Rod Drive
Mechanism Schematic

Figure 4.2-23

BEFORE LOAD TRANSFER

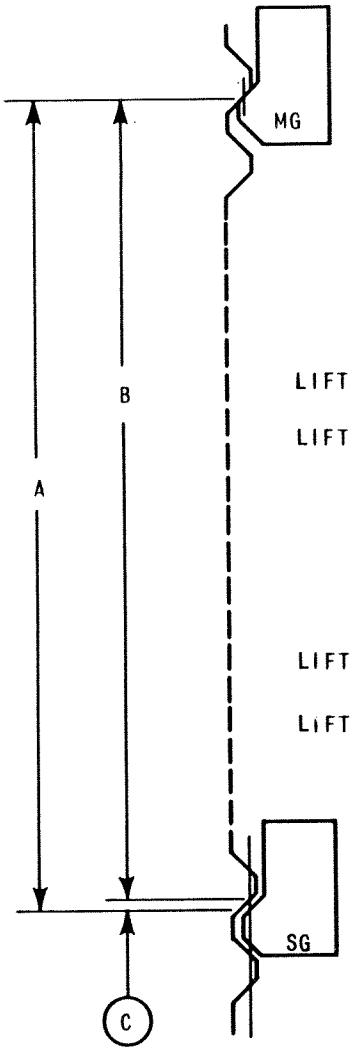

	AT 70°		
	A	B	C
LIFT COIL OFF	15.640	15.625	0.015
LIFT COIL ON	16.265	16.250	0.015

	AT 650°		
	A	B	C
LIFT COIL OFF	15.725	15.679	0.046
LIFT COIL ON	16.375	16.387	0.068

AFTER LOAD TRANSFER

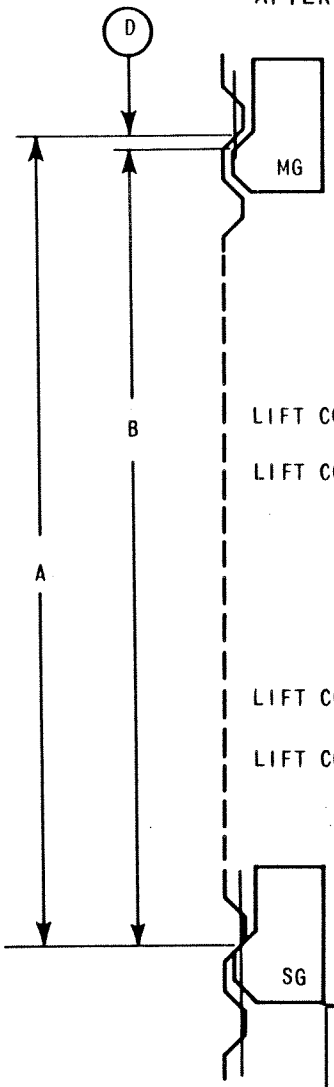

	AT 70°		
	A	B	D
LIFT COIL OFF	15.625	15.578	0.047
LIFT COIL ON	16.258	16.203	0.047

	AT 650°		
	A	B	D
LIFT COIL OFF	15.679	15.641	0.038
LIFT COIL ON	16.387	16.291	0.016

SOUTH CAROLINA ELECTRIC & GAS CO.
VIRGIL C. SUMMER NUCLEAR STATION

Nominal Latch Clearance at Minimum and Maximum Temperature

Figure 4.2-26

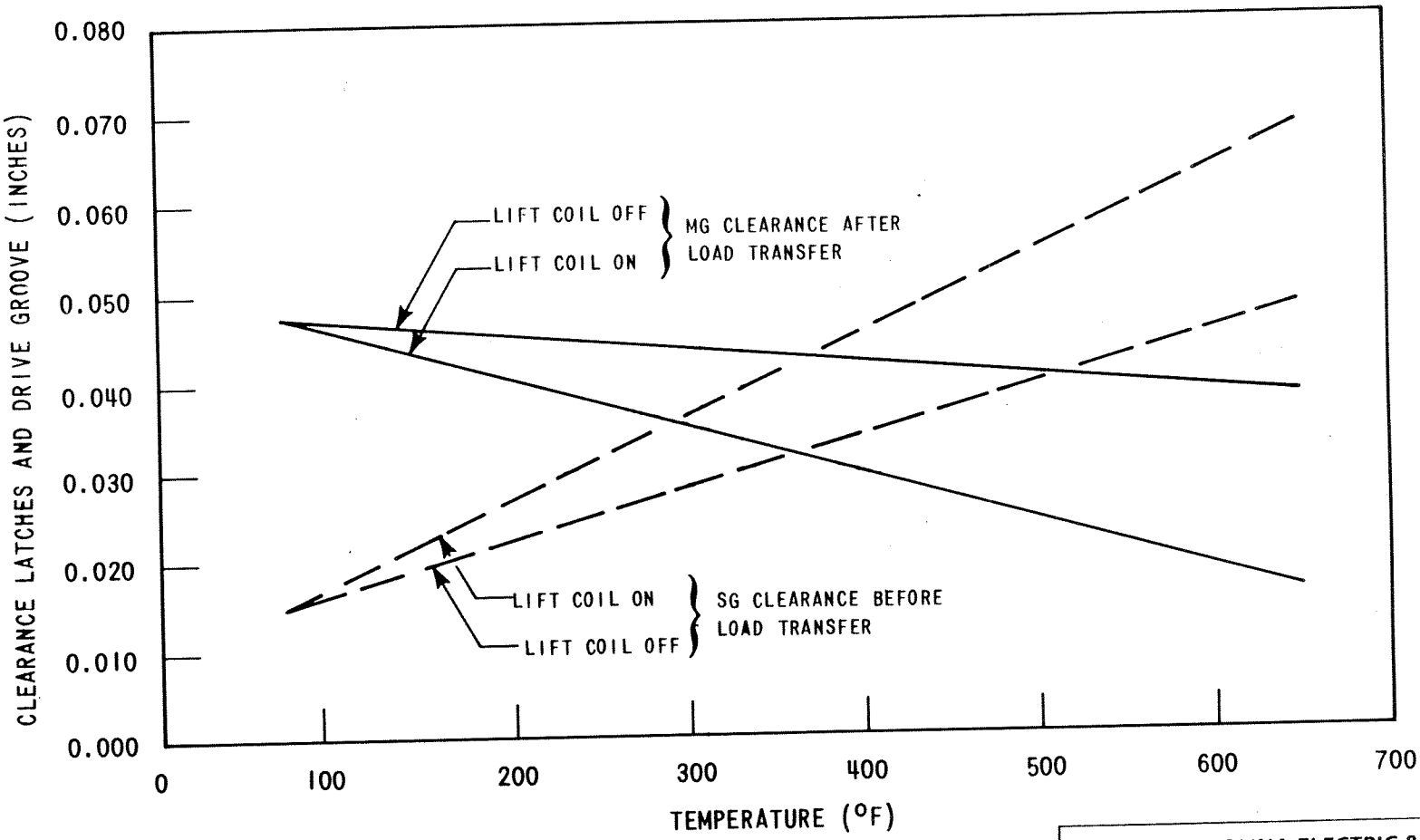

SOUTH CAROLINA ELECTRIC & GAS CO.
VIRGIL C. SUMMER NUCLEAR STATION

Control Rod Drive Mechanism Latch Clearance Thermal Effect

Figure 4.2-27

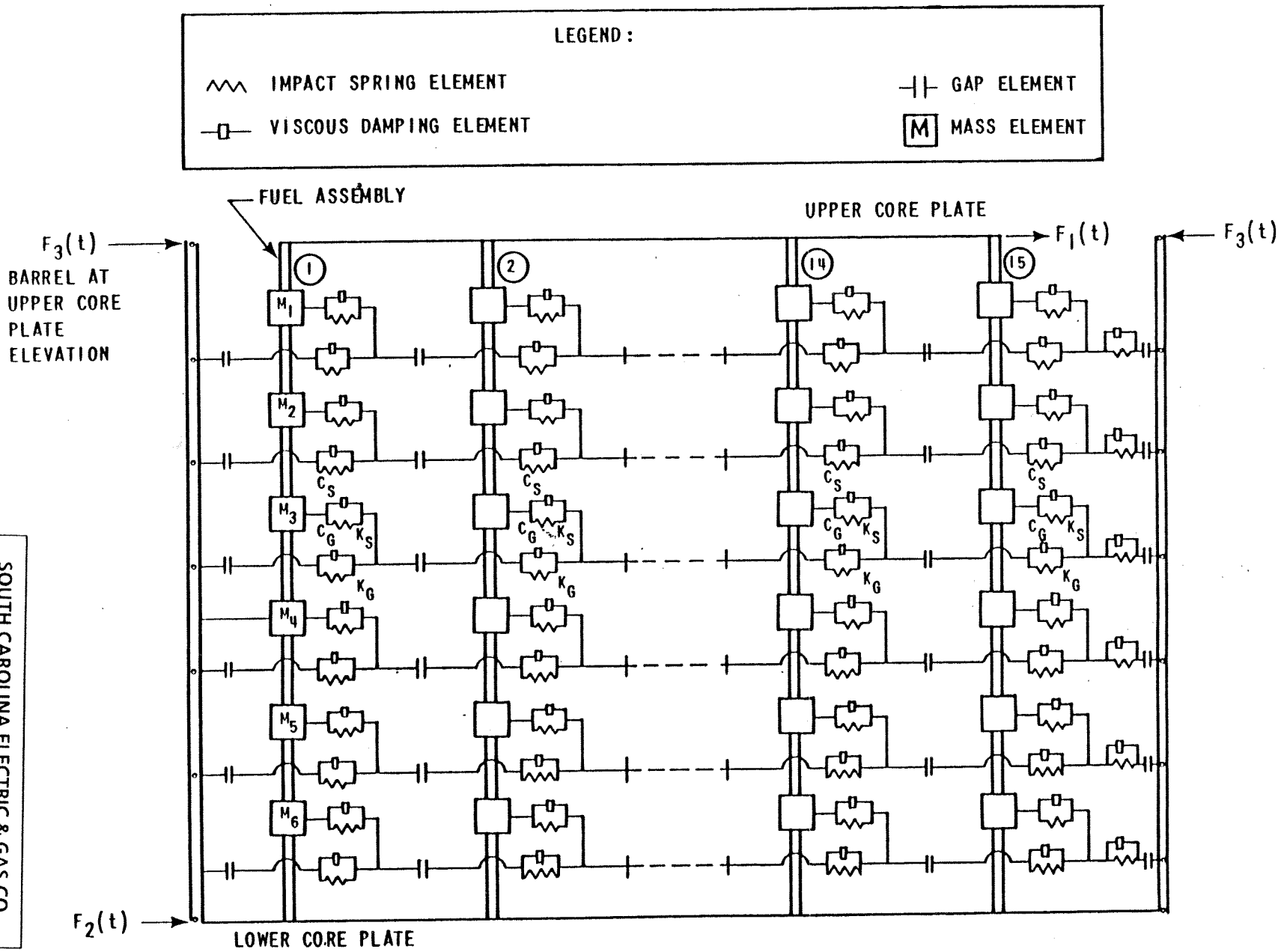

SOUTH CAROLINA ELECTRIC & GAS CO.
VIRGIL C. SUMMER NUCLEAR STATION

Schematic Representation of Reactor Core Model

Figure 4.2-28

Amendment 0
August 1984

4.3 NUCLEAR DESIGN

4.3.1 DESIGN BASES

This section describes the design bases and functional requirements used in the nuclear design of the fuel and reactivity control system and relates these design bases to the General Design Criteria (GDC) of July 1971. Where appropriate, supplemental criteria such as the Final Acceptance Criteria for Emergency Core Cooling Systems are addressed. Before discussing the nuclear design bases, it is appropriate to briefly review the 4 major categories ascribed to the conditions of plant operation.

The full spectrum of plant conditions is divided into 4 categories, in accordance with the anticipated frequency of occurrence and risk to the public:

1. Condition I - Normal Operation

2. Condition II - Incidents of Moderate Frequency

3. Condition III - Infrequent Faults

4. Condition IV - Limiting Faults

In general, the Condition I occurrences are accommodated with margin between any plant parameter and the value of that parameter which would require either automatic or manual protective action. Condition II incidents are accommodated with, at most, a shutdown of the reactor with the plant capable of returning to operation after corrective action. Fuel damage (as used here is defined as penetration of the fission product barrier, i.e., the fuel rod clad) is not expected during Condition I and Condition II events. It is not possible, however, to preclude a very small number of rod failures. These are within the capability of the plant cleanup system and are consistent with the plant design basis.

Condition III incidents shall not cause more than a small fraction of the fuel elements in the reactor to be damaged, although sufficient fuel element damage might occur to preclude immediate resumption of operation. The release of radioactive material due to Condition III incidents should not be sufficient to interrupt or restrict public use of these areas beyond the exclusion radius. Furthermore, a Condition III incident shall not, by itself generate a Condition IV fault or result in a consequential loss of function of the reactor coolant or reactor containment barriers.

Condition IV occurrences are faults that are not expected to occur but are defined as limiting faults which must be designed against. Condition IV faults shall not cause a release of radioactive material that results in an undue risk to public health and safety.

Condition II, III, and IV events or accidents requiring the minimum shutdown margin are assumed to start from normal operating conditions. Normal operation does not require maintaining the minimum shutdown margin; but some accidents which start from normal

operation require that the minimum shutdown margin be available, i.e., at anytime during Condition I operation, the plant must be able to go to zero power and be subcritical by at least the minimum shutdown margin. If this condition is met, then the consequences of accidents assumed to start from normal operation will be within acceptable limits.

The core design power distribution limits related to fuel integrity are met for Condition I occurrences through conservative design and maintained by the action of the control system. The requirements for Condition II occurrences are met by providing an adequate protection system which monitors reactor parameters. The control and protection systems are described in Chapter 7.0 and the consequences of Condition II, III, and IV occurrences are given in Chapter 15.0.

4.3.1.1 Fuel Burnup

4.3.1.1.1 Basis

The fuel rod design basis is described in Section 4.2. The nuclear design basis is to install sufficient reactivity in the fuel to attain the desired core lifetime and energy requirements while meeting all safety related criteria. The above along with the design basis in Section 4.3.1.3, satisfies GDC-10.

4.3.1.1.2 Discussion

Fuel burnup is a measure of fuel depletion which represents the integrated energy output of the fuel (MWD/MTU) and is a convenient means for quantifying fuel exposure criteria.

The core design lifetime or design discharge burnup is achieved by installing sufficient initial excess reactivity in each fuel region and by following a fuel replacement program (such as that described in Section 4.3.2) that meets all safety-related criteria in each cycle of operation.

Initial excess reactivity installed in the fuel, although not a design basis, must be sufficient to maintain core criticality at full power operating conditions throughout cycle life with equilibrium xenon, samarium, and other fission products present. The end of design cycle life is defined to occur when the chemical shim concentration is essentially zero with control rods present to the degree necessary for operational requirements. In terms of chemical shim boron concentration this represents approximately 10 ppm with no control rod insertion.

A limitation on initial installed excess reactivity is not required, other than as is quantified in terms of other design bases, such as core negative reactivity feedback and shutdown margin discussed below.

4.3.1.2 Negative Reactivity Feedbacks (Reactivity Coefficient)

4.3.1.2.1 Basis

The fuel temperature coefficient will be negative and the moderator temperature coefficient of reactivity will be nonpositive for full power operating conditions, thus providing negative reactivity feedback characteristics. Below 70% power, an MTC of up to +7 pcm (percent mille)/°F is allowed. From 70% to 100%, the MTC limit decreases linearly from +7 to 0 pcm/°F. The design basis meets GDC-11.

4.3.1.2.2 Discussion

When compensation for a rapid increase in reactivity is considered, there are 2 major effects. These are the resonance absorption effects (Doppler) associated with changing fuel temperature and the spectrum effect resulting from changing moderator density. These basic physics characteristics are often identified by reactivity coefficients. The use of slightly enriched uranium ensures that the Doppler coefficient of reactivity is negative. This coefficient provides the most rapid reactivity compensation. The core is also designed to have an overall negative moderator temperature coefficient of reactivity at full power operating conditions so that average coolant temperature or void content provides another, slower compensatory effect. Nominal full power operation is permitted only in a range of overall negative moderator temperature coefficient. The negative moderator temperature coefficient at full power can be achieved through the use of fixed burnable absorbers and/or boride absorber coated fuel pellets and/or control rods by limiting the reactivity controlled by soluble boron.

Burnable absorber content (quantity and distribution) is not stated as a design basis other than as it relates to accomplishment of a nonpositive moderator temperature coefficient at power operating conditions discussed above.

4.3.1.3 Control of Power Distribution

4.3.1.3.1 Basis

The nuclear design basis is that, with at least a 95% confidence level:

1. The fuel will not be operated at greater than 13.9 (1.02) = 14.02 kW/ft under normal operating conditions including an allowance of 2% for calorimetric error and not including power spike factor due to densification.

2. Under abnormal conditions including the maximum overpower condition, the fuel peak power will not cause melting as defined in Section 4.4.1.2.

3. The fuel will not operate with a power distribution that violates the departure from nucleate boiling (DNB) design basis (i.e., the DNBR shall not be less than the design limit DNBR as discussed in Section 4.4.1) under Condition I and II events including the maximum overpower condition.

4. Fuel management will be such as to produce rod powers and burnups consistent with the assumptions in the fuel rod mechanical integrity analysis of Section 4.2.

The above basis meets GDC-10.

4.3.1.3.2 Discussion

Calculation of extreme power shapes which affect fuel design limits is performed with proven methods and verified frequently with measurements from operating reactors. The conditions under which limiting power shapes are assumed to occur are chosen conservatively with regard to any permissible operating state.

Even though there is good agreement between measured peak power calculations and measurements, a nuclear uncertainty margin is applied to calculated peak local power. Such a margin is provided both for the analysis during normal operating states and anticipated transients.

4.3.1.4 Maximum Controlled Reactivity Insertion Rate

4.3.1.4.1 Basis

The maximum reactivity insertion rate due to withdrawal of rod cluster control assemblies or by boron dilution is limited. During normal at power operation, the maximum controlled reactivity rate change is less than 105 pcm/sec. A maximum reactivity change rate (90 pcm/sec)[(1)] for accidental withdrawal of control banks is set such that peak heat generation rate and DNBR do not exceed the maximum allowable at overpower conditions. This satisfies GDC-25.

The maximum reactivity worth of control rods and the maximum rates of reactivity insertion employing control rods are limited so as to preclude rupture of the coolant pressure boundary or disruption of the core internals to a degree which would impair core cooling capacity due to a rod withdrawal or ejection accident (see Chapter 15.0).

Following any Condition IV event (rod ejection, steamline break, etc.), the reactor can be brought to the shutdown condition and the core will maintain acceptable heat transfer geometry. This satisfies GDC-28.

(1) 1 pcm = 10^{-5} $\Delta\rho$ (See footnote on Table 4.3-2)

4.3.1.4.2 Discussion

Reactivity addition, associated with an accidental withdrawal of a control bank(s) is limited by the maximum rod speed (or travel rate) and by the worth of the bank(s). For this reactor, the maximum normal operation control rod speed is 45 inches per minute and the maximum rate of reactivity change considering 2 control banks moving is less than 90 pcm/sec. During normal at power operation and with normal control rod overlap, the maximum reactivity change rate is less than 105 pcm/sec. The reactivity change rates are conservatively calculated assuming unfavorable axial power and xenon distributions. The peak xenon burnout rate is 25 pcm/min, significantly lower than the maximum reactivity addition rate of 105 pcm/sec for normal operation and 90 pcm/sec for accidental withdrawal of 2 banks.

4.3.1.5 Shutdown Margins

4.3.1.5.1 Basis

Minimum shutdown margin, as specified in the Technical Specifications, is required at any power operating condition in both the hot standby and the cold shutdown condition.

In all analyses involving reactor trip, the single, highest worth rod cluster control assembly is postulated to remain untripped in its fullout position (stuck rod criterion). This satisfies GDC-26.

4.3.1.5.2 Discussion

Two (2) independent reactivity control systems are provided, namely control rods and soluble boron in the coolant. The control rod system can compensate for the reactivity effects of the fuel and water temperature changes accompanying power level changes over the range from full-load to no-load. In addition, the control rod system provides the minimum shutdown margin under Condition I events and is capable of making the core subcritical rapidly enough to prevent exceeding acceptable fuel damage limits assuming that the highest worth control rod is stuck at its furthest withdrawn position during a reactor trip.

The boron system can compensate for all xenon burnout reactivity changes and will maintain the reactor in the cold shutdown condition. Thus, backup and emergency shutdown provisions are provided by a mechanical and a chemical shim control system which satisfies GDC-26.

4.3.1.5.3 Basis

When fuel assemblies are in the pressure vessel and the vessel head is not in place, K_{eff} will be maintained at or below 0.95 with control rods and soluble boron. Further, the fuel will be maintained sufficiently subcritical that removal of all rod cluster control assemblies will not result in criticality.

4.3.1.5.4 Discussion

ANS Standard N18.2 [1] specifies a K_{eff} not to exceed 0.95 in spent fuel storage racks and transfer equipment flooded with pure water and a K_{eff} not to exceed 0.98 in normally dry new fuel storage racks assuming optimum moderation. No criterion is given for the refueling operation, however a 5% margin, which is consistent with spent fuel storage and transfer and the new fuel storage, is adequate for the controlled and continuously monitored operations involved.

The boron concentration required to meet the refueling shutdown criteria is specified in the Technical Specifications. Verification that this shutdown criteria is met, including uncertainties, is achieved using standard Westinghouse design methods such as the PHOENIX [35] and ANC [34] codes. The subcriticality of the core is continuously monitored as described in the Technical Specifications.

4.3.1.6 Stability

4.3.1.6.1 Basis

The core will be inherently stable to power oscillations at the fundamental mode. This satisfies GDC-12.

4.3.1.6.2 Discussion

Oscillations of the total power output of the core, from whatever cause, are readily detected by the loop temperature sensors and by the nuclear instrumentation. The core is protected by these systems and a reactor trip would occur if power increased unacceptably, preserving the design margins to fuel design limits. The stability of the turbine/steam generator/core systems and the reactor control system is such that total core power oscillations are not normally possible. The redundancy of the protection circuits ensures an extremely low probability of exceeding design power levels.

4.3.1.6.3 Basis

Spatial power oscillations, within the core with a constant core power output, can be reliably and readily detected and suppressed if they should occur.

4.3.1.6.4 Discussion

The core is designed so that diametral and azimuthal oscillations due to spatial xenon effects are self-damping and no operator action or control action is required to suppress them. The stability to diametral oscillations is so great that this excitation is highly improbable. Convergent azimuthal oscillations can be excited by prohibited motion of individual control rods. Such oscillations are readily observable and alarmed, using the excore long ion chambers. Indications are also continuously available from incore thermocouples and loop temperature measurements. Moveable incore detectors can be activated to provide more detailed information. Additionally, the BEACON Power Distribution Monitoring System (PDMS), Reference [37], is available on-line above 25% rated thermal power to provide a continuous real time picture of the core. In all presently proposed cores these horizontal plane oscillations are self-damping by virtue of reactivity feedback effects designed into the core. 02-01

However, axial xenon spatial power oscillations may occur late in core life. The control bank and excore detectors are provided for control and monitoring of axial power distributions. Assurance that fuel design limits are not exceeded is provided by reactor overpower ΔT and overtemperature ΔT trip functions which use the measured axial power imbalance as an input.

4.3.1.7 Anticipated Transients Without Trip

The effects of anticipated transients with failure to trip are not considered in the design bases of the plant. Analysis has shown that the likelihood of such a hypothetical event is negligibly small. Furthermore, analysis of the consequences of a hypothetical failure to trip following anticipated transients has shown that no significant core damage would result, system peak pressures would be limited to acceptable values, and no failure of the reactor coolant system would result. These analyses were documented [4] in August 1974 in accordance with the policy outlined in WASH-1270, "Technical Report on Anticipated Transients Without Scram for Water-Cooled Power Reactors," September, 1973.

4.3.2 DESCRIPTION

4.3.2.1 Nuclear Design Description

The reactor core consists of a specified number of fuel rods which are held in bundles by spacer grids and top and bottom fittings. The fuel rods are constructed of Zirconium alloy cylindrical tubes containing UO_2 fuel pellets. The bundles, known as fuel assemblies, are arranged in a pattern which approximates a right circular cylinder.

Each fuel assembly contains a 17 x 17 rod array composed of 264 fuel rods, 24 rod cluster control thimbles and an incore instrumentation thimble. Figure 4.2-1 shows a cross sectional view of a 17 x 17 fuel assembly and the related rod cluster control locations. Further details of the fuel assembly are given in Section 4.2.1. Limited substitutions of Zircaloy 4, ZIRLO®, and/or or stainless steel filler rods for fuel rods, if justified by a cycle specific reload analysis using NRC approved methodology, may be used. RN 11-013

The VANTAGE 5 fuel rods contain 6 inches of natural uranium in top and bottom portions of the rods. In VANTAGE+ assemblies, this 6 inch blanket contains annular pellets of natural uranium. The diameter of this annulus is 1/2 the outer diameter of the fuel pellet. Fuel assemblies are placed in the core to establish favorable axial and radial power distributions. 98-01

Figure 4.3-1 shows a typical fuel loading pattern. The feed fuel is loaded in a checkerboard pattern among the burned fuel to provide a flat radial power distribution. Burned fuel is placed on the core periphery to reduce neutron leakage. The cores will operate for approximately 18 months between refueling, accumulating approximately 18,000 MWD/MTU burnup. The exact reloading pattern, initial and final positions of assemblies, number of fresh assemblies and their placement are dependent on the energy requirement for the next cycle and burnup and power histories of the previous cycles. 98-01

The core average enrichment is determined by the amount of fissionable material required to provide the desired core lifetime and energy requirements. The physics of the burnout process is such that operation of the reactor depletes the amount of fuel available due to the absorption of neutrons by the U-235 atoms and their subsequent fission. The rate of U-235 depletion is directly proportional to the power level at which the reactor is operated. In addition, the fission process results in the formation of fission products, some of which readily absorb neutrons. These effects, depletion and buildup of fission products, are partially offset by the buildup of plutonium shown in Figure 4.3-2 for a typical 17 x 17 fuel assembly, which occurs due to the non-fission absorption of neutrons in U-238. Therefore, at the beginning of any cycle a reactivity reserve equal to the depletion of the fissionable fuel and the buildup of fission product poisons over the specified cycle life must be incorporated in the reactor design. This excess reactivity is controlled by removable neutron absorbing material in the form of boron dissolved in the primary coolant and boride absorber coated fuel pellets and/or burnable absorber rods.

The concentration of boric acid in the primary coolant is varied to provide control and to compensate for long term reactivity requirements. The concentration of the soluble neutron absorber is varied to compensate for reactivity changes due to fuel burnup, fission product poisoning including xenon and samarium, burnable absorber depletion, and the cold-to-operating moderator temperature change. Using its normal makeup path, the chemical and volume control system (CVCS) is capable of inserting negative reactivity at a rate of approximately 30 pcm/min when the reactor coolant boron concentration is 1000 ppm and approximately 35 pcm/min when the reactor coolant boron concentration is 100 ppm. If the emergency boration path is used, the CVCS is capable of inserting negative reactivity at a rate of approximately 65 pcm/min when the reactor coolant concentration is 1000 ppm and approximately 75 pcm/min when the reactor coolant boron concentration is 100 ppm. The peak burnout rate for xenon is 25 pcm/min (Section 9.3.4.3.1 discusses the capability of the CVCS to counteract xenon decay). Rapid transient reactivity requirements and safety shutdown requirements are met with control rods.

As the boron concentration is increased, the moderator temperature coefficient becomes less negative. The use of a soluble absorber alone would result in a positive moderator coefficient at beginning of life for the first cycle. Therefore, burnable absorber rods are used to reduce the soluble boron concentration sufficiently to ensure that the moderator temperature coefficient is negative for power operating conditions. During operation the absorber content in these rods is depleted thus adding positive reactivity to offset some of the negative reactivity from fuel depletion and fission product buildup. The depletion rate of the burnable absorber rods is not critical since chemical shim is always available and flexible enough to cover any possible deviations in the expected burnable absorber depletion rate. Figure 4.3-3 is a graph of critical boron concentration versus cycle burnup for a typical transition core and an equilibrium core.

98-01

In addition to reactivity control, the burnable absorbers are strategically located to provide a favorable radial power distribution. Figure 4.3-4 shows the burnable absorber distributions within a fuel assembly for the several integral fuel burnable absorber pin patterns used in a 17 x 17 array. A typical burnable absorber loading pattern to be used in the core is shown in Figure 4.3-5.

Tables 4.3-1 through 4.3-3 contain a summary of the reactor core design parameters for typical reload cycles including reactivity coefficients, delayed neutron fractions and neutron lifetimes. Sufficient information is included to permit an independent calculation of the nuclear performance characteristics of typical reload cores.

4.3.2.2 Power Distributions

The accuracy of power distribution calculations has been confirmed through approximately 1000 flux maps during some 20 years of operation under conditions very similar to those expected for the Virgil C. Summer Nuclear Station. Details of this confirmation are given in Reference [5] and in Section 4.3.2.2.6.

4.3.2.2.1 Definitions

Power distributions are quantified in terms of hot channel factors. These factors are a measure of the peak pellet power within the reactor core and the total energy produced in a coolant channel and are expressed in terms of quantities related to the nuclear or thermal design namely:

Power density is the thermal power produced per unit volume of the core (kW/liter).

Linear power density is the thermal power produced per unit length of active fuel (kW/ft). Since fuel assembly geometry is standardized this is the unit of power density most commonly used. For all practical purposes it differs from kW/liter by a constant factor which includes geometry and the fraction of the total thermal power which is generated in the fuel rod.

Average linear power density is the total thermal power produced in the fuel rods divided by the total active fuel length of all rods in the core.

Local heat flux is the heat flux at the surface of the cladding ($Btu\text{-}ft^{2}\text{-}hr^{1}$). For nominal rod parameters this differs from linear power density by a constant factor.

Rod power or rod integral power is the length integrated linear power density in 1 rod (kW).

Average rod power is the total thermal power produced in the fuel rods divided by the number of fuel rods (assuming all rods have equal length).

The hot channel factors used in the discussion of power distributions in this section are defined as follows:

F_Q, Heat Flux Hot Channel Factor, is defined as the maximum local heat flux on the surface of a fuel rod divided by the average fuel rod heat flux, allowing for manufacturing tolerances on fuel pellets and rods.

F_Q^N, Nuclear Heat Flux Hot Channel Factor, is defined as the maximum local fuel rod linear power density divided by the average fuel rod linear power density, assuming nominal fuel pellet and rod parameters.

F_Q^E, Engineering Heat Flux Hot Channel Factor, is the allowance on heat flux required for manufacturing tolerances. The engineering factor allows for local variations in enrichment, pellet density and diameter, surface area of the fuel rod and eccentricity of the gap between pellet and clad.

Combined statistically the net effect is a factor of 1.03 to be applied to fuel rod surface heat flux.

$F_{\Delta H}^N$, Nuclear Enthalpy Rise Hot Channel Factor, is defined as the ratio of the integral of linear power along the rod with the highest integrated power to the average rod power.

Manufacturing tolerances, hot channel power distribution and surrounding channel power distributions are treated explicitly in the calculation of the DNBR described in Section 4.4.

It is convenient for the purposes of discussion to define subfactors of F_Q, however, design limits are set in terms of the total peaking factor.

F_Q = Total peaking factor or heat flux hot channel factor

$$= \frac{\text{MaximumkW/ft}}{\text{AveragekW/ft}}$$

without densification effects:

$$F_Q = F_Q^N \times F_Q^E$$

$$= F_{XY}^N \times F_Z^N \times F_U^N \times F_Q^E$$

Where:

F_Q^N and F_Q^E are defined above.

F_U^N = factor for conservatism, assumed to be 1.05.

F_{XY}^N = ratio of peak power density to average power density in the horizontal plane of peak local power.

F_Z^N = ratio of the power per unit core height in the horizontal plane of peak local power to the average value of power per unit core height. If the plane of peak local power coincides with the plane of maximum power per unit core height then F_Z^N is the core average axial peaking factor.

To include the allowances made for densification effects, which are height dependent, the following quantities are defined.

S(Z) = the allowance made for densification effects at height Z in the core (see Section 4.3.2.2.5).

P(Z) = ratio of the power per unit core height in the horizontal plane at height Z to the average value of power per unit core height.

Then:

F_Q = Total peaking factor

$$F_Q = \frac{\text{Maximum kW/ft}}{\text{Average kW/ft}}$$

Including densification allowance:

$F_Q = \max\ (F^N_{XY}(Z) x P(Z) x S(Z) x F^N_U x F^E_Q$

4.3.2.2.2 Radial Power Distributions

The power shape in horizontal sections of the core at full power is a function of the fuel and burnable absorber loading patterns, and the presence or absence of a single bank of control rods. Thus, at any time in the cycle any horizontal section of the core can be characterized as unrodded or with group D control rods. These two situations combined with burnup effects determine the radial power shapes which can exist in the core at full power. The effect on radial power shapes of power level, xenon, samarium and moderator density effects are also considered but these are quite small. The effect of nonuniform flow distribution is negligible. While radial power distributions in various planes of the core are often illustrated, the core radial enthalpy rise distribution, as determined by the integral of power up each channel, is of greater interest. For representative operating conditions, Figures 4.3-6 through 4.3-10 show representative radial power distributions for 1/4 of the core for a transition cycle. These conditions are; 1) Hot Full Power (HFP) at Beginning of Life (BOL) - unrodded - no xenon, 2) HFP at BOL - unrodded - equilibrium xenon, 3) HFP at BOL - Bank D at the HFP insertion limit in - equilibrium xenon, 4) HFP at Middle of Life (MOL) - unrodded - equilibrium xenon, and 5) HFP at End of Life (EOL) - unrodded - equilibrium xenon. Figures 4.3-11 through 4.3-15 show the same information for a typical equilibrium reload. 98-01

Since the position of the hot channel varies from time to time, a single reference radial design power distribution is selected for DNB calculations. This reference power distribution is chosen conservatively to concentrate power in one area of the core, minimizing the benefits of flow redistribution. Assembly powers are normalized to core average power.

4.3.2.2.3 Assembly Power Distributions

For the purpose of illustration, rodwise power distributions for a typical assembly for BOL and EOL conditions are shown in Figures 4.3-16 and 4.3-17, respectively.

Since the detailed power distribution surrounding the hot channel varies from time to time, a conservatively flat assembly power distribution is assumed in the DNB analysis, described in Section 4.4, with the rod of maximum integrated power artificially raised to the design value of $F^N_{\Delta H}$.

Care is taken in the nuclear design of all fuel cycles and all operating conditions to ensure that a flatter assembly distribution does not occur with limiting values of $F^N_{\Delta H}$.

4.3.2.2.4 Axial Power Distributions

The shape of the power profile in the axial or vertical direction is largely under the control of the operator either through the manual operation of the control rods or automatic motion of the rods responding to manual operation of the CVCS. Nuclear effects which cause variations in the axial power shape include moderator density, Doppler effect on resonance absorption, spatial xenon, burnup and distribution of fuel and burnable absorber material. Automatically controlled variations in total power output and full length rod motion are also important in determining the axial power shape at any time. Signals are available to the operator from the excore ion chambers which are long ion chambers outside the reactor vessel running parallel to the axis of the core. Separate signals are taken from the top and bottom halves of the chambers. The difference between top and bottom signals from each of 4 pairs of detectors is displayed on the control panel and called the flux difference, ΔI. Calculations of core average peaking factor for many plants and measurements from operating plants under many operating situations are associated with either ΔI or axial offset in such a way that an upper bound can be placed on the peaking factor. For these correlations axial offset is defined as:

$$\text{axial offset} = \frac{\Phi_t - \Phi_b}{\Phi_t + \Phi_b}$$

and Φ_t and Φ_b are the top and bottom detector readings.

Representative axial power shapes for a typical transition and a fully transitioned core for BOL, MOL, and EOL conditions are displayed in Figures 4.3-18 through 4.3-20. 98-01

4.3.2.2.5 Local Power Peaking

Fuel densification, which has been observed to occur under irradiation in several operating reactors, causes the fuel pellets to shrink both axially and radially. The pellet shrinkage combined with random hang-up of fuel pellets results in gaps in the fuel column when the pellets below the hung-up pellet settle in the fuel rod. The gaps vary in length and location in the fuel rod. Because of decreased neutron absorption in the vicinity of the gap, power peaking occurs in the adjacent fuel rods resulting in an increased power peaking factor. A quantitative measure of this local peaking is given by the power spike factor S(Z) where Z is the axial location in the core.

The method used to compute the power spike factor is described in Reference [7] and is summarized in Figure 4.3-22. The information flow outlined in Figure 4.3-22 is as follows:

1. The probability that an axial gap of a certain size will occur at a given location in the core is determined from fuel performance data.

2. The magnitude of the power spike caused by a single axial gap of a certain size is determined from nuclear calculations as shown in Figure 4.3-23. This curve is valid for uranium fuel enrichments up to 4.5 w/o.

3. For each axial interval to be analyzed, axial gap occurrence probabilities and the single event power spikes are entered into the DRAW [7] computer code. The code produces a curve of power spike versus probability of exceeding power spike for each elevation in the core. The power census for a core is then statistically combined with the power spike probability curve to obtain a power spike penalty for the core such that less than 1 rod will exceed F_Q^N at 95% confidence level.

The power spike factor due to densification is assumed to be a local perturbation applicable to overpower transients. Thus, densification affects F_Q but not $F_{\Delta H}$. The magnitude of the increased power peaking increases from no effect at the bottom of the core to a few percent at the top of the core as shown in Figure 4.3-24, which is applicable to the nominal 95% (geometric) dense pellets.

For fuel produced by processes other than those for which Reference [7] is applicable, specifications will be followed to ensure that the effects of densification will be no greater than has been allowed for in the design. The specifications for quantifying the extent of densification will be based on the NRC report on fuel densification (Reference [33]).

Results reported in a Westinghouse Topical Report concerning the spike penalty in LOCA analysis (Reference [8]) show that the power spike penalty should not be included in the LOCA envelope.

4.3.2.2.6 Limiting Power Distributions

According to the ANS classification of plant conditions (see Chapter 15.0), Condition I occurrences are those which are expected frequently or regularly in the course of power operation, maintenance, or maneuvering of the plant. As such, Condition I occurrences are accommodated with margin between any plant parameter and the value of that parameter which would require either automatic or manual protective action. Inasmuch as Condition I occurrences occur frequently or regularly, they must be considered from the point of view of affecting the consequences of fault conditions (Conditions II, III, and IV). In this regard, analysis of each fault condition described is generally based on a conservative set of initial conditions corresponding to the most adverse set of conditions which can occur during Condition I operation.

The list of steady-state and shutdown conditions, permissible deviations (such as 1 coolant loop out of service), and operational transients is given in Section 15.1. Implicit in the definition of normal operation is proper and timely action by the reactor operator. That is, the operator follows recommended operating procedures for maintaining appropriate power distributions and takes any necessary remedial actions when alerted to do so by the plant instrumentation. Thus, as stated above, the worst or limiting power distribution which can occur during normal operation is to be considered as the starting point for analysis of ANS Conditions II, III, and IV events.

Improper procedural actions or errors by the operator are assumed in the design as occurrences of moderate frequency (ANS Condition II). Some of the consequences which might result are listed in Section 15.2. Therefore, the limiting power shapes which result from such Condition II events, are those power shapes which deviate from the normal operating condition at the recommended axial offset band, e.g., due to lack of proper action by the operator during a xenon transient following a change in power level brought about by control rod motion. Power shapes which fall in this category are used for determination of the reactor protection system setpoints so as to maintain margin to overpower or DNB limits.

The means for maintaining power distributions within the required hot channel factor limits are described in the Technical Specifications. A complete discussion of power distribution control in Westinghouse PWRs is included in Reference [9]. Detailed background information on the design constraints on local power density in a Westinghouse PWR, on the defined operating procedures and on the measures taken to preclude exceeding design limits is presented in the Westinghouse Topical Reports and power distribution control and load following procedures (Reference [10]). The following paragraphs summarize these reports and describe the calculations used to establish the upper bound on peaking factors.

The calculations used to establish the upper bound on peaking factors, F_Q and $F_{\Delta H}$, include all of the nuclear effects which influence the radial and/or axial power distributions throughout core life for various modes of operation including load follow, reduced power operation, and axial xenon transients.

Radial power distributions are calculated for the full power condition and fuel and moderator temperature feedback effects are included for the average enthalpy plane of the reactor. The steady-state nuclear design calculations are done for normal flow with the same mass flow in each channel and flow redistribution effects neglected. The effect of flow redistribution is calculated explicitly where it is important in the DNB analysis of accidents. The effect of xenon on radial power distribution is small (compare Figures 4.3-6 and 4.3-7) but is included as part of the normal design process. Radial power distributions are relatively fixed and easily bounded with upper limits.

The core average axial profile, however, can experience significant changes which can occur rapidly as a result of rod motion and load changes and more slowly due to xenon distribution. For the study of points of closest approach to axial power distribution limits, several thousand cases are examined. Since the properties of the nuclear design dictate what axial shapes can occur, boundaries on the limits of interest can be set in terms of the parameters which are readily observed on the plane. Specifically, the nuclear design parameters which are significant to the axial power distribution analysis are:

1. Core power level

2. Core height

3. Coolant temperature and flow

4. Coolant temperature program as a function of reactor power

5. Fuel cycle lifetimes

6. Rod bank worths

7. Rod bank overlaps

Normal operation of the plant assumes compliance with the following conditions:

1. Control rods in a single bank move together with no individual rod insertion differing by more than 13 steps (indicated) from the bank demand position;

2. Control banks are sequenced with overlapping banks;

3. The control bank insertion limits are not violated;

4. Axial power distribution procedures, which are given in terms of flux difference control and control bank position, are observed.

The axial power distribution procedures referred to above are part of the required operating procedures which are followed in normal operation. Briefly, they require control of the axial offset (flux difference divided by fractional power) at all power levels within a permissible operating band.

Calculations are performed for normal operation of the reactor beginning, middle, and end of cycle conditions. Different histories of operation are implicitly included in the methodology. These different histories assume base loaded operation and extensive load following.

These cases represent many possible reactor states in the life of 1 fuel cycle. The cases are described in detail in Reference [10] and they are considered to be necessary and sufficient to generate a local power density limit which, when increased by 5% for conservatism, will not be exceeded with a 95% confidence level. Many of the points do not approach the limiting envelope, however they are generated as part of the process which lead to the shapes which do define the envelope.

It is not possible to single out any transient or steady-state condition which defines the most limiting case. It is not even possible to separate out a small number which form an adequate analysis. The process of generating a myriad of shapes is essential to the philosophy that leads to the required level of confidence. A set of parameters that produce a limiting case for 1 reactor fuel cycle, (defined as approaching the line of Figure 4.3-25) is not necessarily a limiting case for another reactor or fuel cycle with different control bank worths, enrichments, burnup, reactivity coefficients, etc. Each shape depends on the detailed history of operation up to that time and on the manner in which xenon was conditional in the days immediately prior to the time at which the power distribution is calculated. 98-01

The calculated points are synthesized from axial calculations combined with radial factors appropriate for rodded and unrodded planes. In these calculations the effects on the radial peak of xenon redistribution that occurs following the withdrawal of a control bank (or banks) from a rodded region is obtained from three-dimensional calculations. The factor applied on the unrodded radial peak is obtained from calculations in which the xenon distribution is preconditioned by the presence of control rods and then allowed to redistribute for several hours. A detailed discussion of this effect may be found in References [10] and [11]. The calculated values are increased by a factor of 1.05 for conservatism and a factor of 1.03 for the engineering factor F_Q^E.

The envelope drawn over the calculated ([F_Q • Power] max) points in Figure 4.3-25 represents an upper bound envelope on local power density versus elevation in the core. It should be emphasized that this envelope is a conservative representation of the bounding values of local power density. Expected values are considerably smaller and, in fact, less conservative bounding values may be justified with additional analysis or surveillance requirements. For example, Figure 4.3-25 bounds BOL, MOL, and EOL conditions. Figure 4.3-25 is based on a radial power distribution invariant with core elevation.

Finally, as previously discussed, this upper bound envelope is based on operation within an allowed range of axial flux difference limits. These limits are detailed in the Technical Specifications and are predicted only upon excore surveillance supplemented by the periodic full core map requirement and by computer based alarms on deviation and time of deviation from the allowed flux difference band. An alternative to performing the periodic full core flux map while above 25% RTP is to use the BEACON Power Distribution Monitoring System, Reference [37]. 02-01

Allowing for fuel densification effects, the average kW/ft at 2900 MWt is 5.69 kW/ft. From Figure 4.3-25, the conservative upper bound value of normalized local power density, including uncertainty allowances, is 2.45 corresponding to a peak local power density of 14.2 kW/ft at 102% of 2900 MWt.

To determine reactor protection system setpoints, with respect to power distributions, 3 categories of events are considered, namely rod control equipment malfunctions, operator errors of commission and operator errors of omission. In evaluating these 3 categories of events, the core is assumed to be operating within the 4 constraints described above.

The first category comprises uncontrolled rod withdrawal (with rods moving in the normal bank sequence). Also included are motions of the control banks below their insertion limits, which could be caused, for example, by uncontrolled dilution or primary coolant cooldown. Power distributions were calculated throughout these occurrences assuming short term corrective action, that is, no transient xenon effects were considered to result from the malfunction. The event was assumed to occur from typical normal operating situations which did not include normal xenon transients. It was further assumed in determining the power distributions that total power level would be limited by reactor trip to below 118%. Results are given in Figure 4.3-26 in units of kW/ft. The peak power density which can occur in such events, assuming reactor trip at or below 118%, is less than that required for center-line melt including uncertainties and densification effects.

As shown in Figure 4.3-26, the maximum linear heat generation rate does not exceed 16 kW/ft. For the uncontrolled RCCA bank withdrawal from subcritical accident, which starts from zero power, the reactor reaches prompt critical causing the nuclear flux to briefly rise to several times full power. Therefore, the linear heat generation rate instantaneously rises to a high value and then decreases.

For rapid transients such as the RCCA withdrawal from subcritical accident, in order to determine that the fuel temperature criterion is not exceeded (peak fuel temperature less than 4700°F), a transient heat transfer calculation must be performed. The peak fuel centerline temperature during the transient conservatively evaluated at the hot spot did not exceed 4000°F. This is below the limiting value of 4700°F, and is equivalent to a steady-state peak linear heat generation rate of only 18 kW/ft.

The second category, also appearing in Figure 4.3-26, assumes that the operator mispositions the control rod bank in violation of the insertion limits and creates short term conditions not included in normal operating conditions.

The third category assumes that the operator fails to take action to correct a flux difference violation. The results shown on Figure 4.3-27 are F_Q multiplied by 102% power including an allowance for calorimetric error. The figure shows that provided the assumed error in operation does not continue for a period which is long compared to the xenon time constant, the maximum local power does not exceed 22.8 kW/ft including the above factors.

Analyses of possible operating power shapes for the reactor described herein show that the appropriate hot channel factors F_Q and $F^N_{\Delta H}$ for peak local power density and for DNB analysis at full power are the values given in Table 4.3-2 and addressed in the Technical Specifications.

F_Q can be increased with decreasing power as shown in the Technical Specifications. Increasing $F^N_{\Delta H}$ with decreasing power is permitted by the DNB protection setpoints and allows radial power shape changes with rod insertion to the insertion limits as described in Section 4.4.3.2. The allowance for increased $F^N_{\Delta H}$ permitted is $F^N_{\Delta H} = (1.62)[1 + 0.3(1-P)]$ (1) where P is the fraction of allowed power level. This becomes a design basis criterion which is used for establishing acceptable control rod patterns and control bank sequencing. Likewise fuel loading patterns for each cycle are selected with consideration of this design criterion. The worst values of $F^N_{\Delta H}$ for possible rod configurations occurring in normal operation are used in verifying that this criterion is met. Typical radial factors are given in Table 4.3-2 and the radial power distributions are shown in Figures 4.3-6 through 4.3-15. The worst values generally occur when the rods are assumed to be at their insertion limits. As discussed in Section 3.2 of Reference [12], it has been determined that provided the above Conditions 1 through 4 are observed, the Technical Specification limits, are met. These limits are taken as input to the thermal-hydraulic design basis as described in Section 4.4.3.2.1. When a situation is possible in normal operation which could result in local power densities in excess of those assumed as the pre-condition for a subsequent hypothetical accident, but which would not itself cause fuel failure, administrative controls and alarms are provided for returning the core to a safe condition. These alarms are described in detail in Chapters 7.0 and Technical Specifications. 02-01

4.3.2.2.7 Experimental Verification of Power Distribution Analysis 00-01

This subject is discussed in depth in Reference [5]. A summary of this report is given here.

In a measurement of peak local power density, F_Q, with the movable detector system described in Sections 7.7.1 and 4.4.5, the following uncertainties have to be considered:

1. Reproducibility of the measured signal,

2. Errors in the calculated relationship between detector current and local flux,

3. Errors in the calculated relationship between detector flux and peak rod power some distance from the measurement thimble.

---

(1) See Table 4.3-2

The appropriate allowance for category 1 above has been quantified by repetitive measurements made with several inter-calibrated detectors by using the common thimble features of the incore detector system. This system allows more than one detector to access any thimble. Errors in category 2, above, are quantified to the extent possible, by using the fluxes measured at 1 thimble location to predict fluxes at another location which is also measured. Local power distribution predictions are verified in critical experiments on arrays of rods with simulated guide thimbles, control rods, burnable absorber, etc. These critical experiments provide quantification of errors of types 2 and 3, above.

Reference [5] describes critical experiments performed at the Westinghouse Reactor Evaluation Center and measurements taken on 2 Westinghouse plants with incore systems of the same type as used in the Virgil C. Summer Nuclear Station. The report concludes that the uncertainty associated with the peak nuclear heat flux factor, F_Q is 4.58% at the 95% confidence level with only 5% of the measurements greater than the inferred value. This is the equivalent of a 2σ limit on a normal distribution, and is the uncertainty to be associated with a full core flux map with movable detectors reduced with a reasonable set of input data incorporating the influence of burnup on the radial power distribution. The uncertainty is usually rounded up to 5%.

In comparing measured power distributions (or detector currents) against the calculations for the same situation, it is not possible to subtract out the detector reproducibility. Thus a comparison between measured and predicted power distributions has to include some measurement error. Such a comparison is given in Figure 4.3-28 for 1 of the maps used in Reference [5]. Since the first publication of the report, hundreds of maps have been taken on these and other reactors. The results confirm the adequacy of the 5% uncertainty allowance on F_Q.

A similar analysis for the uncertainty in $F_{\Delta H}$ (rod integral power) measurements results in an allowance of 3.65% at the equivalent of a 2σ confidence level. For historical reasons an 8% uncertainty factor is allowed in the nuclear design basis; that is, the predicted rod integrals at full power must not exceed the design $F_{\Delta H}$ less 8%. This 8% may be reduced in final design to 4% to allow a wider range of acceptable axial power distributions in the DNB analysis and still meet the design bases of Section 4.3.1.3.

As an example, a recent measurement in the second cycle of a 121 assembly, 12 foot, core is compared with a simplified one dimensional core average axial calculation in Figure 4.3-29. This calculation does not give explicit representation to the fuel grids.

The accumulated data on power distributions in actual operation is basically of 3 types:

1. Much of the data is obtained in steady-state operation at constant power in the normal operating configuration;

2. Data with unusual values of axial offset are obtained as part of the excore detector calibration exercise which is performed monthly;

3. Special tests have been performed in load follow and other transient xenon conditions which have yielded useful information on power distributions.

These data are presented in detail in Reference [10]. Figure 4.3-30 contains a summary of measured values of F_Q as a function of axial offset for 5 plants from that report.

4.3.2.2.8 Testing

A very extensive series of physics tests is performed on first cores. These tests and the criteria for satisfactory results are described in detail in Chapter 14.0. Since not all limiting situations can be created at BOL, the main purpose of the tests is to provide a check on the calculational methods used in the predictions for the conditions of the test.

4.3.2.2.9 Monitoring Instrumentation

The adequacy of instrument numbers, spatial deployment, required correlations between readings and peaking factors, calibration, and errors are described in References [5], [9], and [12]. The relevant conclusions are summarized here in Sections 4.3.2.2.7 and 4.4.5.

Provided the limitations given in Section 4.3.2.2.6 on rod insertion and flux difference are observed, the excore detector system provides adequate monitoring of power distributions.

Further details of specific limits on the observed rod positions and flux difference are given in the Technical Specifications together with a discussion of their bases.

Limits for alarms, reactor trip, etc. are given in the Technical Specifications. Descriptions of the systems provided are given in Section 7.7.

4.3.2.3 Reactivity Coefficients

The kinetic characteristics of the reactor core determine the response of the core to changing plant conditions or to operator adjustments made during normal operation, as well as the core response during abnormal or accidental transients. These kinetic characteristics are quantified in reactivity coefficients. The reactivity coefficients reflect the changes in the neutron multiplication due to varying plant conditions such as power, moderator or fuel temperatures, or less significantly due to a change in pressure or void conditions. Since reactivity coefficients change during the life of the core, ranges of coefficients are employed in transient analysis to determine the response of the plant throughout life. The results of such simulations and the reactivity coefficients used are presented in Chapter 15.0.

The reactivity coefficients are calculated on a corewise basis by radial and axial diffusion theory methods. The effect of radial and axial power distribution on core average reactivity coefficients is implicit in those calculations and is not significant under normal operating conditions. For example, a skewed xenon distribution which results in changing axial offset by 5% changes the moderator and Doppler temperature coefficients by less than 0.01 pcm/°F and 0.03 pcm/°F, respectively. An artificially skewed xenon distribution which results in changing the radial $F_{\Delta H}$ by 3% changes the moderator and Doppler temperature coefficients by less than 0.03 pcm/°F and 0.001 pcm/°F, respectively. The spatial effects are accentuated in some transient conditions; for example, in postulated rupture of the main steamline break and rupture of rod cluster control assembly mechanism housing described in Sections 15.4.2 and 15.4.6, and are included in these analyses.

The analytical methods and calculational models used in calculating the reactivity coefficients are given in Section 4.3.3. These models have been confirmed through extensive testing of more than 30 cores similar to the plant described herein; results of these tests are discussed in Section 4.3.3.

Quantitative information for calculated reactivity coefficients, (density, temperature, pressure, void) and power coefficient is given in the following sections.

4.3.2.3.1 Fuel Temperature (Doppler) Coefficient

The fuel temperature (Doppler) coefficient is defined as the change in reactivity per degree change in effective fuel temperature and is primarily a measure of the Doppler broadening of U-238 and Pu-240 resonance absorption peaks. Doppler broading of other isotopes such as U-236, Np-237, etc. are also considered, but their contributions to the Doppler effect is small. An increase in fuel temperature increases the effective resonance absorption cross sections of the fuel and produces a corresponding reduction in reactivity.

The fuel temperature coefficient is calculated by performing 2-group two or three dimensional calculations. Moderator temperature is held constant and the power level is varied. Spatial variation of fuel temperature is taken into account by calculating the effective fuel temperature as a function of power density as discussed in Section 4.3.3.1.

Typical Doppler temperature coefficients are shown in Figure 4.3-31 as a function of the effective fuel temperature (at BOL and EOL conditions). The effective fuel temperature is lower than the volume averaged fuel temperature since the neutron flux distribution is non-uniform through the pellet and gives preferential weight to the surface temperature. The Doppler-only contribution to the power coefficient, defined later, is shown in Figure 4.3-32 as a function of relative core power. The integral of the differential curve on Figure 4.3-32 is the Doppler contribution to the power defect and is shown in Figure 4.3-33 as a function of relative power. The Doppler coefficient becomes more negative as a function of life as the Pu-240 content increases, thus increasing the Pu-240 resonance absorption but less negative as the fuel temperature changes with burnup as described in Section 4.3.3.1. The upper and lower limits of Doppler coefficient used in accident analyses are given in Chapter 15.0.

4.3.2.3.2 Moderator Coefficients

The moderator coefficient is a measure of the change in reactivity due to a change in specific coolant parameters such as density, temperature, pressure or void. The coefficients obtained are moderator density, temperature, pressure, and void coefficients.

4.3.2.3.2.1 Moderator Density and Temperature Coefficients

The moderator temperature (density) coefficient is defined as the change in reactivity per degree change in the moderator temperature. Generally, the effect of the changes in moderator density as well as the temperature are considered together. A decrease in moderator density means less moderation which results in a negative moderator coefficient. An increase in coolant temperature, keeping the density constant, leads to a hardened neutron spectrum and results in an increase in resonance absorption in U-238, Pu-240 and other isotopes. The hardened spectrum also causes a decrease in the fission-to-capture ratio in U-235 and Pu-239. Both of these effects make the moderator coefficient more negative. Since water density changes more rapidly with temperature as temperature increases, the moderator temperature (density) coefficient becomes more negative with increasing temperature.

The soluble boron used in the reactor as a means of reactivity control also has an effect on moderator density coefficient since the soluble boron absorber density, as well as, the water density is decreased when the coolant temperature rises. A decrease in the soluble absorber concentration introduces a positive component in the moderator coefficient.

Thus, if the concentration of soluble absorber is large enough, the net value of the coefficient may be positive. With the burnable absorber rods present, however, the initial hot boron concentration is sufficiently low that the moderator temperature coefficient is negative at full power operating conditions. The effect of control rods is to make the moderator coefficient more negative by reducing the required soluble boron concentration and by increasing the "leakage" of the core.

With burnup, the moderator coefficient becomes more negative primarily as a result of boric acid dilution but also to a significant extent from the effects of the buildup of plutonium and fission products.

The moderator coefficient is calculated for the various plant conditions discussed above by performing 2-group two or three dimensional calculations, varying the moderator temperature (and density) by about ± 5°F about each of the mean temperatures. The moderator coefficient is shown as a function of core temperature and boron concentration for the unrodded and rodded core in Figures 4.3-34 through 4.3-36. The temperature range covered is from cold (68°F) to about 600°F. The contribution due to Doppler coefficient (because of change in moderator temperature) has been subtracted from these results. Figure 4.3-37 shows the hot, full power moderator temperature coefficient plotted as a function of cycle lifetime at the critical boron concentration for a transition cycle and a typical equilibrium reload cycle.

The moderator coefficients presented here are calculated on a corewise basis, since they are used to describe the core behavior in normal and accident situations when the moderator temperature changes can be considered to affect the whole core.

4.3.2.3.2.2 Moderator Pressure Coefficient

The moderator pressure coefficient relates the change in moderator density, resulting from a reactor coolant pressure change, to the corresponding effect on neutron production. This coefficient is much less significant in comparison with the moderator temperature coefficient. A change of 50 psi in pressure has approximately the same effect on reactivity as a half-degree change in moderator temperature. This coefficient can be determined from the moderator temperature coefficient by relating change in pressure to the corresponding change in density. The moderator pressure coefficient is negative over a portion of the moderator temperature range at BOL (-0.004 pcm/psi, BOL) but is always positive at operating conditions and becomes more positive during life (+0.5 pcm/psi, EOL).

4.3.2.3.2.3 Moderator Void Coefficient

The moderator void coefficient relates the change in neutron multiplication to the presence of voids in the moderator. In a PWR this coefficient is not very significant because of the low void content in the coolant. The core void content is less than 1/2 of 1% and is due to local or statistical boiling. The void coefficient varies from 50 pcm/percent void at BOL, and at low temperatures to -250 pcm/percent void at EOL and at operating temperatures. The negative void coefficient at operating temperature becomes more negative with fuel burnup.

4.3.2.3.3 Power Coefficient

The combined effect of moderator temperature and fuel temperature change as the core power level changes is called the total power coefficient and is expressed in terms of reactivity change per percent power change. The power coefficient at BOL and EOL conditions for a typical reload cycle is given in Figure 4.3-38.

It becomes more negative with burnup reflecting the combined effect of moderator and fuel temperature coefficients with burnup. The power defect (integral reactivity effect) at BOL and EOL for a typical reload cycle is given in Figure 4.3-39.

4.3.2.3.4 Comparison of Calculated and Experimental Reactivity Coefficients

Section 4.3.3 describes the comparison of calculated and experimental reactivity coefficients in detail. Based on the data presented there, the accuracy of the current analytical model is:

± 0.2% $\Delta\rho$ for Doppler and power defect
± 2 pcm/°F for the moderator coefficient

Experimental evaluation of the calculated coefficients is done during the physics startup testing described in Chapter 14.0.

4.3.2.3.5 Reactivity Coefficients Used in Transient Analysis

Table 4.3-2 gives the representative ranges for the reactivity coefficients used in transient analysis. The exact values of the coefficient used in the analysis depend on whether the transient of interest is examined at the BOL or EOL, whether most negative or the most positive (least negative) coefficients are appropriate, and whether spatial nonuniformity must be considered in the analysis. Conservative values of coefficients, considering various aspects of analysis are used in the transient analysis. This is completely described in Chapter 15.0.

The values listed in Table 4.3-2 and illustrated in Figures 4.3-31 through 4.3-39 apply to the core described in Table 4.3-1. The coefficients appropriate for use in subsequent cycles depends on the core's operating history, the number and enrichment of fresh fuel assemblies, the loading pattern of burned and fresh fuel, the type, number and location of any absorbers rods, etc. The need for a re-evaluation of any accident in a subsequent cycle is contingent upon whether or not the coefficients for that cycle fall within the identified range used in the analysis presented in Chapter 15.0 with due allowance for the calculational uncertainties given in Section 4.3.3.3. Control rod requirements are given in Table 4.3-3 for a typical reload cycle.

4.3.2.4 Control Requirements

To ensure the shutdown margin stated in the Technical Specifications under conditions where a cooldown to ambient temperature is required, concentrated soluble boron is added to the coolant. Boron concentrations for several core conditions are listed in Table 4.3-2. For all core conditions including refueling, the boron concentration is well below the solubility limit. The rod cluster control assemblies are employed to bring the reactor to the hot shutdown condition. The minimum required shutdown margin is given in the Technical Specifications.

The ability to accomplish the shutdown for hot conditions is demonstrated in Table 4.3-3 by comparing the difference between the rod cluster control assembly reactivity available with an allowance for the worst stuck rod with that required for control and protection purposes. The shutdown margin includes an allowance of 10% for analytic uncertainties (see Section 4.3.2.4.9). The largest reactivity control requirement appears at the EOL when the moderator temperature coefficient reaches its peak negative value as reflected in the larger power defect.

The control rods are required to provide sufficient reactivity to account for the power defect from full power to zero power and to provide the required shutdown margin. The reactivity addition resulting from power reduction consists of contributions from Doppler, variable average moderator temperature, flux redistribution, and reduction in void content as discussed below.

4.3.2.4.1 Doppler

The Doppler effect arises from the broadening of U-238 and Pu-240 resonance peaks with an increase in effective pellet temperature. This effect is most noticeable over the range of zero power to full power due to the large pellet temperature increase with power generation.

4.3.2.4.2 Variable Average Moderator Temperature

When the core is shutdown to the hot, zero power condition, the average moderator temperature changes from the equilibrium full load value determined by the steam generator and turbine characteristics (steam pressure, heat transfer, tube fouling, etc.) to the equilibrium no load value, which is based on the steam generator shell side design pressure. The design change in temperature is conservatively increased by 4°F to account for the control dead band and measurement errors.

The moderator coefficient becomes more negative as the fuel depletes because the boron concentration is reduced. This effect is the major contributor to the increased requirement at EOL.

4.3.2.4.3 Redistribution

During full power operation the coolant density decreases with core height, and this, together with any partial insertion of control rods, results in less fuel depletion near the top of the core. Under steady-state conditions, the relative power distribution will be slightly asymmetric towards the bottom of the core. On the other hand, at hot zero power conditions, the coolant density is uniform up the core, and there is no flattening due to Doppler. The result will be a flux distribution which at zero power can be skewed toward the top of the core. The reactivity insertion due to the skewed distribution is calculated with an allowance for effects of xenon distribution.

4.3.2.4.4 Void Content

A small void content in the core is due to nucleate boiling at full power. The void collapse coincident with power reduction makes a small reactivity contribution.

4.3.2.4.5 Rod Insertion Allowance

At full power, the control bank is operated within a prescribed band of travel to compensate for small periodic changes in boron concentration, changes in temperature and very small changes in the xenon concentration not compensated for by a change in boron concentration. When the control bank reaches either limit of this band, a change in boron concentration is required to compensate for additional reactivity changes. Since the insertion limit is set by a rod travel limit, a conservatively high calculation of the inserted worth is made which exceeds the normally inserted reactivity.

The rod insertion limits are a function of several design criteria. The usual procedure is to base the insertion limits on the limiting design criteria, which experience has shown to be the required shutdown margin. The remaining criteria, e.g., the $F_{\Delta H}$ design basis and the statically misaligned rod safety criteria, are checked to insure that they are met. For the Virgil C. Summer Nuclear Station, the Technical Specification limit is based on the shutdown criteria and is slightly conservative with respect to the misaligned rod criteria. Therefore, with bank D inserted to its full power insertion limit and 1 RCCA fully withdrawn, the DNB design criteria is met, i.e., minimum DNBR is greater than the design limit.

4.3.2.4.6 Burnup

Excess reactivity is installed at the beginning of each cycle to provide sufficient reactivity to compensate for fuel depletion and fission products throughout the cycle. This reactivity is controlled by the addition of soluble boron to the coolant and by boride absorber coated fuel pellets and/or burnable absorber rods. Typical soluble boron concentration for several core configurations and unit boron worths for reload cycles are given in Table 4.3-2. Since the excess reactivity for burnup is controlled by soluble boron and/or burnable absorbers, it is not included in control rod requirements.

4.3.2.4.7 Xenon and Samarium Poisoning

Changes in xenon and samarium concentrations in the core occur at a sufficiently slow rate, even following rapid power level changes, that the resulting reactivity change is controlled by changing the soluble boron concentration.

4.3.2.4.8 pH Effects

Changes in reactivity due to a change in coolant pH, if any, are sufficiently small in magnitude and occur slowly enough to be controlled by the boron system. Further details are available in Reference [14].

4.3.2.4.9 Experimental Confirmation

Following a normal shutdown, the total core reactivity change during cooldown with a stuck rod has been measured on a 121 assembly 10 foot high core and a 121 assembly 12 foot high core. In each case, the core was allowed to cooldown until it reached criticality simulating the steamline break accident. For the 10 foot core, the total reactivity change associated with the cooldown is overpredicted by about 0.3% $\Delta\rho$ with respect to the measured result. This represents an error of about 5% in the total reactivity change and is about half the uncertainty allowance for this quantity. For the 12 foot core, the difference between the measured and predicted reactivity change was an even smaller 0.2% $\Delta\rho$. These measurements and others demonstrate the ability of the methods described in Section 4.3.3 to accurately predict the total shutdown reactivity of the core.

4.3.2.5 Control

Core reactivity is controlled by means of a chemical absorber dissolved in the coolant, rod cluster control assemblies, and boride absorber coated fuel pellets and/or burnable absorber rods, as described below.

4.3.2.5.1 Chemical Absorber

Boron in solution as boric acid is used to control relatively slow reactivity changes associated with:

1. The moderator temperature defect in going from cold shutdown at ambient temperature to the hot operating temperature at zero power,

2. The transient xenon and samarium poisoning, such as that following power changes or changes in rod cluster control position,

3. The excess reactivity required to compensate for the effects of fissile inventory depletion and buildup of long-life fission products,

4. The burnable absorber depletion.

The boron concentrations for various core conditions are presented in Table 4.3-2.

4.3.2.5.2 Rod Cluster Control Assemblies

The rod cluster control assemblies are used for shutdown and control purposes to offset fast reactivity changes associated with:

1. The required shutdown margin in the hot zero power, stuck rods condition,

2. The reactivity compensation as a result of an increase in power above hot zero power (power defect including Doppler, and moderator reactivity changes),

3. Unprogrammed fluctuations in boron concentration, coolant temperature, or xenon concentration (with rods not exceeding the allowable rod insertion limits),

4. Reactivity ramp rates resulting from load changes.

The allowed control rod bank reactivity insertion is limited at full power to maintain shutdown capability. As the power level is reduced, control rod reactivity requirements are also reduced and more rod insertion is allowed. The control bank position is monitored and the operator is notified by an alarm if the limit is approached. The determination of the insertion limit uses conservative xenon distributions. In addition, the rod cluster control assembly withdrawal pattern determined from these analyses is used in determining power distribution factors and in determining the maximum worth of an inserted rod cluster control assembly ejection accident. For further discussion, refer to the Technical Specifications on rod insertion limits.

Power distribution, rod ejection and rod misalignment analyses are based on the arrangement of the shutdown and control groups of the rod cluster control assemblies shown in Figure 4.3-40. All shutdown rod cluster control assemblies are withdrawn before withdrawal of the control banks is initiated. In going from zero to 100% power, control banks A, B, C, and D are withdrawn sequentially. The limits of rod positions and further discussion on the basis for rod insertion limits are provided in the Technical Specifications.

4.3.2.5.3 Burnable Absorbers

The burnable absorbers (either discrete or integral type) provide partial control of the excess reactivity available during the fuel cycle. In doing so, these rods prevent the moderator temperature coefficient from being positive at normal operating conditions. They perform this function by reducing the requirement for soluble absorber in the moderator at the beginning of the cycle, as described previously. A typical burnable absorber pattern in the core together with the number of rods per assembly is shown in Figure 4.3-5, while the arrangements within an assembly are displayed in Figure 4.3-4. The burnable absorber is depleted with burnup but at a sufficiently slow rate so that the resulting critical concentration of soluble boron is such that the moderator temperature coefficient remains negative at all times for full power operating conditions.

4.3.2.5.4 Peak Xenon Startup

Compensation for the peak xenon buildup is accomplished using the boron control system. Startup from the peak xenon condition is accomplished with a combination of rod motion and boron dilution. The boron dilution may be made at any time, including during the shutdown period, provided the shutdown margin is maintained.

4.3.2.5.5 Load Follow Control and Xenon Control

During load follow maneuvers, power changes are accomplished using control rod motion and dilution or boration by the boron system as required. Control rod motion is limited by the control rod insertion limits as provided in the Technical Specifications and discussed in Sections 4.3.2.5.2 and 4.3.2.5.3. The power distribution is maintained within acceptable limits. Reactivity changes due to the changing xenon concentration can be controlled by rod motion and/or changes in the soluble boron concentration.

4.3.2.5.6 Burnup

Control of the excess reactivity for burnup is accomplished using soluble boron and/or burnable absorber. The boron concentration must be limited during full power operating conditions to ensure the moderator temperature coefficient is negative. Sufficient burnable absorber is installed at the beginning of a cycle to give the desired cycle lifetime without exceeding the boron concentration limit. The practical minimum boron concentration is 10 ppm.

4.3.2.6 Control Rod Patterns and Reactivity Worth

The rod cluster control assemblies are designated by function as the control groups and the shutdown groups. The terms "group" and "bank" are used synonymously throughout this report to describe a particular grouping of control assemblies. The rod cluster assembly pattern is displayed in Figure 4.3-40 which is not expected to change during the life of the plant. The control banks are labeled A, B, C, and D and the shutdown banks are labeled SA, SB, etc., as applicable. Each bank, although operated and controlled as a unit, is comprised of 2 subgroups. The axial position of the rod cluster control assemblies may be controlled manually or automatically. The rod cluster control assemblies are all dropped into the core following actuation of reactor trip signals.

Two (2) criteria have been employed for selection of the control groups. First the total reactivity worth must be adequate to meet the requirements specified in Table 4.3-3. Second, in view of the fact that these rods may be partially inserted at power operation, the total power peaking factor should be low enough to ensure that the power capability requirements are met. Analyses indicate that the first requirement can be met either by a single group or by 2 or more banks whose total worth equals at least the required amount. The axial power shape would be more peaked following movement of a single group of rods worth 3 to 4% $\Delta\rho$; therefore, 4 banks (described as A, B, C, and D in Figure 4.3-40) each worth approximately 1% $\Delta\rho$ have been selected.

The positions of control banks for criticality under any reactor condition is determined by the concentration of boron in the coolant. On an approach to criticality, boron is adjusted to ensure that criticality will be achieved with control rods above the insertion limit set by shutdown and other considerations (see the Technical Specifications). Early in the cycle there may also be a withdrawal limit at low power to maintain a negative moderator temperature coefficient more negative than the Technical Specification limit.

Ejected rod worths are given in Section 15.4.6 for several different conditions. Experimental confirmation of these worths can be found by reference to startup test reports such as Reference [15].

Allowable deviations due to misaligned control rods are discussed in the Technical Specifications.

A representative calculation for 2 banks of control rods withdrawn simultaneously (rod withdrawal accident) is given in Figure 4.3-41.

Calculation of control rod reactivity worth versus time following reactor trip involves both control rod velocity and differential reactivity worth. The rod position versus time of travel after rod release assumed is given in Figure 4.3-42. For nuclear design purposes, the reactivity worth versus rod position is calculated by a series of steady-state calculations at various control rod positions assuming all rods out of the core as the initial position in order to minimize the initial reactivity insertion rate. Also to be conservative, the rod of highest worth is assumed to be stuck out of the core and the flux distribution (and thus reactivity importance) is assumed to be skewed to the bottom of the core. The result of these calculations is shown on Figure 4.3-43.

The shutdown groups provide additional negative reactivity to assure an adequate shutdown margin. Shutdown margin is defined as the amount by which the core would be subcritical at hot shutdown if all rod cluster control assemblies are tripped, but assuming that the highest worth assembly remains fully withdrawn and no changes in xenon or boron take place. The loss of control rod worth due to the material irradiation is negligible since only bank D may be in the core under normal operating conditions.

The values given in Table 4.3-3 show that the available reactivity in withdrawn rod cluster control assemblies provides the design bases minimum shutdown margin allowing for the highest worth cluster to be at its fully withdrawn position. Allowance for uncertainty in the calculated worth of N-1 rods is made before determination of the shutdown margin.

4.3.2.7 Criticality of Fuel Assemblies

Criticality of fuel assemblies outside the reactor is precluded by adequate design of fuel transfer and fuel storage facilities and by administrative control procedures. This section identifies those criteria important to criticality safety analyses. Westinghouse 17 x 17 fuel assemblies (STANDARD, VANTAGE 5, and VANTAGE+) were included in the analyses with the most limiting being assumed in all cases.

4.3.2.7.1 New Fuel Storage

New fuel is normally stored in 21 inch center to center racks in the new fuel storage facility with no water present but which are designed so as to prevent accidental criticality even if unborated water is present. For the flooded condition, assuming new fuel of the highest anticipated enrichment (5.0 w/o U-235) in place, the effective multiplication factor does not exceed 0.95. For the normally dry condition the effective multiplication factor does not exceed 0.98 with new fuel of the highest anticipated enrichment in place, assuming optimum moderation. Credit is taken for the inherent neutron absorbing effect of materials of construction of the racks. RN 14-006

In the analysis for the new fuel storage facilities, the fuel assemblies are assumed to be in their most reactive condition, namely fresh or undepleted and with no control rods or removable neutron absorbers present. Assemblies can not be closer together than the design separation provided by the storage facility except in special cases such as in fuel shipping containers where analyses are carried out to establish the acceptability of the design. The mechanical integrity of the fuel assembly is assumed.

New fuel may also be stored in Region 1 of the spent fuel storage facility, as discussed in Section 4.3.2.7.2.

4.3.2.7.2 Spent Fuel Storage

The high density spent fuel storage racks are designed to assure that a K_{eff} equal to or less than 0.95 is maintained with the racks fully loaded with fuel of the highest anticipated reactivity in each of 2 regions and flooded with unborated water at a temperature corresponding to the highest reactivity. The maximum calculated reactivity is obtained by adding calculational and methodology biases and the statistically combined material and construction tolerances and uncertainties to the nominal reference reactivity. Table 4.3-4 summarizes the biases and statistical uncertainties determined for each spent fuel rack region. The maximum reactivity for each region is less than 0.95 with a 95% probability at a 95% confidence level. RN 03-017

To assure that the true reactivity will always be less than the calculated reactivity, the following conservative assumptions were used to develop the nominal reference reactivity:

1. The effective multiplication factor of an infinite array of fuel assemblies is assumed, except for the assessment of peripheral effects and certain abnormal/accident conditions where neutron leakage is inherent.

2. No credit is taken for spacer grids, spacer grid sleeves, fuel dishing or fuel chamfering.

3. The racks were assumed to be fully loaded with the most reactive fuel authorized to be stored.

4. Depletion calculations assume conservative operating conditions; highest fuel and moderator temperature and an allowance for the soluble boron concentration during in-core operations.

5. All fuel assembly parameters relevant to the criticality analysis are based on the Westinghouse 17 x 17 fuel assembly design (STANDARD, VANTAGE 5, or VANTAGE+) which yields the highest reactivity in each region.

6. For assemblies that use WABAs during in-core depletion, it is assumed that the maximum burnup of the assembly when the WABA is removed is 30 GWD/MTU. RN 03-017

RN 03-017

The moderator is assumed to be pure water (no boron) at a temperature of 68°F and a density of 1.0 gm/cm^3. A reactivity bias is applied to account for the normal range of spent fuel pool water temperatures (39°F to 248°F). A nominal Boral poison material loadings 0.0324 (minimum of 0.0300) grams B-10 per square centimeter are used throughout the lattice for Regions 1 and 2. RN 03-017

The design methods which ensure the criticality safety of the fuel assemblies in the spent fuel storage racks are discussed in Reference [36]. The criticality analysis performed for each of the 2 storage regions produced separate criteria defining the storage limits applicable to each region as follows: RN 03-017

1. Region 1 is designed to accommodate the storage of new and freshly discharged fuel assemblies with a maximum nominal enrichment of 4.95 weight percent U-235.

2. Region 2 is designed to accommodate the storage of fuel assemblies with a maximum nominal initial enrichment of 4.95 weight percent U-235 with a minimum burnup of 41,611 MWD/MTU or fuel of initial enrichment and burnup combinations within the acceptable domain depicted in Figure 4.3-44. RN 03-017

Figure 4.3-44 illustrates, as a function of the initial fuel enrichment, the minimum acceptable burnup which yields the maximum allowable reactivity for Region 2, respectively. This curve is incorporated in the Technical Specifications.

Most accident conditions will not result in an increase in K_{eff} of the spent fuel storage rack. Examples are:

1. Fuel Assembly Drop on Top of Rack - The rack structure pertinent for criticality is not excessively deformed and the dropped assembly which comes to rest horizontally on top of the rack has sufficient water separating it from the active fuel height of stored assemblies to preclude neutronic interaction.

2. Fuel Assembly Drop Between Rack Modules - the design of the spent fuel racks are such that they preclude the insertion of a fuel assembly in other than prescribed locations.

3. Fuel Assembly Drop Between Rack and Wall - the design of the spent fuel racks are such that they preclude the insertion of fuel assembly in other than prescribed locations. RN 03-017

4. Rack Lateral Movement - The racks are constructed with the baseplates extending beyond the edge of the outer cells which assures that the minimum spacing between racks is maintained under all conditions.

5. Bulk Coolant Cooldown - For both regions the moderator temperature coefficient of reactivity is negative. Therefore it is assumed that the moderator is at the temperature (39°F) which results in the highest reactivity, assuring that the true reactivity will always be lower over the expected range of water temperatures.

6. Fuel Assembly Drop into Loaded Cell - For both regions, a vertical impact would at most cause a small compression of the stored assembly, i-educing the water-to-fuel ratio and thereby reducing reactivity. In addition, the distance between the active regions of both assemblies will be more than sufficient to ensure no neutron interaction.

7. Fuel Assembly Drop into Empty Cell - For both regions this postulated accident could result in a localized deformation of the rack baseplate, and therefore result in the active fuel height of that assembly no longer being completely covered by the Boral. Such a misalignment of the active fuel height and Boral of up to three inches would cause a negligible increase in reactivity. RN 03-017

One (1) accident can be postulated which could cause reactivity to increase beyond the analyzed condition. It is:

1. Fuel Assembly Misload - For Region 2, this postulated accident would result in an increase in reactivity. The effect of misplacing a single fresh 4.95 weight percent U-235 fuel assembly that has no integral fuel burnable absorbers into the center of a fully loaded rack would have greatest effect. This event could increase reactivity by as much as 0.42 ΔK. To offset this increase, 500 ppm of soluble boron is required to maintain the maximum reactivity less than 0.95.

For occurrences of any of the above postulated accidents, the double contingency principle of ANSI/ANS 8.1-1983 can be applied. This states that one is not required to assume two unlikely, independent, concurrent events to ensure protection against criticality accidents. Thus, for these conditions, the presence of soluble boron in the storage pool water can be assumed as a realistic initial condition since not assuming its presence would be a second unlikely event.

Since the V. C. Summer spent fuel pool boron concentration is maintained at a minimum of 2000 ppm whenever fuel handling operation are active, and since it is expected this level of boron would remain in the pool between outages, should a postulated accident occur which causes reactivity to increase, K_{eff} will be maintained less than or equal to 0.95 due to the negative reactivity effect of the dissolved boron.

4.3.2.8 Stability

4.3.2.8.1 Introduction

The stability of the PWR cores against xenon-induced spatial oscillations and the control of such transients are discussed extensively in References [9], [17], [18], and [19]. A summary of these reports is given in the following discussion and the design bases are given in Section 4.3.1.6.

In a large reactor core, xenon-induced oscillations can take place with no corresponding change in the total power of the core. The oscillation may be caused by a power shift in the core which occurs rapidly in comparison with the xenon-iodine time constants. Such a power shift occurs in the axial direction when a plant load change is made by control rod motion and results in a change in the moderator density and fuel temperature distributions. Such a power shift could occur in the diametral plane of the core as a result of abnormal control action.

Protection against total power instabilities is provided by the control and protection system as described in Section 7.7. Hence, the discussion on the core stability will be limited here to xenon-induced spatial oscillations.

4.3.2.8.2 Stability Index

Power distributions, either in the axial direction or in the X-Y plane, can undergo oscillations due to perturbations introduced in the equilibrium distributions without changing the total core power. The xenon-induced oscillations are essentially limited to the first flux overtones in the current PWRs, and the stability of the core against xenon-induced oscillations can be determined in terms of the eigenvalues of the first flux overtones. Writing, either in the axial direction or in the X-Y plane, the eigenvalue ξ of the first flux harmonic as:

$$\xi = b + ic, \qquad (4.3\text{-}1)$$

then b is defined as the stability index and T = 2n/c as the oscillation period of the first harmonic. The time-dependence of the first harmonic $\delta\phi$ in the power distribution can now be represented as:

$$\delta\phi(t) = Ae^{\xi t} = ae^{bt} \cos ct, \qquad (4.3\text{-}2)$$

where A and a are constants. The stability index can also be obtained approximately by:

$$b = \frac{1}{T} \ln \frac{A_n + 1}{A_n} \qquad (4.3\text{-}3)$$

where A_n A_{n+1} are the successive peak amplitudes of the oscillation and T is the time period between the successive peaks.

4.3.2.8.3 Prediction of the Core Stability

The stability of the core described herein (i.e., with 17 x 17 fuel assemblies) against xenon-induced spatial oscillations is expected to be equal to or better than that of earlier designs. The prediction is based on a comparison of the parameters which are significant in determining the stability of the core against the xenon-induced oscillations, namely; 1) the overall core size is unchanged and spatial power distributions will be similar, 2) the moderator temperature coefficient is expected to be similar at full power, and 3) the Doppler coefficient of reactivity is expected to be similar at full power.

Analysis of both the axial and X-Y xenon transient tests, discussed in Section 4.3.2.8.5, shows that the calculational model is adequate for the prediction of core stability.

4.3.2.8.4 Stability Measurements

1. Axial Measurements

   Two (2) axial xenon transient tests conducted in a PWR with a core height of 12 feet and 121 fuel assemblies is reported in Reference [20] , and will be briefly discussed here. The tests were performed at approximately 10% and 50% of cycle life.

   Both a free-running oscillation test and a controlled test were performed during the first test. The second test at mid-cycle consisted of a free-running oscillation test only. In each of the free-running oscillation tests, a perturbation was introduced to the equilibrium power distribution through an impulse motion of the control Bank D and the subsequent oscillation was monitored to measure the stability index and the oscillation period. In the controlled test conducted early in the cycle, the part length rods were used to follow the oscillations to maintain an axial offset within the prescribed limits. The axial offset of power was obtained from the excore ion chamber readings (which had been calibrated against the incore flux maps) as a function of time for both free-running tests as shown in Figure 4.3-46.

   The total core power was maintained constant during these spatial xenon tests. The stability index and the oscillation period were obtained from a least-square fit of the axial offset data in the form of Equation (4.3-2). The axial offset of power is the quantity that properly represents the axial stability in the sense that it essentially eliminates any contribution from even order harmonics including the fundamental mode. The conclusions of the tests are:

a. The core was stable against induced axial xenon transients both at the core average burnups of 1550 MWD/MTU and 7700 MWD/MTU. The measured stability indices are -0.041 hr^{-1} for the first test (Curve 1 of Figure 4.3-46) and-0.014 hr^{-1} for the second test (Curve 2 of Figure 4.3-46). The corresponding oscillation periods are 32.4 and 27.2 hours, respectively.

b. The reactor core becomes less stable as fuel burnup progresses and the axial stability index was essentially zero at 12,000 MWD/MTU.

2. Measurements in the X-Y Plane

Two (2) X-Y xenon oscillation tests were performed at a PWR plant with a core height of 12 feet and 157 fuel assemblies. The first test was conducted at a core average burnup of 1540 MWD/MTU and the second at a core average burnup of 12,900 MWD/MTU. The X-Y xenon tests show that the core was stable in the X-Y plane at both burnups. The second test shows that the core became more stable as the fuel burnup increased and all Westinghouse PWRs with 121 and 157 assemblies are expected to be stable throughout their burnup cycles.

In each of the 2 X-Y tests, a perturbation was introduced to the equilibrium power distribution through an impulse motion of 1 rod cluster control unit located along the diagonal axis. Following the perturbation, the uncontrolled oscillation was monitored using the movable detector and thermocouple system and the excore power range detectors. The quadrant tilt difference (QTD) is the quantity that properly represents the diametral oscillation in the X-Y plane of the reactor core in that the differences of the quadrant average powers over 2 symmetrically opposite quadrants essentially eliminates the contribution to the oscillation from the azimuthal mode. The QTD data were fitted in the form of Equation (4.3-2) through a least-square method. A stability index of -0.076 hr^{-1} with a period of 29.6 hours was obtained from the thermocouple data shown in Figure 4.3-47.

It was observed in the second X-Y xenon test that the PWR core with 157 fuel assemblies had become more stable due to an increased fuel depletion although the stability index was not determined.

4.3.2.8.5 Comparison of Calculations with Measurements

The analysis of the axial xenon transient tests was performed in an axial slab geometry using a flux synthesis technique. The direct simulation of the axial offset data was carried out using an updated version of the PANDA Code [21]. The analysis of the X-Y xenon transient tests was performed in an X-Y geometry using a modified TURTLE [13] Code. Both the PANDA and TURTLE codes solve the 2-group time-dependent neutron diffusion equation with time-dependent xenon and iodine concentrations. The fuel temperature and moderator density feedback is limited to a steady-state model. The X-Y calculations were performed in an average enthalpy plane.

The basic nuclear cross sections used in this study were generated from a unit cell depletion program which has evolved from the codes LEOPARD [2] and CINDER [22]. The detailed experimental data during the tests including the reactor power level, enthalpy rise and the impulse motion of the control rod assembly, as well as the plant follow burnup data were closely simulated in the study.

The results of the stability calculation for the axial tests are compared with the experimental data in Table 4.3-5. The calculations show conservative results for both of the axial tests with a margin of approximately -0.01 hr^{-1} in the stability index.

An analytical simulation of the first X-Y xenon oscillation test shows a calculated stability index of -0.081 hr^{-1}, in good agreement with the measured value of -0.075 hr^{-1}. As indicated earlier, the second X-Y xenon test showed that the core had become more stable compared to the first test and no evaluation of the stability index was attempted. This increase in the core stability in the X-Y plane due to increased fuel burnup is due mainly to the increased magnitude of the negative moderator temperature coefficient.

Previous studies of the physics of xenon oscillations, including three-dimensional analysis, are reported in the series of topical reports, References [17], [18], and [19]. A more detailed description of the experimental results and analysis of the axial and X-Y xenon transient tests is presented in Reference [20] and Section 1 of Reference [23].

4.3.2.8.6 Stability Control and Protection

The excore detector system is utilized to provide indications of xenon-induced spatial oscillations. The readings from the excore detectors are available to the operator and also form part of the protection system.

1. Axial Power Distribution

   For maintenance of proper axial power distributions, the operator is instructed to maintain an axial offset within prescribed limits, based on the excore detector readings. Should the axial offset be permitted to move far enough outside these limits, the protection limit will be reached and the power will be reduced.

   Twelve (12) foot PWR cores become less stable to axial xenon oscillations as fuel burnup progresses. However, free xenon oscillations are not allowed to occur except for special tests. The control rod banks present in all modern Westinghouse PWRs are sufficient to dampen and control any axial xenon oscillations present. Should the axial offset be inadvertently permitted to move far enough outside the limits due to an axial xenon oscillation, or any other reason, the protection limit on axial offset will be reached and the power will be automatically cut back.

2. Radial Power Distribution

The core described herein is calculated to be stable against X-Y xenon induced oscillations at all times in life.

The X-Y stability of large PWRs has been further verified as part of the startup physics test program at a PWR core with 193 fuel assemblies. The measured X-Y stability of the PWR core with 157 assemblies and the good agreement between the calculated and measured stability index for this core, as discussed in Sections 4.3.2.8.4 and 4.3.2.8.5, make it very unlikely that a sustained X-Y oscillation can occur in a core with 193 assemblies. However, in the unlikely event that X-Y oscillations occur, backup actions are possible and would be implemented, if necessary, to increase the natural stability of the core. This is based on the fact that several actions could be taken to make the moderator temperature coefficient more negative, which will increase the stability of the core in the X-Y plane.

Provisions for protection against non-symmetric perturbations in the X-Y power distribution that could result from equipment malfunctions are made in the protection system design. This includes control rod drop, rod misalignment and asymmetric loss of coolant flow.

A more detailed discussion of the power distribution control in PWR cores is presented in Reference [9].

4.3.2.9 Vessel Irradiation

It is beyond the scope of this section to present methods and analyses used in determination of neutron and gamma flux attenuation between the core and the pressure vessel other than a brief review given below. A more complete discussion on the pressure vessel irradiation and surveillance program is given in Section 5.4.3.6.

The primary shielding material that serves to attenuate high energy neutron and gamma flux originating in the core consists primarily of the core baffle, core barrel, the neutron pads, and associated water annuli, all of which are within the region between the core and the pressure vessel.

In general, few group neutron diffusion theory codes are used to determine flux and fission power density distributions within the active core and the accuracy of these analyses is verified by incore measurements on operating reactors. Outside the active core, methods such as those which use multigroup space dependent slowing down codes described in Section 5.4.3.6.2 are used. Regionwise power sharing information from the core calculations is often used as reference source data for the multigroup codes.

The neutron flux distribution and spectrum in the various structural components varies significantly from the core to the pressure vessel. Representative values of the neutron flux distribution and spectrum are presented in Table 4.3-6. The values listed are based on equilibrium cycle reactor core parameters and power distributions, and thus, are suitable for long term net projections and for correlation with radiation damage estimates.

As discussed in Section 5.4.3.6, the irradiation surveillance program utilizes actual test samples to verify the accuracy of the calculated fluxes at the vessel.

4.3.3 ANALYTICAL METHODS

Calculations required in nuclear design consist of 3 distinct types, which are performed in sequence:

1. Determination of effective fuel temperatures,

2. Generation of macroscopic few-group parameters,

3. Space-dependent, few-group diffusion calculations.

These calculations are carried out by computer codes which can be executed individually, however, at Westinghouse most of the codes required have been linked to form an automated design sequence which minimizes design time, avoids errors in transcription of data, and standardizes the design methods.

4.3.3.1 Fuel Temperature (Doppler) Calculations

Temperatures vary radially within the fuel rod, depending on the heat generation rate in the pellet, the conductivity of the materials in the pellet, gap, and clad; and the temperature of the coolant.

The fuel temperatures for use in most nuclear design Doppler calculations are obtained from a simplified version of the Westinghouse fuel rod design model described in Section 4.2.1.3.1 which considers the effect of radial variation of pellet conductivity, expansion-coefficient and heat generation rate, elastic deflection of the clad, and a gap conductance which depends on the initial fill gap, the hot open gap dimension, and the fraction of the pellet over which the gap is closed. The fraction of the gap assumed closed represents an empirical adjustment used to produce good agreement with observed reactivity data at beginning-of-life. Further gap closure occurs with burnup and accounts for the decrease in Doppler defect with burnup which has been observed in operating plants. For detailed calculations of the Doppler coefficient, such as for use in xenon stability calculations, a more sophisticated temperature model is used which accounts for the effects of fuel swelling, fission gas release, and clad creep deformation.

Radial power distributions in the pellet as a function of burnup are obtained from LASER [24] calculations.

The effective U-238 temperature for resonance absorption is obtained from the radial temperature distribution by applying a radially dependent weighting function. The weighting function was determined from REPAD [25] Monte Carlo calculations of resonance escape probabilities in several steady-state and transient temperature distributions. In each case a flat pellet temperature was determined which produced the same resonance escape probability as the actual distribution. The weighting function was empirically determined from these results.

The effective Pu-240 temperature for resonance absorption is determined by a convolution of the radial distribution of Pu-240 densities from LASER burnup calculations and the radial weighting function. The resulting temperature is burnup dependent, but the difference between U-238 and Pu-240 temperatures, in terms of reactivity effects, is small.

The effective pellet temperature for pellet dimensional change is that value which produces the same outer pellet radius in a virgin pellet as that obtained from the temperature model. The effective clad temperature for dimensional change is its average value.

The temperature calculational model has been validated by plant Doppler defect data as shown in Table 4.3-7 and Doppler coefficient data as shown in Figure 4.3-48. Stability index measurements also provide a sensitive measure of the Doppler coefficient near full power(see Section 4.3.2.8). It can be seen that Doppler defect data is typically within 0.2% $\Delta\rho$ of prediction.

4.3.3.2 Macroscopic Group Constants

There are 2 lattice codes used for the generation of macroscopic group constants for use in the spatial few group diffusion codes. The first code is a linked version of LEOPARD (Reference [2]) and CINDER (Reference [26]) and the second code is PHOENIX-P (Reference [35]). A description of each code follows.

Macroscopic few-group constants and analogous microscopic cross sections (needed for feedback and microscopic depletion calculations) can be generated for fuel cells by a recent version of the LEOPARD [2] and CINDER [26] codes, which are linked internally and provide burnup dependent cross sections. Normally a simplified approximation of the main fuel chains is used; however, where needed, a complete solution for all the significant isotopes in the fuel chains from Th-232 to Cm-244 is available [27]. Fast and thermal cross-section library tapes contain microscopic cross-sections taken for the most part from the ENDF/B [27] library, with a few exceptions where other data provided better agreement with critical experiments, isotopic measurements, and plant critical boron values. The effect on the unit fuel cell of non-lattice components in the fuel assembly is obtained by supplying an appropriate volume fraction of these materials in an extra region which is homogenized with the unit cell in the fast (MUFT) and thermal (SOFOCATE) flux calculations. In the thermal calculation, the fuel rod, clad, and moderator are homogenized by energy-dependent disadvantage factors derived from an analytical fit to integral transport theory results.

Group constants for burnable absorber cells, guide thimbles, instrument thimbles and interassembly gaps are generated in a manner analogous to the fuel cell calculation. Reflector group constants are taken from infinite medium LEOPARD calculations. Baffle group constants are calculated from an average of core and radial reflector microscopic group constants for stainless steel.

The group constants for core materials, calculated above, are placed in a pin-by-pin discrete 2-group diffusion theory code, an updated version of the TURTLE code, to solve for 2-group nodal macroscopic and microscopic cross sections, through flux-volume weighting homogenization.

Group constants for control rods are calculated in a linked version of the HAMMER [28] and AIM [29] codes to provide an improved treatment of self shielding in the broad resonance structure of these isotopes at epithermal energies than is available in LEOPARD. The Doppler broadened cross-sections of the control rod materials are represented as smooth cross-sections in the 54 group LEOPARD fast group structure and in 30 thermal groups. The 4 group constants in the rod cell and appropriate extra region are generated in the coupled space-energy transport HAMMER calculation. A corresponding AIM calculation of the homogenized rod cell with extra region is used to adjust the absorption cross-sections of the rod cell to match the reaction rates in HAMMER. These transport-equivalent group constants are reduced to 2-group constants for use in space-dependent diffusion calculations. In discrete X-Y calculations, only 1 mesh interval per cell is used, and the rod group constants are further adjusted for use in this standard mesh by reaction rate matching the standard mesh unit assembly to a fine-mesh unit assembly calculation.

Validation of the cross-section method is based on analysis of critical experiments as shown in Table 4.3-4, isotopic data as shown in Table 4.3-8, plant critical boron (C_B) values at HZP, BOL, as shown in Table 4.3-9 and at HFP as a function of burnup as shown in Figures 4.3-49 through 4.3-51. Control rod worth measurements are shown in Table 4.3-10.

Confirmatory critical experiments on burnable absorbers are described in Reference [30].

The PHOENIX-P computer code is a two-dimensional, multigroup, transport based lattice code and capable of providing all necessary data for PWR analysis. Being a dimensional lattice code, PHOENIX-P does not rely on pre-determined spatial/spectral interaction assumptions for a heterogeneous fuel lattice, hence, will provide a more accurate multi-group flux solution than versions of LEOPARD/CINDER. The PHOENIX-P computer code is approved by the USNRC as the lattice code for generating macroscopic and microscopic few group cross sections for PWR analysis (Reference [35]).

The solution for the detailed spatial flux and energy distribution is divided into 2 major steps in PHOENIX-P (Reference [35]). In the first step, a two-dimensional fine energy group nodal solution is obtained which couples individual subcell regions (pellet, clad, and moderator) as well as surrounding pins. PHOENIX-P uses a method based on the Carlvik's collision probability approach and heterogeneous response fluxes which preserves the heterogeneity of the pin cells and their surroundings. The nodal solution provides accurate and detailed local flux distribution which is then used to spatially homogenize the pin cells to fewer groups.

The second step in the solution process solves for the angular flux distribution using a standard S^4 discrete ordinates calculation. This step is based on the group-collapsed and homogenized cross sections obtained from the first step of the solution. The S^4 fluxes are then used to normalize the detailed spatial and energy nodal fluxes. The normalized nodal fluxes are used to compute reaction rates, power distribution and to deplete the fuel and burnable absorbers. A standard B1 calculation is employed to evaluate the fundamental mode critical spectrum and to provide an improved fast diffusion coefficient for the core spatial codes.

The PHOENIX-P code employs a 42 energy group library which has been derived mainly from ENDF/B-V files. The PHOENIX-P cross sections library was designed to properly capture integral properties of the multi-group data during group collapse, and enabling proper modeling of important resonance parameters. The library contains all neutronic data necessary for modeling fuel, fission products, cladding and structural, coolant, and control/burnable absorber materials present in Light Water Reactor cores.

Group constants for burnable absorber cells, guide thimbles, instruments thimbles, control rod cells, and other non-fuel cells can be obtained directly from PHOENIX-P without any adjustments such as those required in the cell or ID lattice codes.

4.3.3.3 Spatial Few-Group Diffusion Calculations

Spatial few-group diffusion calculations have primarily consisted of 2 group X-Y calculations using an updated version of the TURTLE code, and 2-group axial calculations using an updated version of the PANDA code. However, with the advent of VANTAGE 5 fuel, and hence, axial features such as axial blankets and part length burnable absorbers, there will be a greater reliance on three-dimensional nodal codes such as 3D ANC (Advanced Nodal Code) (Reference [34]). The three-dimensional nature of the nodal codes provide both the radial and axial power distributions.

Nodal three-dimensional calculations are carried out to determine the critical boron concentrations and power distributions. The moderator coefficient is evaluated by varying the inlet temperature in the same calculations used for power distribution and reactivity predictions.

Validation of TURTLE reactivity calculations is associated with the validation of the group constants themselves, as discussed in Section 4.3.3.2. Validation of the Doppler calculations is associated with the fuel temperature validation discussed in Section 4.3.3.1. Validation of the moderator coefficient calculations is obtained by comparison with plant measurements at hot zero power conditions as shown in Table 4.3-11.

ANC is used in two-dimensional and three-dimensional calculations. ANC can be used for safety analyses and to calculate critical boron concentrations, control rod worths, reactivity coefficients, etc.

Axial calculations are used to determine differential control rod worth curves (reactivity versus rod insertion) and axial power shapes during steady-state and transient xenon conditions (flyspeck curve). Group constants are obtained from ANC three-dimensional calculations homogenized by flux-volume weighting.

Validation of the spatial codes for calculating power distributions involves the use of incore and excore detectors and is discussed in Section 4.3.2.2.7.

Based on comparison with measured data it is estimated that the accuracy of current analytical methods is:

± 0.2% $\Delta\rho$ for Doppler defect

± 2 x 10^{-5}/°F for moderator coefficient

± 50 ppm for critical boron concentration with depletion

± 3% for power distributions

± 0.2% $\Delta\rho$ for rod bank worth

± 4 pcm/step for differential rod worth

± 0.5 pcm/ppm for boron worth

± 0.1% $\Delta\rho$ for moderator defect

4.3.4 REFERENCES

1. American Nuclear Society, "Nuclear Safety Criteria for the Design of Stationary Pressurized Water Reactor Plants," ANS N18.2, Draft, August, 1970; sponsored by Power Reactor System Engineering Committee; issued November 1970.

2. Barry, R. F., "LEOPARD - A Spectrum Dependent Non-Spatial Depletion Code for the IBM-7094," WCAP-3269-26, September 1963.

3. Dominick, I. E. and Orr, W. L., "Experimental Verification of Wet Fuel Storage Criticality Analyses," WCAP-8682 (Proprietary) and WCAP-8683 (Non-Proprietary), December 1975.

4. "Westinghouse Anticipated Transient Without Reactor Trip Analysis," WCAP-8330, August 1974.

5. Langford, F. L. and Nath, R. J., "Evaluation of Nuclear Hot Channel Factor Uncertainties," WCAP-7308-L (Proprietary) and WCAP-7810 (Non- Proprietary), December 1971.

6. McFarlane, A. F., "Core Power Capability in Westinghouse PWRs," WCAP-7267-L (Proprietary), October, 1969 and WCAP-7809 (Non- Proprietary), December 1971.

7. Hellman, J. M., (Ed), "Fuel Densification Experimental Results and Model for Reactor Application," WCAP-8218-P-A (Proprietary) and WCAP-8219-A (Non-Proprietary), March 1975.

8. Hellman, J. M. and Yang, J. W., "Effects of Fuel Densification Power Spikes on Clad Thermal Transients," WCAP-8359, July 1974.

9. Moore, J. S., "Power Distribution Control of Westinghouse Pressurized Water Reactors," WCAP-7811 (Non-Proprietary), December 1971.

10. Morita, T., et al., "Power Distribution Control and Load Follow Procedures," WCAP-8385 (Proprietary) and WCAP-8403 (Non-Proprietary), September 1974.

11. Morita, T. and Lucoff, D. M., "Calculational Methods for Prediction of Elevation-Dependent Power Peaking Factor," WCAP-8718 (Proprietary) and WCAP-8719 (Non-Proprietary), to be published.

12. McFarlane, A. F., "Power Peaking Factors," WCAP-7912-P-A (Proprietary) and WCAP-7912-A (Non-Proprietary), January 1975.

13. Altomare, S. and Barry, R. F., "The TURTLE 24.0 Diffusion Depletion Code," WCAP-7213-P-A (Proprietary) and WCAP-7758-A (Non-Proprietary), January 1975.

14. Cermak, J. O., et al., "Pressurized Water Reactor pH - Reactivity Effect Final Report," WCAP-3696-8 (EURAEC-2074), October 1968.

15. Ouzts, J. E., "Plant Startup Test Report, H. B. Robinson Unit No. 2," WCAP-7844, January 1972.

16. Poncelet, C. G. and Christie, A. M., "Xenon-Induced Spatial Instabilities in Large PWRs," WCAP-3680-20, (EURAEC-1974) March 1968.

17. Skogen, F. B. and McFarlane, A. F., "Control Procedures for Xenon-Induced X-Y Instabilities in Large PWRs," WCAP-3680-21, (EURAEC-2111), February 1969.

18. Skogen, F. B. and McFarlane, A. F., "Xenon-Induced Spatial Instabilities in Three-Dimensions," WCAP-3680-22 (EURAEC-2116), September 1969.

19. Lee, J. C., et al., "Axial Xenon Transient Tests at the Rochester Gas and Electric Reactor," WCAP-7964, June 1971.

20. Barry, R. F., et al., "The PANDA Code," WCAP-7048-P-A (Proprietary) and WCAP-7757-A (Non-Proprietary), January 1975.

21. England, T. R., "CINDER - A One-Point Depletion and Fission Product Program," WAPD-TM-334, August 1962.

22. Eggleston, F. T., "Safety-Related Research and Development for Westinghouse Pressurized Water Reactors, Program Summaries, Spring 1976, “WCAP-8768, June 1976.

23. Poncelet, C. G., "LASER - A Depletion Program for Lattice Calculations Based on MUFT and THERMOS," WCAP-6073, April 1966.

24. Olhoeft, J. E., "The Doppler Effect for a Non-Uniform Temperature Distribution in Reactor Fuel Elements," WCAP-2048, July 1962.

25. Nodvik, R. J., et al., "Supplementary Report on Evaluation of Mass Spectrometric and Radiochemical Analyses of Yankee Core I Spent Fuel, Including Isotopes of Elements Thorium Through Cirium," WCAP-6086, August 1969.

26. Drake, M. K. (Ed), "Data Formats and Procedure for the ENDF/B Neutron Cross Section Library," BNL-50274, ENDF-102, Vol. 1, 1970.

27. Suich, J. E. and Honeck, H. C., "The HAMMER System, Hetergeneous Analysis by Multigroup Methods of Exponentials and Reactors," DP-1064, January 1967.

28. Flatt, H. P. and Buller, D. C., "AIM-5, A Multigroup, One Dimensional Diffusion Equation Code," NAA-SR-4694, March 1960.

29. Moore, J. S., "Nuclear Design of Westinghouse Pressurized Water Reactors with Burnable Poison Rods," WCAP-7806 (Non-Proprietary), December 1971.

30. Nodvik, R. J., "Saxton Core II Fuel Performance Evaluation," WCAP-3385-56, Part II, "Evaluation of Mass Spectrometric and Radiochemical Analyses of Irradiated Saxton Plutonium Fuel," July 1970.

31. Leamer, R. D., et al., "PUO_2-UO_2 Fueled Critical Experiments," WCAP-3726-1, July 1967.

32. Meyer, R. O., "The Analysis of Fuel Densification," Division of Systems Safety, United States Nuclear Regulatory Commission, NUREG- 0085, July 1976.

33. Liu, Y. S., et al., "ANC: A Westinghouse Advanced Nodal Code," WCAP-10965-P-A (Proprietary), September 1986.

34. Nguyen, T. Q., et al., "Qualification of the Phoenix-P/ANC Nuclear Design System for Pressurized Water Reactor Cores," WCAP-11596-P-A, June 1988.

35. Ford, W. E., "CSRL-V: Processed ENDFIB-V 227-Neutron-Group and Pointwise Cross-Section Libraries for Criticality Safety, Reactor and Shielding Studies," ORNL/CSD/TM-160, June 1982.

36. J. L. Skolds, SCE&G, to Document Control Desk, December 13, 1993 - RC-93-0304, "Technical Specification Change TSP-930017, Fuel Storage".

37. "BEACON Core Monitoring and Operations Support System," WCAP-12472-P-A, August 1994. 02-01

38. WCAP-12472-P-A, Addendum 1-A, “BEACON Core Monitoring and Operations Support System,” January 2000, (W Proprietary) RN 12-027

This page intentionally left blank.

TABLE 4.3-1

REACTOR CORE DESCRIPTION

Active Core	VANTAGE+ with Perf. + features	
Equivalent Diameter, in.	119.7	
Active Fuel Height, First Core, in.	144.0	
Height-to-Diameter Ratio	1.20	
Total Cross Section Area, ft^2	78.14	
H_2O/U Molecular Ratio, lattice (Colt)	2.73	
Number of Fuel Assemblies	157	
Fuel Weight (as UO_2), lb	162,652	
Zircaloy Weight, lb	37,350	98-01
Weight of Grids, lb	597 INC, 3297 ZIRC	
Fuel Assemblies		
Rod Array	17 x 17	
Rods per Assembly	264	
Rod Pitch, in.	0.496	
Overall Transverse Dimensions, in.	8.426 x 8.426	
Number of Grids per Assembly	2 INC, 6 Zirc, 1 Pro *	
Number if IFMs per Assembly	3	
Composition of Grids	Inconel Zircaloy	98-01
Number of Guide Thimbles per Assembly	24	
Composition of Guide Thimbles	Zircaloy	
Diameter of Guide Thimbles (upper part), in.	0.442 I.D.x 0.474 O.D.	
Diameter of Guide Thimbles (lower part), in.	0.397 I.D.x 0.429 O.D.	
Diameter of Instrument Guide Thimbles, in.	0.442 I.D.x 0.474 O.D.	
Fuel Rods		
Number	41,448	
Outside Diameter, in.	0.360	
Diameter Gap, in.	0.0062	
Clad Thickness, in.	0.0225	
Clad Material	ZIRLO®/Optimized ZIRLO (TM)	RN 11-013

* VANTAGE+ with Performance + features contains 1 Robust Protective Grid. RN 11-013

TABLE 4.3-1 (Continued)

REACTOR CORE DESCRIPTION

Fuel Pellets	VANTAGE 5/VANTAGE+
Material	UO_2 Sintered
Density (percent of Theoretical)	95
Diameter, in.	0.3088*
Length, in.	0.370 Enriched 0.507 Unenriched
Mass of UO_2 per foot of Fuel Rod, lb/ft	0.334
Rod Cluster Control Assemblies	
Neutron Absorber	Ag-IN-CD
Composition, %	80, 15, 5
Diameter, in.	0.341
Density, lb/in^3	0.367
Cladding Material	Type 304, Cold worked, Stainless Steel
Clad Thickness, in.	0.0185
Number of Clusters	
Full Length	48
Part Length	0
Number of Absorber Rods per Cluster	24
Full Length Assembly Weight (dry), lb	157
Burnable Absorber Rods (Borosilicate)	
Number	1072
Material	Borosilicate Glass
Outside Diameter, in.	0.381
Inner Tube, O.D., in.	0.1815
Clad Material	Stainless Steel
Inner Tube Material	Stainless Steel
Boron Loading (w/o B203 in glass rod)	12.5
Weight of Boron - 10 per foot of rod, lb/ft	0.000419
Initial Reactivity Worth, % Δp	7.0 (hot), ~ 5.5
Wet Annular Burnable Absorber (WABA) Rods	
Material	Aluminum Oxide Boron Carbide
Outside Diameter, in.	0.381
Inner Tube, O.D., in.	00267
Clad Material	Zircaloy-4
Inner Tube Material	Zircaloy-4
Weight of Boron 10, gms/cm	0.00603

* IFBA coated fuel pellets have a thin (less than 1 mil) boride coating on the pellet cylindrical surface.

TABLE 4.3-2

NUCLEAR DESIGN PARAMETERS
(Typical Reload Cycle)

Core Average Linear Power, kW/ft, Including Densification Effects	5.69
Total Heat Flux Hot Channel Factor, F_Q	2.45
Nuclear Enthalpy Rise Hot Channel Factor, $F^N_{\Delta H}$	1.62
Reactivity Coefficients	
Doppler Coefficient	See Figures 4.3-31 and 4.3-32
Moderator Temperature Coefficient at Operating Conditions, pcm/°F (1)	0 to -50
Boron Coefficient in Primary Coolant, pcm/ppm (1)	-16 to -8
Rodded Moderator Density Coefficient at Operating Conditions, pcm/gm/cc	$\leq + 0.50 \times 10^5$
Delayed Neutron Fraction and Lifetime	
β_{eff} BOL, (EOL)	0.0075 (0.0044)
ℓ *, BOL, (EOL) μsec	14.0 (17.0)
Control Rod Worths	
Rod Requirements	See Table 4.3-3
Maximum Bank Worth, pcm	< 2300
Maximum Ejected Rod Worth	See Chapter 15.0
Boron Concentrations	
Refueling	2000
Zero Power, K_{eff} = 0.99, Hot Rod Cluster Control Assemblies Out	2133
Full Power, No Xenon, K_{eff} = 1.0, Hot Rod Cluster Control Assemblies Out	1857
Reduction with Fuel Burnup	See Figure 4.3-3*

(1) 1 pcm ≡ (percent mille) 10^{-4} $\Delta\rho$ where $\Delta\rho$ is calculated from two statepoint values of K_{eff} by In (K_2/K_1).

* Figure 4.3-3 is a graph of critical boron concentration versus cycle burnup for a typical transition core and a full core. 98-01

TABLE 4.3-3

REACTIVITY REQUIREMENTS FOR ROD CLUSTER CONTROL ASSEMBLIES
(Typical Reload Cycle)

Reactivity Effects, Percent	Beginning of Life	End of Life
1. Control Requirements		
Fuel temperature (Doppler), %$\Delta\rho$	1.11	1.06
Moderator temperature[1], %$\Delta\rho$	0.06	1.06
Redistribution, %$\Delta\rho$	0.85	1.00
Rod Insertion Allowance, %$\Delta\rho$	0.50	0.50
2. Total Control, %$\Delta\rho$	2.52	3.62
3. Estimated Rod Cluster Control Assembly Worth (52 Rods)		
a. All assemblies inserted, %$\Delta\rho$	10.18	8.40
b. All but one (highest worth) assemblies inserted, %$\Delta\rho$	6.43	7.61
4. Estimated Rod Cluster Control Assembly credit with 10 % adjustment to accommodate uncertainties (3b - 10 percent), %$\Delta\rho$	5.79	6.85
5. Shutdown Margin Available (4-2), %$\Delta\rho$	3.27	3.23[2]

(1) Includes void effects.
(2) The design basis minimum shutdown is 1.77%.

TABLE 4.3-4

SUMMARY OF SPENT FUEL RACK CRITICALITY BIASES
AND STATISTICAL UNCERTAINTIES

	REGION 1	REGION 2	
CALCULATIONAL & METHODOLOGY BIASES			
Methodology (Benchmark) Bias	+0.0009	+0.0009	
Pool Water Temperature Variation	+0.0016	+0.0021	
Axial Burnup Distribution	N/A	+0.0062	
TOTAL Bias	+0.0025	+0.0092	
TOLERANCES & UNCERTAINTIES			
UO_2 Enrichment Tolerance	+0.0016	+0.0032	
UO_2 Density Tolerance	+0.0022	+0.0030	
Storage Cell ID Tolerance	N/A	+0.0011[1]	
Boral Width Tolerance	+0.0006	+0.0008	
Boral Minimum B10 Content	+0.0019	+0.0028	
Depletion Uncertainty	N/A	+0.0146	
Calculational Uncertainty (95/95)	+0.0016	+0.0012	
Methodology Bias Uncertainty	+0.0011	+0.0011	RN 03-017
TOTAL Uncertainty (statistical)	+0.0086	+0.0157	
TOTAL OF BIASES & UNCERTAINTIES	+0.0111	+0.0249	

1 As the box I.D. and cell pitch are interrelated a change in one of these parameters will necessarily the other parameter. It is assumed that both the cell pitch and box I.D. are manufactured at their minimum.

2 This assumes the maximum possible change in the water gap, predicated on the box I.D. and cell pitch being manufactured at their greatest tolerance in opposition to each other (i.e. maximum box I.D. and minimum cell pitch).

TABLE 4.3-5

AXIAL STABILITY INDEX PRESSURIZER WATER
REACTOR CORE WITH A 12 FOOT HEIGHT

Burnup (MWD/T)	F_Z	C_B (ppm)	Stability Index (hr^{-1})	
			Exp	Calc
1550	1.34	1065	-0.041	-0.032
7700	1.27	700	-0.014	-0.006
		Difference	+0.027	+0.026

02-01

TABLE 4.3-6

TYPICAL NEUTRON FLUX LEVELS (n/cm^2 - sec) AT FULL POWER

	$E > s1.0$ Mev	5.53 Kev $< E <$ 1.0 Mev	0.625 ev $\leq E <$ 5.53 Kev	$E <$ 0.625 ev $(nv)_0$
Core Center	6.73×10^{13}	1.18×10^{14}	8.92×10^{13}	3.14×10^{13}
Core Outer Radius at Midheight	3.39×10^{13}	6.03×10^{13}	4.85×10^{13}	9.03×10^{12}
Core Top, on Axis	1.60×10^{13}	2.54×10^{13}	2.20×10^{13}	1.71×10^{13}
Core Bottom, on Axis	2.48×10^{13}	4.13×10^{13}	3.67×10^{13}	1.53×10^{13}
Pressure Vessel Inner Wall, Azimuthal Peak, Core Midheight	2.90×10^{10}	6.03×10^{10}	6.32×10^{10}	8.78×10^{10}

02-01

TABLE 4.3-7

COMPARISON OF MEASURED AND CALCULATED DOPPLER DEFECTS

Plant	Fuel Type	Core Burnup (MWD/MTU)	Measured (pcm) [1]	Calculated (pcm)
1	Air - Filled	1800	1700	1710
2	Air - Filled	7700	1300	1440
3	Air and Helium - Filled	8460	1200	1210

(1) pcm = $10^5 \times \ln k_1/k_2$ 02-01

TABLE 4.3-8

SAXTON CORE II ISOTOPICS ROD MY, AXIAL ZONE 6

Atom Ratio	Measured [1]	2σ Precision (%)	LEOPARD Calculation	02-01
U-234/U	4.65×10^{-5}	± 29	4.60×10^{-5}	
U-235/U	5.74×10^{-3}	± 0.9	5.73×10^{-3}	02-01
U-236/U	3.55×10^{-4}	± 5.6	3.74×10^{-4}	
U-238/U	0.993816	± 0.01	0.99385	
Pu-238/Pu	1.32×10^{-3}	± 2.3	1.222×10^{-3}	
Pu-239/Pu	0.73971	± 0.03	0.74497	
Pu-240/Pu	0.19302	± 0.2	0.19102	
Pu-241/Pu	6.014×10^{-2}	± 0.3	5.74×10^{-2}	
Pu-242/Pu	5.81×10^{-3}	± 0.9	5.38×10^{-3}	
Pu/U [2]	5.938×10^{-2}	± 0.7	5.970×10^{-2}	
Np-237/U-238	1.14×10^{-4}	± 15	0.86×10^{-4}	
Am-241/Pu-239	1.23×10^{-2}	± 15	1.08×10^{-2}	
Cm-242/Pu-239	1.05×10^{-4}	± 10	1.11×10^{-4}	
Cm-244/Pu-239	1.09×10^{-4}	± 20	0.98×10^{-4}	

(1) Reported in Reference [31]
(2) Weight ratio

TABLE 4.3-9

CRITICAL BORON CONCENTRATIONS, HZP, BOL

Plant Type	Measured	Calculated
2-Loop, 121 Assemblies 10-foot Core	1583	1589
2-Loop, 121 Assemblies 12-foot Core	1625	1624
2-Loop, 121 Assemblies 12-foot Core	1517	1517
2-Loop, 157 Assemblies 12-foot Core	1169	1161

TABLE 4.3-10

COMPARISON OF MEASURED AND CALCULATED ROD WORTH

2-Loop Plant, 121 Assemblies, 10-foot Core	Measured (pcm)	Calculated (pcm)
Group B	1885	1893
Group A	1530	1649
Shutdown Group	3050	2917
ESADA Critical [1], 0.69" Pitch, 2 w/o PuO_2 8% Pu-240 9 Control Rods		
6.21" Rod Separation	2250	2250
2.07" Rod Separation	4220	4160
1.38" Rod Separation	4100	4019

02-01

(1) Reported in Reference [32]

TABLE 4.3-11

COMPARISON OF MEASURED AND CALCULATED MODERATOR COEFFICIENTS AT HZP, BOL

Plant Type/ Control Bank Configuration	Measured α_{iso} (1) (pcm/°F)	Calculated α_{iso} (pcm/°F)
3-Loop, 157 Assemblies, 12-foot Core		
D at 160 steps	-0.50	-0.50
D in, C at 190 steps	-3.01	-2.75
D in, C at 28 steps	-7.67	-7.02
B, C, and D in	-5.16	-4.45
2-Loop, 121 Assemblies, 12-foot Core		
D at 180 steps	+0.85	+1.02
D in, C at 180 steps	-2.40	-1.90
C and D in, B at 165 steps	-4.40	-5.58
B, C, and D in, A at 174 steps	-8.70	-8.12

02-01

(1) Isothermal coefficients, which include the Doppler effect in the fuel.

$$\alpha_{in} = 10^5 \ln \frac{k_2}{k_1} / \Delta T°F$$

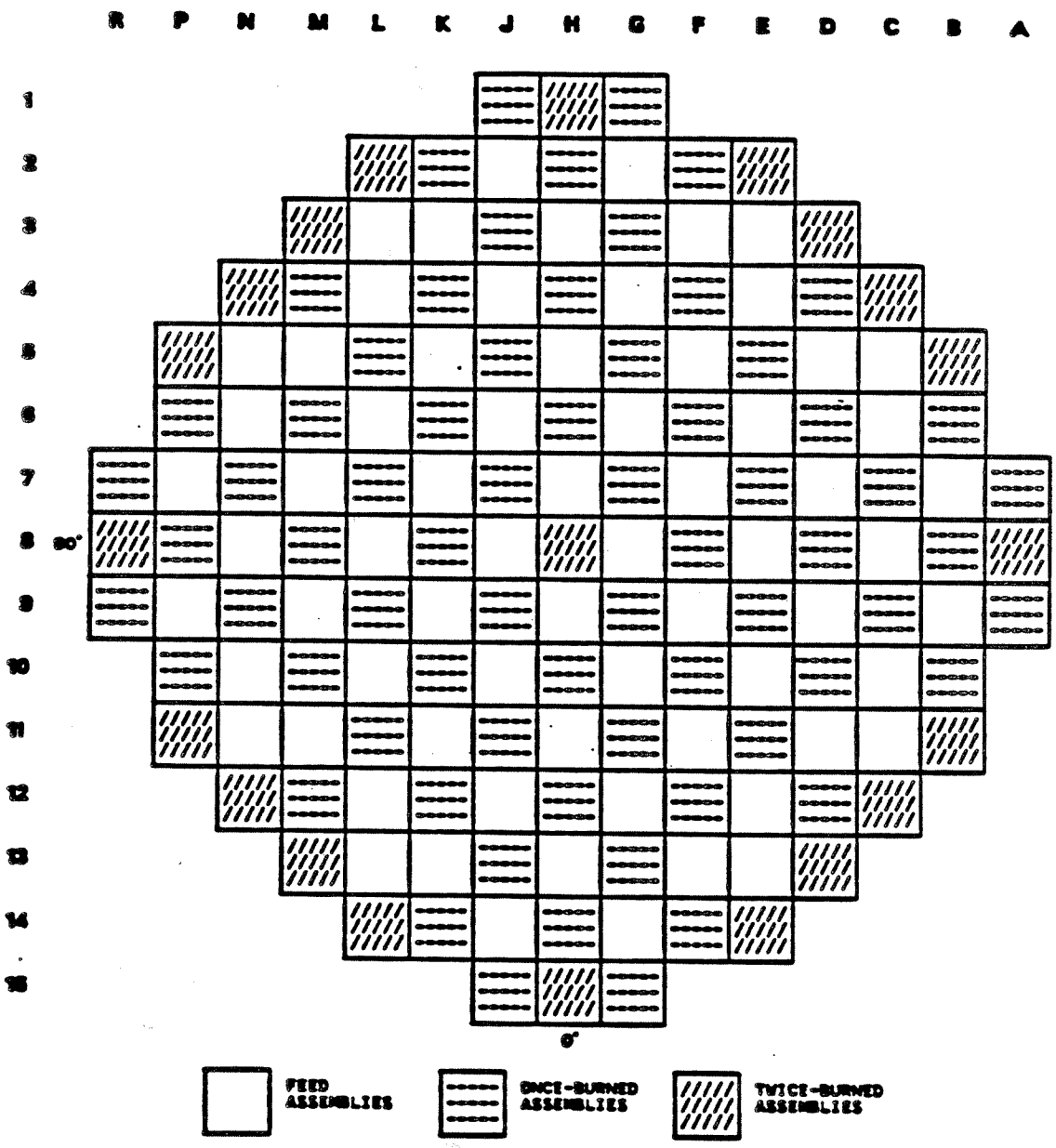

AMENDMENT 6
AUGUST, 1990

SOUTH CAROLINA ELECTRIC & GAS CO.
VIRGIL C. SUMMER NUCLEAR STATION

Typical Reload Core Fuel
Loading Arrangement

Figure 4.3-1

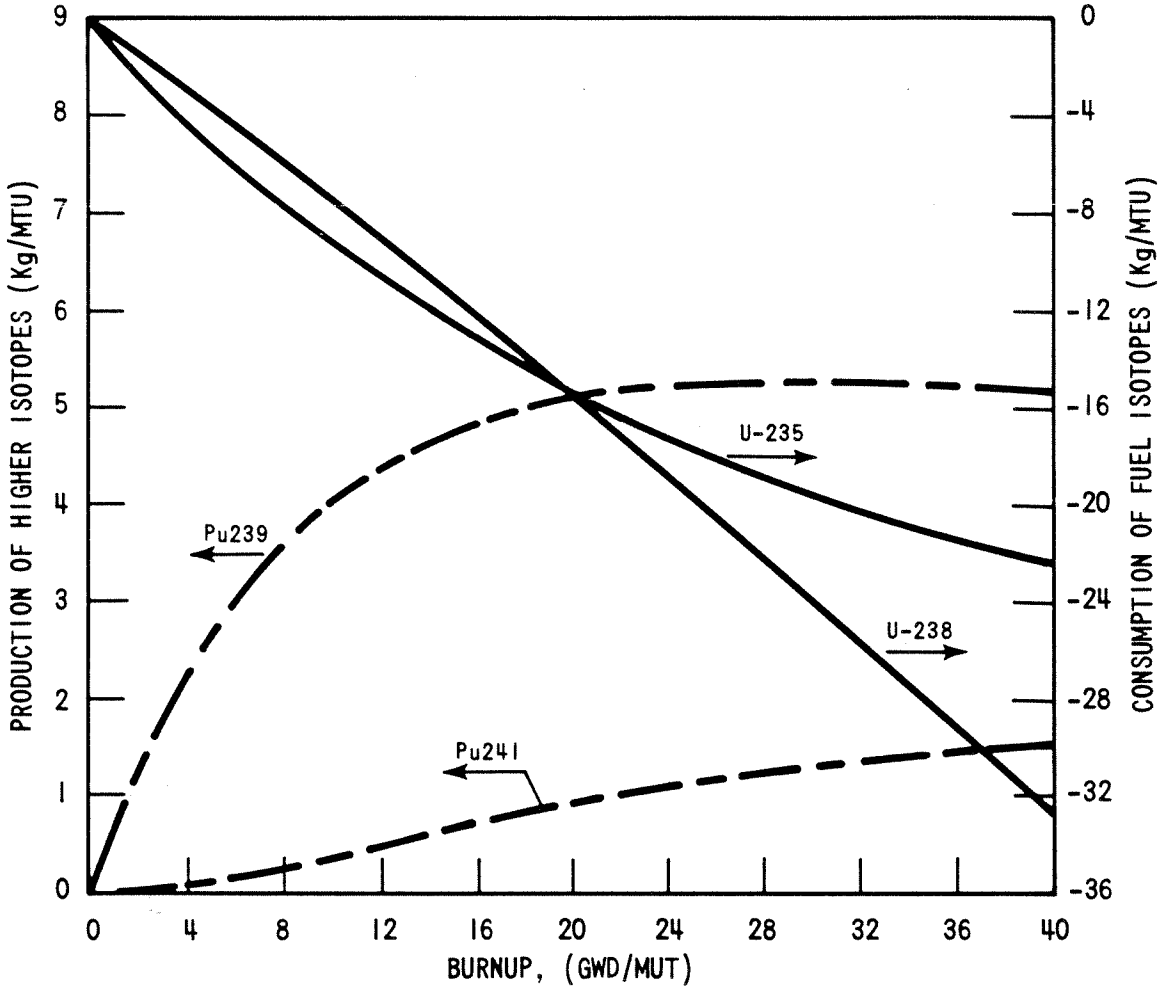

SOUTH CAROLINA ELECTRIC & GAS CO.
VIRGIL C. SUMMER NUCLEAR STATION

Production and Consumption
of Higher Isotopes

Figure 4.3-2

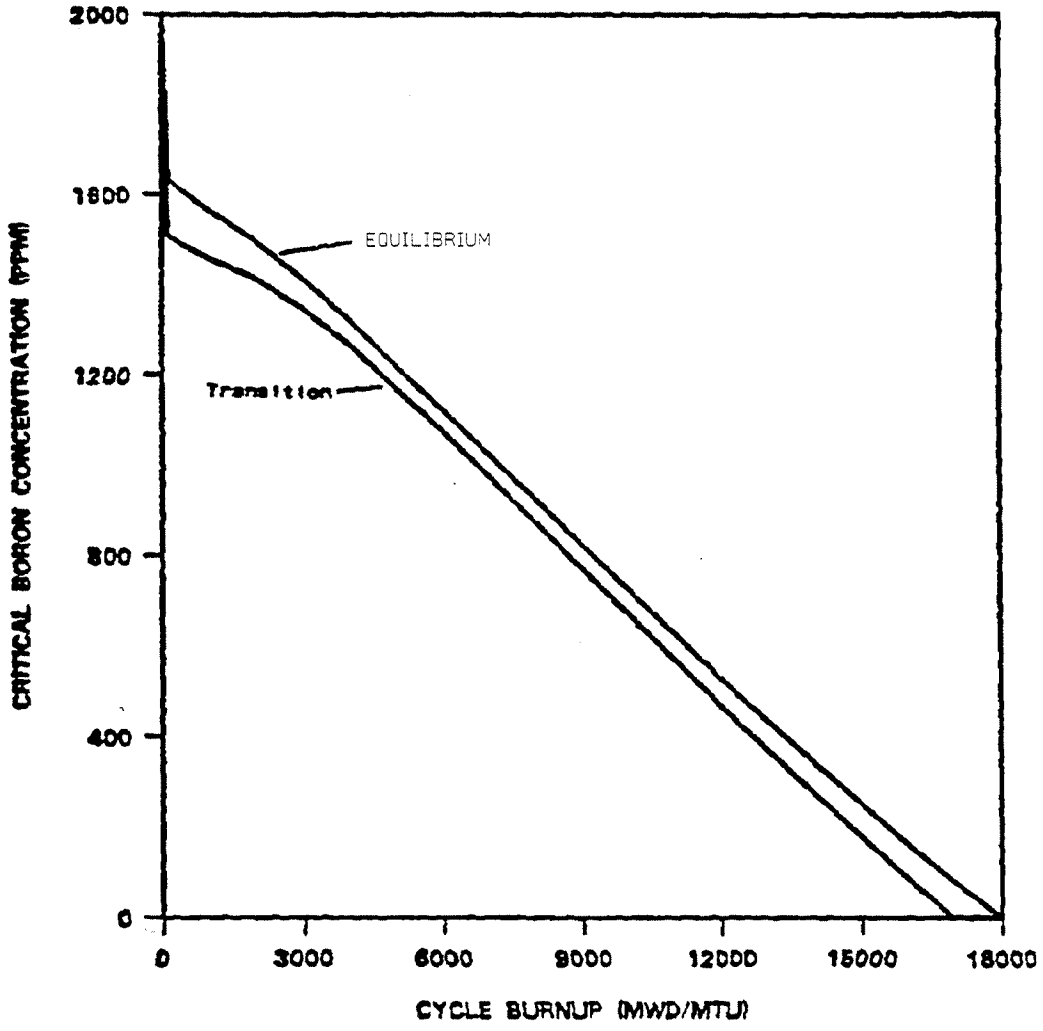

SOUTH CAROLINA ELECTRIC & GAS CO. VIRGIL C. SUMMER NUCLEAR STATION
Boron Concentration Versus Burnup For Transition and Equilibrium Cores Figure 4.3-3

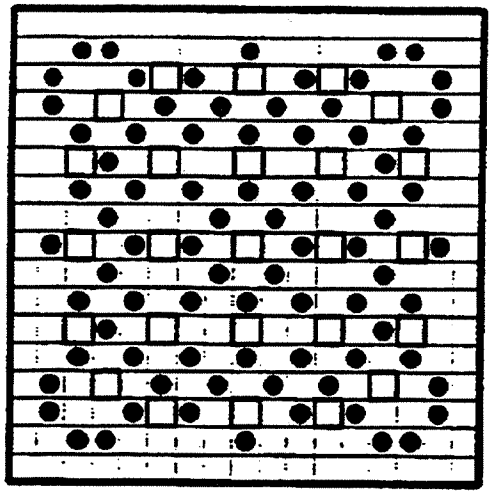

80 IFBA ASSEMBLY

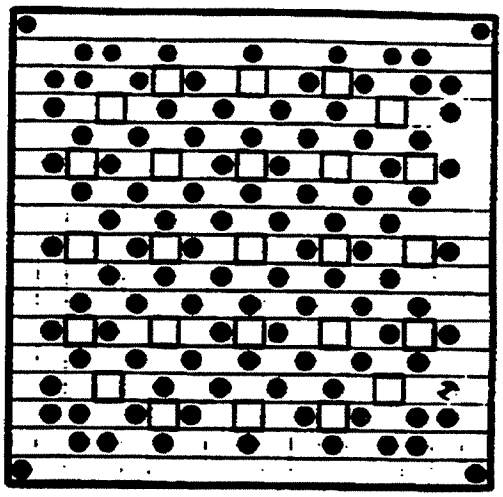

104 IFBA ASSEMBLY

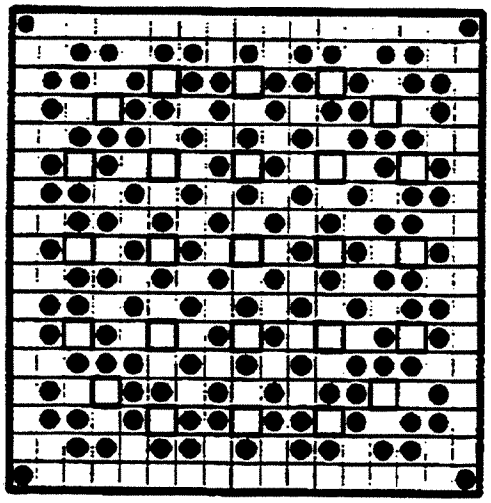

128 IFBA ASSEMBLY

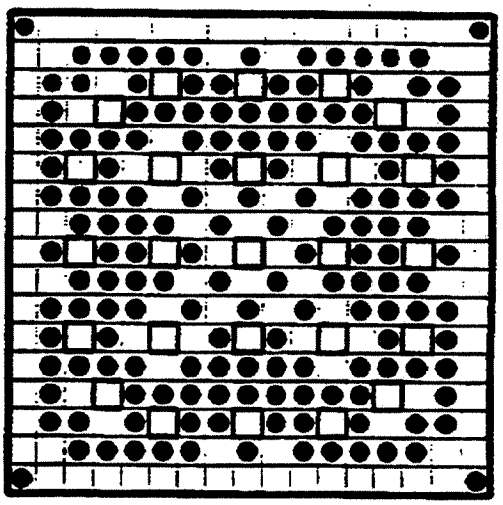

156 IFBA ASSEMBLY

NOTE: ALL FIGURES ARE TOP VIEW

LEGEND :

- FUEL ROD
- GUIDE TUBE OR INSTRUMENTATION TUBE
- IFBA ROD

SOUTH CAROLINA ELECTRIC & GAS CO.
VIRGIL C. SUMMER NUCLEAR STATION

Integral Fuel Burnable Absorber Rod Arrangement Within an Assembly
(Sheet 1 of 2)

Figure 4.3-4

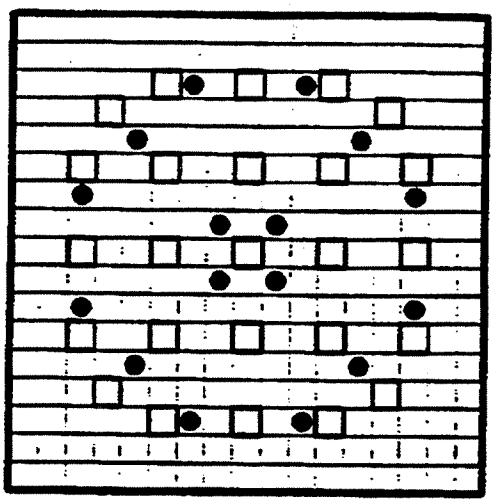

16 IFBA ASSEMBLY

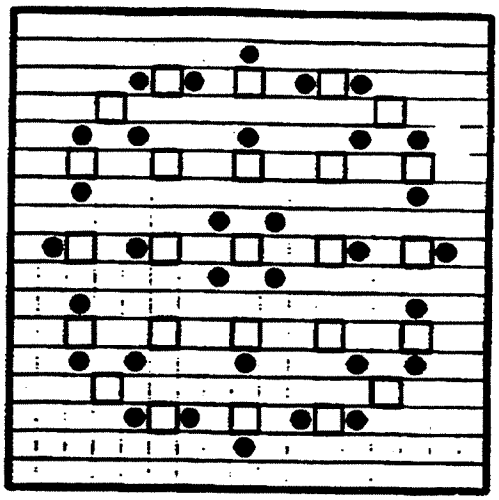

32 IFBA ASSEMBLY

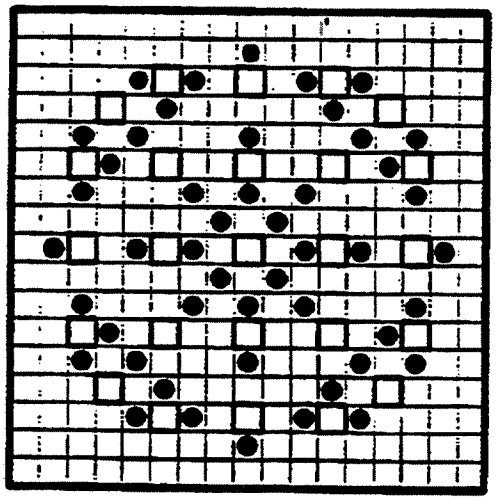

48 IFBA ASSEMBLY

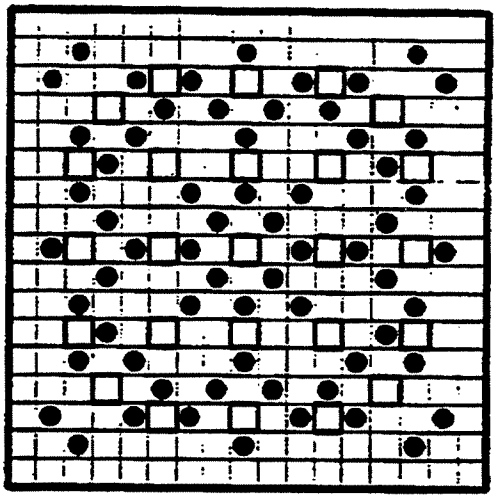

64 IFBA ASSEMBLY

LEGEND :

- FUEL ROD
- GUIDE TUBE OR INSTRUMENTATION TUBE
- IFBA ROD

NOTE: ALL FIGURES ARE TOP VIEW

SOUTH CAROLINA ELECTRIC & GAS CO.
VIRGIL C. SUMMER NUCLEAR STATION

Integral Fuel Burnable Absorber Rod
Arrangement Within an Assembly
(Sheet 2 of 2)

Figure 4.3-4

AMENDMENT 96-02
JULY 1996

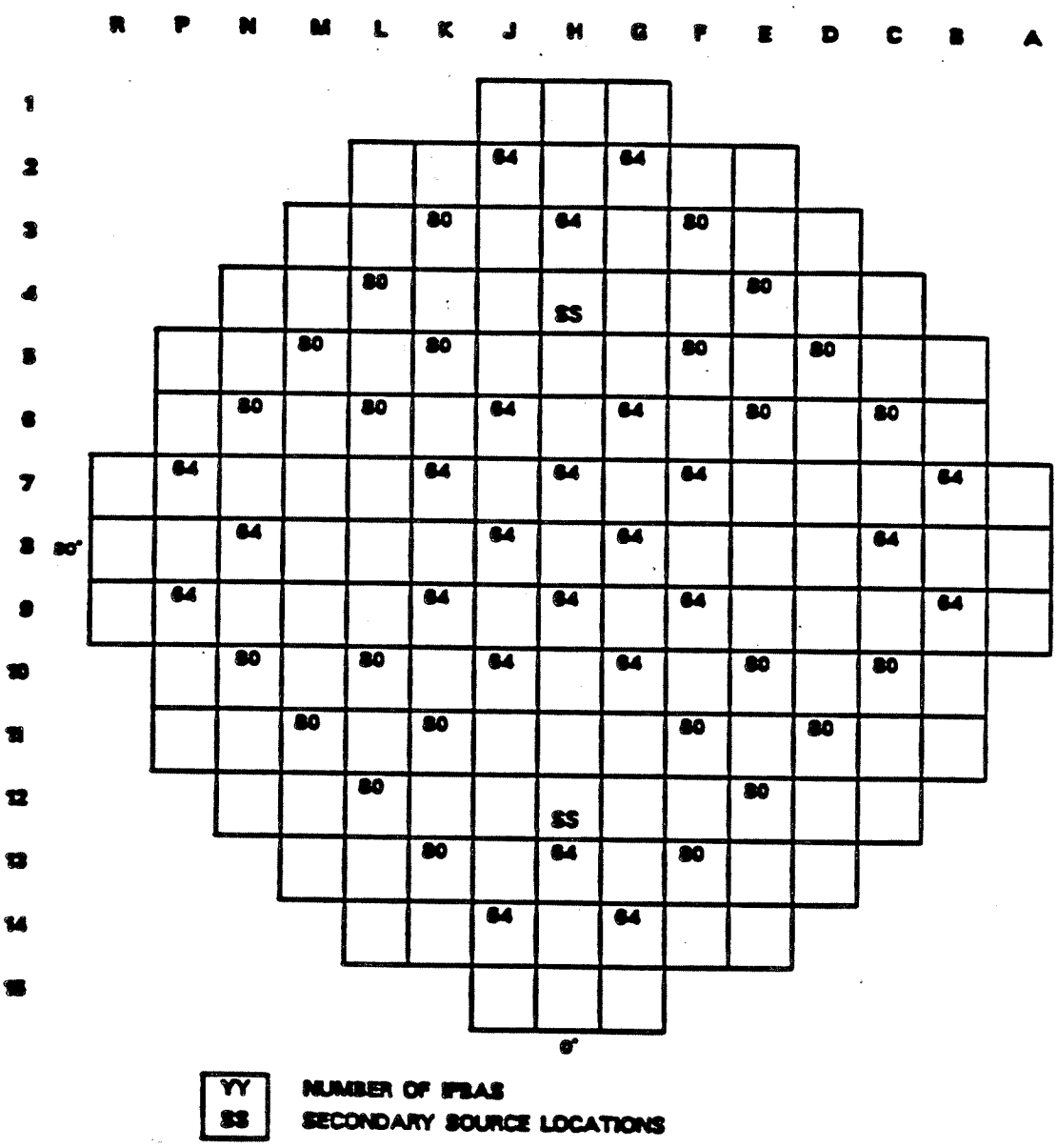

AMENDMENT 6
AUGUST, 1990

SOUTH CAROLINA ELECTRIC & GAS CO.
VIRGIL C. SUMMER NUCLEAR STATION

Typical Burnable Absorber
Loading Pattern

Figure 4.3-5

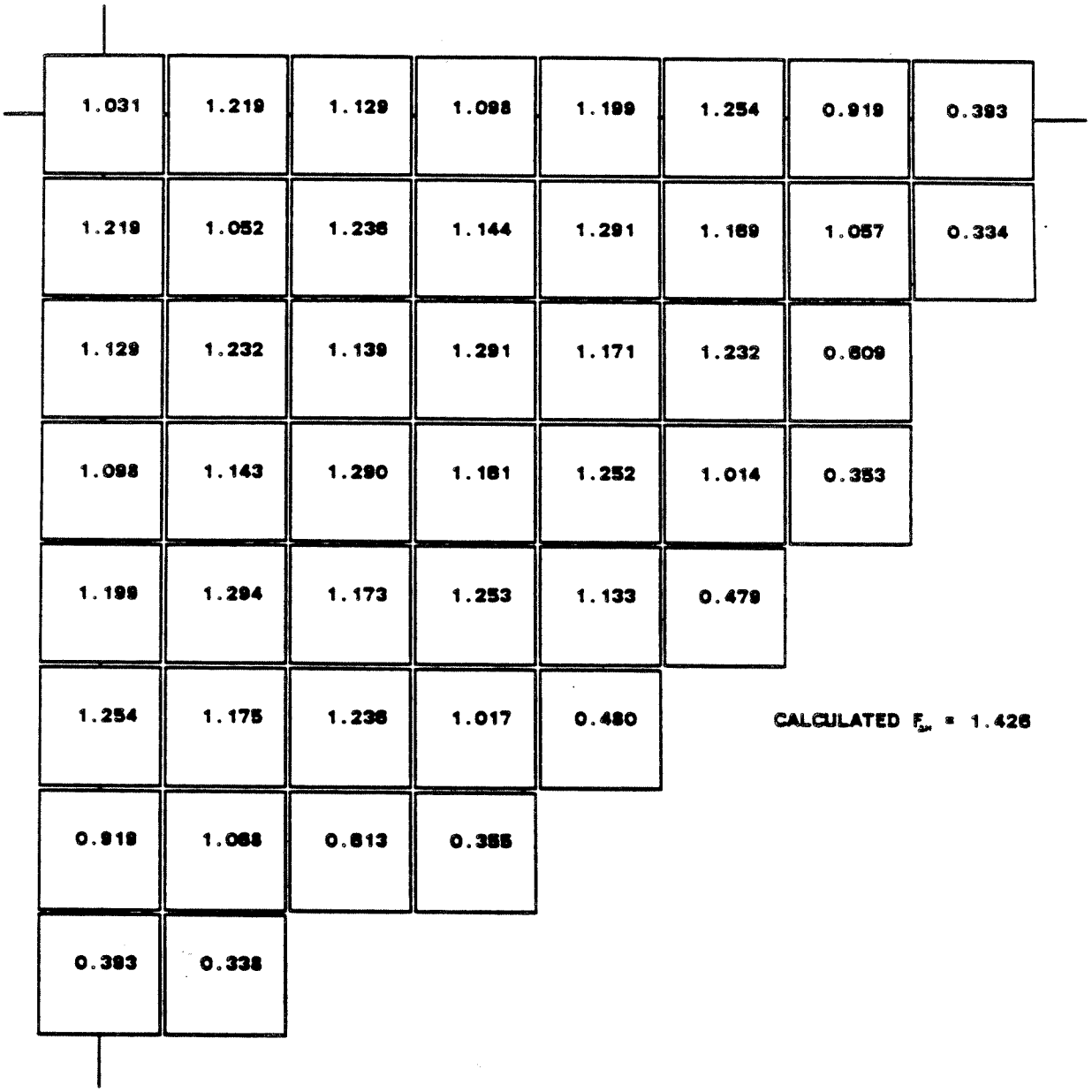

AMENDMENT 6
AUGUST, 1990

SOUTH CAROLINA ELECTRIC & GAS CO.
VIRGIL C. SUMMER NUCLEAR STATION

Normalized Power Density Distribution
Near Beginning of Life, Unrodded Core,
Hot Full Power, No Xenon
(Transition Core)

Figure 4.3-6

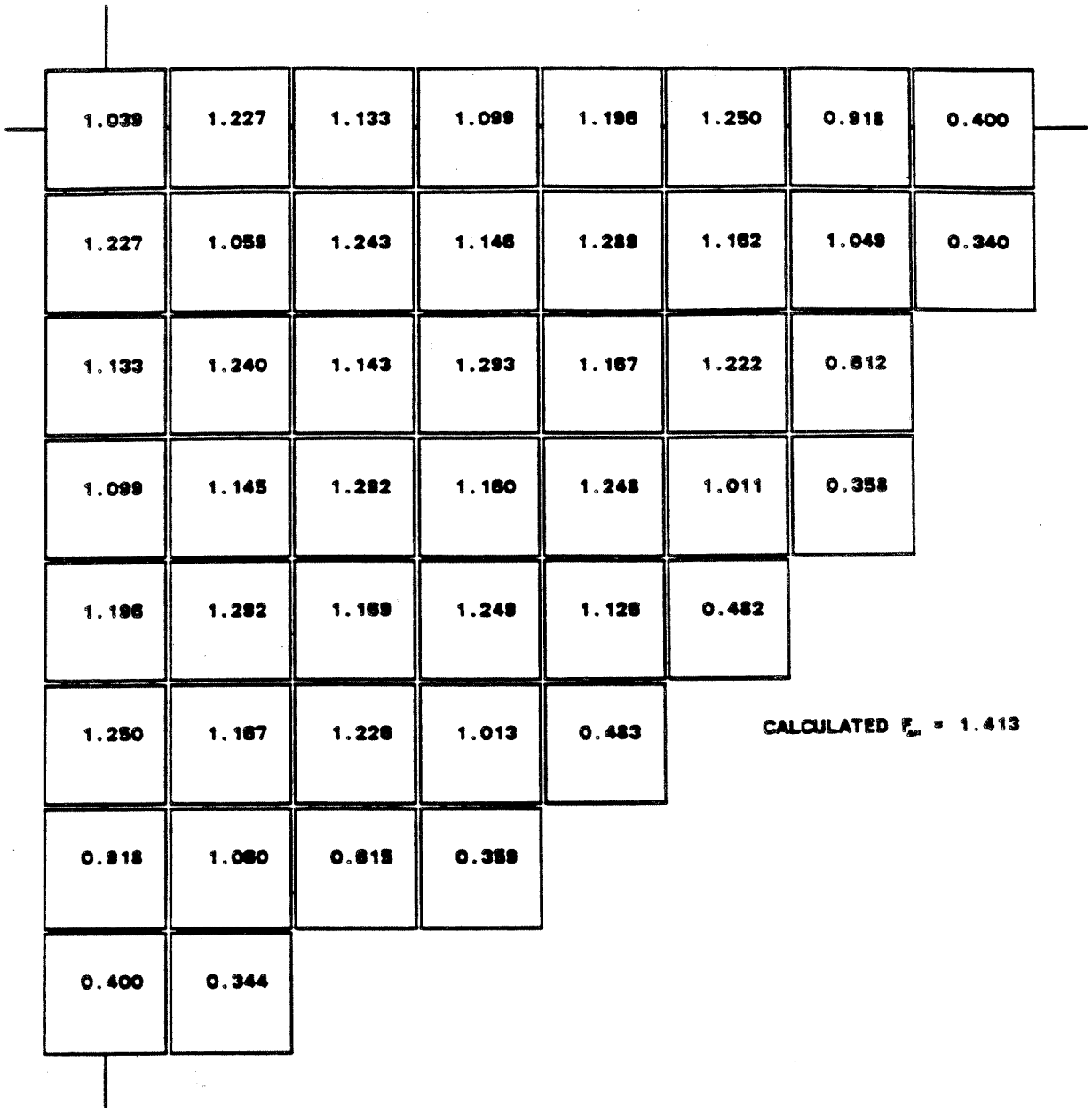

AMENDMENT 6
AUGUST, 1990

SOUTH CAROLINA ELECTRIC & GAS CO.
VIRGIL C. SUMMER NUCLEAR STATION

Normalized Power Density Distribution
Near Beginning of Life, Unrodded Core,
Hot Full Power, Equilibrium Xenon
(Transition Core)

Figure 4.3-7

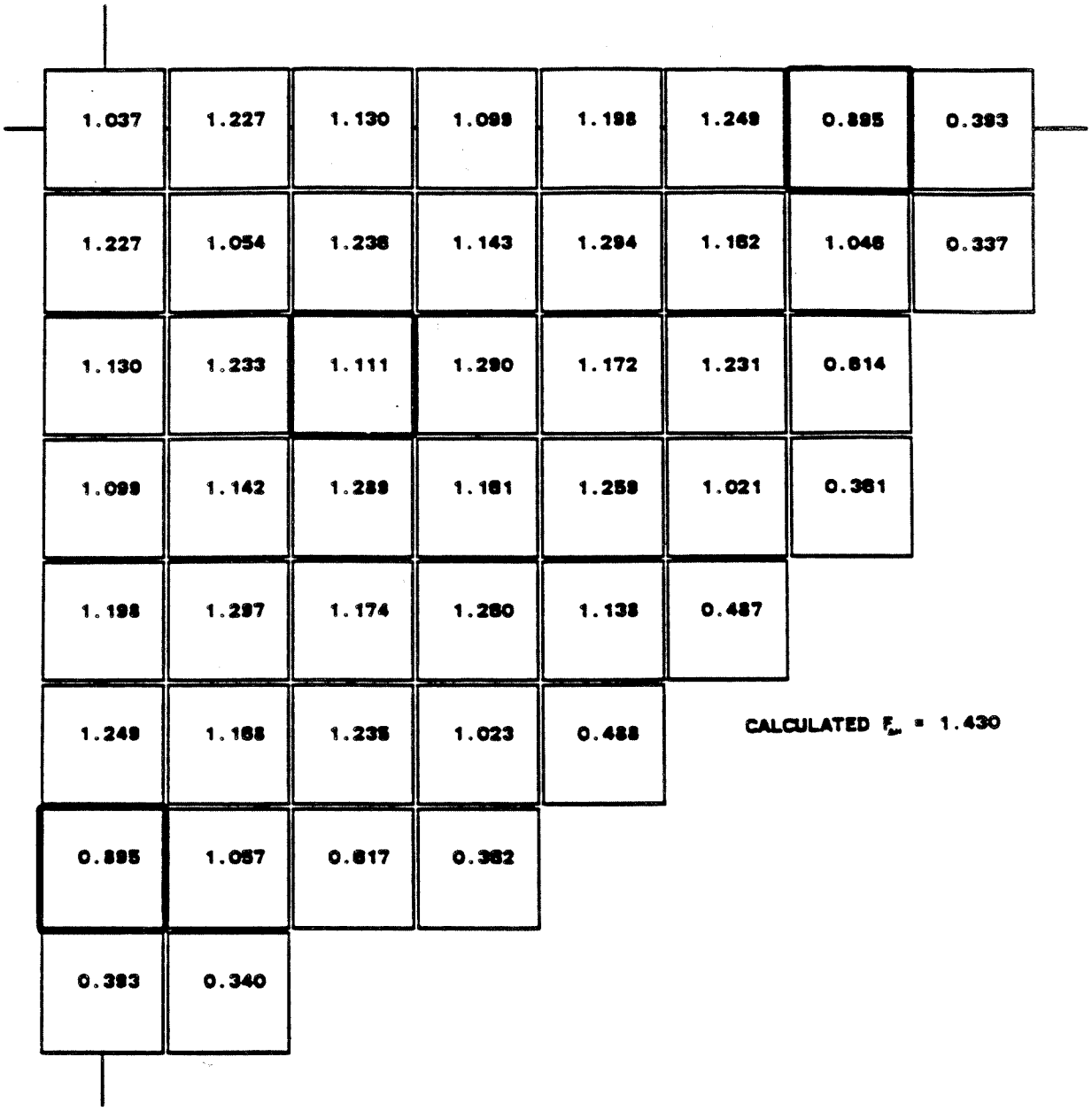

AMENDMENT 6
AUGUST, 1990

SOUTH CAROLINA ELECTRIC & GAS CO.
VIRGIL C. SUMMER NUCLEAR STATION

Normalized Power Density Distribution
Near Beginning of Life, Group D at
HFP Insertion Limit, Hot Full Power,
Equilibrium Xenon (Transition Core)

Figure 4.3-8

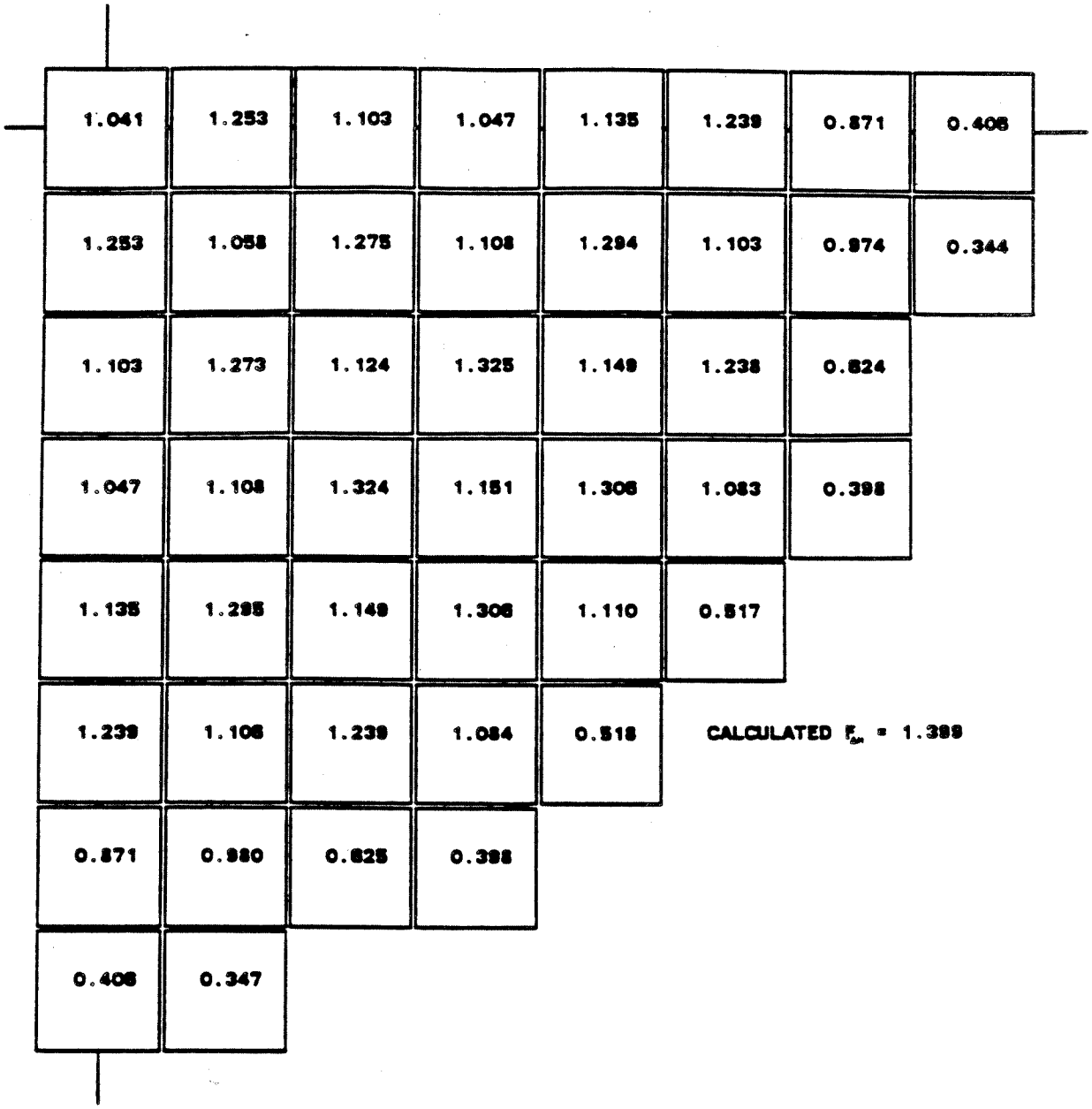

AMENDMENT 6
AUGUST, 1990

SOUTH CAROLINA ELECTRIC & GAS CO.
VIRGIL C. SUMMER NUCLEAR STATION

Normalized Power Density Distribution
Near Middle of Life, Unrodded Core,
Hot Full Power, Equilibrium Xenon
(Transition Core)

Figure 4.3-9

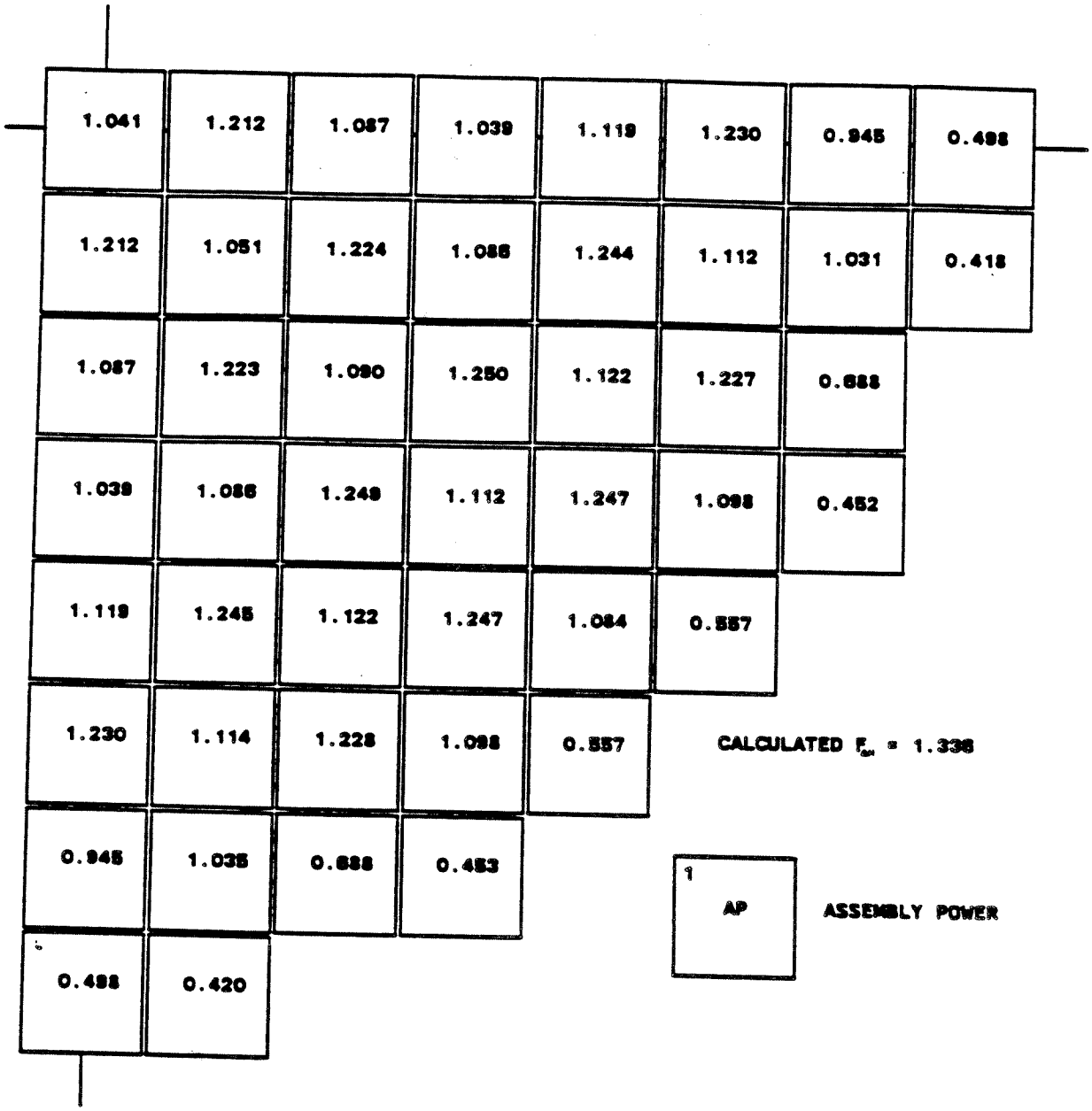

AMENDMENT 6
AUGUST, 1990

SOUTH CAROLINA ELECTRIC & GAS CO.
VIRGIL C. SUMMER NUCLEAR STATION

Normalized Power Density Distribution
Near End of Life, Unrodded Core,
Hot Full Power, Equilibrium Xenon
(Transition Core)

Figure 4.3-10

0.811	1.131	1.019	1.293	1.196	1.384	0.855	0.304
1.131	0.978	1.220	1.174	1.361	1.205	1.030	0.285
1.019	1.221	1.074	1.350	1.234	1.295	0.564	
1.293	1.173	1.349	1.283	1.373	1.118	0.318	
1.196	1.359	1.231	1.371	0.755	0.378		
1.384	1.200	1.291	1.115	0.378			
0.855	1.021	0.561	0.317				
0.304	0.282						

CALCULATED $F_{\Delta H} = 1.556$

SOUTH CAROLINA ELECTRIC & GAS CO.
VIRGIL C. SUMMER NUCLEAR STATION

Normalized Power Density Distribution
Near Beginning of Life, Unrodded Core,
Hot Full Power, No Xenon
(Equilibrium Core)

Figure 4.3-11

0.837	1.155	1.034	1.296	1.191	1.372	0.859	0.315
1.155	0.999	1.232	1.174	1.352	1.196	1.030	0.293
1.034	1.233	1.081	1.344	1.223	1.282	0.570	
1.296	1.174	1.343	1.271	1.357	1.110	0.324	
1.191	1.351	1.221	1.356	0.758	0.383		
1.372	1.191	1.279	1.108	0.383			
0.859	1.022	0.567	0.323				
0.315	0.291						

CALCULATED $F_{\Delta H} = 1.530$

SOUTH CAROLINA ELECTRIC & GAS CO.
VIRGIL C. SUMMER NUCLEAR STATION

Normalized Power Density Distribution
Near Beginning of Life, Unrodded Core,
Hot Full Power, Equilibrium Xenon
(Equilibrium Core)

Figure 4.3-12

0.837	1.157	1.033	1.298	1.193	1.369	0.836	0.310
1.157	0.995	1.224	1.172	1.357	1.198	1.028	0.292
1.033	1.225	1.046	1.338	1.227	1.291	0.573	
1.298	1.171	1.337	1.271	1.366	1.121	0.327	
1.193	1.355	1.225	1.365	0.764	0.387		
1.369	1.193	1.288	1.119	0.387			
0.836	1.020	0.570	0.327				
0.310	0.289						

CALCULATED $F_{\Delta H} = 1.484$

SOUTH CAROLINA ELECTRIC & GAS CO.
VIRGIL C. SUMMER NUCLEAR STATION

Normalized Power Density Distribution
Near Beginning of Life, Group D at
HFP Insertion Limit, Hot Full Power,
Equilibrium Xenon (Equilibrium Core)

Figure 4.3-13

0.933	1.288	1.087	1.355	1.149	1.326	0.843	0.346
1.288	1.072	1.333	1.168	1.355	1.126	0.994	0.318
1.087	1.334	1.099	1.366	1.158	1.245	0.580	
1.355	1.167	1.365	1.206	1.311	1.055	0.341	
1.149	1.354	1.158	1.310	0.759	0.400		
1.326	1.124	1.244	1.055	0.400			
0.843	0.989	0.579	0.341				
0.346	0.316						

CALCULATED $F_{\Delta H} = 1.439$

SOUTH CAROLINA ELECTRIC & GAS CO.
VIRGIL C. SUMMER NUCLEAR STATION

Normalized Power Density Distribution
Near Middle of Life, Unrodded Core,
Hot Full Power, Equilibrium Xenon
(Equilibrium Core)

Figure 4.3-14

0.955	1.269	1.063	1.277	1.107	1.312	0.919	0.448
1.269	1.059	1.271	1.116	1.280	1.117	1.059	0.400
1.063	1.271	1.064	1.281	1.118	1.249	0.653	
1.277	1.115	1.281	1.152	1.285	1.078	0.403	
1.107	1.280	1.118	1.285	0.814	0.461		
1.312	1.116	1.249	1.078	0.461			
0.919	1.056	0.652	0.403				
0.448	0.400						

CALCULATED $F_{\Delta H} = 1.373$

SOUTH CAROLINA ELECTRIC & GAS CO.
VIRGIL C. SUMMER NUCLEAR STATION

Normalized Power Density Distribution
Near End of Life, Unrodded Core,
Hot Full Power, Equilibrium Xenon
(Equilibrium Core)

Figure 4.3-15

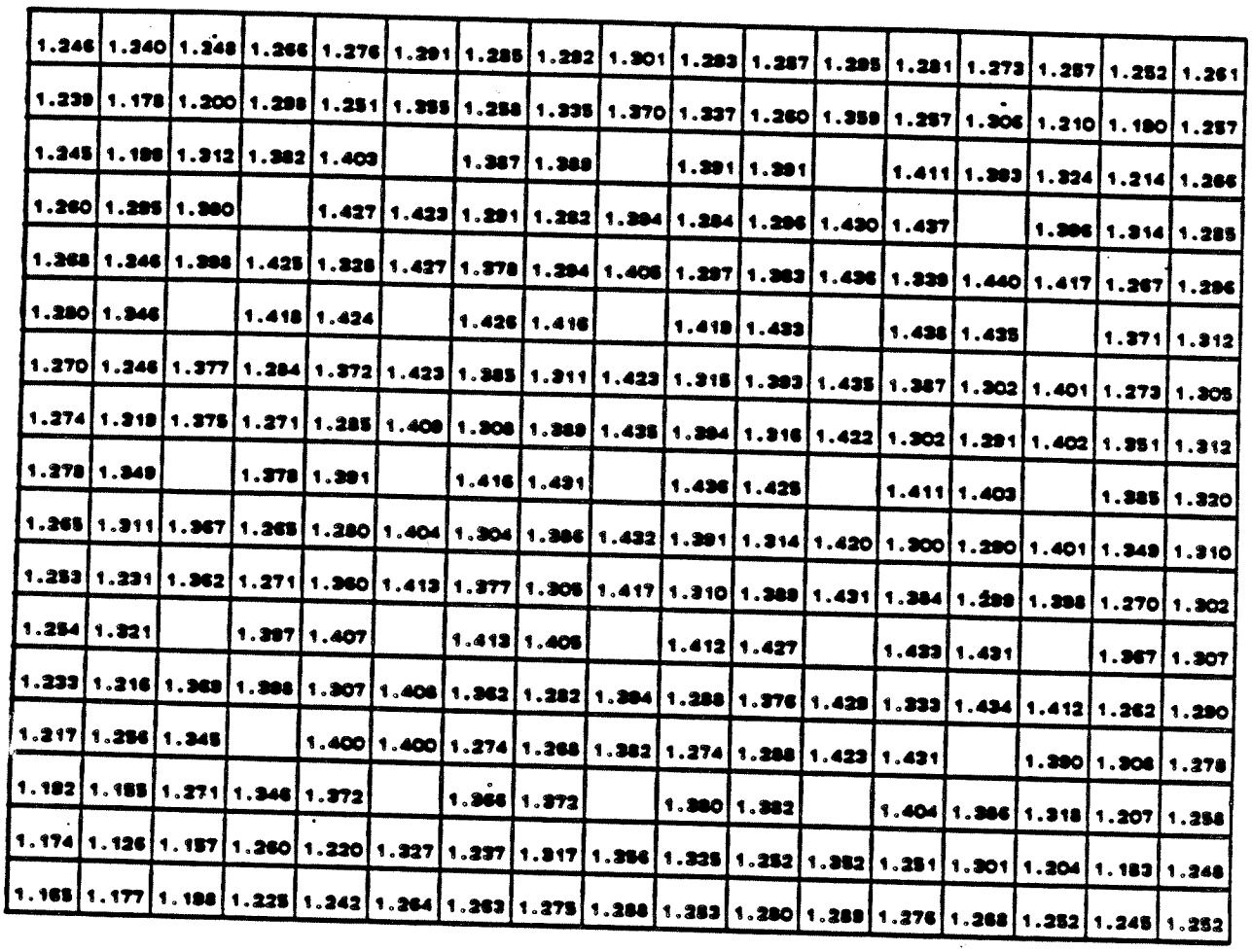

1.246	1.240	1.248	1.266	1.276	1.291	1.285	1.282	1.301	1.293	1.287	1.285	1.281	1.273	1.257	1.252	1.261
1.239	1.178	1.200	1.298	1.251	1.355	1.258	1.335	1.370	1.337	1.260	1.359	1.257	1.306	1.210	1.190	1.257
1.245	1.198	1.312	1.382	1.403		1.387	1.389		1.391	1.391		1.411	1.383	1.324	1.214	1.266
1.260	1.295	1.380		1.427	1.423	1.291	1.282	1.384	1.284	1.296	1.430	1.437		1.396	1.314	1.285
1.268	1.346	1.398	1.425	1.328	1.427	1.378	1.284	1.406	1.287	1.382	1.436	1.339	1.440	1.417	1.267	1.296
1.280	1.346		1.418	1.424		1.426	1.416		1.419	1.433		1.438	1.435		1.371	1.312
1.270	1.346	1.377	1.284	1.372	1.423	1.385	1.311	1.423	1.315	1.393	1.435	1.387	1.302	1.401	1.273	1.305
1.274	1.318	1.375	1.271	1.285	1.408	1.308	1.389	1.435	1.394	1.316	1.422	1.302	1.291	1.402	1.351	1.312
1.278	1.349		1.378	1.391		1.416	1.431		1.436	1.429		1.411	1.403		1.385	1.320
1.265	1.311	1.367	1.265	1.280	1.404	1.304	1.386	1.432	1.391	1.314	1.420	1.300	1.290	1.401	1.349	1.310
1.253	1.231	1.362	1.271	1.360	1.413	1.377	1.306	1.417	1.310	1.389	1.431	1.384	1.299	1.398	1.270	1.302
1.254	1.321		1.397	1.407		1.413	1.406		1.412	1.427		1.423	1.431		1.367	1.307
1.233	1.216	1.369	1.398	1.307	1.408	1.362	1.282	1.394	1.288	1.376	1.428	1.333	1.434	1.412	1.262	1.290
1.217	1.256	1.345		1.400	1.400	1.274	1.268	1.382	1.274	1.288	1.423	1.431		1.390	1.306	1.278
1.192	1.185	1.271	1.346	1.372		1.366	1.372		1.380	1.382		1.404	1.386	1.318	1.207	1.258
1.174	1.126	1.157	1.260	1.220	1.327	1.237	1.317	1.356	1.335	1.252	1.382	1.251	1.301	1.204	1.183	1.248
1.165	1.177	1.198	1.225	1.242	1.264	1.263	1.275	1.288	1.283	1.280	1.288	1.276	1.268	1.252	1.245	1.252

AMENDMENT 6
AUGUST, 1990

SOUTH CAROLINA ELECTRIC & GAS CO.
VIRGIL C. SUMMER NUCLEAR STATION

Rodwise Power Distribution in a Typical Assembly (G-10) Near BOL, HFP, Equilibrium Xenon, Unrodded Core

Figure 4.3-16

1.138	1.136	1.142	1.155	1.167	1.180	1.177	1.179	1.185	1.180	1.181	1.186	1.175	1.165	1.155	1.151	1.156
1.133	1.164	1.181	1.181	1.227	1.233	1.236	1.212	1.238	1.213	1.240	1.239	1.235	1.191	1.184	1.180	1.153
1.138	1.179	1.190	1.245	1.266		1.264	1.264		1.266	1.268		1.275	1.256	1.204	1.187	1.160
1.148	1.177	1.243		1.288	1.288	1.276	1.274	1.279	1.277	1.282	1.296	1.298		1.259	1.196	1.173
1.159	1.221	1.262	1.286	1.299	1.292	1.288	1.284	1.288	1.286	1.284	1.301	1.311	1.301	1.280	1.243	1.186
1.169	1.225		1.284	1.290		1.282	1.283		1.296	1.298		1.303	1.301		1.250	1.198
1.163	1.225	1.286	1.270	1.284	1.289	1.262	1.291	1.287	1.285	1.270	1.300	1.268	1.289	1.278	1.252	1.196
1.162	1.198	1.253	1.265	1.276	1.288	1.289	1.266	1.289	1.270	1.287	1.300	1.283	1.286	1.278	1.228	1.187
1.166	1.221		1.266	1.278		1.282	1.296		1.300	1.301		1.296	1.289		1.254	1.204
1.157	1.193	1.248	1.261	1.273	1.285	1.286	1.264	1.288	1.269	1.287	1.300	1.283	1.286	1.278	1.228	1.188
1.152	1.214	1.246	1.262	1.247	1.284	1.258	1.288	1.285	1.294	1.269	1.300	1.269	1.290	1.279	1.254	1.187
1.152	1.210		1.272	1.280		1.285	1.288		1.294	1.298		1.304	1.303		1.252	1.201
1.136	1.200	1.244	1.270	1.286	1.282	1.280	1.277	1.284	1.284	1.283	1.301	1.312	1.303	1.283	1.246	1.190
1.120	1.191	1.230		1.272	1.278	1.266	1.267	1.274	1.274	1.281	1.297	1.300		1.263	1.201	1.177
1.102	1.147	1.183	1.222	1.247		1.252	1.256		1.263	1.268		1.277	1.260	1.208	1.202	1.166
1.089	1.125	1.149	1.185	1.206	1.216	1.223	1.202	1.232	1.210	1.239	1.240	1.238	1.195	1.189	1.185	1.160
1.083	1.091	1.107	1.126	1.144	1.161	1.163	1.169	1.179	1.177	1.180	1.187	1.178	1.169	1.160	1.157	1.163

AMENDMENT 6
AUGUST, 1990

SOUTH CAROLINA ELECTRIC & GAS CO.
VIRGIL C. SUMMER NUCLEAR STATION

Rodwise Power Distribution in a Typical Assembly (G-10) Near EOL, HFP, Equilibrium Xenon, Unrodded Core

Figure 4.3-17

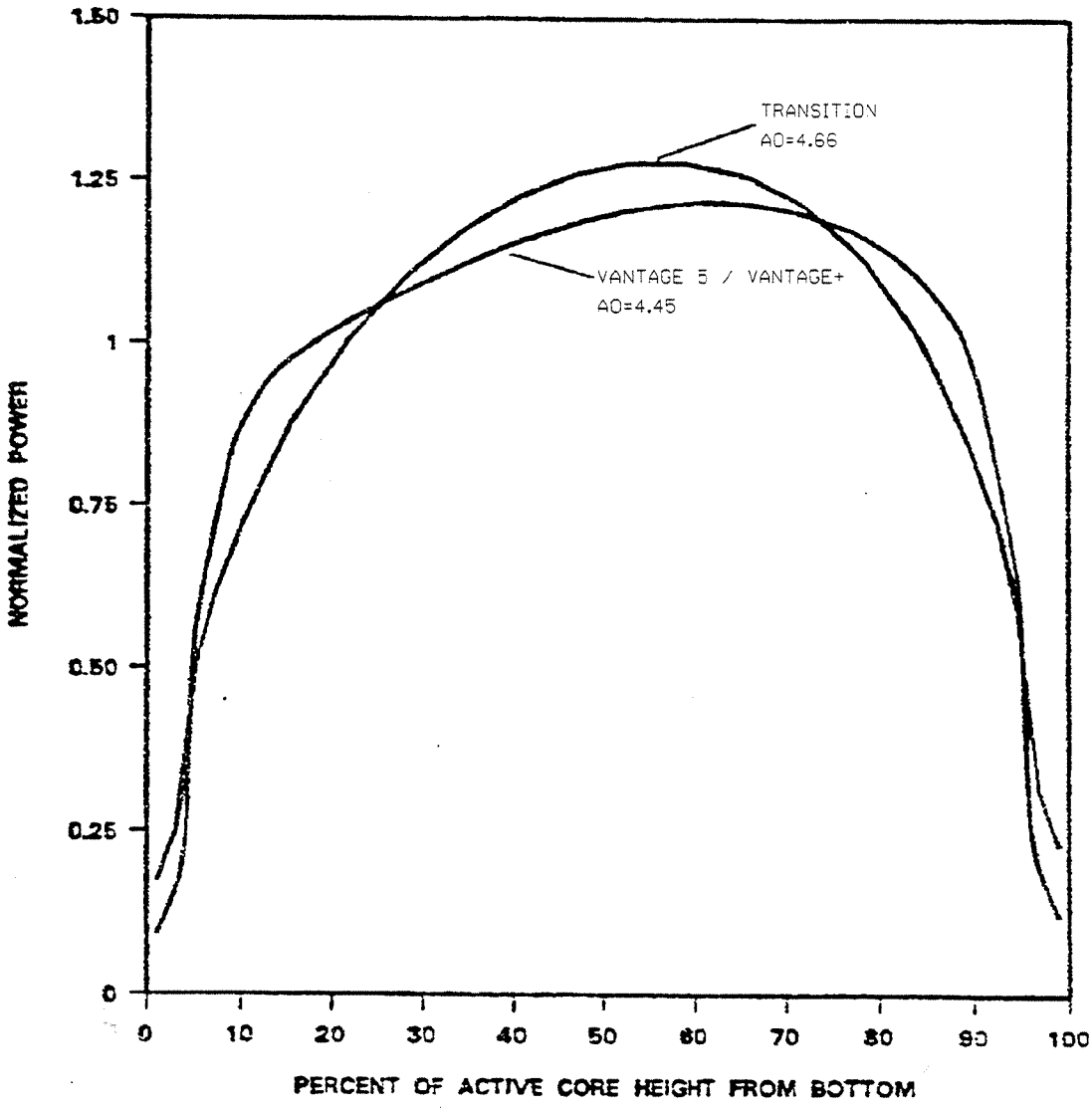

SOUTH CAROLINA ELECTRIC & GAS CO. VIRGIL C. SUMMER NUCLEAR STATION
Typical Axial Power Shapes Occurring at Beginning of Life Figure 4.3-18

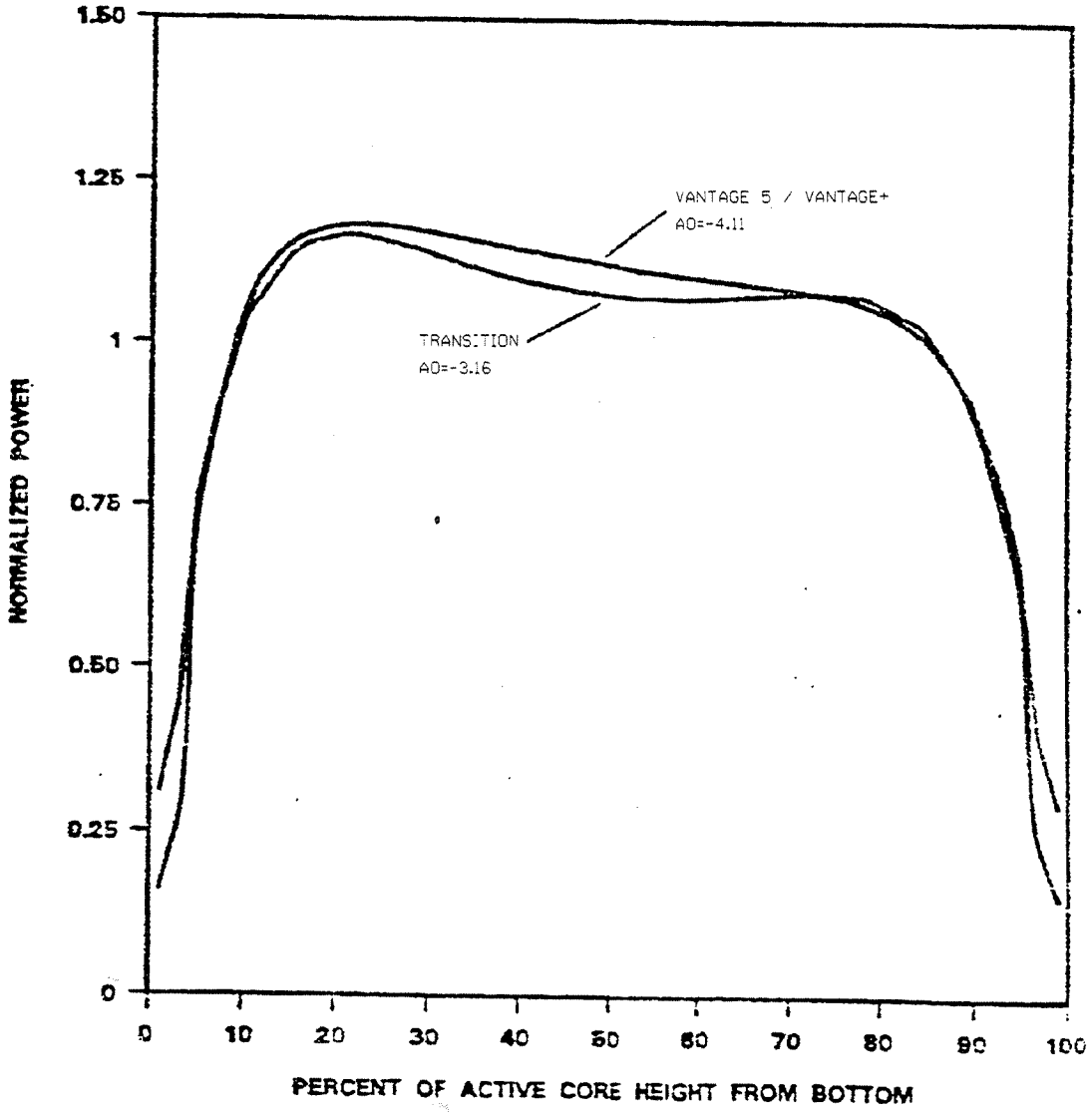

SOUTH CAROLINA ELECTRIC & GAS CO. VIRGIL C. SUMMER NUCLEAR STATION
Typical Axial Power Shapes Occurring at Middle of Life Figure 4.3-19

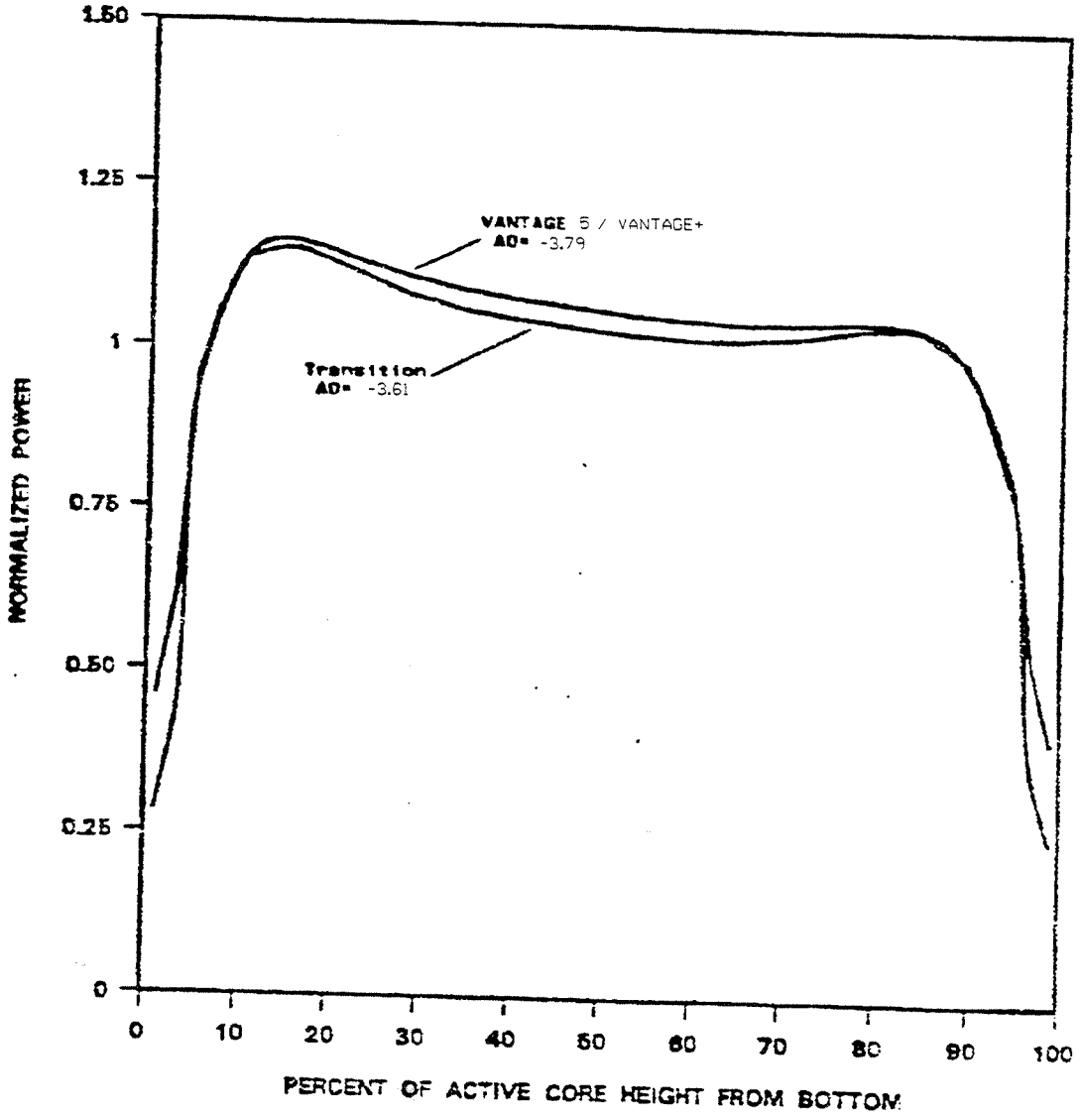

SOUTH CAROLINA ELECTRIC & GAS CO. VIRGIL C. SUMMER NUCLEAR STATION
Typical Axial Power Shapes Occurring at End of Life Figure 4.3-20

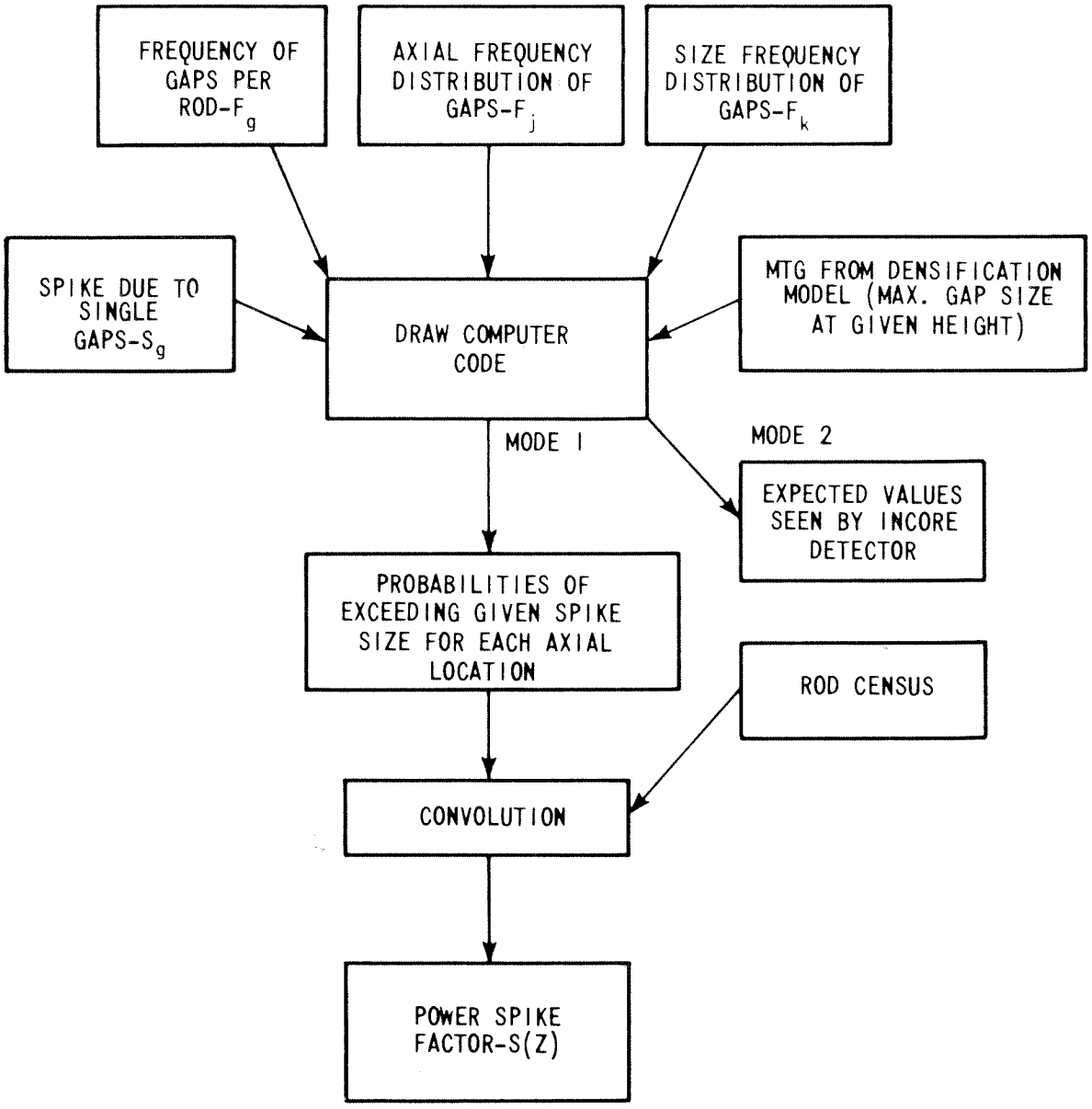

AMENDMENT 6
AUGUST, 1990

SOUTH CAROLINA ELECTRIC & GAS CO.
VIRGIL C. SUMMER NUCLEAR STATION

Flowchart for Determining Spike Model

Figure 4.3-22

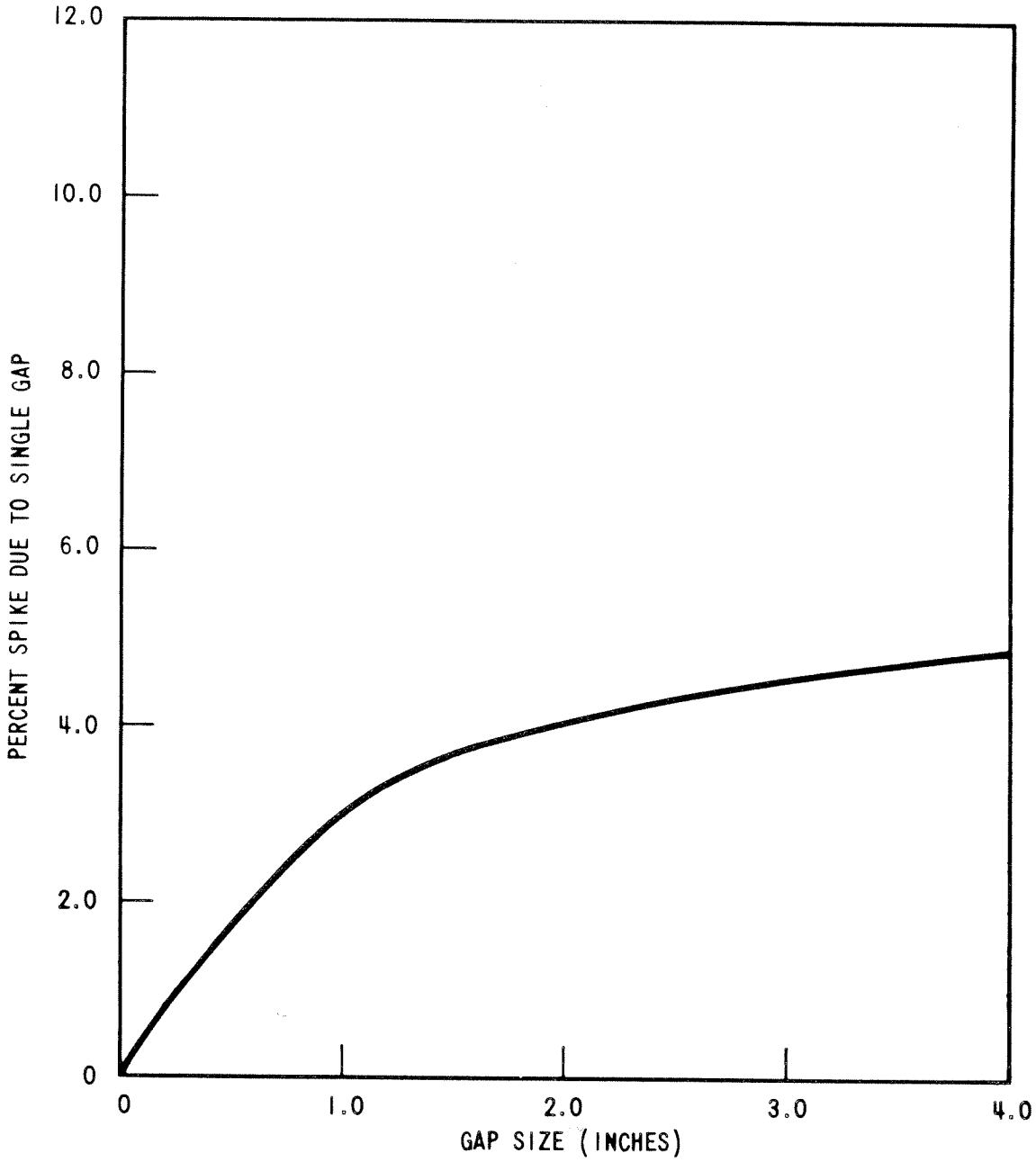

AMENDMENT 6
AUGUST, 1990

SOUTH CAROLINA ELECTRIC & GAS CO.
VIRGIL C. SUMMER NUCLEAR STATION

Predicted Power Spike Due to Single Non-Flattened Gap in the Adjacent Fuel

Figure 4.3-23

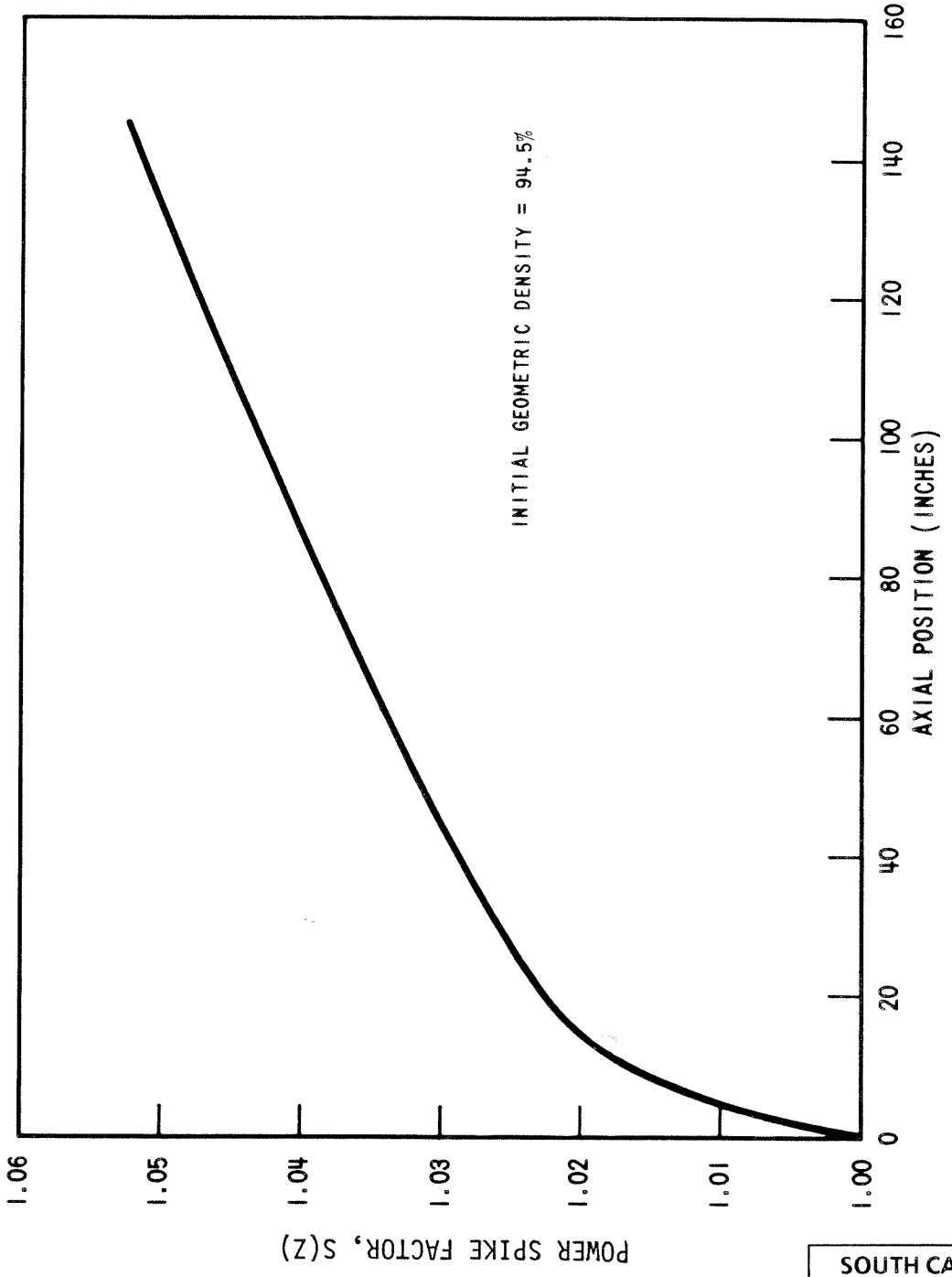

AMENDMENT 6
AUGUST, 1990

SOUTH CAROLINA ELECTRIC & GAS CO.
VIRGIL C. SUMMER NUCLEAR STATION

Power Spike Factor as a
Function of Axial Position

Figure 4.3-24

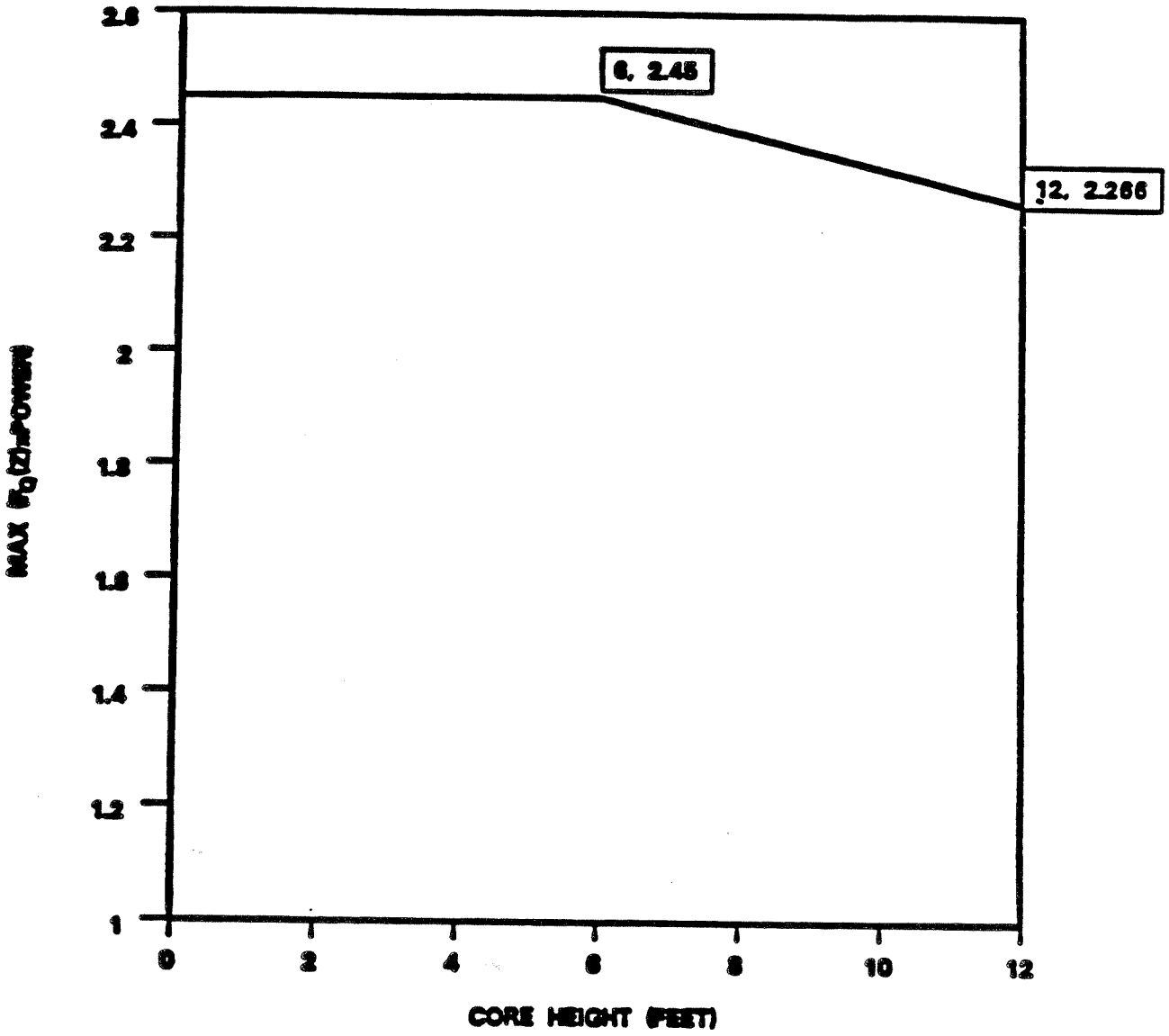

AMENDMENT 6
AUGUST, 1990

SOUTH CAROLINA ELECTRIC & GAS CO.
VIRGIL C. SUMMER NUCLEAR STATION

Maximum F_Q x Power Versus Axial Height During Normal Operation

Figure 4.3-25

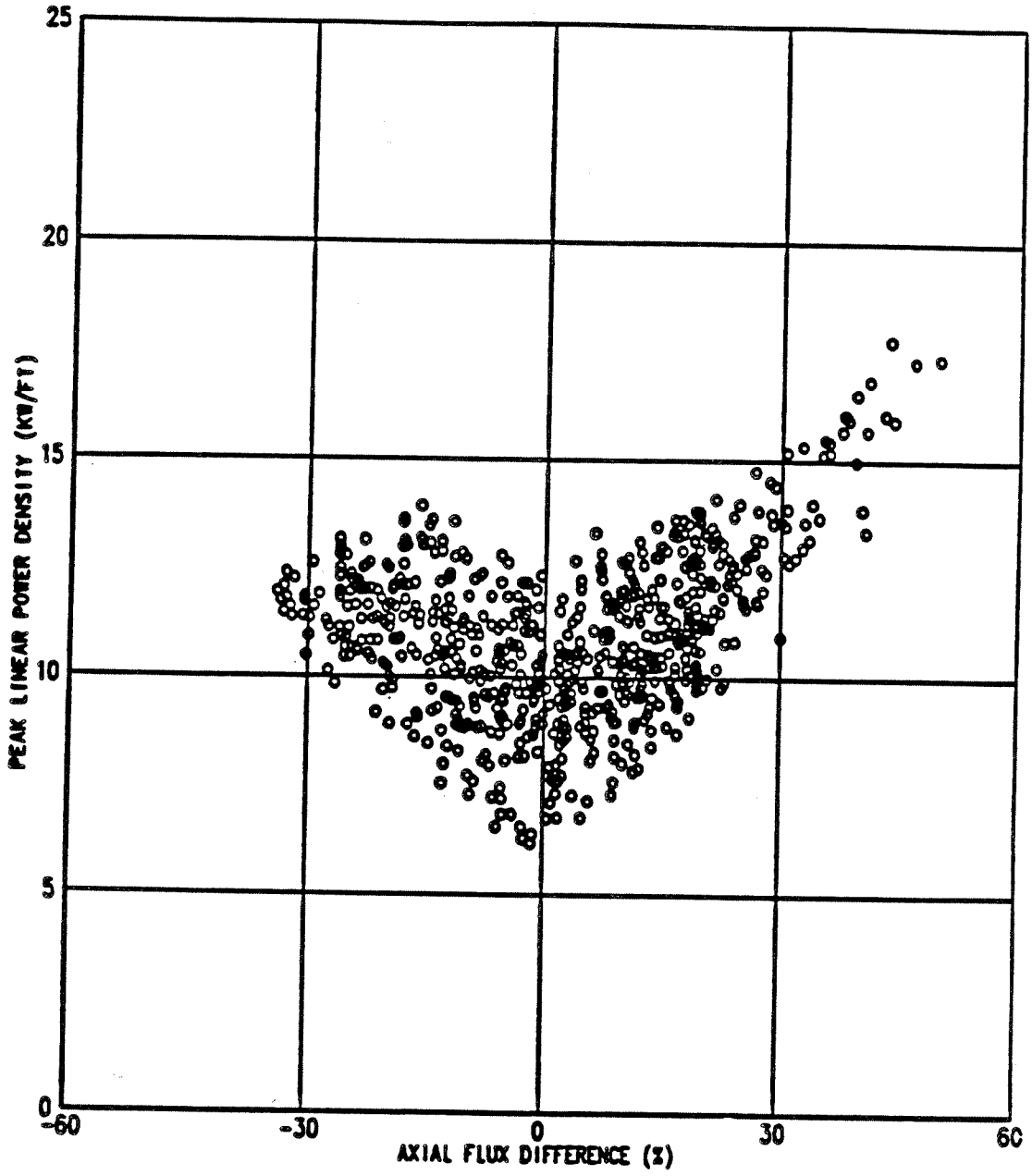

AMENDMENT 6
AUGUST, 1990

SOUTH CAROLINA ELECTRIC & GAS CO.
VIRGIL C. SUMMER NUCLEAR STATION

Peak Power During Control Rod Malfunction Overpower Transients

Figure 4.3-26

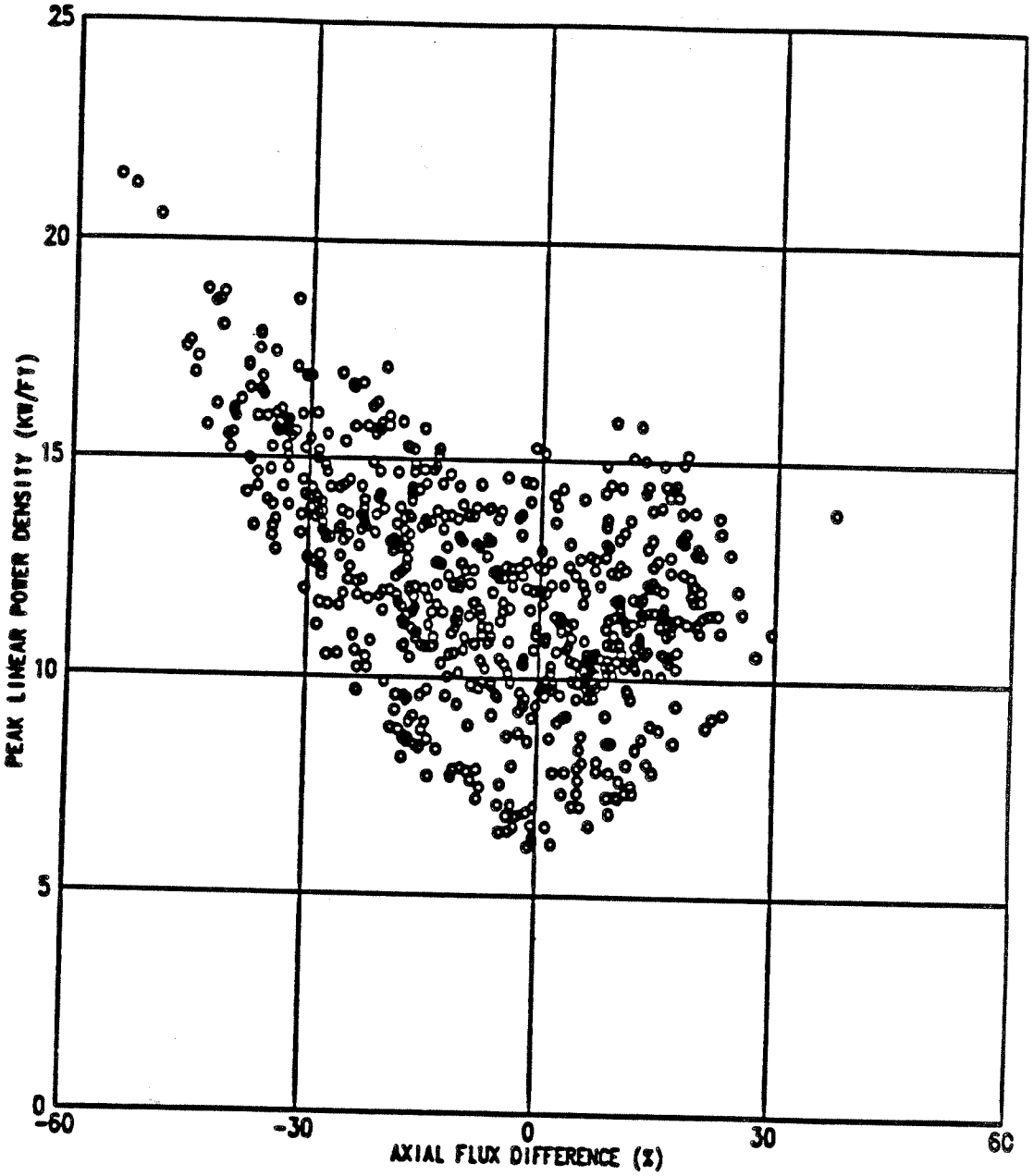

AMENDMENT 6
AUGUST, 1990

SOUTH CAROLINA ELECTRIC & GAS CO.
VIRGIL C. SUMMER NUCLEAR STATION

Peak Power During Boration/Dilution Overpower Transients

Figure 4.3-27

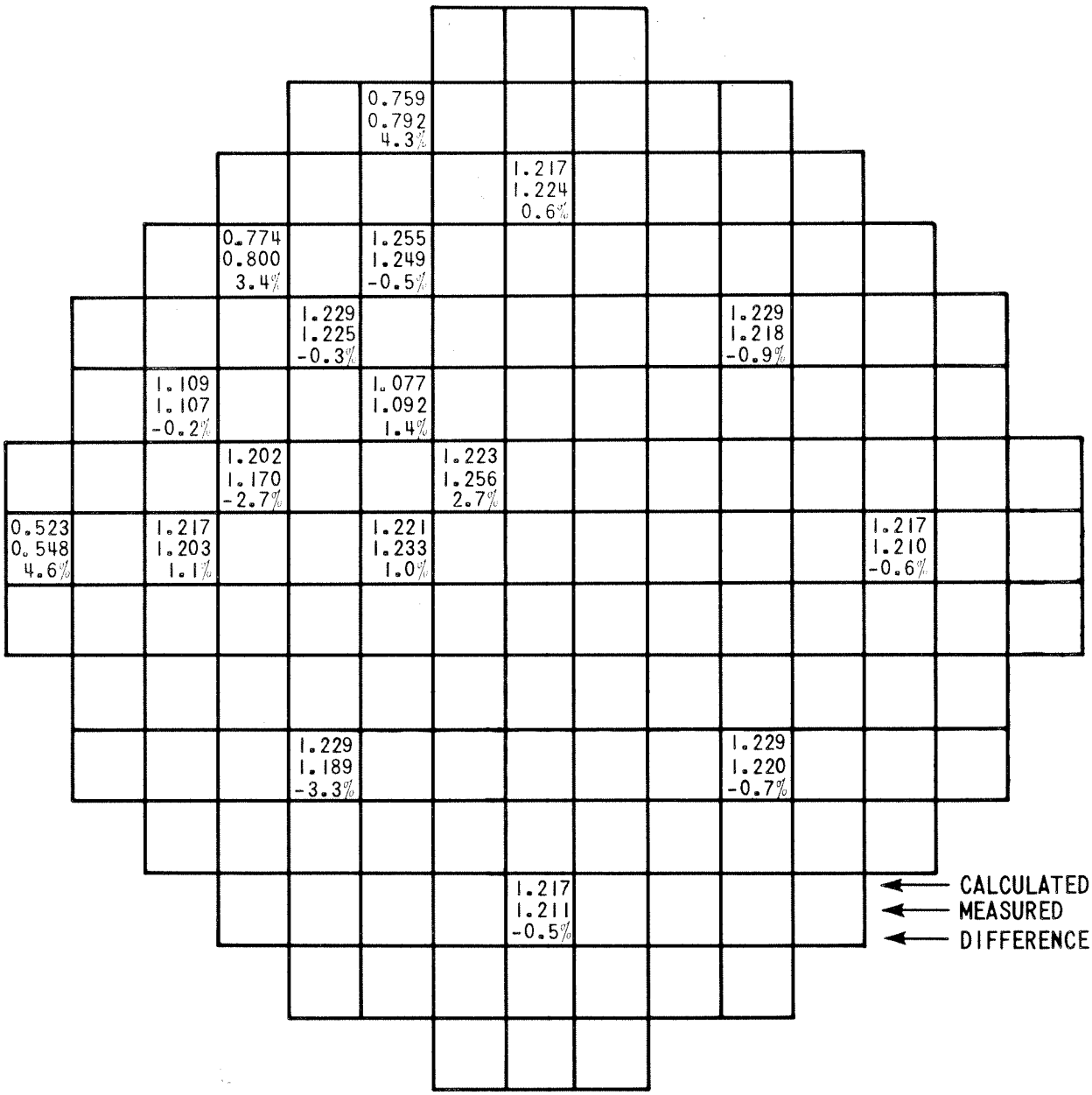

PEAKING FACTORS

$\bar{F}_z$ = 1.5

$F^N_{\Delta H}$ = 1.357

F^N_Q = 2.07 LOCATED AT M-8 SOUTH

AMENDMENT 6
AUGUST, 1990

SOUTH CAROLINA ELECTRIC & GAS CO.
VIRGIL C. SUMMER NUCLEAR STATION

Comparison Between Calculated and Measured Relative Fuel Assembly Power Distribution

Figure 4.3-28

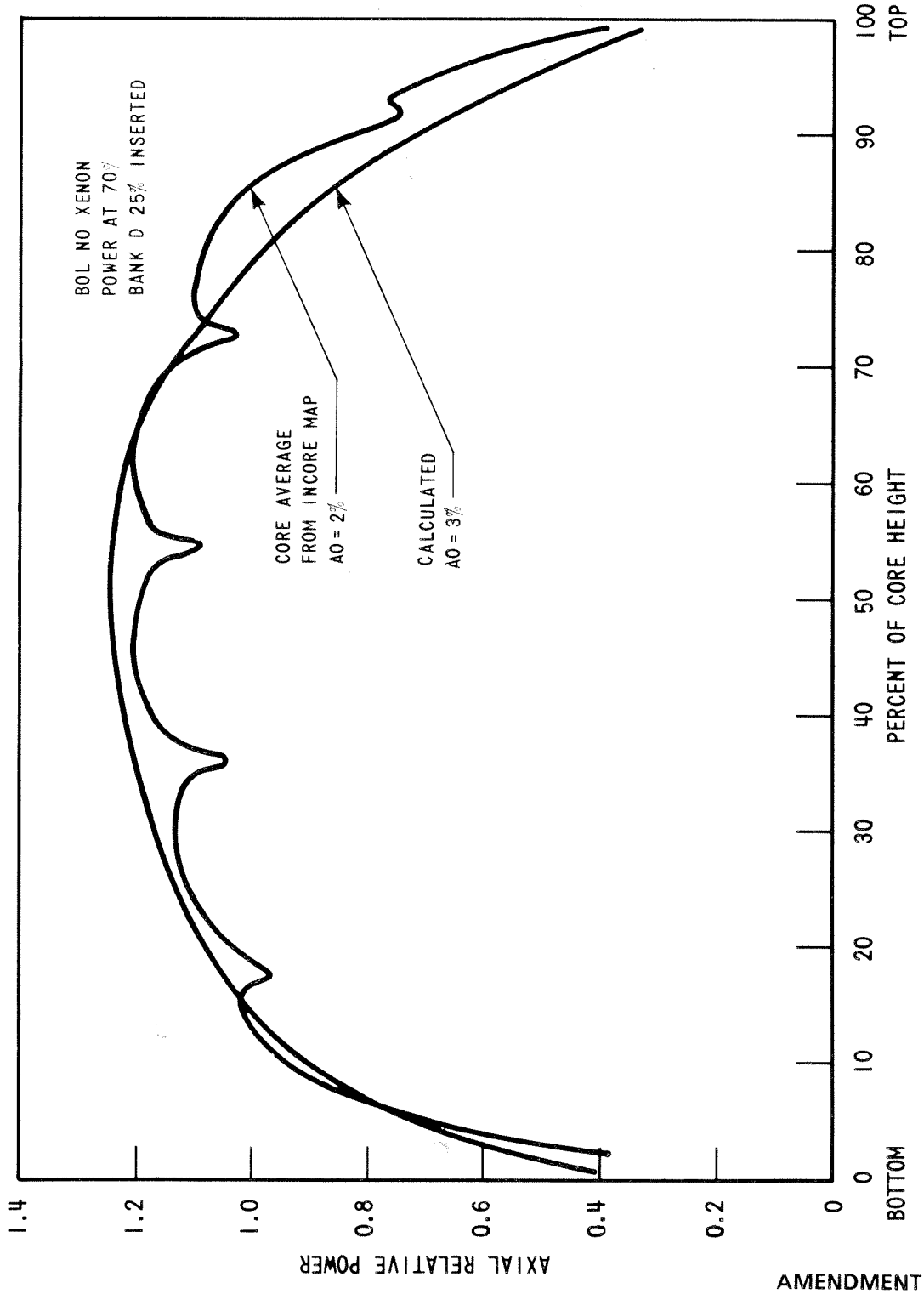

AMENDMENT 6
AUGUST, 1990

SOUTH CAROLINA ELECTRIC & GAS CO.
VIRGIL C. SUMMER NUCLEAR STATION

Comparison of Calculated
and Measured Axial Shape

Figure 4.3-29

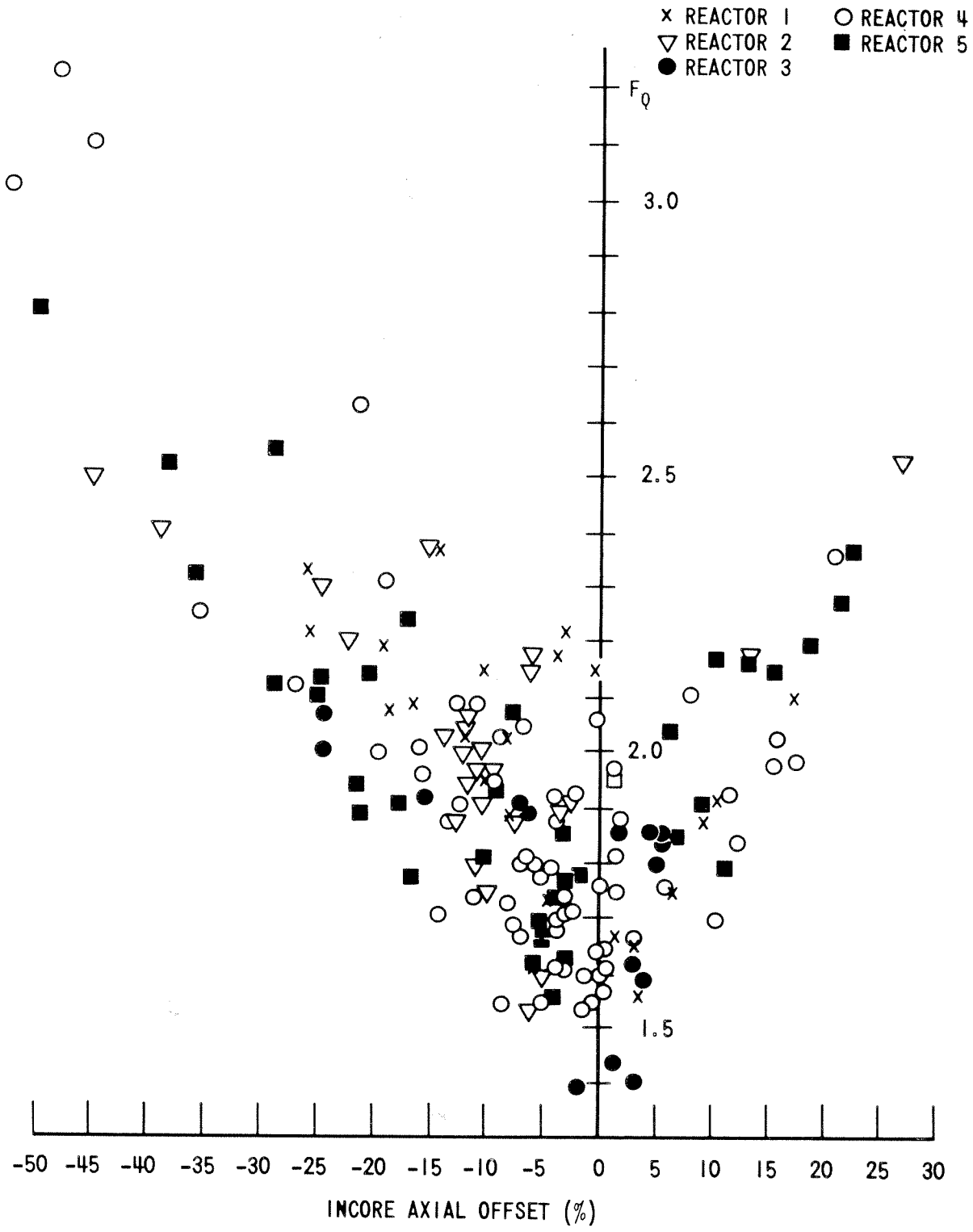

AMENDMENT 6
AUGUST, 1990

SOUTH CAROLINA ELECTRIC & GAS CO.
VIRGIL C. SUMMER NUCLEAR STATION

Measured Values of F_Q for
Full Power Rod Configurations

Figure 4.3-30

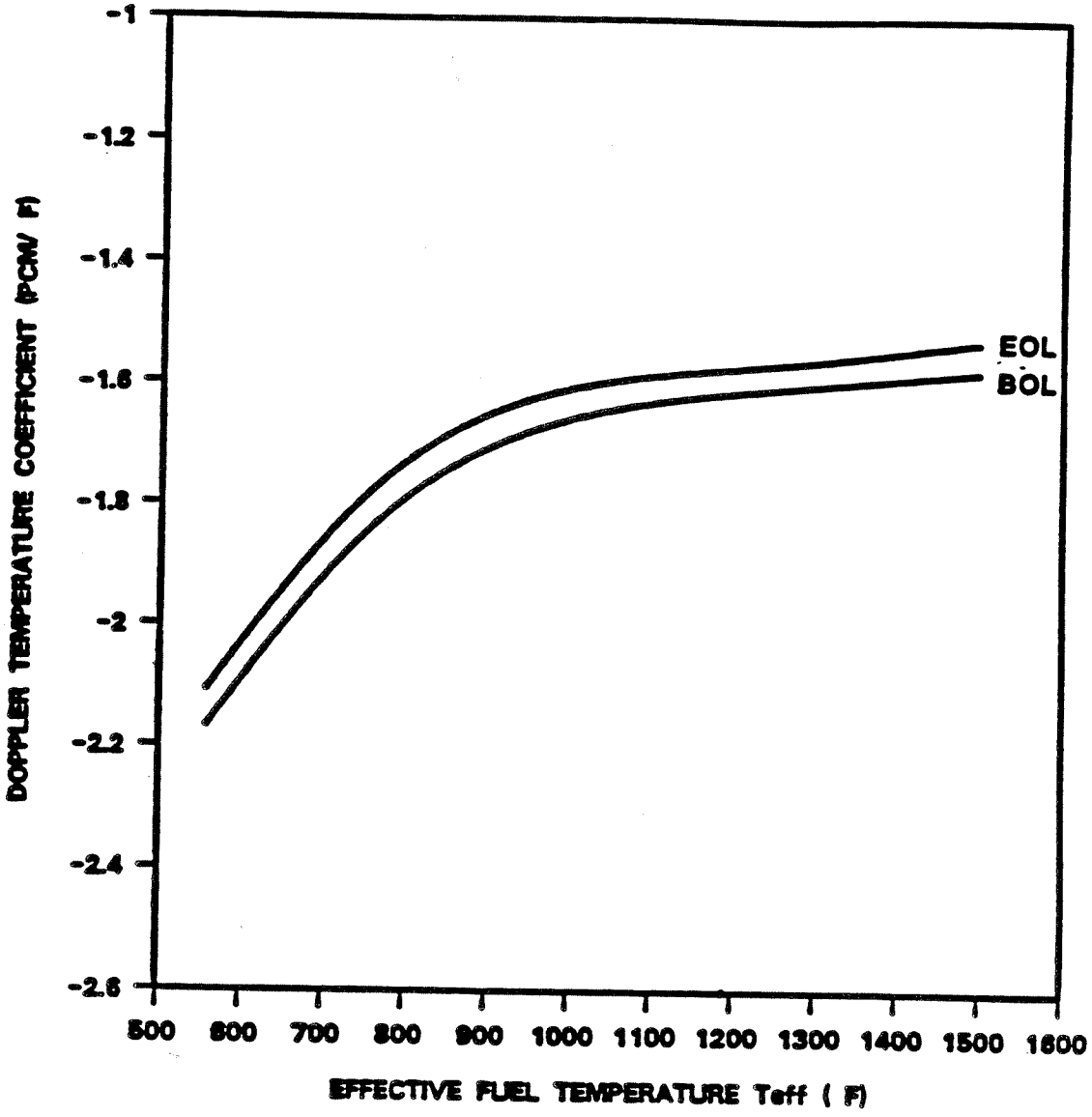

AMENDMENT 6
AUGUST, 1990

SOUTH CAROLINA ELECTRIC & GAS CO.
VIRGIL C. SUMMER NUCLEAR STATION

Doppler Temperature Coefficient at BOL and EOL Versus T_{eff} for a Typical Reload Core

Figure 4.3-31

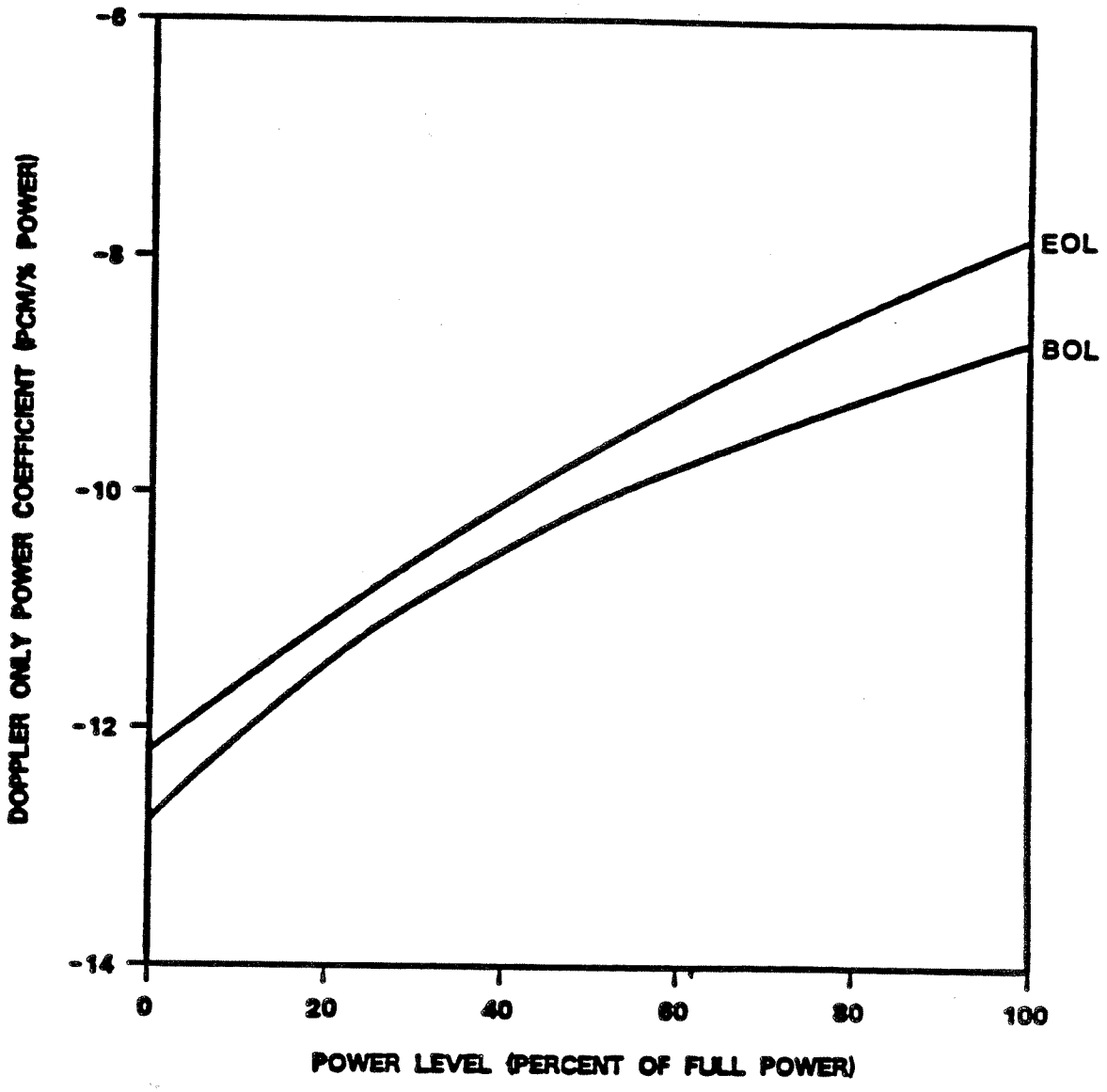

AMENDMENT 6
AUGUST, 1990

SOUTH CAROLINA ELECTRIC & GAS CO.
VIRGIL C. SUMMER NUCLEAR STATION

Doppler Only Power Coefficient
Versus Power Level at BOL and EOL
for a Typical Reload Core

Figure 4.3-32

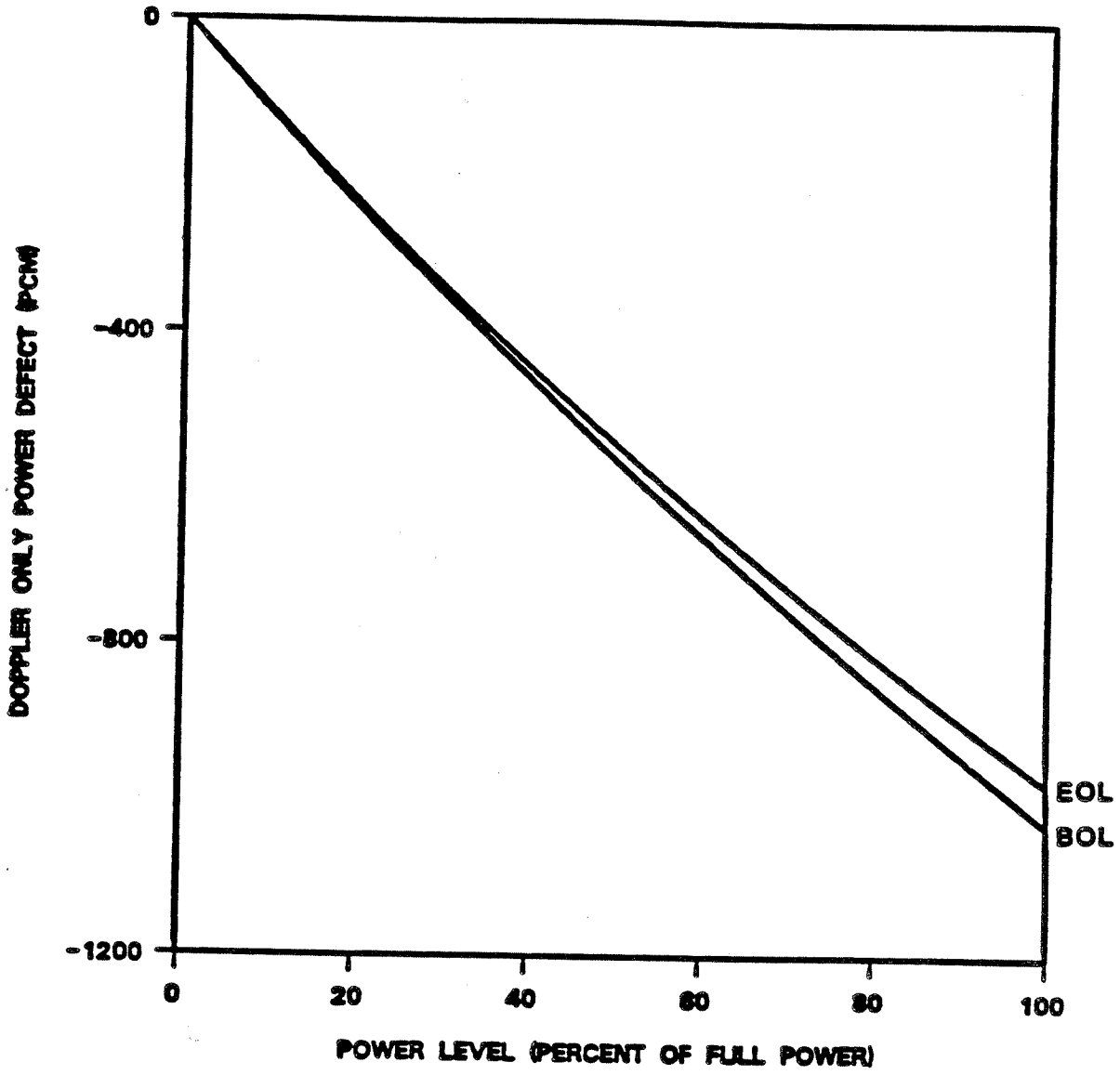

AMENDMENT 6
AUGUST, 1990

SOUTH CAROLINA ELECTRIC & GAS CO.
VIRGIL C. SUMMER NUCLEAR STATION

Doppler Only Power Defect Versus
Percent Power BOL and EOL
for a Typical Reload Core

Figure 4.3-33

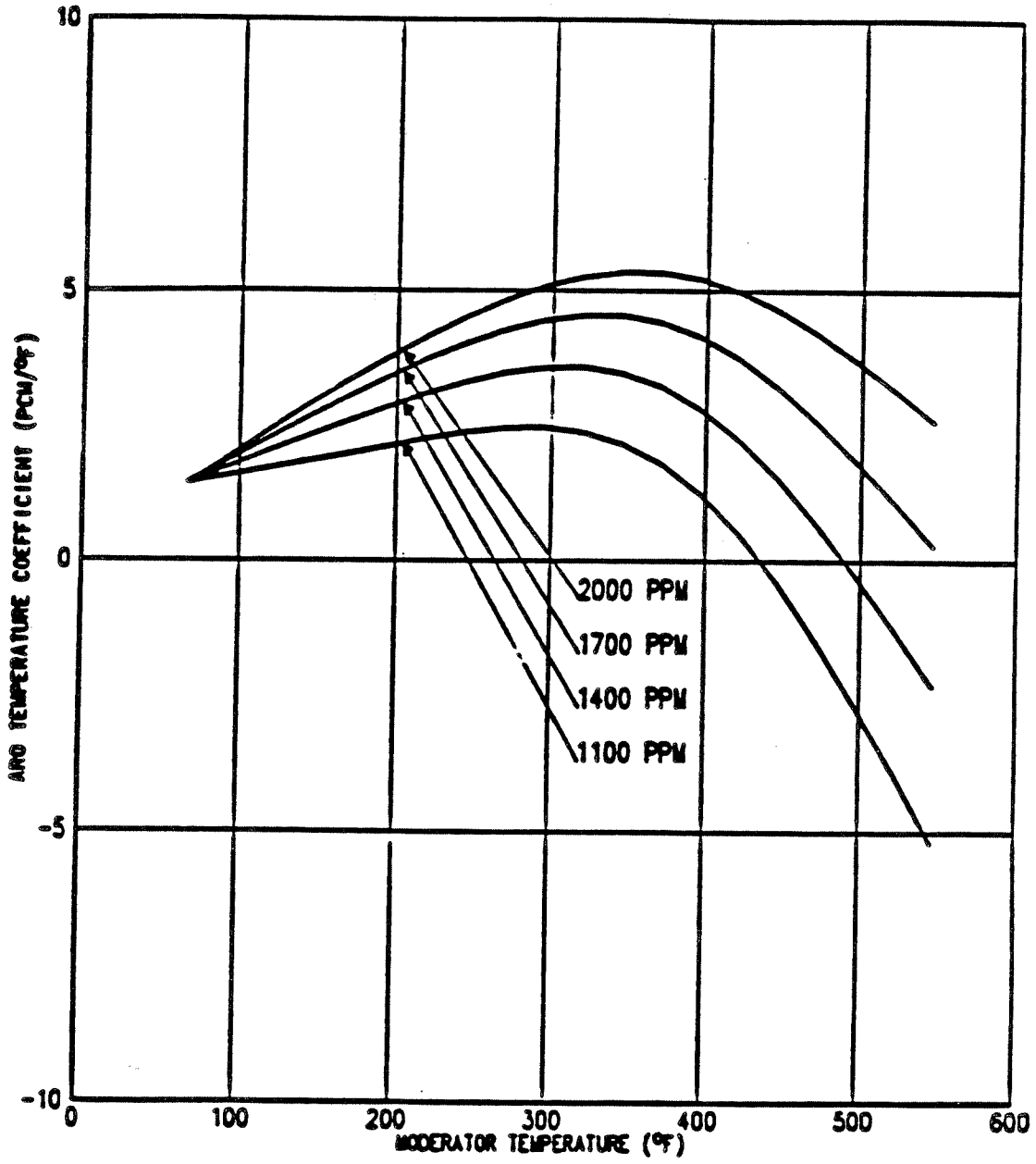

AMENDMENT 6
AUGUST, 1990

SOUTH CAROLINA ELECTRIC & GAS CO.
VIRGIL C. SUMMER NUCLEAR STATION

Moderator Temperature Coefficient
BOL, No Rods, for a Typical Reload Core

Figure 4.3-34

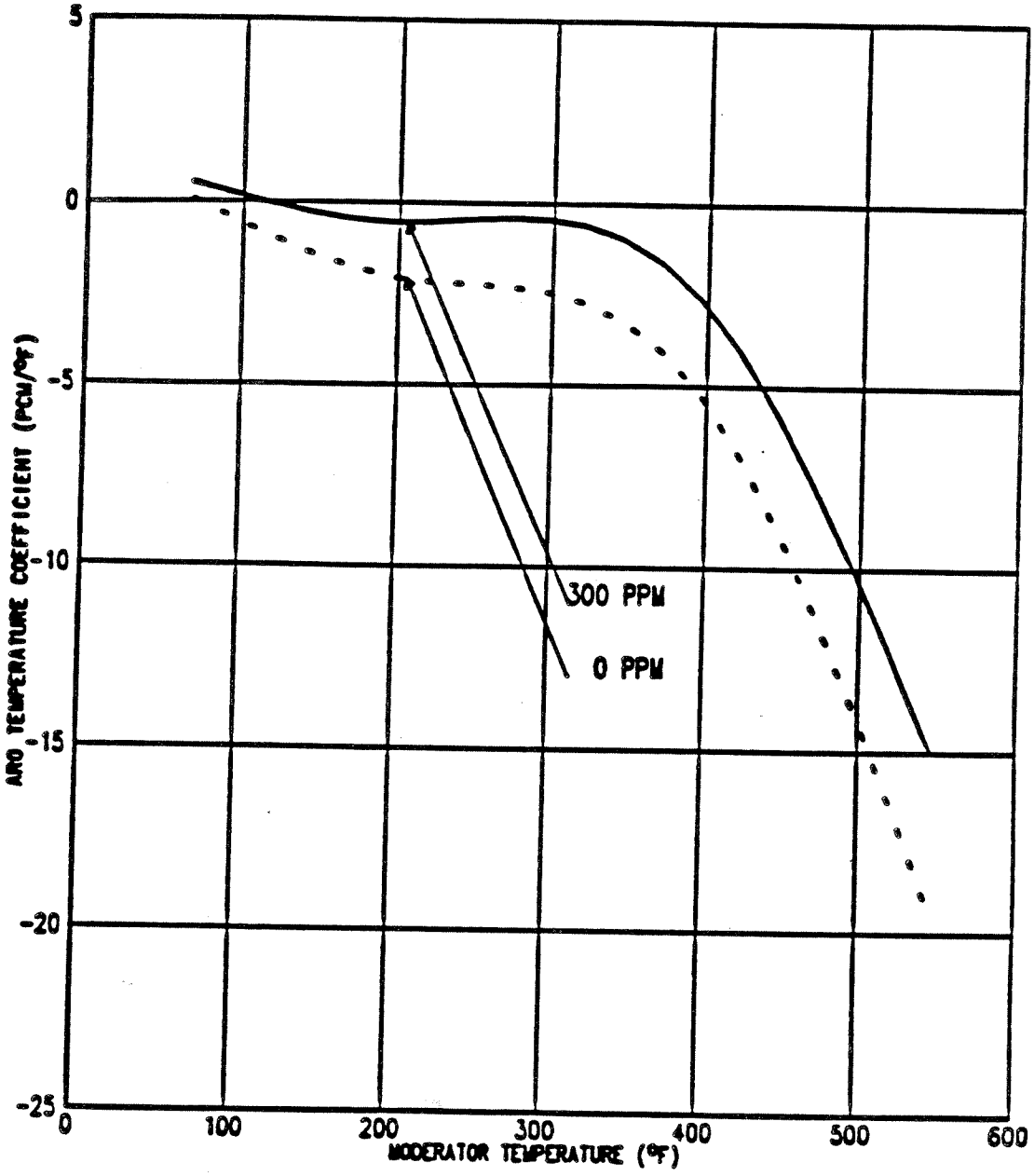

AMENDMENT 6
AUGUST, 1990

SOUTH CAROLINA ELECTRIC & GAS CO.
VIRGIL C. SUMMER NUCLEAR STATION

Moderator Temperature Coefficient
EOL for a Typical Reload Core

Figure 4.3-35

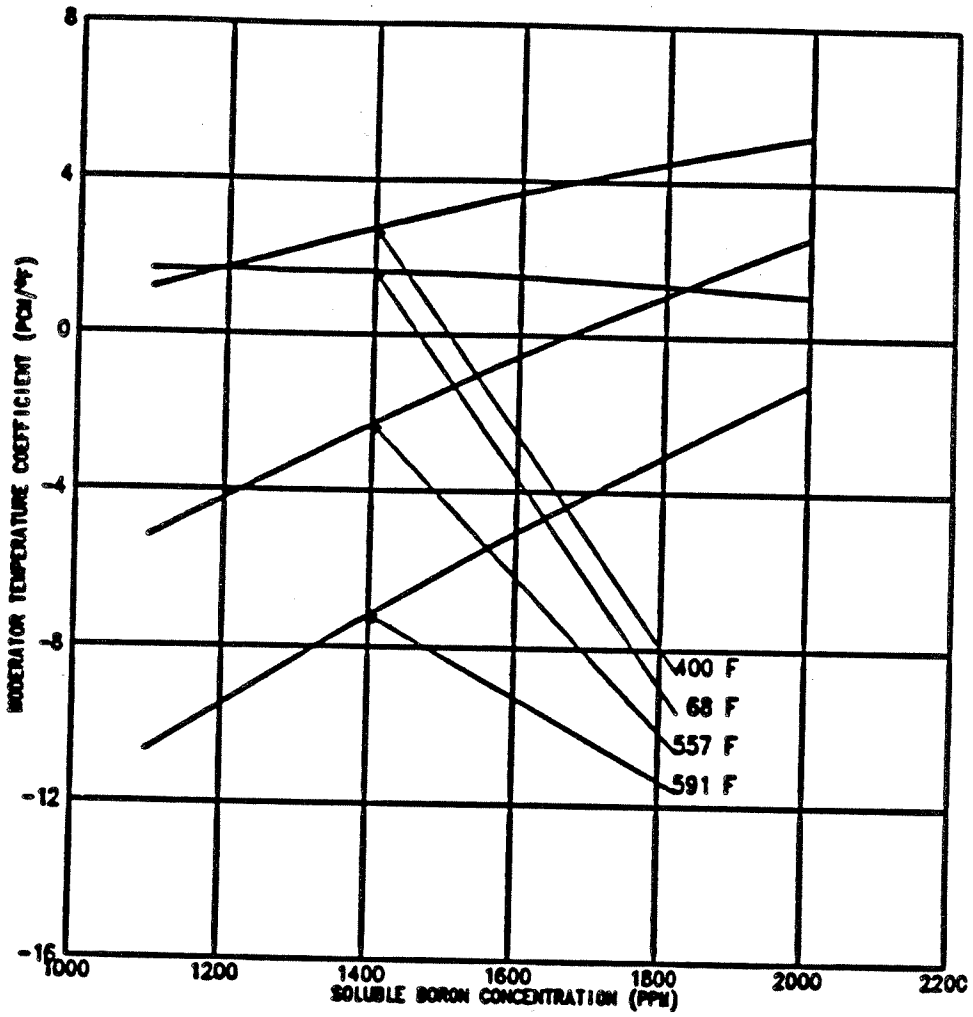

AMENDMENT 6
AUGUST, 1990

SOUTH CAROLINA ELECTRIC & GAS CO.
VIRGIL C. SUMMER NUCLEAR STATION

Moderator Temperature Coefficient
as a Function of Boron Concentration
BOL, No Rods, for a Typical Reload Core

Figure 4.3-36

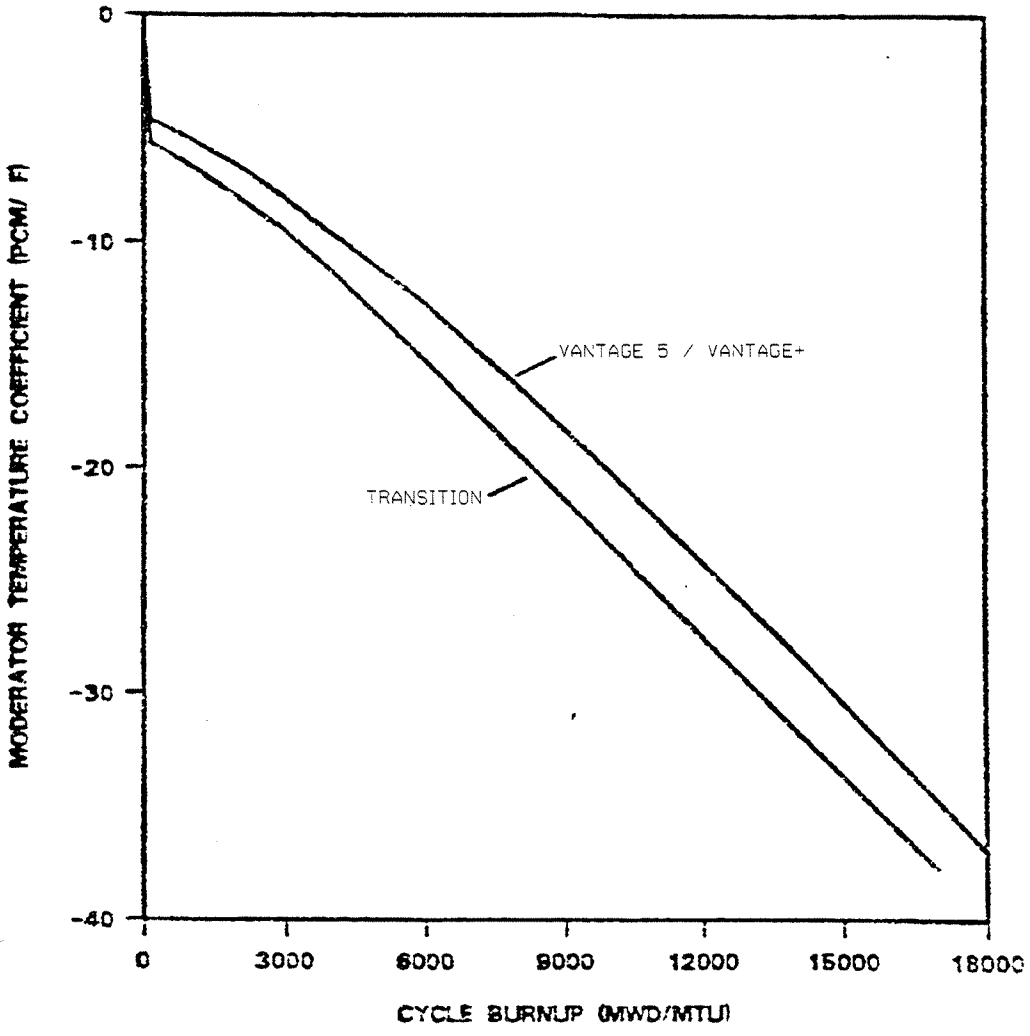

SOUTH CAROLINA ELECTRIC & GAS CO. VIRGIL C. SUMMER NUCLEAR STATION
Hot Full Power Temperature Coefficient at Critical Boron Concentration versus Burnup Figure 4.3-37

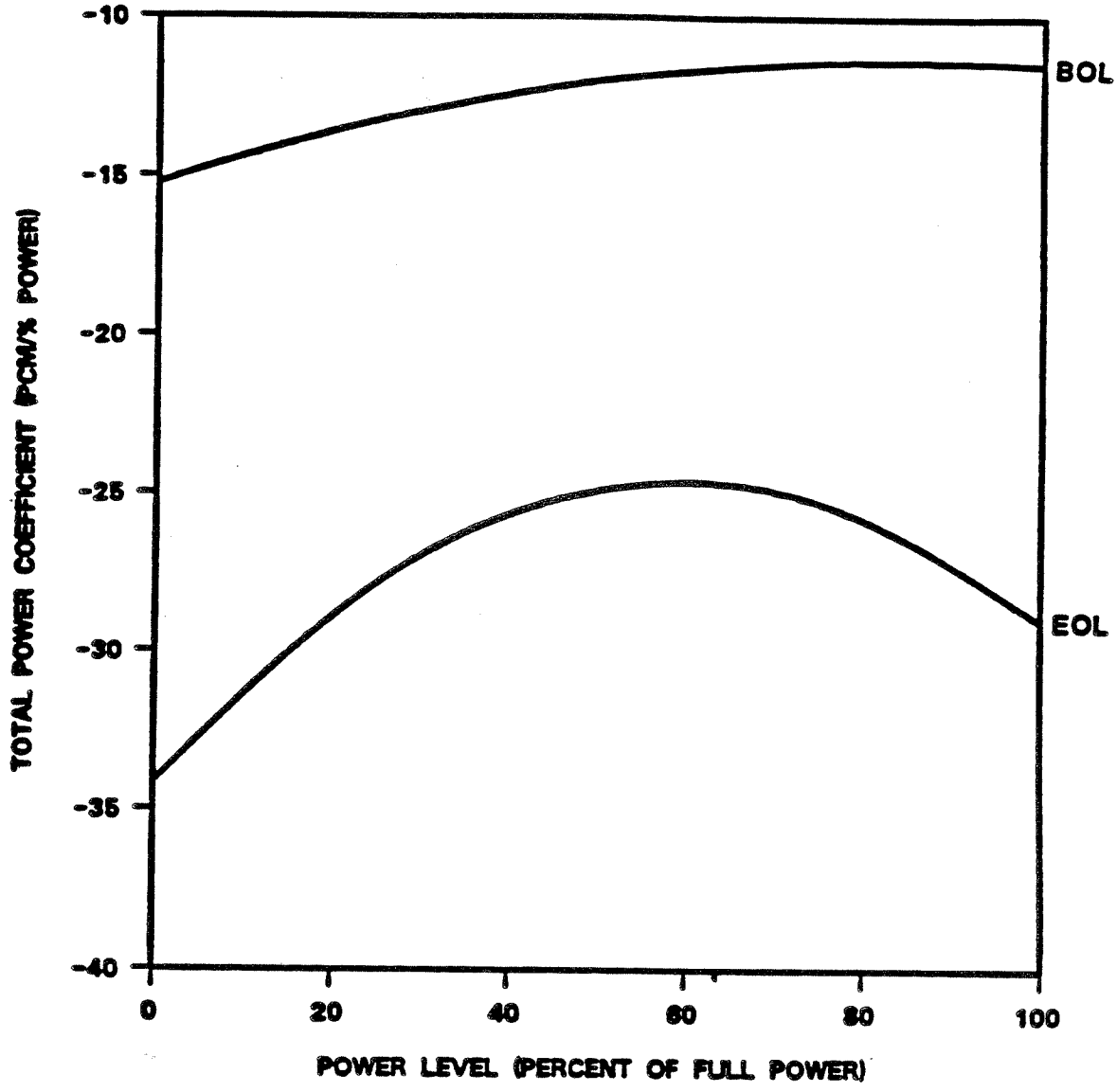

AMENDMENT 6
AUGUST, 1990

SOUTH CAROLINA ELECTRIC & GAS CO.
VIRGIL C. SUMMER NUCLEAR STATION

Total Power Coefficient Versus
Percent Power for BOL and EOL
on a Typical Reload Core

Figure 4.3-38

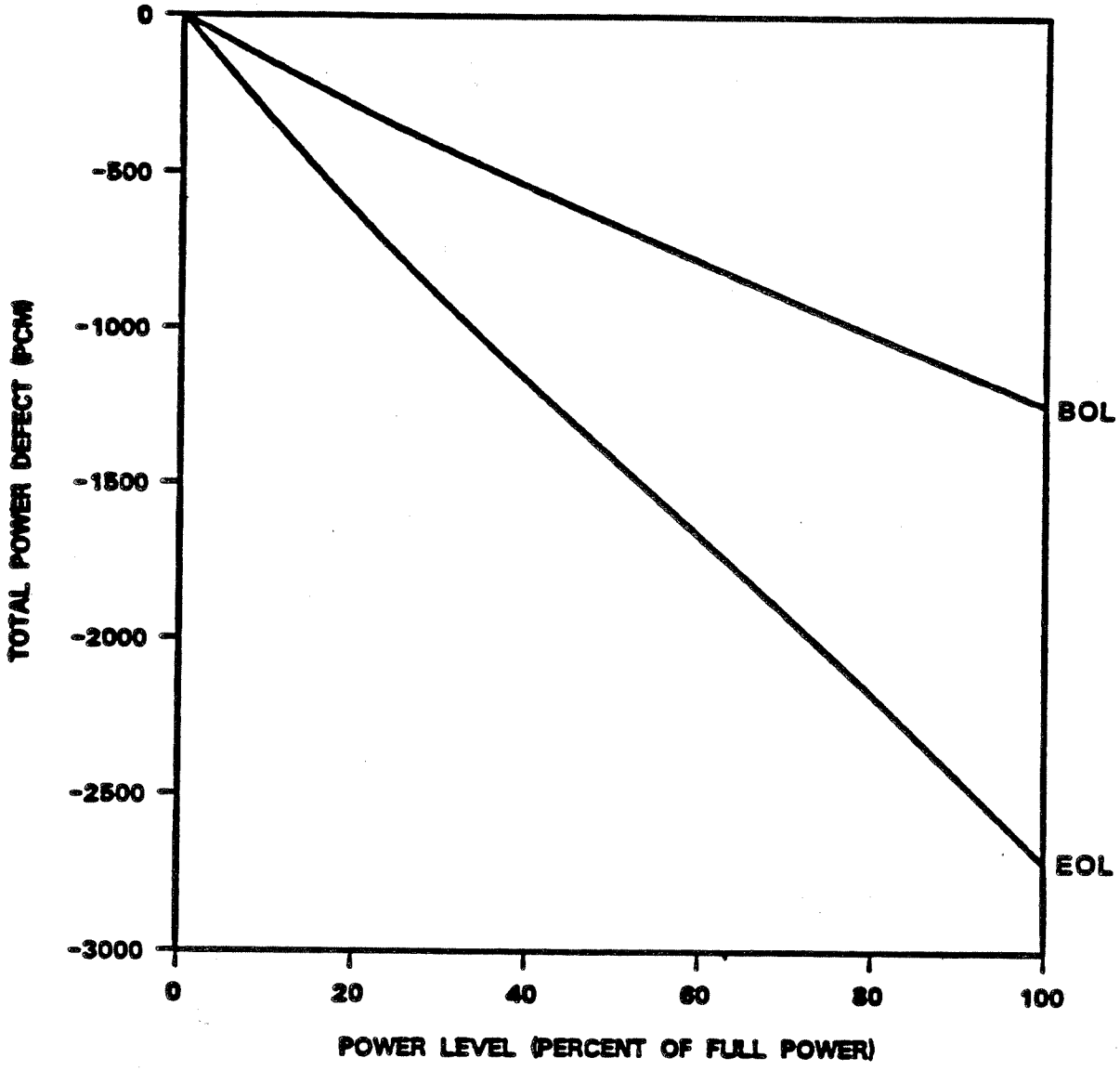

AMENDMENT 6
AUGUST, 1990

SOUTH CAROLINA ELECTRIC & GAS CO. VIRGIL C. SUMMER NUCLEAR STATION
Total Power Defect BOL, EOL, for a Typical Reload Core Figure 4.3-39

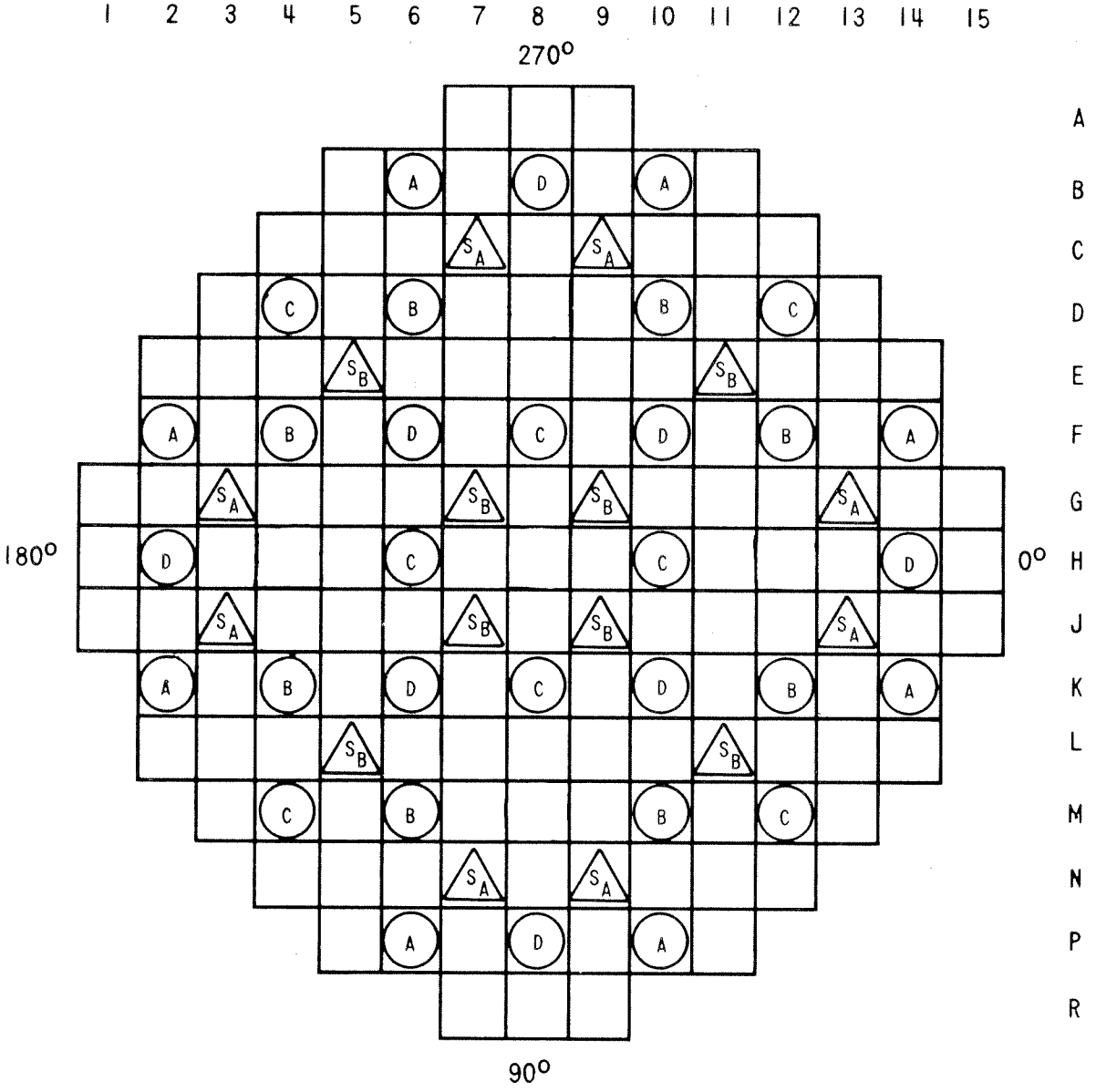

FUNCTION	NUMBER OF CLUSTERS
CONTROL BANK D	8
CONTROL BANK C	8
CONTROL BANK B	8
CONTROL BANK A	8
SHUTDOWN BANK S_B	8
SHUTDOWN BANK S_A	8

AMENDMENT 6
AUGUST, 1990

SOUTH CAROLINA ELECTRIC & GAS CO.
VIRGIL C. SUMMER NUCLEAR STATION

Rod Cluster Control Assembly Pattern

Figure 4.3-40

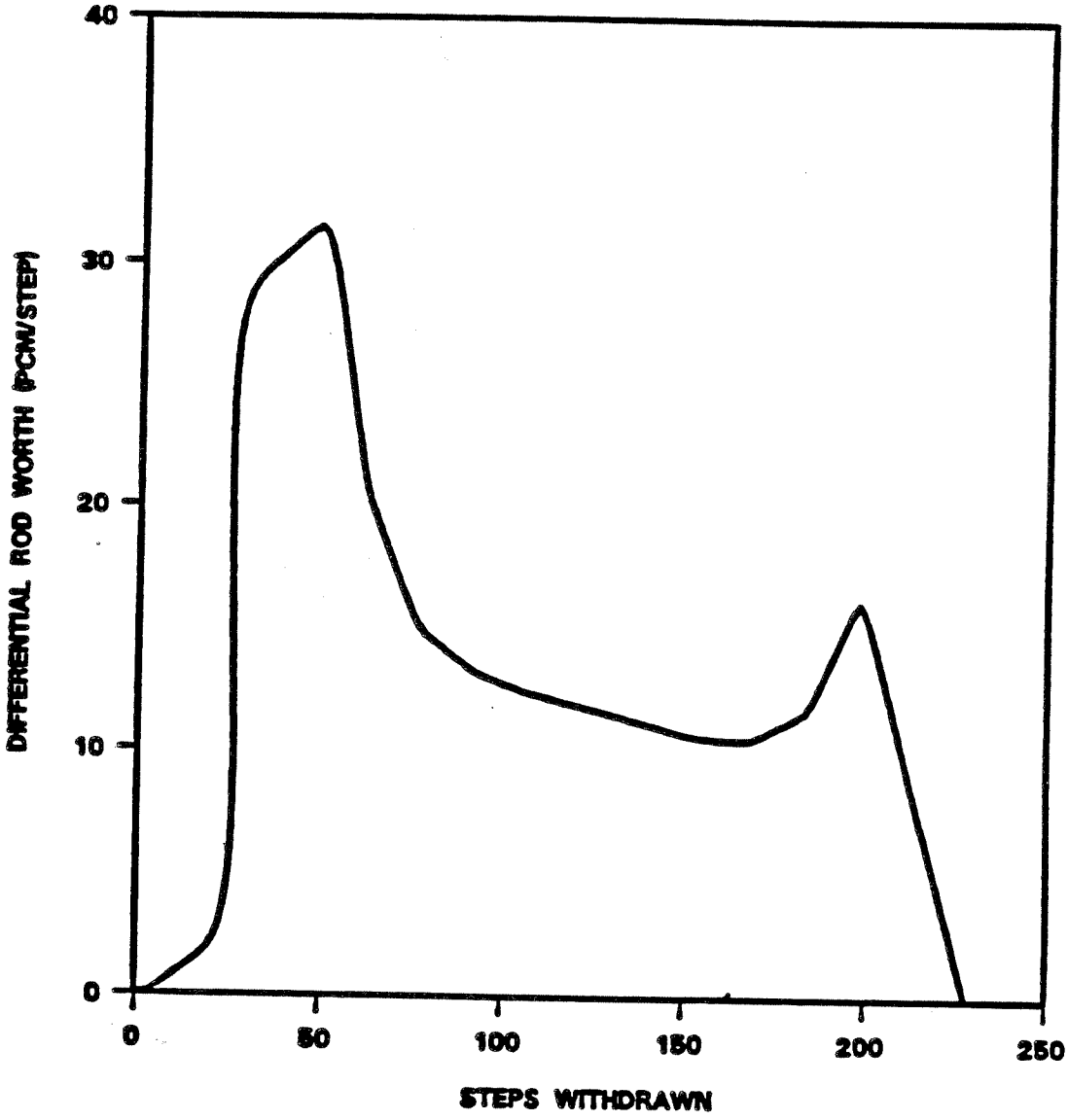

AMENDMENT 6
AUGUST, 1990

SOUTH CAROLINA ELECTRIC & GAS CO. VIRGIL C. SUMMER NUCLEAR STATION
Accidental Simultaneous Withdrawal of Two Control Banks EOL, HZP Banks D and B Moving in the Same Plane Figure 4.3-41

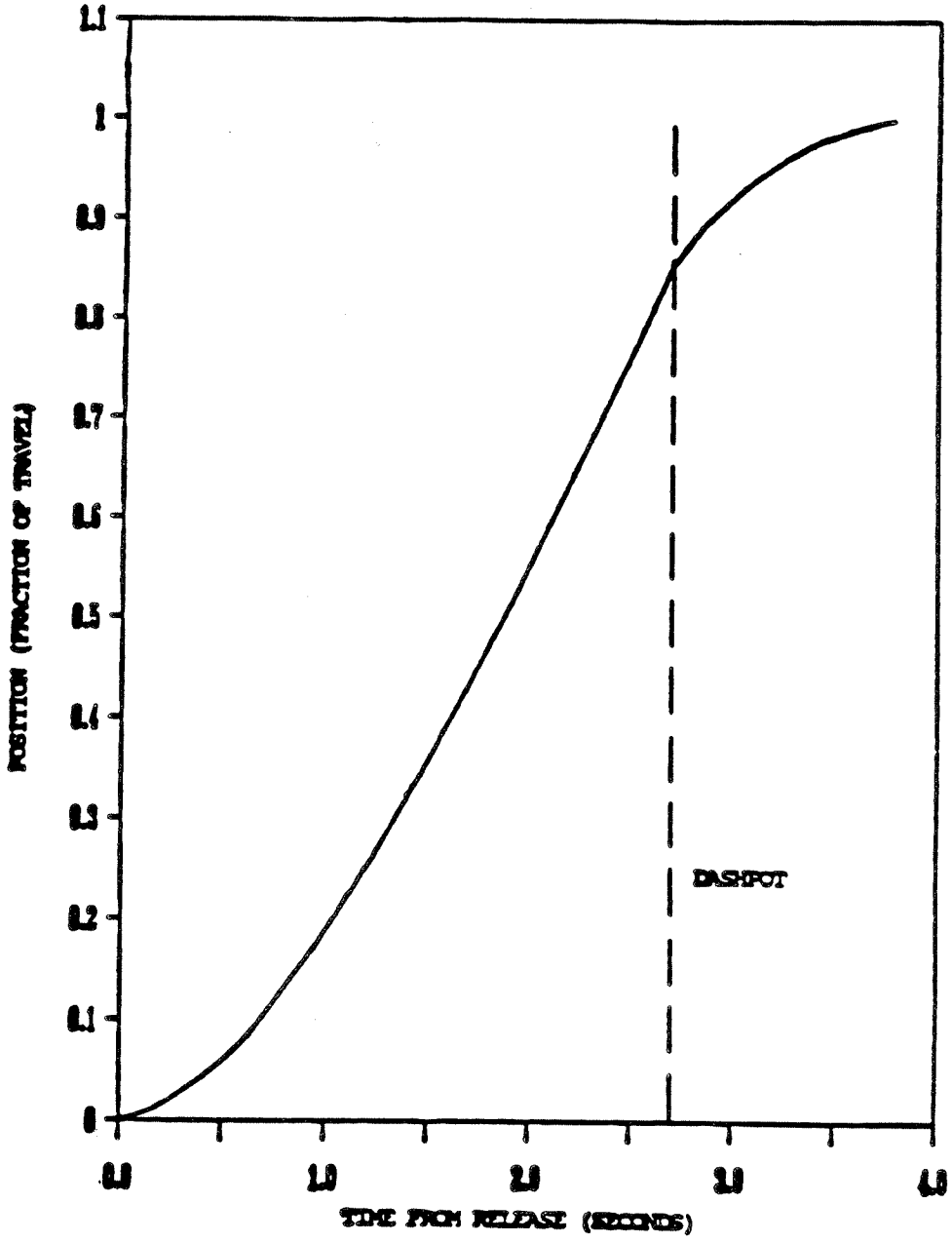

AMENDMENT 6
AUGUST, 1990

SOUTH CAROLINA ELECTRIC & GAS CO.
VIRGIL C. SUMMER NUCLEAR STATION

Rod Position Versus Time on Reactor Trip

Figure 4.3-42

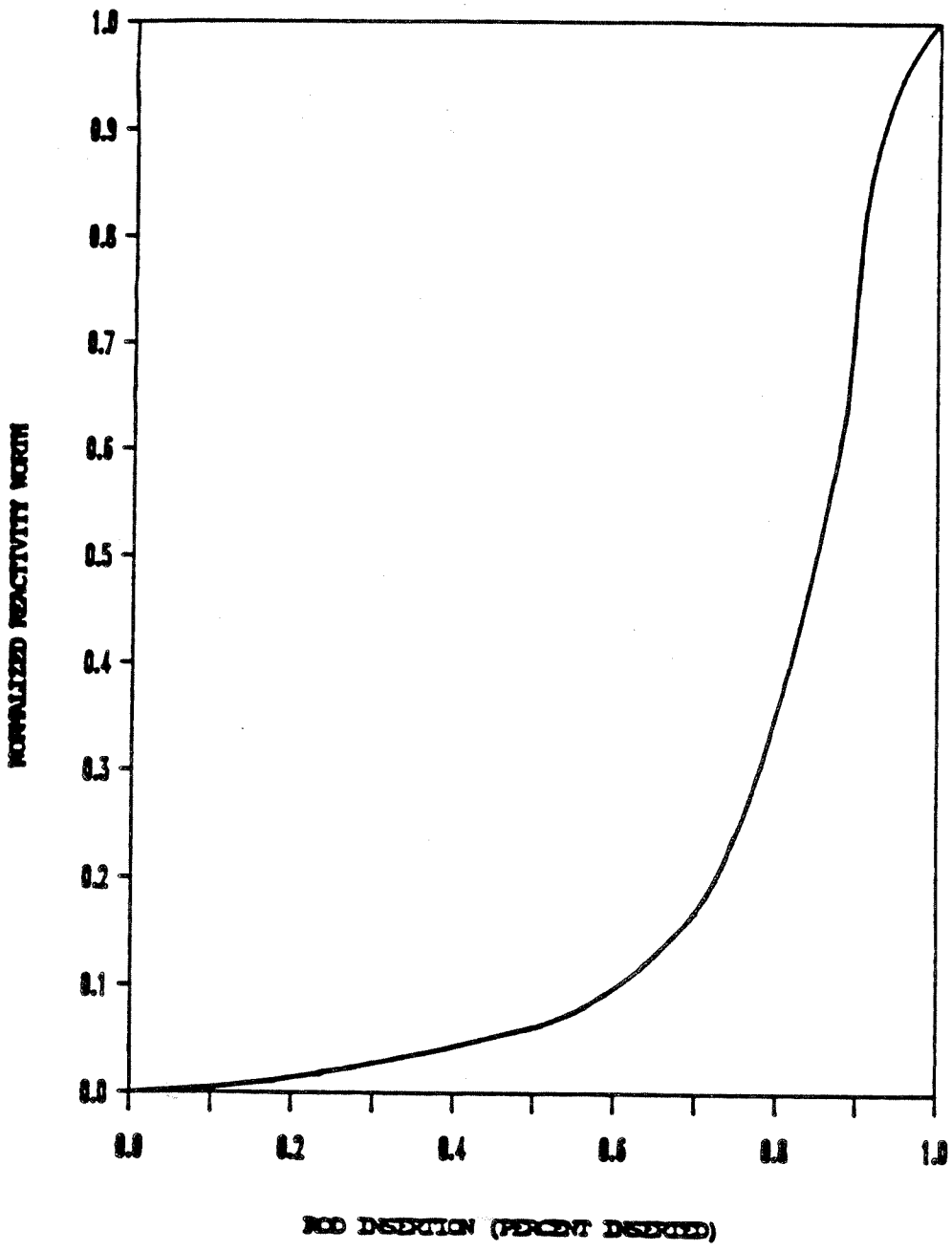

AMENDMENT 6
AUGUST, 1990

SOUTH CAROLINA ELECTRIC & GAS CO.
VIRGIL C. SUMMER NUCLEAR STATION

Normalized RCCA Reactivity Worth
Versus Percent Insertion

Figure 4.3-43

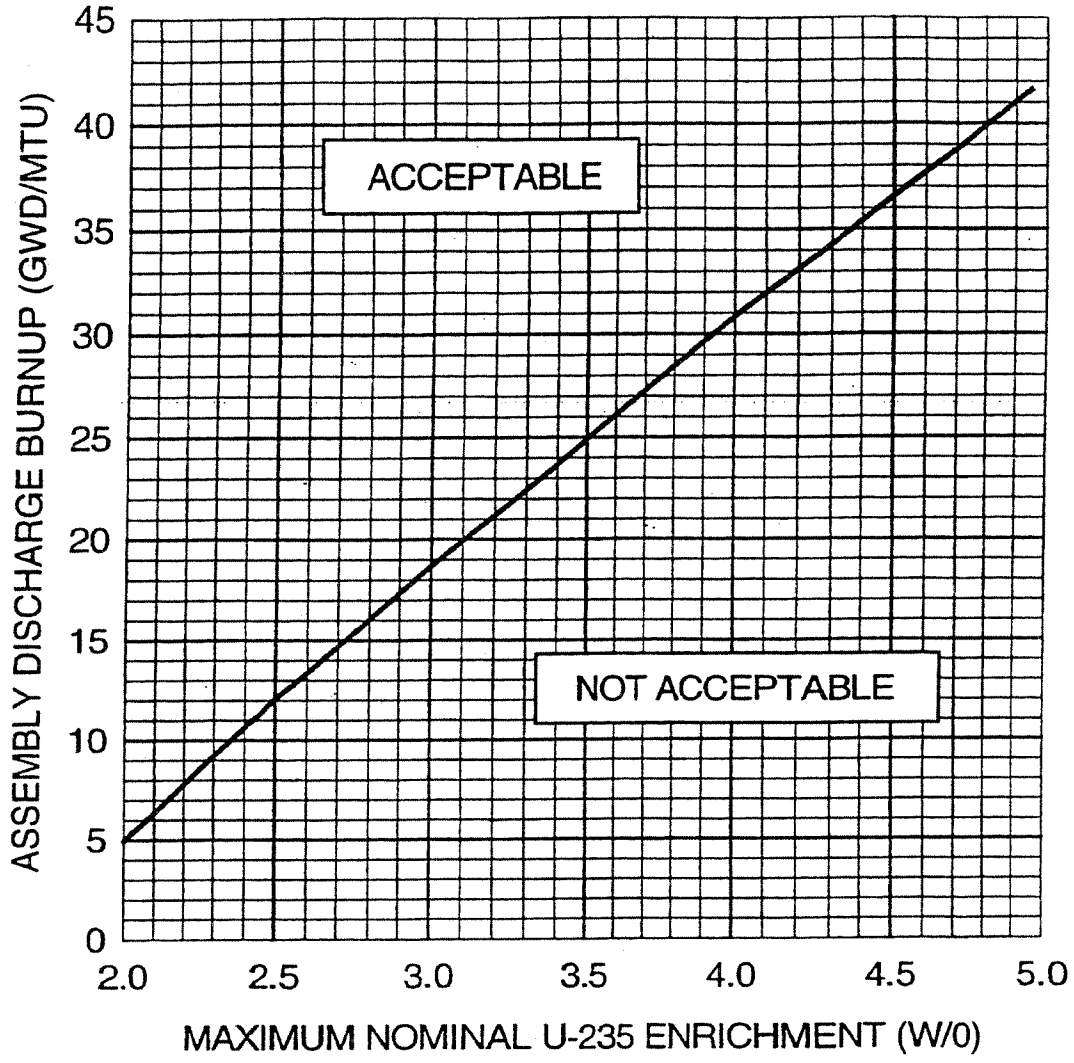

Notes

1. Fuel assemblies with enrichments less than 2.0 W/O must meet the burn-up requirements of 2.0 W/O assemblies.

2. Use of the following polynomial fit is acceptable where E = Enrichment W/O:

   Assembly Discharge burnup = $0.1246\ E^3 - 1.91\ E^2 + 20.9205\ E - 30.2482$

RN 03-017
December 2003

SOUTH CAROLINA ELECTRIC & GAS CO.
VIRGIL C. SUMMER NUCLEAR STATION

Required Fuel Assembly Burn-up as a Function of Initial Enrichment to permit Storage in Region 2 Racks

Figure 4.3-44

Figure 4.3-45 Deleted per RN 03-017, December 2003

RN
03-017

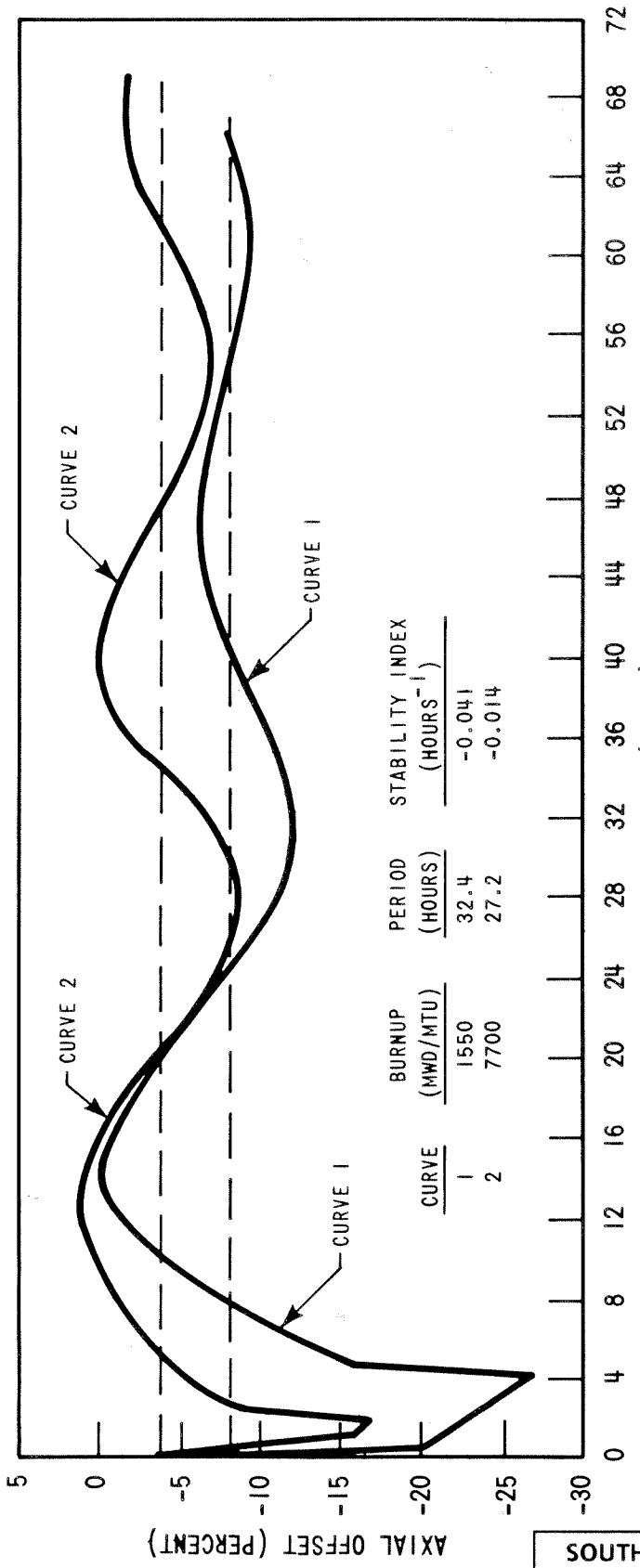

AMENDMENT 6
AUGUST, 1990

SOUTH CAROLINA ELECTRIC & GAS CO.
VIRGIL C. SUMMER NUCLEAR STATION

Axial Offset Versus Time PWR Core with a 12-ft. Height and 121 Assemblies

Figure 4.3-46

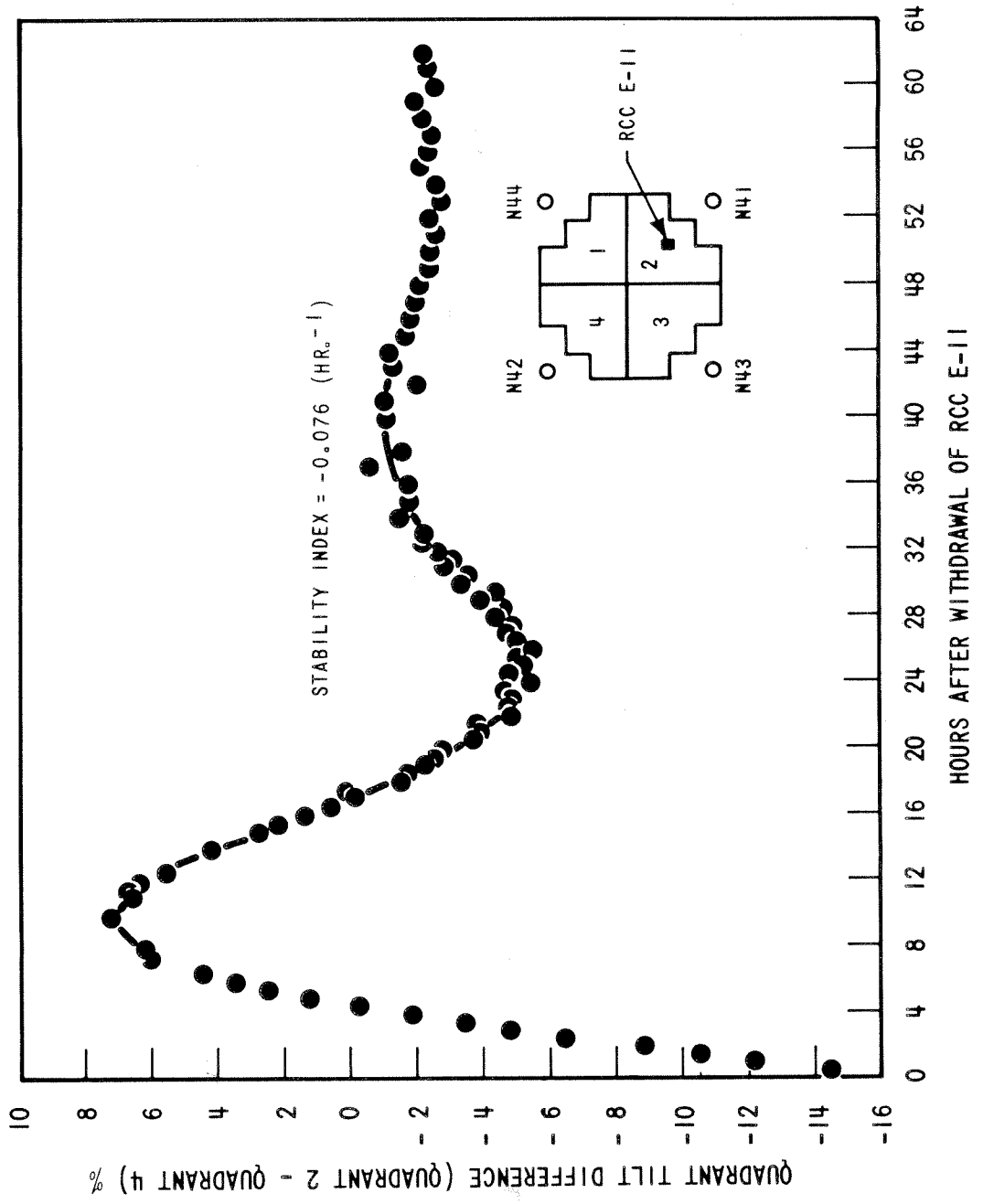

AMENDMENT 6
AUGUST, 1990

SOUTH CAROLINA ELECTRIC & GAS CO.
VIRGIL C. SUMMER NUCLEAR STATION

XY Xenon Test Thermocouple Response
Quadrant Tilt Difference Versus Time

Figure 4.3-47

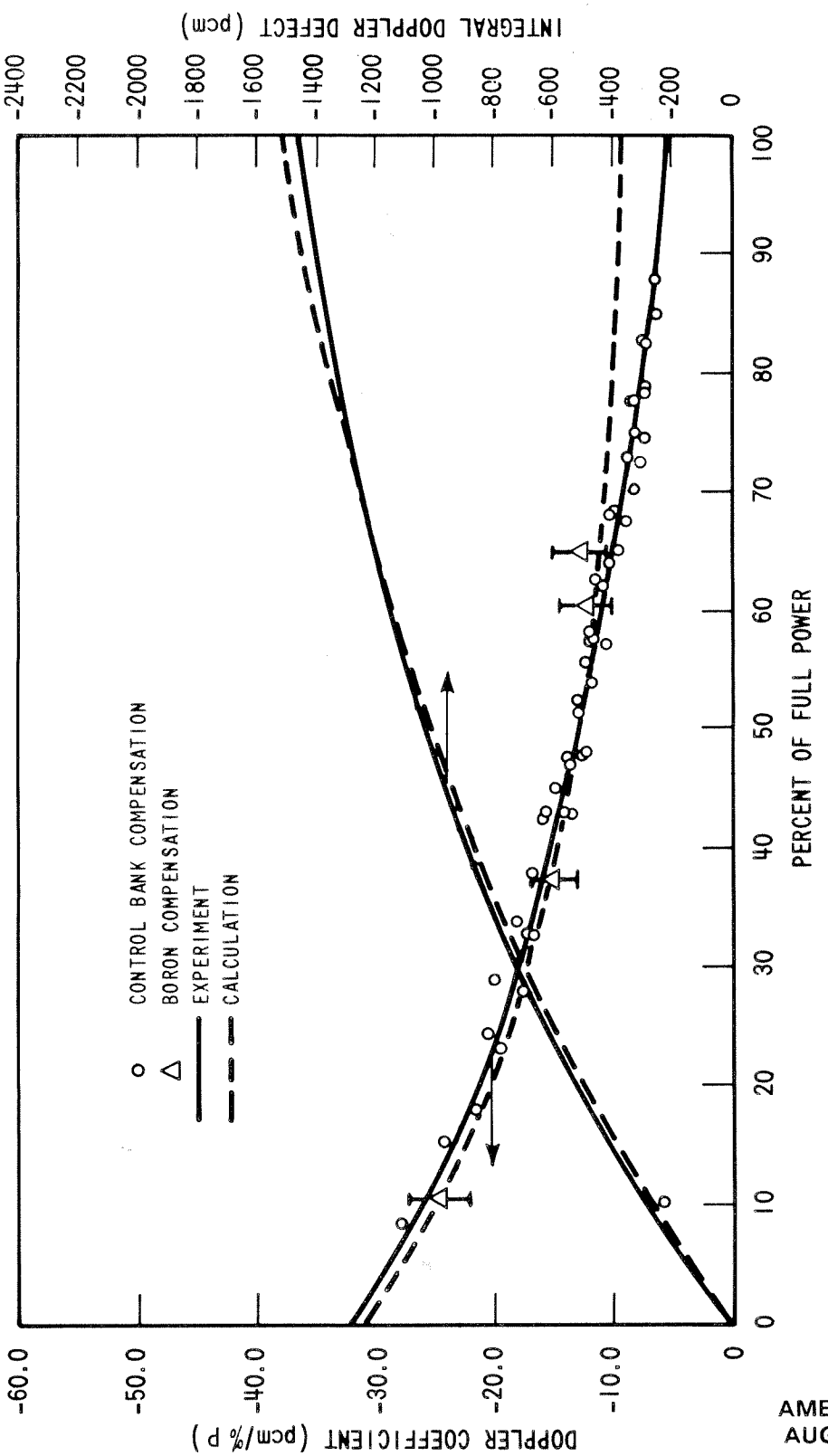

AMENDMENT 6
AUGUST, 1990

SOUTH CAROLINA ELECTRIC & GAS CO.
VIRGIL C. SUMMER NUCLEAR STATION

Calculated and Measured Doppler Defect and Coefficients at BOL, Two-Loop Plant, 121 Assemblies, 12-ft. Core

Figure 4.3-48

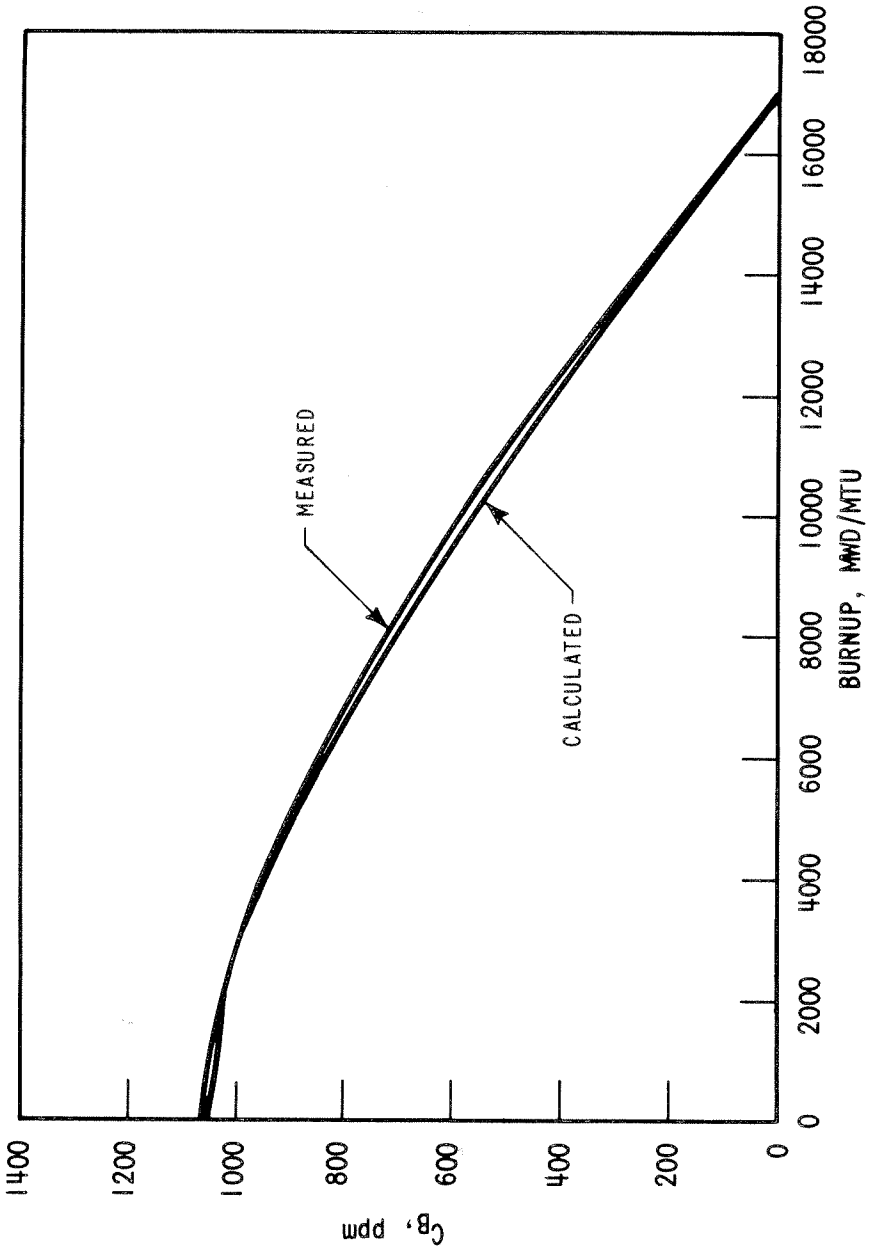

AMENDMENT 6
AUGUST, 1990

SOUTH CAROLINA ELECTRIC & GAS CO.
VIRGIL C. SUMMER NUCLEAR STATION

Comparison of Calculated and Measured Boron Concentration for Two-Loop Plant, 121 Assemblies, 12-ft. Core

Figure 4.3-49

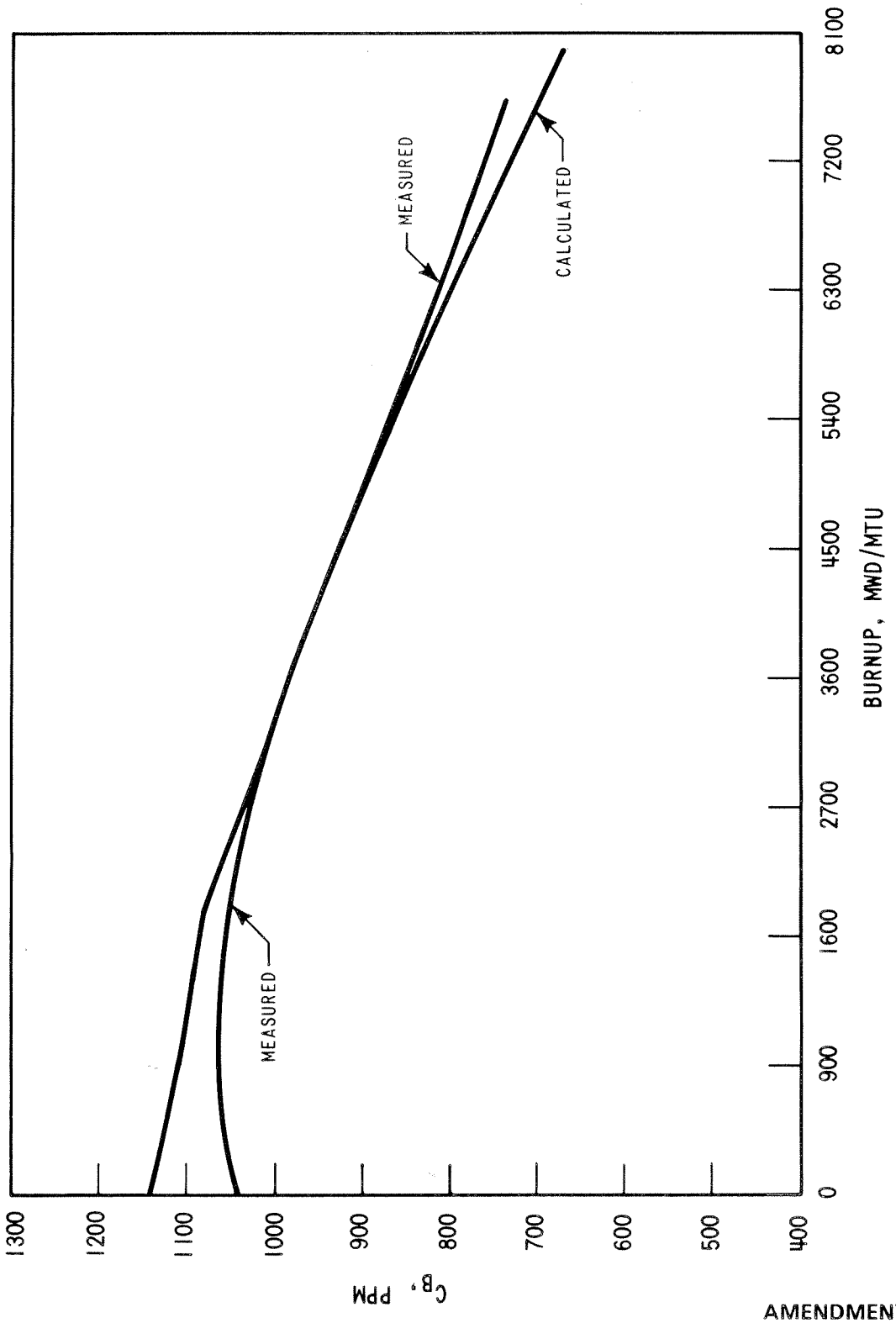

AMENDMENT 6
AUGUST, 1990

SOUTH CAROLINA ELECTRIC & GAS CO.
VIRGIL C. SUMMER NUCLEAR STATION

Comparison of Calculated and Measured C_B in Two-Loop Plant, 121 Assemblies, 12-ft. Core

Figure 4.3-50

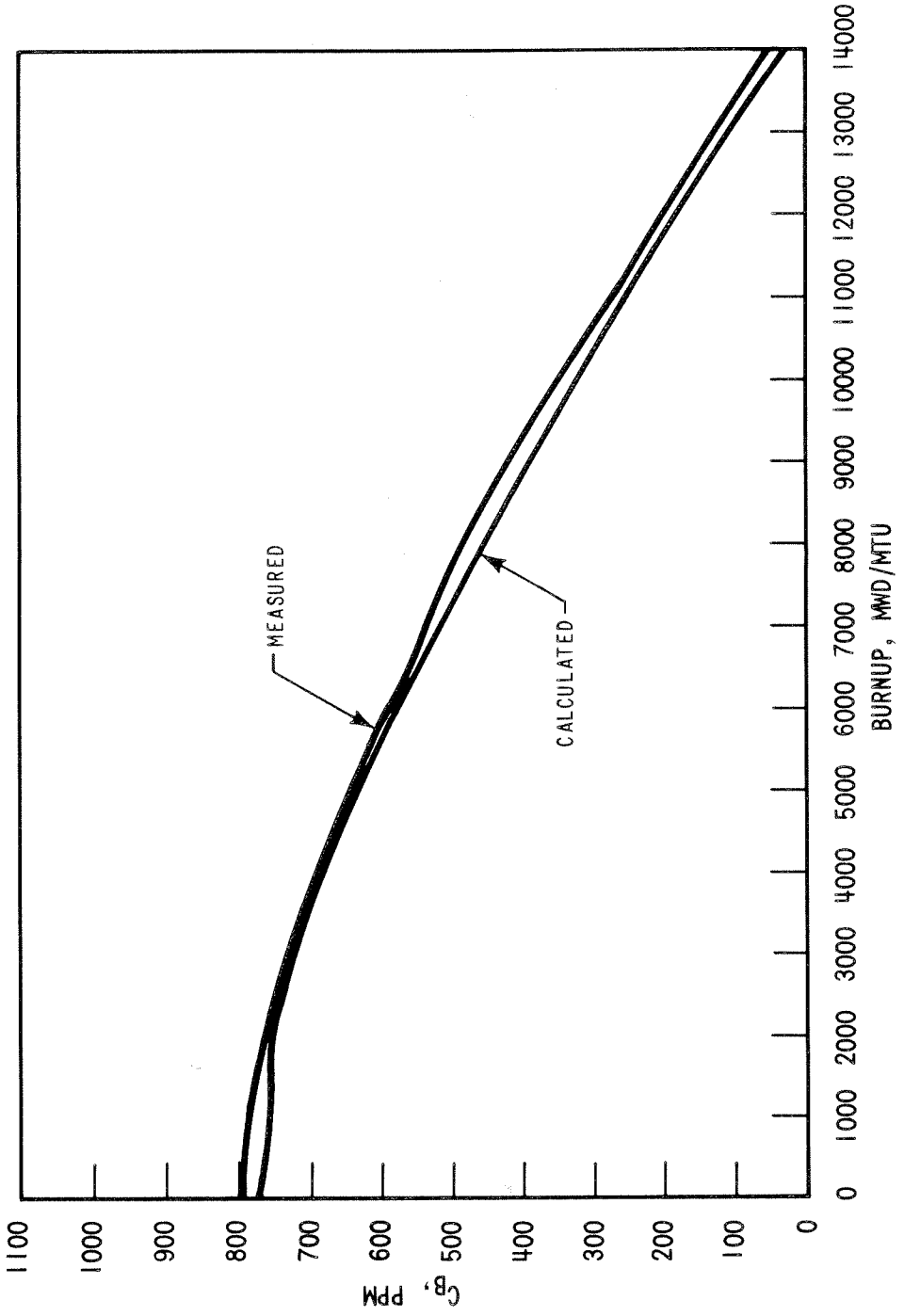

AMENDMENT 6
AUGUST, 1990

SOUTH CAROLINA ELECTRIC & GAS CO.
VIRGIL C. SUMMER NUCLEAR STATION

Comparison of Calculated and Measured C_B in Three-Loop Plant, 157 Assemblies, 12-ft. Core

Figure 4.3-51

4.4 THERMAL AND HYDRAULIC DESIGN

4.4.1 DESIGN BASES

The overall objective of the thermal and hydraulic design of the reactor core is to provide adequate heat transfer which is compatible with the heat generation distribution in the core such that heat removal by the reactor coolant system or the emergency core cooling system (when applicable) assures that the following performance and safety criteria requirements are met:

1. Fuel damage (defined as penetration of the fission product barrier, i.e., the fuel rod clad) is not expected during normal operation and operational transients (Condition I) or any transient conditions arising from faults of moderate frequency (Condition II). It is not possible, however, to preclude a very small number of rod failures. These will be within the capability of the plant cleanup system and are consistent with the plant design bases.

2. The reactor can be brought to a safe state following a Condition III event with only a small fraction of fuel rods damaged (see above definition) although sufficient fuel damage might occur to preclude resumption of operation without considerable outage time.

3. The reactor can be brought to a safe state and the core can be kept subcritical with acceptable heat transfer geometry following transients arising from Condition IV events.

In order to satisfy the above criteria, the following design bases have been established for the thermal and hydraulic design of the reactor core.

4.4.1.1 Departure from Nucleate Boiling Design Basis

4.4.1.1.1 Basis

There shall be at least a 95% probability (at a 95% confidence level) that departure from nucleate boiling (DNB) will not occur on the most limiting fuel rod during normal operation and operational transients and any transient conditions arising from faults of moderate frequency (Condition I and II events).

The design method employed to meet the DNB design basis is the Revised Thermal Design Procedure (RTDP), Reference [110]. Uncertainties in plant operating parameters, nuclear and thermal parameters, fuel fabrication parameters, computer code and DNB correlation predictions are considered statistically to obtain DNB uncertainty factors. Based on the DNB uncertainty factors, RTDP design limit DNBR values are determined such that there is at least a 95% probability at a 95% confidence level that DNB will not occur on the most limiting fuel rod. Plant parameter uncertainties

RN 95-022

are used to determine the plant uncertainties. Since the parameter uncertainties are considered in determining the design DNBR value, the plant safety analyses are performed using values of input parameters without uncertainties.

For this application, the minimum required DNBR value for fuel analysis is 1.23 for both thimble cold wall cells (3 fuel rods and a thin tube) and typical cells (4 fuel rods). RN 95-022 96-043

To maintain DNBR margin to offset DNB penalties such as those due to fuel rod bow (see paragraph 4.4.2.3.4.3), the safety analyses were performed to DNBR limits higher than the design limit DNBR values. The differences between the design limit DNBRs and the safety analysis limit DNBRs results in available DNBR margin. The net DNBR margin, after consideration of all penalties, is available for operating and design flexibility. RN 95-022

For those accident cases where statistical methods are not applied, the Standard Thermal Design Procedure (STDP) is used. (Plant uncertainties are directly accounted for in the calculations.) RN 95-022

4.4.1.1.2 Discussion

By preventing DNB, adequate heat transfer is assured between the fuel clad and the reactor coolant, thereby preventing clad damage as a result of inadequate cooling. Maximum fuel rod surface temperature is not a design basis as it will be within a few degrees of coolant temperature during operation in the nucleate boiling region. Limits provided by the nuclear control and protection systems are such that this design basis will be met for transients associated with Condition II events including overpower transients. There is an additional large DNBR margin at rated power operation and during normal operating transients.

4.4.1.2 Fuel Temperature Design Basis

4.4.1.2.1 Basis

During modes of operation associated with Condition I and II events, the maximum fuel temperature shall be less than the melting temperature of UO_2. The UO_2 melting temperature for at least 95% of the peak kW/ft fuel rods will not be exceeded at the 95% confidence level. The melting temperature of UO_2 is taken as 5080°F, Reference [1], unirradiated and decreasing 58°F per 10,000 MWD/MTU. By precluding UO_2 melting, the fuel geometry is preserved and possible adverse effects of molten UO_2 on the cladding are eliminated. To preclude center melting and as a basis for overpower protection system setpoints, a calculated centerline fuel temperature of 4700°F has been selected as the overpower limit. This provides sufficient margin for uncertainties in the thermal evaluations as described in Section 4.4.2.10.1.

4.4.1.2.2 Discussion

Fuel rod thermal evaluations are performed at rated power, maximum overpower and during transients at various burnups. These analyses assure that this design basis as well as the fuel integrity design bases given in Section 4.2 are met. They also provide input for the evaluation of Condition III and IV faults given in Chapter 15.0.

4.4.1.3 Core Flow Design Basis

4.4.1.3.1 Basis

A minimum of 91.1% of the thermal flow rate will pass through the fuel rod region of the core and be effective for fuel rod cooling. Coolant flow through the thimble tubes as well as the leakage from the core barrel-baffle region into the core are not considered effective for heat removal.

4.4.1.3.2 Discussion

Core cooling evaluations are based on the thermal flow rate (minimum flow) entering the reactor vessel. A maximum of 8.9% (non-RTDP) of this value is allotted as bypass flow. This includes rod cluster control guide thimble cooling flow, head cooling flow, baffle leakage, and leakage to the vessel outlet nozzle, and includes the effect of thimble plug removal.

RN 95-022

4.4.1.4 Hydrodynamic Stability Design Bases

Modes of operation associated with Condition-I and II events shall not lead to hydrodynamic instability.

4.4.1.5 Other Considerations

The above design bases together with the fuel clad and fuel assembly design bases given in Section 4.2.1.1 are sufficiently comprehensive so additional limits are not required.

Fuel rod diametral gap characteristics, moderator-coolant flow velocity and distribution, and moderator void are not inherently limiting. Each of these parameters is incorporated into the thermal and hydraulic models used to ensure the above mentioned design criteria are met. For instance, the fuel rod diametral gap characteristics change with time (see Section 4.2.1.3.1) and the fuel rod integrity is evaluated on that basis. The effect of the moderator flow velocity and distribution (see Section 4.4.2.3) and moderator void distribution (see Section 4.4.2.5) are included in the core thermal (THINC) evaluation and thus affect the design bases.

Meeting the fuel clad integrity criteria covers possible effects of clad temperature limitations. As noted in Section 4.2.1.3.1, the fuel rod conditions change with time. A single clad temperature limit for Condition I or Condition II events is not appropriate since of necessity it would be overly conservative. A clad temperature limit is applied to the loss of coolant accident (Section 15.4.1),control rod ejection accident, Reference [2], and locked rotor accident, Reference [3].

4.4.2 DESCRIPTION

4.4.2.1 (Deleted)

4.4.2.2 Fuel and Cladding Temperatures

Consistent with the thermal-hydraulic design bases described in Section 4.4.1, the following discussion pertains mainly to fuel pellet temperature evaluation. A discussion of fuel clad integrity is presented in Section 4.2.1.3.1.

The thermal-hydraulic design assures that the maximum fuel temperature is below the melting point of UO_2 (melting point of 5080°F [1] unirradiated and decreasing by 58°F per 10,000 MWD/MTU). To preclude center melting and as a basis for overpower protection system setpoints, a calculated centerline fuel temperature of 4700°F has been selected as the overpower limit. This provides sufficient margin for uncertainties in the thermal evaluations as described in Section 4.4.2.10.1. The temperature distribution within the fuel pellet is predominantly a function of the local power density and the UO_2 thermal conductivity. However, the computation of radial fuel temperature distributions combines crud, oxide, clad gap, and pellet conductances. The factors which influence these conductances, such as gap size (or contact pressure), internal gas pressure, gas composition, pellet density, and radial power distribution within the pellet, etc., have been combined into a semi-empirical thermal model (see Section 4.2.1.3.1) which includes a model for time dependent fuel densification as given in References [6], [38], [105], and [106]. This thermal model enables the determination of these factors and their net effects on temperature profiles. The temperature predictions have been compared to in-pile fuel temperature measurements, References [7] through [13], [38], [105], and [106], and melt radius data, References [14] and [15], with good results.

RN 95-022 01-113 14-036

Fuel rod thermal evaluations (fuel centerline, average and surface temperatures) are performed at several times in the fuel rod lifetime (with consideration of time dependent densification) to determine the maximum fuel temperatures. The principal factors which are employed in the determination of the fuel temperature are discussed below.

RN 95-022

4.4.2.2.1 UO_2 Thermal Conductivity

The thermal conductivity of uranium dioxide was evaluated from data reported in References [16] through [28].

At the higher temperatures, thermal conductivity is best obtained by utilizing the integral conductivity to melt which can be determined with more certainty.

From an examination of the data, it has been concluded that the best estimate for the value of $\int_0^{2800^\circ C}$ Kdt is 93 watts/cm. This conclusion is based on the integral values reported in References [14] and [28] through [32].

The design curve for the thermal conductivity is shown in Figure 4.4-3. The section of the curve at temperatures between 0°C and 1300°C is in excellent agreement with the recommendation of the IAEA panel in Reference [33]. The section of the curve above 1300°C is derived for an integral value of 93 watts/cm (References [14], [28], [32]). RN 14-036

Thermal conductivity for UO_2 at 95% theoretical density can be represented best by the following equation:

$$K = \frac{1}{11.8 + 0.0238T} + 8.775 \times 10^{-13} T^3 \qquad (4.4\text{-}1)$$

Where:

K = watts/cm-°C

T = °C

4.4.2.2.2 Radial Power Distribution in UO_2 Fuel Rods

An accurate description of the radial power distribution as a function of burnup is needed for determining the power level for incipient fuel melting and other important performance parameters such as pellet thermal expansion, fuel swelling and fission gas release rates.

This information on radial power distributions in UO_2 fuel rods is determined with the neutron transport theory code, LASER. The LASER Code has been validated by comparing the code predictions on radial burnup and isotopic distributions with measured radial microdrill data, References [34] and [35]. A "radial power depression factor," f, is determined using radial power distributions predicted by LASER. The factor f enters into the determination of the pellet centerline temperature, T_c, relative to the pellet surface temperature, T_s, through the expression:

$$\int_{T_s}^{T_c} K(T)\,dT = \frac{q'f}{4\Pi} \qquad (4.4\text{-}2)$$

RN 95-022 96-043

Where:

K(T) = the thermal conductivity for UO_2 with a uniform density distribution

q' = the linear power generation rate

4.4.2.2.3 Gap Conductance

The temperature drop across the pellet clad gap is a function of the gap size and the thermal conductivity of the gas in the gap. The gap conductance model is selected such that when combined with the UO_2 thermal conductivity model, the calculated fuel centerline temperatures reflect the in-pile temperature measurements. A more detailed discussion of the gap conductance model is presented in References [38] and [105].

RN 95-022 14-036

4.4.2.2.4 Surface Heat Transfer Coefficients

The fuel rod surface heat transfer coefficients during subcooled forced convection and nucleate boiling are presented in Section 4.4.2.8.1.

4.4.2.2.5 Fuel Clad Temperatures

The outer surface of the fuel rod at the hot spot operates at a temperature of approximately 660°F for steady-state operation at rated power throughout core life due to the onset of nucleate boiling. Initially (beginning-of-life), this temperature is that of the clad metal outer surface.

RN 95-022

During operation over the life of the core, the buildup of oxides and crud on the fuel rod surface causes the clad surface temperature to increase. Allowance is made in the fuel center melt evaluation for this temperature rise. Since the thermal-hydraulic design basis limits DNB, adequate heat transfer is provided between the fuel clad and the reactor coolant so that the core thermal output is not limited by considerations of clad temperature.

RN 95-022

4.4.2.2.6 Treatment of Peaking Factors

The total heat flux hot channel factor, F_Q, is defined by the ratio of the maximum to core average heat flux. As presented in Table 4.3-2 and discussed in Section 4.3.2.2.6, the design value of F_Q for normal operation is 2.45.

This results in a peak local power of 13.9 kW/ft at full power conditions. As described in Section 4.3.2.2.6 the peak linear power for determination of protection setpoints is < 22.6 kW/ft. The centerline temperature at this kW/ft must be below the UO_2 melt temperature over the lifetime of the rod, including allowances for uncertainties. The melt temperature of unirradiated UO_2 is 5080°F [1] and decreases by 58°F per 10,000 MWD/MTU. The centerline temperature at the peak linear power for determination of protection setpoints is below that required to produce melting. Fuel centerline temperature at the peak linear power for the determination of protection setpoints are presented in Table 4.4-1.

RN 95-022

4.4.2.3 Critical Heat Flux Ratio or Departure from Nucleate Boiling Ratio and Mixing Technology

The minimum DNBR's for the rated power conditions are given in Table 4.4-1. The core average DNBR is not a safety related item as it is not directly related to the minimum DNBR in the core, which occurs at some elevation in the limiting flow channel. Similarly, the DNBR at the hot spot is not directly safety related. The minimum DNBR in the limiting flow channel will be downstream of the peak heat flux location (hot spot) due to the increased downstream enthalpy rise.

DNBR's are calculated by using the correlation and definitions described in the following Sections 4.4.2.3.1 and 4.4.2.3.2. The THINC-IV computer code (discussed in Section 4.4.3.4.1) is used to determine the flow distribution in the core and the local conditions in the hot channel for use in the DNB correlation. The use of hot channel factors is discussed in Section 4.4.3.2.1 (nuclear hot channel factors) and in Section 4.4.2.3.4 (engineering hot channel factors).

4.4.2.3.1 Departure from Nucleate Boiling Technology

RN 95-022

The WRB-2 (Reference [102]) correlation was developed based on CHF data for Westinghouse fuel designs which employ grids with mixing vanes of the same design as the 17 x 17 standard fuel mixing vane design. This includes CHF data with the VANTAGE 5 fuel design.

The applicable ranges of variables for the WRB-2 correlation are:

Pressure	$1440 \leq P \leq 2490$ psia
Local Mass Velocity	$0.9 \leq G_{loc}/10^6 \leq 3.7$ lb/ft^2-hr
Local Quality	$-0.1 \leq X_{loc} \leq 0.3$
Heated Length, Inlet to CHF Location	$L_h \leq 14$ feet
Grid Spacing	$10 \leq g_{sp} \leq 26$ inches
Equivalent Hydraulic Diameter	$0.37 \leq d_e \leq 0.51$ inch
Equivalent Heated Hydraulic Diameter	$0.46 \leq d_h \leq 0.59$ inch

Figure 4.4-6 shows measured critical heat flux plotted against predicted critical heat flux using the WRB-2 correlation.

The correlation limit DNBR is 1.17 for both the WRB-1 and WRB-2 correlation.

The W-3 DNB correlation, References [39] and [108], is used where the primary DNBR correlations are not applicable. The WRB-2 correlation was developed based on mixing vane data and, therefore, is only applicable in the heated rod spans above the first mixing vane grid. The W-3 correlation, which does not take credit for mixing vane grids, is used to calculate DNBR values in the heated region below the first mixing vane grid. In addition, the W-3 correlation is applied in the analysis of accident conditions where the system pressure is below the range of the primary correlations. For system pressures in the range of 500 to 1000 psia, the W-3 correlation limit is 1.45 (Reference [107]). For system pressures greater than 1000 psia, the W-3 correlation limit is 1.30. A cold wall factor, Reference [109], is applied to the W-3 DNB correlation to account for the presence of the unheated thimble surfaces.

RN 95-022

4.4.2.3.2 Definition of Departure from Nucleate Boiling Ratio

The DNB heat flux ratio (DNBR) as applied to this design for both typical and thimble (cold wall) cells is:

$$DNBR = \frac{q''_{DNB,N}}{q''_{loc}} \qquad (4.4\text{-}9)$$

Where:

$$q''_{DNB,N} = \frac{q''_{DNB,EU}}{F} \qquad (4.4\text{-}10)$$

and $q''_{DNB,EU}$ is the uniform DNB heat flux as predicted by the WRB-1 or WRB-2 DNB correlation, References [44] and [102].

F is the flux shape factor to account for nonuniform axial heat flux distributions, References [44], with the "C" term modified as in Reference [39].

q''_{loc} is the actual local heat flux.

4.4.2.3.3 Mixing Technology

The rate of heat exchange by mixing between flow channels is proportional to the difference in the local mean fluid enthalpy of the respective channels, the local fluid density and flow velocity. The proportionality is expressed by the dimensionless thermal diffusion coefficient (TDC) which is defined as:

$$TDC = \frac{w'}{\rho V a} \qquad (4.4\text{-}14)$$

Where:

w' = flow exchange rate per unit length, $lb_m/ft\text{-}sec$

ρ = fluid density, lb_m/ft^3

V = fluid velocity, ft/sec

a = lateral flow area between channels per unit length, ft^2/ft

The application of the TDC in the THINC analysis for determining the overall mixing effect or heat exchange rate is presented in Reference [41].

As part of its research and development program, Westinghouse has sponsored and directed mixing tests at Columbia University [46]. These series of tests, using the "R" mixing vane grid design on 13, 26, and 32 inch grid spacing, were conducted in pressurized water loops at Reynolds numbers similar to that of a PWR core under the following single and 2 phase (subcooled boiling) flow conditions:

1.	Pressure	1500 to 2400 psia
2.	Inlet temperature	332 to 642°F
3.	Mass velocity	1.0 to 3.5 x 10^6 $lb_m/hr\text{-}ft^2$
4.	Reynolds number	1.34 to 7.45 x 10^5
5.	Bulk outlet quality	-52.1 to -13.5%

TDC is determined by comparing the THINC Code predictions with the measured subchannel exit temperatures. Data for 26-inch axial grid spacing are presented in Figure 4.4-8 where the thermal diffusion coefficient is plotted versus the Reynolds number. TDC is found to be independent of Reynolds number, mass velocity, pressure, and quality over the ranges tested. The 2 phase data (local, subcooled boiling) fell within the scatter of the single phase data. The effect of two-phase flow on the value of TDC has been demonstrated by Cadek [46], Rowe and Angle [47, 48], and Gonzalez-Santalo and Griffith [49]. In the subcooled boiling region the values of TDC were

indistinguishable from the single phase values. In the quality region, Rowe and Angle show that in the case with rod spacing similar to that in PWR reactor core geometry, the value of TDC increased with quality to a point and then decreased, but never below the single phase value. Gonzalez-Santalo and Griffith showed that the mixing coefficient increased as the void fraction increased.

A mixing test program similar to the one described above was conducted at Columbia University for the 17 x 17 geometry and mixing vane grids on 26-inch spacing [50]. The mean value of TDC obtained from these tests was 0.059.

Since the actual reactor grid spacing for the lower region of the VANTAGE 5 and VANTAGE+ design is approximately 20 inches, and approximately 10 inches in the upper region of VANTAGE 5 or VANTAGE+, additional margin is available for these designs, as the value of TDC increases grid spacing decreases [46]. RN 95-022

Based on the above test results, a TDC value of 0.038 is used for the VANTAGE 5 and VANTAGE+ fuel assemblies.

4.4.2.3.4 Hot Channel Factors

The total hot channel factors for heat flux and enthalpy rise are defined as the maximum to core average ratios of these quantities. The heat flux hot channel factor considers the local maximum linear heat generation rate at a point (the hot spot), and the enthalpy rise hot channel factor involves the maximum integrated value along a channel (the hot channel).

Each of the total hot channel factors considers a nuclear hot channel factor (see Section 4.4.3.2) describing the neutron power distribution and an engineering hot channel factor, which allows for variations in fabrication tolerances.

4.4.2.3.4.1 Heat Flux Engineering Hot Channel Factor, F_Q^E

The kW/ft engineering hot channel factor is used to evaluate the maximum linear heat generation rate in this core. This subfactor is determined by statistically combining the fabrication variances for the fuel pellet diameter, density and enrichment, and has a value of 1.03 at the 95% probability level with 95% confidence. As shown in Reference [104], no DNB penalty need be taken for the short relatively low intensity heat flux spikes caused by variations in the above parameters, as well as fuel pellet eccentricity and fuel rod diameter variation.

4.4.2.3.4.2 Enthalpy Rise Engineering Hot Channel Factor, $F^{E}_{\Delta H}$

The effect of variations in and fabrication tolerances on the hot channel enthalpy rise is directly considered in the THINC core thermal subchannel analysis (see Section 4.4.3.4.1) under any reactor operating condition. The items considered contributing to the enthalpy rise engineering hot channel factor are discussed below:

1. Pellet diameter, density and enrichment and fuel rod diameter:

   Variations in pellet diameter, density and enrichment, and fuel rod diameter, are considered statistically in establishing the limit DNBR's (see Subsection 4.4.1.1) for the improved thermal design procedure (Reference [99]) employed in this application. Uncertainties in these variables are determined from sampling of manufacturing data.

2. Inlet Flow Maldistribution:

   The consideration of inlet flow maldistribution in core thermal performances is discussed in Section 4.4.3.1.2. A design basis of 5% reduction in coolant flow to the hot assembly is used in the THINC-IV analysis.

3. Flow Redistribution:

   The flow redistribution accounts for the reduction in flow in the hot channel resulting from the high flow resistance in the channel due to the local or bulk boiling. The effect of the nonuniform power distribution is inherently considered in the THINC analysis for every operating condition which is evaluated.

4. Flow Mixing:

   The subchannel mixing model incorporated in the THINC Code and used in reactor design is based on experimental data [46 to 51] discussed in Sections 4.4.3.4.1 and 4.4.2.3.3. The mixing vanes incorporated in the spacer grid design induce additional flow mixing between the various flow channels in a fuel assembly as well as between adjacent assemblies. This mixing reduces the enthalpy rise in the hot channel resulting from local power peaking or unfavorable mechanical tolerances. RN 01-113

4.4.2.3.4.3 Effects of Rod Bow on DNBR

The phenomenon of fuel rod bowing, as described in Reference [95], must be accounted for in the DNBR safety analysis of Condition I and II events for each plant application. Applicable generic credits for margin resulting from retained conservatism in the evaluation of the DNBR and/or margin obtained from the measured plant operating parameters (such as $F^N_{\Delta H}$, reactor power or core flow) -- which are less limiting than those required by the plant safety analysis -- can be used to offset the effect of rod bow.

For the safety analysis of the Virgil C. Summer Nuclear Station, sufficient margin was maintained (see Section 4.4.3.11) to accommodate full and low flow DNBR penalties (<2% for the worst case, which is a burnup of 24,000 MWD/MTU) identified in Reference [96]. RN 14-023

The maximum rod bow penalties accounted for in the design safety analysis are based on an assembly average burnup of 24,000 MWD/MTU. At burnups greater than 24,000 MWD/MTU, credit is taken for the effect of F^N burndown, due to the decrease in fissionable isotopes and the buildup of fission product inventory, and no additional rod bow penalty is required.

4.4.2.4 Flux Tilt Considerations

Significant quadrant power tilts are not anticipated during normal operation since this phenomenon is caused by some asymmetric perturbation. A dropped or misaligned rod cluster control assembly could cause changes in hot channel factors; however, these events are analyzed separately in Chapter 15.0. This discussion will be confined to flux tilts caused by x-y xenon transients, inlet temperature mismatches, enrichment variations within tolerances and so forth.

The design value of the enthalpy rise hot channel factor $F^N_{\Delta H}$, which includes an 8% uncertainty (as discussed in Section 4.3.2.2.7), is assumed to be sufficiently conservative that flux tilts up to and including the alarm point (see Technical Specifications) will not result in values of $F^N_{\Delta H}$ greater than the assumed in this submittal. The design value of F_Q does not include a specific allowance for quadrant flux tilts.

4.4.2.5 (Deleted)

4.4.2.6 (Deleted)

4.4.2.7 Core Pressure Drops and Hydraulic Loads

4.4.2.7.1 Core Pressure Drops

The analytical model and experimental data used to calculate the pressure drops shown in Table 4.4-1 are described in Section 4.4.2.8. The core pressure drop includes the fuel assembly, lower core plate, and upper core plate pressure drops. The full power operation pressure drop values shown in Table 4.4-1 are the unrecoverable pressure drops across the vessel, including the inlet and outlet nozzles, and across the core. Section 5.1.1 also defines and describes the best estimate flow, the thermal design flow (minimum flow) which is the basis for reactor core thermal performance and the mechanical design flow (maximum flow) which is used in the mechanical design of the reactor vessel internals and fuel assemblies.

Uncertainties associated with the core pressure drop values are discussed in Section 4.4.2.10.2.

4.4.2.7.2 Hydraulic Loads

The fuel assembly hold down springs, Figure 4.2-2, are designed to keep the fuel assemblies in contact with the lower core plate under all Condition I and II events with the exception of the turbine overspeed transient associated with a loss of external load. The hold down springs are designed to tolerate possible over deflection associated with fuel assembly lift off for this case and provide contact between the fuel assembly and the lower core plate following this transient. More adverse flow conditions can occur during a LOCA. These conditions are presented in Section 15.4.1.

Hydraulic loads at normal operating conditions are calculated considering the mechanical design flow which is described in Section 5.1 and accounting for the minimum core bypass flow based on manufacturing tolerances. Core hydraulic loads at cold plant startup conditions are adjusted to account for the coolant density difference. Conservative core hydraulic loads for a pump overspeed transient, which could possibly create flow rates 20% greater than the mechanical design flow, are evaluated to be approximately twice the fuel assembly weight.

Core hydraulic loads were measured during the prototype assembly tests described in Section 1.5. Reference [5] contains a detailed discussion of the results.

4.4.2.8 Correlation and Physical Data

4.4.2.8.1 Surface Heat Transfer Coefficients

Forced convection heat transfer coefficients are obtained from the familiar Dittus-Boelter correlation [53], with the properties evaluated at bulk fluid conditions:

$$\frac{hD_e}{K} = 0.023\left(\frac{D_e G}{\mu}\right)0.8\left(\frac{C_p \mu}{K}\right)0.4 \qquad (4.4\text{-}15)$$

Where:

h = heat transfer coefficient, Btu/hr-ft^2-°F

D_e = equivalent diameter, ft

K = thermal conductivity, Btu/hr-ft-°F

G = mass velocity, lb_m/hr-ft^2

m = dynamic viscosity, lb_m/ft-hr

C_P = heat capacity, Btu/lb_m-°F

This correlation has been shown to be conservative [54] for rod bundle geometries with pitch to diameter ratios in the range used by PWRs.

The onset of nucleate boiling occurs when the clad wall temperature reaches the amount of superheat predicted by Thom's [55] correlation. After this occurrence the outer clad wall temperature is determined by:

$$\Delta T_{sat} = [0.072 \exp(-P/1260)]\,(q")^{0.5} \qquad (4.4\text{-}16)$$

Where:

ΔT_{sat} = wall superheat, $T_w - T_{sat}$ °F

q" = wall heat flux, Btu/hr-ft^2

P = pressure, psia

T_w = outer clad wall temperature, °F

T_{sat} = saturation temperature of coolant at P, °F

4.4.2.8.2 Total Core and Vessel Pressure Drop

Unrecoverable pressure losses occur as a result of viscous drag (friction) and/or geometry changes (form) in the fluid flow path. The flow field is assumed to be incompressible, turbulent, single-phase water. These assumptions apply to the core and vessel pressure drop calculations for the purpose of establishing the primary loop flow rate. Two (2)-phase considerations are neglected in the vessel pressure drop evaluation because the core average void is negligible. Two (2) phase flow considerations in the core thermal subchannel analyses are considered and the models are discussed in Section 4.4.3.1.3. Core and vessel pressure losses are calculated by equations of the form:

$$\Delta P_L = \left(K + F \frac{L}{D_e} \right) \frac{\rho V^2}{2 g_c (144)} \qquad (4.4\text{-}17)$$

Where:

ΔP_L = unrecoverable pressure drop, lb_f/in^2

ρ = fluid density, lb_m/ft^3

L = length, ft

D_e = equivalent diameter, ft

V = fluid velocity, ft/sec

g_c = 32.174 $\frac{lb_m - ft}{lb_f - sec^2}$

K = form loss coefficient, dimensionless

F = friction loss coefficient, dimensionless

Fluid density is assumed to be constant at the appropriate value for each component in the core and vessel. Because of the complex core and vessel flow geometry, precise analytical values for the form and friction loss coefficients are not available. Therefore, experimental values for these coefficients are obtained from geometrically similar models.

Values are quoted in Table 4.4-1 for unrecoverable pressure loss across the reactor vessel, including the inlet and outlet nozzles, and across the core. The results of full scale tests of core components and fuel assemblies were utilized in developing the core pressure loss characteristic. The pressure drop for the vessel was obtained by combining the core loss with correlation of 1/7th scale model hydraulic test data on a number of vessels [56, 57] and form loss relationships [58]. Moody [59] curves were used to obtain the single phase friction factors.

Tests of the primary coolant loop flow rates will be made (see Section 4.4.4.1) prior to initial criticality to verify that the flow rates used in the design, which were determined in part from the pressure losses calculated by the method described here, are conservative.

4.4.2.8.3 Void Fraction Correlation

There are 3 separate void regions considered in flow boiling in a PWR as illustrated in Figure 4.4-12. They are the wall void region (no bubble detachment), the subcooled boiling region (bubble detachment) and the bulk boiling region.

In the wall void region, the point where local boiling begins is determined when the clad temperature reaches the amount of superheat predicted by Thom's [55] correlation (discussed in Section 4.4.2.8.1). The void fraction in this region is calculated using Maurer's [60] relationship. The bubble detachment point, where the superheated bubbles break away from the wall, is determined by using Griffith's [61] relationship.

The void fraction in the subcooled boiling region (that is, after the detachment point) is calculated from the Bowring [62] correlation. This correlation predicts the void fraction from the detachment point to the bulk boiling region.

The void fraction in the bulk boiling region is predicted by using homogeneous flow theory and assuming no slip. The void fraction in this region is therefore a function only of the thermodynamic quality.

4.4.2.9 Thermal Effects of Operational Transients

DNB core safety limits are generated as a function of coolant temperature, pressure, core power and axial and radial power distributions. Operation within these DNB safety limits ensures that the DNB design basis is met for both steady-state operation and for most anticipated operational transients that are slow with respect to fluid transport delays in the primary system. In addition, for other transients, e.g., uncontrolled rod bank withdrawal at power incident (Section 15.2.2) specific protection functions are provided as described in Section 7.2 and the use of these protection functions are described in Chapter 15.0 (see Table 15.1-3). The thermal response of the fuel rod is discussed in Section 4.4.3.7.

Transients which affect only 1 steam generator are analyzed using a multi-loop system simulation; e.g., the LOFTRAN code (see code description in Section 15.1.8.2). The variation in core inlet temperature distribution is taken into account for such asymmetric events. In general, mixing among the streams from the reactor coolant loops is assumed such that the core reactivity and nuclear power transients are conservatively calculated. Also, in calculating the DNB ratio, the highest inlet temperature from among the reactor coolant loops is used.

Excessive heat removal due to Feedwater System Malfunctions (Section 15.2.10) is an example of an event analyzed in the FSAR which affects only 1 steam generator. The accidental opening of one feedwater control valve with the reactor at power causes excess feedwater to be delivered to 1 steam generator. This results in a reduction in cold leg temperature and an increase in ΔT in the affected reactor coolant loop. For this analysis, no mixing was assumed in the reactor vessel inlet plenum, and the reactivity calculation was based on the loop with the greatest cooldown (the loop with the steam generator to which excess feedwater flow is being delivered), providing a conservatively high prediction of nuclear power. In calculating the DNB ratio during the transient, the initial value of core inlet temperature (including appropriate error allowances) was used. No credit was taken for the cooldown of the reactor coolant system due to the excessive heat removal in the affected steam generator. Thus, margin to core thermal limits is conservatively minimized throughout the transient.

4.4.2.10 Uncertainties in Estimates

4.4.2.10.1 Uncertainties in Fuel and Clad Temperatures

As discussed in Section 4.4.2.2, the fuel temperature is a function of crud, oxide, clad, gap, and pellet conductances. Uncertainties in the fuel temperature calculation are essentially of 2 types: fabrication uncertainties such as variations in the pellet and clad dimensions and the pellet density; and model uncertainties such as variations in the pellet conductivity and the gap conductance. These uncertainties have been quantified by comparison of the thermal model to the in-pile thermocouple measurements, References [7] through [13], by out-of-pile measurements of the fuel and clad properties, References [16] through [27], and by measurements of the fuel and clad dimensions during fabrication. The resulting uncertainties are then used in all evaluations involving the fuel temperature. The effect of densification on fuel temperature uncertainties is presented in Reference [6].

In addition to the temperature uncertainty described above, the measurement uncertainty in determining the local power, and the effect of density and enrichment variations on the local power are considered in establishing the heat flux hot channel factor. These uncertainties are described in Section 4.3.2.2.1.

Reactor trip setpoints as specified in the Technical Specification include allowance for instrument and measurement uncertainties such as calorimetric error, instrument drift and channel reproducibility, temperature measurement uncertainties, noise, and heat capacity variations.

Uncertainty in determining the cladding temperature results from uncertainties in the crud and oxide thicknesses. Because of the excellent heat transfer between the surface of the rod and the coolant, the film temperature drop does not appreciably contribute to the uncertainty.

4.4.2.10.2 Uncertainties in Pressure Drops

Core and vessel pressure drops based on the best estimate flow, as described in Section 5.1, are quoted in Table 4.4-1. The uncertainties quoted are based on the uncertainties in both the test results and the analytical extension of these values to the reactor application.

Operating experience to date has indicated that a flow resistance-allowance for possible crud deposition is not required. There has been no detectable long-term flow reduction reported at any Westinghouse plant. Inspection of the inside surfaces of steam generator tubes removed from operating plants has confirmed that there is no significant surface deposition that would affect system flow. Although all of the coolant piping surfaces have not been inspected, the small piping friction contribution to the total system resistance and the lack of significant deposition on piping near steam generator nozzles support the conclusion that an allowance for piping deposition is not necessary. The effect of crud enters into the calculation of core pressure drop through the fuel rod frictional component by use of a surface roughness factor. Present analyses utilize a surface roughness value which is a factor of 3 greater than the best estimate obtained from crud sampling from several operating Westinghouse reactors.

A major use of the core and vessel pressure drops is to determine the primary system coolant flow rates as discussed in Section 5.1. In addition, as discussed in Section 4.4.4.1, tests on the primary system prior to initial criticality will be made to verify that a conservative primary system coolant flow rate has been used in the design and analyses of the Virgil C. Summer Nuclear Station.

4.4.2.10.3 Uncertainties Due to Inlet Flow Maldistribution

The effects of uncertainties in the inlet flow maldistribution criteria used in the core thermal analyses is discussed in Section 4.4.3.1.2.

4.4.2.10.4 Uncertainty in DNB Correlation

The uncertainty in the DNB correlation (Section 4.4.2.3) can be written as a statement on the probability of not being in DNB based on the statistics of the DNB data. This is discussed in Section 4.4.2.3.2.

4.4.2.10.5 Uncertainties in DNBR Calculations

The uncertainties in the DNBRs calculated by THINC analysis (see Section 4.4.3.4.1) due to uncertainties in the nuclear peaking factors are accounted for by applying conservatively high values of the nuclear peaking factors and including measurement error allowances in the statistical evaluation of the limit DNBR (see Section 4.4.1.1.1) using the Revised Thermal Design Procedure, Reference [110]. In addition, conservative values for the engineering hot channel factors are used as discussed in Section 4.4.2.3.4. The results of a sensitivity study[52] with THINC-IV show that the minimum DNBR in the hot channel is relatively insensitive to variations in the core-wide radial power distribution (for the same value of $F^N_{\Delta H}$).

RN 95-022

The ability of the THINC-IV computer code to accurately predict flow and enthalpy distributions in rod bundles is discussed in Section 4.4.3.4.1 and in Reference [63]. Studies have been performed [52] to determine the sensitivity of the minimum DNBR in the hot channel to the void fraction correlation (see Section 4.4.2.8.3); the inlet velocity and exit pressure distributions assumed as boundary conditions for the analysis; and the grid pressure loss coefficients. The results of these studies show that the minimum DNBR in the hot channel is relatively insensitive to variations in these parameters. The range of variations considered in these studies covered the range of possible variations in these parameters. As required in Reference [98], an uncertainty of 4% in DNBR is included in the design procedure to account for any THINC-IV code uncertainty.

4.4.2.10.6 Uncertainties in Flow Rates

The uncertainties associated with loop flow rates are discussed in Section 5.1. For core thermal performance evaluations, a thermal design loop flow is defined which is less than the best estimate loop flow and accounts for both prediction and measurement uncertainties. In addition, another 8.9% of the thermal design flow is assumed to be ineffective for core heat removal capability because it bypasses the core through the various available vessel flow paths described in Section 4.4.3.1.1.

4.4.2.10.7 Uncertainties in Hydraulic Loads

As discussed in Section 4.4.2.7.2, hydraulic loads on the fuel assembly are evaluated for a pump overspeed transient which create flow rates 20% greater than the mechanical design flow. The mechanical design flow as stated in Section 5.1 is greater than the best estimate or most likely flow rate value for the actual plant operating condition.

4.4.2.10.8 Uncertainty in Mixing Coefficient

The value of the mixing coefficient--TDC--used in THINC analysis for this application is 0.038. The results of the mixing tests done on 17 x 17 geometry, as discussed in Section 4.4.2.3.3, had a mean value for TDC of 0.059 for 26-inch grid spacing. Because the actual grid spacing is approximately 20 inches in the lower region of the VANTAGE 5/VANTAGE+ fuel assemblies and approximately 10 inches in the upper region, additional margin is available for these designs, since the value of TDC increases as grid spacing decreases (Reference [46]). RN 95-022 RN 01-113

4.4.2.11 Plant Configuration Data

Plant configuration data for the thermal hydraulic and fluid systems external to the core are provided in the appropriate Chapters 5.0, 6.0, and 9.0. Implementation of the emergency core cooling system (ECCS) is discussed in Chapter 15.0. Some specific areas of interest are the following:

1. Total coolant flow rates for the reactor coolant system (RCS) and each loop are provided in Table 5.5-1. Flow rates employed in the evaluation of the core are presented in Section 4.4.

2. Total RCS volume including pressurizer and surge line, RCS liquid volume including pressurizer water at steady-state power conditions are given in Table 5.5-1.

3. The flow path length through each volume may be calculated from physical data provided in the above referenced tables.

4. The height of fluid in each component of the RCS may be determined from the physical data presented in Section 5.5. The components of the RCS are water filled during power operation with the pressurizer being approximately 60% water filled.

5. Components of the ECCS are to be located so as to meet the criteria for net positive suction head described in Section 6.3.

6. Line lengths and sizes for the safety injection system are determined so as to guarantee a total system resistance which will provide, as a minimum, the fluid delivery rates assumed in the safety analyses described in Chapter 15.0.

7. The minimum flow areas for components of the RCS are presented in Section 5.5, component and subsystem design.

8. The steady-state pressure drops and temperature distributions through the RCS are presented in Table 5.1-1.

4.4.3 EVALUATION

4.4.3.1 Core Hydraulics

4.4.3.1.1 Flow Paths Considered in Core Pressure Drop and Thermal Design

The following flow paths or core bypass flow are considered:

1. Flow through the spray nozzles into the upper head for head cooling purposes.

2. Flow entering into the RCC guide thimbles to cool the control rods.

3. Leakage flow from the vessel inlet nozzle directly to the vessel outlet nozzle through the gap between the vessel and the barrel.

4. Flow introduced between the baffle and the barrel for the purpose of cooling these components, and which is not considered available for core cooling.

5. Flow in the gaps between the fuel assemblies on the core periphery and the adjacent baffle wall.

The above contributions are evaluated to confirm that the design value of the core bypass flow is met. The design value of core bypass flow for the Virgil C. Summer Nuclear Station is equal to 8.9% of the total vessel flow assuming removal of all thimble plugs from the core. Of the total allowance, 4.9% is associated with the internals (Items 1, 3, 4, and 5 above) and 4.0% for the core. Calculations have been performed using drawing tolerances on a worst case basis and accounting for uncertainties in pressure losses. Based on these calculations, the core bypass flow for the Virgil C. Summer Nuclear Station is $\leq$ 8.9%. This design bypass value is also used in the evaluation of the core pressure drops quoted in Table 4.4-1, and the determination of reactor flow rates in Section 5.1.

Flow model test results for the flow path through the reactor are discussed in Section 4.4.2.8.2.

4.4.3.1.2 Inlet Flow Distributions

Data has been considered from several 1/7 scale hydraulic reactor model tests, References [56], [57], and [64], in arriving at the core inlet flow maldistribution criteria to be used in the THINC analyses (see Section 4.4.3.4.1). THINC I analyses made, using this data, have indicated that a conservative design basis is to consider 5% reduction in the flow to the hot assembly, Reference [65]. The same design basis of 5% reduction to the hot assembly inlet is used in THINC IV analyses.

The experimental error estimated in the inlet velocity distribution has been considered as outlined in Reference [52] where the sensitivity of changes in inlet velocity distributions to hot channel thermal performance is shown to be small. Studies [52] made with the improved THINC model (THINC IV) show that it is adequate to use the 5% reduction in inlet flow to the hot assembly for a loop out of service based on the experimental data in References [56] and [57].

The effect of the total flow rate on the inlet velocity distribution was studied in the experiments of Reference [56]. As was expected, on the basis of the theoretical analysis, no significant variation could be found in inlet velocity distribution with reduced flow rate.

4.4.3.1.3 Empirical Friction Factor Correlations

Two (2) empirical friction factor correlations are used in the THINC-IV computer code (described in Section 4.4.3.4.1).

The friction factor in the axial direction, parallel to the fuel rod axis, is evaluated using the Novendstern-Sandberg correlation [66]. This correlation consists of the following:

1. For isothermal conditions, this correlation used the Moody [59] friction factor including surface roughness effects.

2. Under single-phase heating conditions a factor is applied based on the values of the coolant density and viscosity at the temperature of the heated surface and at the bulk coolant temperature, and

3. Under 2-phase flow conditions the homogeneous flow model proposed by Owens [67] is used with a modification to account for a mass velocity and heat flux effect.

The flow in the lateral directions, normal to the fuel rod axis, views the reactor core as a large tube bank. Thus, the lateral friction factor proposed by Idel'chik [58] is applicable. This correlation is of the form:

$$F_L = ARe_L^{-0.2} \qquad (4.4\text{-}18)$$

Where:

A is a function of the rod pitch and diameter as given in Reference [58].

Re_L is the lateral Reynolds number based on the rod diameter.

Extensive comparisons of THINC-IV predictions using these correlations to experimental data are given in Reference [63], and verify the applicability of these correlations in PWR design.

4.4.3.2 Influence of Power Distribution

The core power distribution which is largely established at beginning-of-life by fuel enrichment, loading pattern, and core power level is also a function of variables such as control rod worth and position, and fuel depletion throughout lifetime. Radial power distributions in various planes of the core are often illustrated for general interest, however, the core radial enthalpy rise distribution as determined by the integral of power up each channel is of greater importance for DNB analyses. These radial power distributions, characterized by $F^N_{\Delta H}$ (defined in Section 4.3.2.2.2) as well as axial heat flux profiles are discussed in the following 2 sections.

4.4.3.2.1 Nuclear Enthalpy Rise Hot Channel Factor, $F^N_{\Delta H}$

Given the local power density q' (kW/ft) at a point x, y, z in a core with N fuel rods and height H,

$$F^N_{\Delta H} = \frac{\text{hot rod power}}{\text{average rod power}} = \frac{\text{Max}\int_o^H q'(xo, yo, z)dz}{\frac{1}{N}\sum_{\text{all rods}}\int_o^H q'(x, y, z)dz} \qquad (4.4\text{-}19)$$

RN 95-022

The way in which $F^N_{\Delta H}$ is used in the DNB calculation is important. The location of minimum DNBR depends on the axial profile and the value of DNBR depends on the enthalpy rise to that point. Basically, the maximum value of the rod integral is used to identify the most likely rod for minimum DNBR. An axial power profile is obtained which, when normalized to the design value of $F^N_{\Delta H}$, recreates the axial heat flux along the limiting rod. The surrounding rods are assumed to have the same axial profile with rod average powers which are typical distributions found in hot assemblies. In this manner worst case axial profiles can be combined with worst case radial distributions for reference DNB calculations.

It should be noted again that $F^N_{\Delta H}$ is an integral and is used as such in DNB calculations. Local heat fluxes are obtained by using hot channel and adjacent channel explicit power shapes which take into account variations in horizontal power shapes throughout the core. The sensitivity of the THINC-IV analysis to radial power shapes is discussed in Reference [52].

For operation at a fraction of full power, the design $F^N_{\Delta H}$ used is given by: RN 95-022

$$F^N_{\Delta H} = F^{RTP}_{\Delta H} [1 + PF_{\Delta H}(1 - P)] \quad (4.4\text{-}20)$$ RN 95-022

where:

$F^{RTP}_{\Delta H}$ is the limit at Rated Thermal Power (RTP) specified in the Core Operating Limits Report (COLR), $PF_{\Delta H}$ is the Power Factor Multiplier for $F^{RTP}_{\Delta H}$ specified in the COLR, and P is the fraction of Rated Thermal Power. RN 95-022

The permitted relaxation of $F^N_{\Delta H}$ is included in the DNB protection setpoints and allows radial power shape changes with rod insertion to the insertion limits [68], thus allowing greater flexibility in the nuclear design.

4.4.3.2.2 Axial Heat Flux Distributions

As discussed in Section 4.3.2.2, the axial heat flux distribution can vary as a result of rod motion, power change, or due to spatial xenon transients which may occur in the axial direction. Consequently, it is necessary to measure the axial power imbalance by means of the ex-core nuclear detectors(as discussed in Section 4.3.2.2.7) and protect the core from excessive axial power imbalance.

The reference axial shape used in establishing core DNB limits (that is overtemperature ΔT protection system setpoints) is a chopped cosine shape with a peak to average value of 1.55. The Reactor Trip System provides automatic reduction of the trip setpoints on excessive axial power imbalance.

To determine the magnitude of the setpoint reduction, the reference shape is supplemented by other axial shapes skewed to the bottom and top of the core. The course of those accidents in which DNB is a concern is analyzed in Chapter 15.0, assuming that the protection setpoints have been set on the basis of these shapes. In many cases, the axial power distribution in the hot channel changes throughout the course of the accident due to rod motion, coolant temperature, and power level changes.

The initial conditions for the accidents for which DNB protection is required are assumed to be those permissible within the relaxed axial offset control strategy for the load maneuvers described in Reference [103]. In the case of the loss of flow accident, the hot channel heat flux profile is very similar to the power density profile in normal operation preceding the accident. It is therefore possible to calculate the minimum DNBR for conditions representative of the loss of flow accident as a function of the flux difference initially in the core.

The power shape resulting in the minimum DNBR is selected as the design power shape for non-overpower/overtemperature DNB events. This design shape results in a calculated DNBR that bounds all the normal operation power shapes.

4.4.3.3 Core Thermal Response

A general summary of the steady-state thermal-hydraulic design parameters including thermal output, flow rates, etc., is provided in Table 4.4-1 for all loops in operation.

As stated in Section 4.4.1, the design bases of the application are to prevent DNB and to prevent fuel melting for Condition I and II events. The protective systems described in Chapter 7.0 are designed to meet these bases. The response of the core to Condition II transients is given in Chapter 15.0.

Local fluid conditions during steady-state and transient operation are checked to ensure that they are within the parameter range of the applicable CHF correlation. RN 95-022

4.4.3.4 Analytical Techniques

4.4.3.4.1 Core Analysis

The objective of reactor core thermal design is to determine the maximum heat removal capability in all flow subchannels and show that the core safety limits, as presented in the Technical Specifications are not exceeded while compounding engineering and nuclear effects. The thermal design takes into account local variations in dimensions, power generation, flow redistribution, and mixing. THINC-IV is a realistic three-dimensional matrix model which has been developed to account for hydraulic and nuclear effects on the enthalpy rise in the core, References [52], [63] and [111]. The behavior of the assembly is determined by superimposing the power distribution among the assemblies upon the inlet flow distribution while allowing for flow mixing and flow distribution between assemblies. The average flow and enthalpy in the hottest assembly is obtained from the core-wide, assembly-by-assembly analysis. The local variations in power, fuel rod and pellet fabrication, and mixing within the hottest assembly are then superimposed on the average conditions of the hottest assembly in order to determine the conditions in the hot channel. RN 95-022 RN 95-022

The following sections describe the use of the THINC Code in the thermal-hydraulic design evaluation to determine the conditions in the hot channel and to assure that the safety related design bases are not violated.

4.4.3.4.1.1 Steady-State Analysis

The THINC-IV computer program, as approved by the NRC (Reference [98]) is used to determine coolant density, mass velocity, enthalpy, vapor void, static pressure, and DNBR distributions along parallel flow channels within a reactor core under all expected operating conditions. The THINC-IV Code is described in detail in References [52], [63] and [111], including models and correlations used. In addition, a discussion on experimental verification of THINC-IV is given in Reference [63]. RN 95-022 RN 01-113

The effect of crud on the flow and enthalpy distribution in the core is accounted for directly in the THINC-IV evaluations by assuming a crud thickness several times that which would be expected to occur. This results in slightly conservative evaluations of the minimum DNBR.

Estimates of uncertainties are discussed in Section 4.4.2.10.

RN 95-022

4.4.3.4.1.2 Experimental Verification

Extensive experimental verification of THINC-IV is presented in Reference [63].

The THINC-IV analysis is based on a knowledge and understanding of the heat transfer and hydrodynamic behavior of the coolant flow and the mechanical characteristics of the fuel elements. The use of the THINC-IV analysis provides a realistic evaluation of the core performance and is used in the thermal analyses described above.

4.4.3.4.1.3 Transient Analysis

The THINC-IV thermal-hydraulic computer code does not have a transient capability. Since a transient version of the third section of the THINC-I program [41] does have this capability, this code (THINC-III) continues to be used for transient DNB analysis.

RN 95-022

The conservation equations needed for the transient analysis are included in THINC-III by adding the necessary accumulation terms to the conservation equations used in the steady-state (THINC-I) analysis. The input description must now include one or more of the following time dependent arrays:

1. Inlet flow variation,
2. Heat flux distribution,
3. Inlet pressure history.

At the beginning of the transient, the calculation procedure is carried out as in the steady-state analysis. The THINC-III Code is first run in the steady-state mode to ensure conservatism with respect to THINC-IV and in order to provide the steady-state initial conditions at the start of the transient. The time is incremented by an amount determined either by the user or by the program itself. At each new time step the calculations are carried out with the addition of the accumulation terms which are evaluated using the information from the previous time step. This procedure is continued until a preset maximum time is reached.

RN 95-022

At preselected intervals, a complete description of the coolant parameter distributions within the array as well as DNBR are printed out. In this manner the variation of any parameter with time can be readily determined.

At various times during the transient, steady-state THINC-IV is applied to show that the application of the transient version of THINC-I is conservative. RN 95-022

The THINC-III Code does not have the capability for evaluating fuel rod thermal response. This is treated by the methods described in Section 15.1.9.

4.4.3.4.2 Fuel Temperatures

As discussed in Section 4.4.2.2, the fuel rod behavior is evaluated utilizing a semi-empirical thermal model which considers, in addition to the thermal aspects, such items as clad creep, fuel swelling, fission gas release, release of absorbed gases, cladding corrosion and elastic deflection, and helium solubility.

A detailed description of the thermal model can be found in Reference [3] with the modifications for time dependent densification given in Reference [6].

4.4.3.4.3 Hydrodynamic Instability

The analytical methods used to assess hydraulic instability are discussed in Section 4.4.3.5.

4.4.3.5 Hydrodynamic and Flow Power Coupled Instability

Boiling flows may be susceptible to thermohydrodynamic instabilities [87]. These instabilities are undesirable in reactors since they may cause a change in thermohydraulic conditions that may lead to a reduction in the DNB heat flux relative to that observed during a steady flow condition or to undesired forced vibrations of core components. Therefore, a thermohydraulic design was developed which states that modes of operation under Condition I and II events shall not lead to thermohydrodynamic instabilities.

Two (2) specific types of flow instabilities are considered for Westinghouse Power operation. These are the Ledinegg of flow excursion type of static instability and the density wave type of dynamic instability.

A Ledinegg instability involves a sudden change in flow rate from one steady-state to another. This instability occurs [87] when the slope of the reactor coolant system pressure drop-flow rate curve ($\partial\Delta P/\partial G$ internal) becomes algebraically smaller than the loop supply (pump head) pressure drop-flow rate curve ($\partial\Delta P/\partial G$ external). The criterion for stability is thus $\partial\Delta P/\partial G$ internal > $\partial\Delta P/\partial G$ external. The Westinghouse pump head curve has negative slope ($\partial\Delta P/\partial G$ external < 0) whereas the reactor coolant system pressure drop-flow curve has a positive slope ($\partial\Delta P/\partial G$ external < 0) whereas the reactor coolant system pressure drop-flow curve has a positive slope ($\partial\Delta P/\partial G$ internal > 0) over the Condition I and Condition II operational ranges. Thus, the Ledinegg instability will not occur.

The mechanism of density wave oscillations in a heated channel has been described by Lahey and Moody [88]. Briefly, an inlet flow fluctuation produces an enthalpy perturbation. This perturbs the length and the pressure drop of the single phase region and causes quality or void perturbations in the 2-phase regions which travel up the channel with the flow. The quality and length perturbations in the 2-phase region create 2-phase pressure drop perturbations. However, since the total pressure drop across the core is maintained by the characteristics of the fluid system external to the core, then the 2-phase pressure drop perturbation feeds back to the single phase region. These resulting perturbations can be either attenuated or self-sustained.

A simple method has been developed by Ishii [89] for parallel closed channel systems to evaluate whether a given condition is stable with respect to the density wave type of dynamic instability. This method had been used to assess the stability of typical Westinghouse reactor designs [90, 91, 92], including the Virgil C. Summer Nuclear Station, under Condition I and II operation. The results indicate that a large margin to density wave instability exists, e.g., increases on the order of 200% of rated reactor power would be required for the predicted inception of this type of instability.

The application of the method of Ishii [89] to Westinghouse reactor designs is conservative due to the parallel open channel feature of Westinghouse PWR Cores. For such cores, there is little resistance to lateral flow leaving the flow channels of high power density. There is also energy transfer from channels of high power density to lower power density channels. This coupling with cooler channels has led to the opinion that an open channel configuration is more stable than the above closed channel analysis under the same boundary conditions. Flow stability tests [93] have been conducted where the closed channel systems were shown to be less stable than when the same channels were cross connected at several locations. The cross connections were such that the resistance to channel to channel cross flow and enthalpy perturbations would be greater than that which would exist in a PWR core which has a relatively low resistance to cross flow.

Flow instabilities which have been observed have occurred almost exclusively in closed channel systems operating at low pressures relative to the Westinghouse PWR operating pressures. Kao, Morgan, and Parker [94] analyzed parallel closed channel stability experiments simulating a reactor core flow. These experiments were conducted at pressures up to 2200 psia. the results showed that for flow and power levels typical of power reactor conditions, no flow oscillations could be induced above 1200 psia.

Additional evidence that flow instabilities do not adversely affect thermal margin is provided by the data from the rod bundle DNB tests. Many Westinghouse rod bundles have been tested over wide ranges of operating conditions with no evidence of premature DNB or of inconsistent data which might be indicative of flow instabilities in the rod bundle.

In summary, it is concluded that thermohydrodynamic instabilities will not occur under Condition I and II modes of operation for Westinghouse PWR reactor designs. A large power margin, greater than doubling rated power, exists to predicted inception of such instabilities. Analysis has been performed which shows that minor plant to plant differences in Westinghouse reactor designs such as fuel assembly arrays, core power to flow ratios, fuel assembly length, etc. will not result in gross deterioration of the above power margins.

4.4.3.6 Temperature Transient Effects Analysis

Waterlogging damage of a fuel rod could occur as a consequence of a power increase on a rod after water has entered the fuel rod through a clad defect. Water entry will continue until the fuel rod internal pressure is equal to the reactor coolant pressure. A subsequent power increase raises the temperature and, hence, could raise the pressure of the water contained within the fuel rod. The increase in hydrostatic pressure within the fuel rod then drives a portion of the water from the fuel rod through the water entry defect. Clad distortion and/or rupture can occur if the fuel rod internal pressure increase is excessive due to insufficient venting of water to the reactor coolant. This occurs when there is both a rapid increase in the temperature of the water within the fuel rod and a small defect. Zircaloy clad fuel rods which have failed due to waterlogging [80, 81] indicate that very rapid power transients are required for fuel failure. Normal operational transients are limited to about 40 cal/gm-min (peak rod), while the Spert tests [80] indicate that 120 to 150 cal/gm is required to rupture the clad even with very short transients (5.5 msec period). Release of the internal fuel rod pressure is expected to have a minimal effect on the reactor coolant system [80] and is not expected to result in failure of additional fuel rods [81]. Ejection of fuel pellet fragments into the coolant stream is not expected [80, 81]. A clad breech due to waterlogging is thus expected to be similar to any fuel rod failure mechanism which exposes fuel pellets to the reactor coolant stream. Waterlogging has not been identified as the mechanism for clad distortion or perforation of any Westinghouse Zircaloy-4 fuel rods.

An excessively high fuel rod internal gas pressure could cause clad failure. One of the fuel rod design bases (Section 4.2.1.1.1) is that the fuel rod internal gas pressure does not exceed the nominal coolant pressure even at the overpower condition. During operational transients, fuel rod clad rupture due to high internal gas pressure is precluded by meeting the above design basis.

4.4.3.7 Potentially Damaging Temperature Effects During Transients

The fuel rod experiences many operational transients (intentional maneuvers) during its residence in the core. A number of thermal effects must be considered when analyzing the fuel rod performance.

The clad can be in contact with the fuel pellet at some time in the fuel lifetime. Clad-pellet interaction occurs if the fuel pellet temperature is increased after the clad is in contact with the pellet. Clad-pellet interaction is discussed in Section 4.2.1.3.1.

Increasing the fuel temperature results in an increased fuel rod internal pressure. One of the fuel rod design bases is that the fuel rod internal pressures do not exceed the nominal coolant pressure even at the overpower condition (see Section 4.2.1.1.1).

The potential effects of operation with waterlogged fuel are discussed in Section 4.4.3.6, which concluded that waterlogging is not a concern during operational transients.

Clad flattening, as noted in Section 4.2.1.3.1, has been observed in some operating power reactors. Thermal expansion (axial) of the fuel rod stack against a flattened section of clad could cause failure of the clad. This is no longer a concern because clad flattening is precluded during the fuel residence in the core (see Section 4.2.1.3.1).

There can be a differential thermal expansion between the fuel rods and the guide thimbles during a transient. Excessive bowing of the fuel rods could occur if the grid assemblies did not allow axial movement of the fuel rods relative to the grids. Thermal expansion of the fuel rods is considered in the grid design so that axial loads imposed on the fuel rods during a thermal transient will not result in excessively bowed fuel rods (see Section 4.2.1.2.2).

4.4.3.8 Energy Release During Fuel Element Burnout

As discussed in Section 4.4.2.3, the core is protected from going through DNB over the full range of possible operating conditions. At full power nominal operation, the minimum DNBR was found to be 2.21 (for 2900 MWt). This means that for these conditions, the probability of a rod going through DNB is less than 0.01% at a 95% confidence level, based on the statistics of the WRB-2 correlation. In the extremely unlikely event that DNB should occur, the clad temperature will rise due to the steam blanketing at the rod surface and the consequent degradation in heat transfer. During this time, there is a potential for chemical reaction between the cladding and the coolant. However, because of the relatively good film boiling heat transfer following DNB, the energy release resulting from this reaction is insignificant compared to the power produced by the fuel.

RN 95-022

1. DNB With Physical Burnout

RN 95-022

Westinghouse [73] has conducted DNB tests in a 25 rod bundle where physical burnout occurred with 1 rod. After this occurrence, the 25 rod test section was used for several days to obtain more DNB data from the other rods in the bundle. The burnout and deformation of the rod did not affect the performance of neighboring rods in the test section during the burnout or the validity of the subsequent DNB data points as predicted by the W-3 correlation. No occurrences of flow instability or other abnormal operation were observed.

2. DNB With Return to Nucleate Boiling

Additional DNB tests have been conducted by Westinghouse [82] in 19 and 21 rod bundles. In these tests, DNB without physical burnout was experienced more than once on single rods in the bundles for short periods of time. Each time, a reduction in power of approximately 10% was sufficient to re-establish nucleate boiling on the surface of the rod. During these and subsequent tests, no adverse effects were observed on this rod or any other rod in the bundle as a consequence of operating in DNB.

4.4.3.9 Energy Release or Rupture of Waterlogged Fuel Elements

A full discussion of waterlogging including energy release is contained in Section 4.4.3.6. It is noted that the resulting energy release is not expected to affect neighboring fuel rods.

4.4.3.10 Fuel Rod Behavior Effects from Coolant Flow Blockage

Coolant flow blockages can occur within the coolant channels of a fuel assembly or external to the reactor core. The effects of fuel assembly blockage within the assembly on fuel rod behavior is more pronounced than external blockages of the same magnitude. In both cases the flow blockages cause local reductions in coolant flow. The amount of local flow reduction, where it occurs in the reactor, and how far along the flow stream the reduction persists are considerations which will influence the fuel rod behavior. The effects of coolant flow blockages in terms of maintaining rated core performance are determined both by analytical and experimental methods. The experimental data are usually used to augment analytical tools such as computer programs similar to the THINC-IV program. Inspection of the DNB correlation (Section 4.4.2.3 and Reference [44]) shows that the predicted DNBR is dependent upon the local values of quality and mass velocity.

The THINC-IV Code is capable of predicting the effects of local flow blockages on DNBR within the fuel assembly on subchannel basis, regardless of where the flow blockage occurs. In Reference [63], it is shown that for a fuel assembly similar to the Westinghouse design, THINC-IV accurately predicts the flow distribution within the fuel assembly when the inlet nozzle is completely blocked. Full recovery of the flow was found to occur about 30 inches downstream of the blockage. With the reference reactor operating at the nominal full power conditions specified in Table 4.4-1, the effects of an increase in enthalpy and decrease in mass velocity in the lower portion of the fuel assembly would not result in the reactor reaching the DNBR limit.

RN 95-022

From a review of the open literature it is concluded that flow blockage in "open lattice cores" similar to the Westinghouse cores causes flow perturbations which are local to the blockage. For instance, A. Oktsubo [83], et al., show that the mean bundle velocity is approached asymptotically about 4 inches downstream from a flow blockage in a single flow cell. Similar results were also found for 2 and 3 cells completely blocked. P. Basmer [84], et al., tested an open lattice fuel assembly in which 41% of the subchannels were completely blocked in the center of the test bundle between spacer grids. Their results show the stagnant zone behind the flow blockage essentially disappears after 1.65 L/De or about 5 inches for their test bundle. They also found that leakage flow through the blockage tended to shorten the stagnant zone or, in essence, the complete recovery length. Thus, local flow blockages within a fuel assembly have little effect on subchannel enthalpy rise. The reduction in local mass velocity is then the main parameter which affects the DNBR. If the Virgil C. Summer Nuclear Station was operating at full power and nominal steady state conditions as specified in Table 4.4-1, a reduction in local mass velocity greater than 60% would be required to reduce the DNBR to the DNBR limit. The above mass velocity effect on the DNB correlation was based on the assumption of fully developed flow along the full channel length. In reality a local flow blockage is expected to promote turbulence and thus would not adversely affect DNBR at all [85].

RN 95-022

Coolant flow blockages induce local crossflows as well as promote turbulence. Fuel rod behavior is changed under the influence of a sufficiently high crossflow component. Fuel rod vibration could occur, caused by this crossflow component, through vortex shedding or turbulent mechanisms. If the crossflow velocity exceeds the limit established for fluid elastic stability, large amplitude whirling results. The limits for a controlled vibration mechanism are established from studies of vortex shedding and turbulent pressure fluctuations. The crossflow velocity required to exceed fluid elastic stability limits is dependent on the axial location of the blockage and the characterization of the crossflow (jet flow or not). These limits are greater than those for vibratory fuel rod wear. Crossflow velocity above the established limits can lead to mechanical wear of the fuel rods at the grid support locations. Fuel rod wear due to flow induced vibration is considered in the fuel rod fretting evaluation (Section 4.2).

4.4.3.11 DNBR Margins

The minimum required DNBR value for the VANTAGE 5 or VANTAGE+ fuel analysis are 1.23 for both thimble cold wall cells (3 fuel rods and a thimble tube) and typical cells (4 fuel rods).

To maintain DNBR margin to offset DNB penalties such as those due to fuel rod bow (see paragraph 4.4.2.3.4.3), the safety analyses were performed to DNBR limits higher than the design limit DNBR values. The differences between the design limit DNBRs and the safety analysis limit DNBRs results in available DNBR margin. The net DNBR margin, after consideration of all penalties, is available for operating and design flexibility. RN 95-022

4.4.4 TESTING AND VERIFICATION

NOTE 4.4.4.1
Section 4.4.4.1 is being retained for historical purposes only. RN 00-023

4.4.4.1 Tests Prior to Initial Criticality

A reactor coolant flow test, as noted in Table 14.1-58, is performed following fuel loading but prior to initial criticality. Coolant loop pressure drop data is obtained in this test. This data in conjunction with coolant pump performance information allows determination of the coolant flow rates at reactor operating conditions. This test verifies that proper coolant flow rates have been used in the core thermal and hydraulic analysis. RN 98-151

4.4.4.2 Initial Power and Plant Operation

Core power distribution measurements are made at several core power levels (see Section 4.3.2.2.7). These tests are used to ensure that conservative peaking factors are used in the core thermal and hydraulic analysis.

Additional demonstration of the overall conservatism of the THINC analysis was obtained by comparing THINC predictions to incore thermocouple measurements. These measurements were performed on the Zion reactor [86]. No further in-reactor testing is planned.

The reactor coolant system total flow rate determined by heat balance measurement at least once per 18 months with the plant greater than or equal to 90% rated thermal power is included in the Technical Specification surveillance requirement. RN 00-023

4.4.4.3 Component and Fuel Inspections

Inspections performed on the manufactured fuel are delineated in Section 4.2.1.4. Fabrication measurements critical to thermal and hydraulic analysis are obtained to verify that the engineering hot channel factors employed in the design analyses (Section 4.4.2.3.4) are met.

4.4.5 INSTRUMENTATION APPLICATION

4.4.5.1 Incore Instrumentation

Instrumentation is located in the core so that by correlating movable neutron detector information with fixed thermocouple information radial, axial, and azimuthal core characteristics may be obtained for all core quadrants.

The incore instrumentation system is comprised of thermocouples, positioned to measure fuel assembly coolant outlet temperatures at preselected positions, and fission chamber detectors positioned in guide thimbles which run the length of selected fuel assemblies to measure the neutron flux distribution. Figure 4.4-19 shows the number and location of instrumented assemblies in the core.

The core-exit thermocouples provide a backup to the flux monitoring instrumentation for monitoring power distribution. The routine, systematic, collection of thermocouple readings by the operator provides a data base. From this data base, abnormally high or abnormally low readings, quadrant temperature tilts, or systematic departure from a prior reference map can be deduced.

The movable incore neutron detector system would be used for more detailed mapping if the thermocouple system were to indicate an abnormality. These 2 complementary systems are more useful when taken together than either system alone would be. The incore instrumentation system is described in more detail in Section 7.7.1.9.

The incore instrumentation is provided to obtain data from which fission power density distribution in the core, coolant enthalpy distribution in the core, and fuel burnup distribution may be determined.

The BEACON Power Distribution Monitoring System (PDMS), Reference [113], for measuring power distribution is available as an alternative to using the movable in-core flux mapping system when power is greater than 25% RTP. This system provides continuous 3-dimensional core power distribution determination and directly relates power distribution to fuel safety limits. This system is described in WCAP-12472-P-A and uses core exit thermocouples, control rod bank position, T_{cold}, reactor power level, and the nuclear instrumentation power range section signals to develop the power distribution map.

RN 00-011

4.4.5.2 Overtemperature and Overpower ΔT Instrumentation

The Overtemperature ΔT trip protects the core against low DNBR. The Overpower ΔT trip protects against excessive power (fuel rod rating protection).

As discussed in Section 7.2.1.1.2, factors included in establishing the overtemperature ΔT and overpower ΔT trip setpoints includes the reactor coolant temperature in each loop and the axial distribution of core power through the use of the 2 section excore neutron detectors.

4.4.5.3 Instrumentation to Limit Maximum Power Output

The output of the 3 ranges (source, intermediate, and power) of detectors, with the electronics of the nuclear instruments, are used to limit the maximum power output of the reactor within their respective ranges.

There are 8 radial locations around the reactor in the primary shield. Seven (7) of these are utilized and have flux measuring detectors installed. One (1) location is a spare. Two (2) Source/Intermediate Range post accident 1E qualified detector assemblies are installed on opposite flat portions of the core containing the startup sources at an elevation corresponding to 1/2 of the core height. Each Source/Intermediate Range detector assembly is comprised of 2 identical fission chamber detectors surrounded by high density polyethylene. The Source Range utilizes the output of both fission chamber detectors and converts the combined signal into an equivalent count rate. The Intermediate Range uses the output of only one of the 2 fission chamber detectors and converts it to percent full power. Additionally, there is a Source Range detector installed in a well that was originally a spare well. It provides input to the remote Source Range instrument. This instrument is installed in the Control Room Evacuation Panel room and is used only in the case of Control Room evacuation. It provides a display and has the capability of providing a signal to the High Flux at Shutdown annunciator in the Control Room. It does not provide any rod control interlocks or any reactor trip signals. Four (4) dual section uncompensated ionization chamber assemblies for the power range are installed vertically at the 4 corners of the core and located equidistant from the reactor vessel at all points. Furthermore, these power range detectors are installed within 1 foot of the reactor vessel in order to minimize neutron flux pattern distortions. Each power range detector provides 2 signals corresponding to the neutron flux in the upper and in the lower sections of a core quadrant. The 3 ranges of detectors are used as inputs to monitor neutron flux from a completely shutdown condition to 120% of full power with the capability of recording overpower excursions up to 200% of full power.

The difference in neutron flux between the upper and lower sections of the power range detectors are used to limit the overtemperature ΔT and overpower ΔT trip setpoints and to provide the operator with an indication of the core power axial offset. In addition, the output of the power range channels are used for:

1. The rod speed control function,
2. To alert the operator to an excessive power unbalance between the quadrants,
3. Protect the core against rod ejection accidents, and
4. Protect the core against adverse power distributions resulting from dropped rods.

Details of the neutron detectors and nuclear instrumentation design and the control and trip logic are given in Chapter 7.0. The limits on neutron flux operation and trip setpoints are given in the Technical Specifications.

4.4.5.4 Loose Parts Monitoring Program (Metal Impact Detection System)

The Virgil C. Summer Nuclear Station Metal Impact Monitor is designed to enable early detection of debris which may collect in the steam generators or the reactor vessel. The developmental prototype of the Westinghouse Metal Impact Monitor is installed in the R. E. Ginna Plant (RGE) to evaluate the long term performance of the system in an operating plant. The system consists of a detector, preamplifier, signal processor and display.

The detectors are high temperature accelerometers mounted on the lower head of each steam generator, on the reactor vessel head flange and on incore instrument conduit near the bottom of the reactor vessel. The system accelerometer sensitivity is 10-100 pico coulombs/g.

RN 01-113

Preamplification of the detector signal is accomplished through use of a signal conditioning amplifier. This amplifier consists of a remote charge preamplifier located inside the reactor building and a signal conditioner located outside the reactor building. The signal is converted from the low level accelerometer charge signal to a voltage signal for transmission to the signal processing equipment in the control room.

Mechanical mounting adapters are provided for attaching the accelerometers to the various vessels. These adapters which are larger than the accelerometers use threaded and/or clamping arrangements to insure excellent mechanical attachment. No epoxies or magnetic attachments are used on a permanent basis to insure maximum signal strength and provide reasonable assurance and that the equipment will remain attached under normal and OBE operation.

The preamplifier housing and conduit for the loose parts monitoring system cables within the Reactor Building are designed and installed to withstand the Safe Shutdown Earthquake (SSE).

The Metal Impact Monitor was designed so that rate of impact incidents, as well as, energy of impact may be monitored continuously. Rate and amplitude latching-type alarms are displayed on the front panel of the monitor. Common alarm outputs are provided for connection to the main control room annunciator panel. An audio system produces the sound equivalent in parallel to the impact signal.

The vendor supplies operator training in the operation, trouble shooting and calibration of the system. Operating procedures detailing response to alarms are used to evaluate problems when detected by the system. Administrative procedures are utilized to ensure that data records are used and maintained for an appropriate period.

Although the metal impact monitor has been designed as a maintenance aid and is not considered as necessary for safe operation of a nuclear power plant, it will be operational during startup testing for obtaining baseline data from which detection sensitivity will be identified and set.

The system is a non-Class 1E system.

The loose parts monitoring system (LMPS) will detect impacts of approximately 0.2 ft/lb at approximately 2 feet from the transducer. This sensitivity meets the requirements of Regulatory Guide 1.133.

Two (2) redundant signal chains consisting of an accelerometer, a charge pre-amplifier, and the required cabling are located to provide broad coverage at the top of the reactor vessel, 2 at the bottom of the reactor vessel and 2 at the bottom of each steam generator. Each redundant channel is physically located to provide mechanical separation inside the containment.

Additionally, each signal chain is connected to it’s own signal conditioner, mounted in a common rack, outside the containment. Each channel is therefore active and provides for continuous audio monitoring. The signal processing to provide an automatic alarm is provided on a per "natural collection point" basis with automatic switching between redundant signal chains.

Electrical noise problems are minimized in the Westinghouse LPM system by:

a. Electrically isolating and shielding the accelerometers, pre-amplifiers and connecting cables.

b. Grounding of shields at electronics cabinet only.

c. Digital signal processing is employed to reduce the sensitivity to electrical noise and allows for the use of a unique impact discrimination technique. This allows for maximizing system sensitivity while minimizing susceptibility to false alarms.

Process noise problems are minimized by providing an inhibit function to reduce the sensitivity of the alarm discrimination circuitry during typical plant operation changes, such as:

a. An inhibit card is provided in the rod control system to prevent alarms during control rod motion.

b. Allows for other "owner furnished" input signals (contact closures) to inhibit the sensitivity during start-up or shut down of pumps, opening and closing of valves, etc.

4.4.6 REFERENCES

1. Christensen, J. A., Allio, R. J. and Biancheria, A., "Melting Point of Irradiated UO_2," WCAP-6065, February 1965.

2. Risher, D. H., "An Evaluation of the Rod Ejection Accident in Westinghouse Pressurized Water Reactors Using Spatial Kinetics Methods," WCAP-7588, Revision 1-A, January 1975.

3. Supplemental information on fuel design transmitted from R. Salvatori, Westinghouse NES, to D. Knuth, AEC, as attachments to letter NS-SL-518 (12/22/72), NS-SL-521 (12/29/72), NS-SL-524 (12/29/72) and NS-SL-543 (1/21/73), (Westinghouse Proprietary), and supplemental information on fuel design transmitted from R. Salvatori, Westinghouse NES, to D. Knuth, AEC, as attachments to letters NS-SL-527 (1/12/73) and NS-SL-544 (1/12/73).

4. Motley, F. E., Wenzel, A. H. and Cadek, F. F., "Critical Heat Flux Testing of 17x17 Fuel Assembly Geometry with 22 Inch Grid Spacing," WCAP-8536 (Proprietary) and WCAP-8537 (Non-Proprietary), May 1975.

5. Nakazato, S. and DeMario, E. E., "Hydraulic Flow Test of the 17 x 17 Fuel Assembly," WCAP-8278 (Proprietary) and WCAP-8279 (Non- Proprietary), February 1974.

6. Hellman, J.M. (Ed.), “Fuel Densification Experimental Results and Model For Reactor Application,” WCAP-8218-P-A (proprietary) and WCAP-8219-A (Non-Proprietary), March 1975.

7. Kjaerheim, G. and Rolstad, E., "In-Pile Determination of UO_2Thermal Conductivity, Density Effects and Gap Conductance," HPR-80, December 1967.

8. Kjaerheim, G., "In-Pile Measurements of Centre Fuel Temperatures and Thermal Conductivity Determination of Oxide Fuels," paper IFA-175 presented at the European Atomic Energy Society Symposium on Performance Experience of Water-Cooled Power Reactor Fuel, Stockholm, Sweden (October 21-22, 1969).

9. Cohen, I., Lustman, B. and Eichenberg, J., "Measurement of the Thermal Conductivity of Metal-Clad Uranium Oxide Rods during Irradiation," WAPD-228, 1960.

10. Clough, D. J. and Sayers, J. B., "The Measurement of the Thermal Conductivity of UO_2 under Irradiation in the Temperature Range 150°- 1600°C," AERE-R-4690, UKAEA Research Group, Harwell, December 1964.

11. Stora, J. P., Debernardy, DeSigoyer, B., Delmas, R., Deschamps, P., Ringot, C. and Lavaud, B., "Thermal Conductivity of Sintered Uranium Oxide under In-Pile Conditions," EURAEC-1095, 1964.

12. Devold, I., "A Study of the Temperature Distribution in UO_2 Reactor Fuel Elements," AE-318, Aktiebolaget Atomenergi, Stockholm, Sweden, 1968.

13. Balfour, M.G., Christensen, J. A. and Ferrari, H. M., "In-Pile Measurement of UO_2 Thermal Conductivity," WCAP-2923, 1966.

14. Duncan, R. N., "Rabbit Capsule Irradiation of UO_2," CVTR Project, CNVA-142, June 1962.

15. Nelson, R. C., Coplin, D. H., Lyons, M. F. and Weidenbaum, B., "Fission Gas Release from UO_2 Fuel Rods with Gross Central Melting," GEAP-4572, July 1964.

16. Howard, V. C., and Gulvin, T. G., "Thermal Conductivity Determinations on Uranium Dioxide by a Radial Flow Method," UKAEA IG- Report 51, November 1960.

17. Lucks, C. F., and Deem, H. W., "Thermal Conductivity and Electrical Conductivity of UO_2," in Progress Reports Relating to Civilian Applications, BMI-1448 (Rev.) for June, 1960; BMI-1489 (Rev.) for December, 1960 and BMI-1518 (Rev.) for May 1961.

18. Daniel, J. L., Matolich, Jr., J., and Deem, H. W. "Thermal Conductivity of UO_2," HW-69945, September 1962.

19. Feith, A. D., "Thermal Conductivity of UO_2 by a Radial Heat Flow Method," TID-21668, 1962.

20. Vogt, J., Grandell L. and Runfors, U., "Determination of the Thermal Conductivity of Unirradiated Uranium Dioxide," AB Atomenergi Report RMB-527, 1964, Quoted by IAEA Technical Report Series No. 59, "Thermal Conductivity of Uranium Dioxide."

21. Nishijima, T., Kawada, T. and Ishihata, A., "Thermal Conductivity of Sintered UO_2 and Al_2O_3 at High Temperatures," J. American Ceramic Society, 48, 31 34 (1965).

22. Ainscough, J. B. and Wheeler, M. J., "The Thermal Diffusivity and Thermal Conductivity of Sintered Uranium Dioxide," in Proceedings of the Seventh Conference of Thermal Conductivity, p. 467, National Bureau of Standards, Washington, 1968.

23. Godfrey, T. G., Fulkerson, W., Killie, T. G., Moore, J. P. and McElroy, D. L. "Thermal Conductivity of Uranium Dioxide and Armco Iron by an Improved Radial Heat Flow Technique," ORNL-3556, June 1964.

24. Stora, J. P., et al., "Thermal Conductivity of Sintered Uranium Oxide Under In-Pile Conditions," EURAEC-1095, August 1964.

25. Bush, A. J., "Apparatus for Measuring Thermal Conductivity to 2500°C," Westinghouse Research Laboratories Report 64-1P6-401-R3 (Proprietary), February 1965.

26. Asamoto, R. R., Anselin, F. L. and Conti, A. E., "The Effect of Density on the Thermal Conductivity of Uranium Dioxide," GEAP-5493, April 1968.

27. Kruger, O. L., "Heat Transfer Properties of Uranium and Plutonium Dioxide," Paper 11-N-68F presented at the Fall meeting of Nuclear Division of the American Ceramic Society, September 1968, Pittsburgh.

28. Gyllander, J. A., "In-Pile Determination of the Thermal Conductivity of UO_2 in the Range 500-2500°C," AE-411, January 1971.

29. Lyons, M. F., et al., "UO_2 Powder and Pellet Thermal Conductivity During Irradiation," GEAP-5100-1, March 1966.

30. Coplin, D. H., et al., "The Thermal Conductivity of UO_2 by Direct In-Reactor Measurements," GEAP-5100-6, March 1968.

31. Bain, A. S., "The Heat Rating Required to Produce Center Melting in Various UO_2 Fuels," ASTM Special Technical Publication, No. 306, pp. 30-46, Philadelphia, 1962.

32. Stora, J. P., "In-Reactor Measurements of the Integrated Thermal Conductivity of UO_2 - Effect of Porosity," Trans. ANS, 13, 137-138 (1970).

33. International Atomic Energy Agency, "Thermal Conductivity of Uranium Dioxide," Report of the Panel held in Vienna, April, 1965, IAEA Technical Reports Series, No. 59, Vienna, The Agency, 1966.

34. Poncelot, C. G., "Burnup Physics of Heterogeneous Reactor Lattices," WCAP-6069, June 1965.

35. Nodvick, R. J., "Saxton Core II Fuel Performance Evaluation," WCAP- 3385-56, Part II, "Evaluation of Mass Spectrometric and Radiochemical Analyses of Irradiated Saxton Plutonium Fuel," July 1970.

36. Dean, R. A., "Thermal Contact Conductance Between UO_2 and Zircaloy-2" CVNA-127, May 1962.

37. Ross, A. M. and Stoute, R. L., "Heat Transfer Coefficient Between UO_2 and Zircaloy-2," AECL-1552, June 1962.

38. Sidener, S., et. al., "Westinghouse Improved Performance Analysis and Design Model (PAD 4.0)," WCAP-15063-P-A Revision 1, with Errata (Proprietary) and WCAP-15064-NP-A Revision 1, with Errata (Non-Proprietary), July 2000. RN 14-036

39. Tong, L. S., "Boiling Crisis and Critical Heat Flux," AEC Critical Review Series, TID-25887, 1972.

40. Deleted

41. Chelemer, H., Weisman, J. and Tong, L. S., "Subchannel Thermal Analysis of Rod Bundle Cores," WCAP-7015, Revision 1, January 1969.

42. Motley, F. E. and Cadek, F. F., "DNB Tests Results for New Mixing Vane Grids (R)," WCAP-7695-P-A (Proprietary) and WCAP-7958-A (Non- Proprietary), January 1975.

43. Deleted

44. Tong, L. S., "Prediction of Departure from Nucleate Boiling for an Axially Non-Uniform Heat Flux Distribution," J. Nucl. Energy, 21, 241-248 (1967).

45. Deleted

46. Cadek, F. F., Motley, F. E. and Dominicis, D. P., "Effect of Axial Spacing on Interchannel Thermal Mixing with R Mixing Vane Grid," WCAP-7941-P-A (Proprietary) and WCAP-7959-A (Non-Proprietary), January 1975.

47. Rowe, D. S., Angle, C. W., "Crossflow Mixing Between Parallel Flow Channels During Boiling, Part II Measurement of Flow and Enthalpy in Two Parallel Channels," BNWL-371, part 2, December 1967.

48. Rowe, D. S., Angle, C. W., "Crossflow Mixing Between Parallel Flow Channels During Boiling, Part III Effect of Spacers on Mixing Between Two Channels," BNWL-371, part 3, January 1969.

49. Gonzalez-Santalo, J. M. and Griffith, P., "Two-Phase Flow Mixing in Rod Bundle Subchannels," ASME Paper 72-WA/NE-19.

50. Motley, F. E., Wenzel, A. H., Cadek, F. F., "The Effect of 17 x 17 Fuel Geometry on Interchannel Thermal Mixing," WCAP-8298-P-A (Proprietary) and WCAP-8299-A (Non-Proprietary), January 1975.

51. Cadek, F. F., "Interchannel Thermal Mixing with Mixing Vane Grids," WCAP-7667-P-A (Proprietary) and WCAP-7755-A (Non-Proprietary), January 1975.

52. Hochreiter, L. E., "Application of the THINC-IV Program to PWR Design," WCAP-8054 (Proprietary) and WCAP-8195 (Non-Proprietary), October 1973.

53. Dittus, F. W., and Boelter, L. M. K., "Heat Transfer in Automobile Radiators of the Tubular Type," Calif. Univ. Publication in Eng., 2, No. 13, 443-461 (1930).

54. Weisman, J., "Heat Transfer to Water Flowing Parallel to Tube Bundles," Nucl. Sci. Eng., 6, 78-79 (1959).

55. Thom, J. R. S., Walker, W. M., Fallon, T. A. and Reising, G. F. S., "Boiling in Sub-cooled Water During Flowup Heated Tubes or Annuli," Prc. Instn. Mech. Engrs., 180, Pt. C, 226-46 (1955-66).

56. Hetsroni, G., "Hydraulic Tests of the San Onofre Reactor Model," WCAP-3269-8, June 1964.

57. Hetsroni, G., "Studies of the Connecticut-Yankee Hydraulic Model," NYO-3250-2, June 1965.

58. Idel'chik, I. E., "Handbook of Hydraulic Resistance," AEC-TR-6630, 1960.

59. Moody, L. F., "Friction Factors for Pipe Flow," Transaction of the American Society of Mechanical Engineers, 66, 671-684 (1944).

60. Maurer, G. W., "A Method of Predicting Steady State Boiling Vapor Fractions in Reactor Coolant Channels," WAPD-BT-19, pp. 59-70. June 1960.

61. Griffith, P., Clark, J. A. and Rohsenow W. M., "Void Volumes in Subcooled Boiling Systems," ASME Paper No 58-HT-19.

62. Bowring, R. W., "Physical Model, Based on Bubble Detachment, and Calculation of Steam Voidage in the Subcooled Region of a Heated Channel," HPR-10, December 1962.

63. Hochreiter, L. E., Chelemer, H. and Chen, K., "THINC-IV An Improved Program for Thermal-Hydraulic Analysis of Rod Bundle Cores," WCAP- 7956, June 1973.

64. Carter, F. D., "Inlet Orificing of Open PWR Cores," WCAP-7836, January 1972.

65. Shefcheck, J., "Application of the THINC Program to PWR Design," WCAP-7359-L (Proprietary), August, 1969 and WCAP-7838 (Non-Proprietary), January 1972.

66. Novendstern, E. H. and Sandberg, R. O., "Single Phase Local Boiling and Bulk Boiling Pressure Drop Correlations," WCAP-2850 (Proprietary), April, 1966 and WCAP-7916 (Non-Proprietary), June 1972.

67. Owens, Jr., W. L., "Two-Phase Pressure Gradient," in International Developments in Heat Transfer, Part II, pp. 363-368, ASME, New York, 1961.

68. McFarlane, A. F., "Power Peaking Factors," WCAP-7912-P-A (Proprietary) and WCAP-7912-A (Non-Proprietary), January 1975.

69. Deleted

70. Vallentine, H. R., "Applied Hydrodynamics," Buttersworth Publishers, London, 1959.

71. Kays, W. M. and London, A. L., "Compact Heat Exchangers," National Press, Palo Alto, 1955.

72. Rowe, D. S., "COBRA-III, a Digital Computer Program for Steady State and Transient Thermal-Hydraulic Analysis of Rod Bundle Nuclear Fuel Elements," BNWL-B-82, 1971.

73. Weisman, J., Wenzel, A. H., Tong, L. S., Fitzsimmons, D., Thorne, W. and Barch, J., "Experimental Determination of the Departure from Nucleate Boiling in Large Rod Bundles at High Pressures," Chem. Eng. Prog. Symp. Ser. 64, No. 82, 114-125 (1968).

74. Reference deleted by Amendment 11.

75. Reference deleted by Amendment 11.

76. Reference deleted by Amendment 11.

77. Reference deleted by Amendment 11.

78. Reference deleted by Amendment 11.

79. Hill, K. W., Motely, F. E., Cadek, F. F., Wenzel, A. H., "Effect of 17 x 17 Fuel Assembly Geometry on DNB," WCAP-8296-P-A (Proprietary) and WCAP-8297-A (Non-Proprietary), February 1975.

80. Stephan, L. A., "The Effects of Cladding Material and Heat Treatment on the Response of Waterlogged UO_2 Fuel Rods to Power Bursts," IM-ITR-111, January 1970.

81. Western New York Nuclear Research Center Correspondence with the AEC on February 11 and August 27, 1971, Docket 50-57.

82. Tong, L. S., et al., "Critical Heat Flux (DNB) in Square and Tri- Angular Array Rod Bundles," presented at the Japan Society of Mechanical Engineers Semi-International Symposium held at Tokyo, Japan, September 4-8, 1967, pages 5-34.

83. Ohtsubo, A., and Uruwashi, S., "Stagnant Fluid due to Local Flow Blockage," J. Nucl. Sci. Technol., 9, No. 7, 433-434, (1972).

84. Basmer, P., Kirsh, D. and Schultheiss, G. F., "Investigation of the Flow Pattern in the Recirculation Zone Downstream of Local Coolant Blockages in Pin Bundles," Atomwirtschaft, 17, No. 8, 416-417, (1972). (In German).

85. Hill, K. W., Motley, F. E., Cadek, F. F. and Casterline, J. E., "Effects on Critical Heat Flux of Local Heat Flux Spikes or Local Flow Blockage in Pressurized Water Reactor Rod Bundles," ASME Paper 74-WA/HT-54, August 12, 1974.

86. Burke, T. M., Meyer, C. E. and Shefcheck, J., "Analysis of Data from the Zion (Unit 1) THINC Verification Test," WCAP-8453-A, May 1976.

87. J. A. Boure, A. E. Bergles, and L. S. Tong, "Review of Two-Phase Flow Instability," Nucl. Engr. Design 25 (1973) p. 165-192.

88. R. T. Lahey and F. J. Moody, "The Thermal Hydraulics of a Boiling Water Reactor," American Nuclear Society, 1977.

89. P. Saha, M. Ishii, and N. Zuber, "An Experimental Investigation of the Thermally Induced Flow Oscillations in Two-Phase Systems," J. of Heat Transfer, Nov. 1976, pp. 616-622.

90. Virgil C. Summer FSAR, Docket #50-395.

91. Byron/Braidwood FSAR, Docket #50-456.

92. South Texas FSAR, Docket #50-498.

93. S. Kakac, T. N. Veziroglu, K. Akyuzlu, O. Berkol, "Sustained and Transient Boiling Flow Instabilities in a Cross-Connected Four-Parallel-Channel Upflow System," Proc. of 5th International Heat Transfer Conference, Tokyo, September 3-7, 1974.

94. H. S. Kao, C. D. Morgan, and W. B. Parker, "Prediction of Flow Oscillation in Reactor Core Channel," Trans. ANS, Vol. 16, 1973, pp. 212-213.

95. Skaritka, J. (Ed.), "Fuel Rod Bow Evaluation," WCAP-8691, Revision 1, July 1979.

96. "Partial Response to Request Number 1 for Additional Information on WCAP-8691, Revision 1" letter, E. P. Rahe, Jr. (Westinghouse) to J. R. Miller (NRC), NS-EPR-2515, dated October 9, 1981; "Remaining Response to Request Number 1 for Additional Information on WCAP-8691, Revision 1" letter, E. P. Rahe, Jr. (Westinghouse) to J. R. Miller (NRC), NS-EPR-2572, dated March 15, 1982.

97. Motley, F. E., Hill, K. W., Cadek, F. F., and Shefcheck, J., "New Westinghouse Correlation WRB-1 for Predicting Critical Heat Flux in Rod Bundles with Mixing Vane Grids," WCAP-8762, July, 1976 (Proprietary) and WCAP-8763, July 1976 (non-Proprietary).

98. Letter from J. F. Stolz (NRC) to C. Eicheldinger (Westinghouse); Subject: Staff Evaluation for WCAP-7956, WCAP-8054, WCAP-8567, and WCAP-8762, April 19, 1978.

99. Chelemer, H., Boman, L. H., and Sharp, D. R., "Improved Thermal Design Procedures," WCAP-8567-P, July 1975 (Proprietary) and WCAP-8568, July 1975 (non-Proprietary).

100. Not Used

101. Motley, F. E. and Cadek, F. F., "Application for Modified Spacer Factor to L-Grid Typical and Cold Wall Cell DNB," WCAP-7988 (Westinghouse Proprietary) and WCAP-8030-A (non-Proprietary), October 1972.

102. Davidson, S. L. and Kramer, W. R., (Ed.), "Reference Core Report VANTAGE 5 Fuel Assemblies," WCAP-10444-P-A (Proprietary), September 1985.

103. Miller, R. W., et al., "Relaxation of Constant Axial Offset Control -F_Q Surveillance Technical Specification," WCAP-10216-P-A (Proprietary) and WCAP-10217-A (non-Proprietary), June 1983.

104. Hill, K. W., Motley, F. E., and Cadek, F. F., "Effect of Local Heat Flux Spikes on DNB in non-Uniform Heated Rod Bundles," WCAP-8174 (Proprietary) and WCAP-8202 (non-Proprietary), August 1973.

105. Weiner, R.A., et.al., "Improved Fuel Performance Models for Westinghouse Fuel Rod Design and Safety Evaluations," WCAP-10851-P-A, August 1988. RN 95-022

106. Leech, W.J. et.al., "Revised PAD Code Thermal Safety Model," WCAP-8720, Addendum 2, October 1982.

107. Letter from A.C. Thadani (NRC) to W.J. Johnson (Westinghouse), January 31, 1989, Subject: Acceptance for Referencing of Licensing Topical Report, WCAP-9226-P/9227-NP, "Reactor Core Response to Excessive Secondary Steam Releases."

108. Tong, L.S., "Critical Heat Fluxes in Rod Bundles, Two Phase Flow and Heat Transfer in Rod Bundles," Annual Winter Meeting ASME, November 1968, p. 3146.

RN 95-022

109. Motley, F.E., Cadek, F.F., "DNB Test Results for R-Grid Thimble Cold Wall Cells," WCAP-7695-L Addendum 1, October 1972.

110. Friedland, A.J. and Ray, S., "Revised Thermal Design Procedure," WCAP-11397-P.A., April 1989.

111. Friedland, A.J., Ray, S., "Improved THINC IV Modeling for PWR Core Design," WCAP-12330-P-A, September 1991.

112. WCAP-13712, "Reactor Pressure Vessel and Internals System Evaluations for the Virgil C. Summer Steam Generator Replacement/Uprating Program," April 1993.

113. WCAP-12472-P-A, "BEACON Core Monitoring and Operations Support System," August 1994.

RN 00-011

TABLE 4.4-1

THERMAL AND HYDRAULIC COMPARISON TABLE

DESIGN PARAMETERS	CURRENT RTP AND ENGINEERED SAFETY DESIGN RATING	
		RN 95-022
Reactor Core Heat Output, MWt	2900	RN 95-022
Reactor Core Heat Output, 10^6 Btu/hr	9898	
Heat Generated in Fuel, Z	97.4	
System Pressure, Nominal, psia	2250	
System Pressure, Minimum Steady State, psia	2200	
Minimum DNBR at Nominal Conditions		
Typical Flow Channel	2.34	RN 95-022
Thimble (Cold Wall) Flow Channel	2.21	
Minimum DNBR Design Limit	1.23	
DNB Correlation	WRB-2	
Coolant Flow		
Total Thermal Design Flow Rate 10^6 lb/hr	104.0	
Minimum Measured Flow Rate, 10^6 lb/hr	106.1	
Effective Flow Rate for Heat Transfer (Based on TDF), 10^6 lb/hr	94.74	RN 95-022
Effective Flow Area for Heat Transfer, ft^2	44.0	
Average Velocity Along Fuel Rods, ft/sec	13.7	
Average Mass Velocity, 10^6 lb/hr-ft^2 (2)	2.15	RN 09-022
Coolant Temperature (Based on TDF)		
Nominal Inlet, °F	552.9	
Average Rise in Vessel, °F	69.0	RN 95-022
Average Rise in Core, °F	74.8	
Average in Core, °F	592.8	
Average in Vessel, °F	587.4	
Heat Transfer		RN 95-022
Active Heat Transfer, Surface Area, ft^2	46,780	
Average Heat Flux, Btu/hr-ft^2	206,100	RN 95-022 09-022
Maximum Heat Flux for Normal Operation, Btu/hr-ft^2	504,900 (1)	

TABLE 4.4-1 (Continued)

THERMAL AND HYDRAULIC COMPARISON TABLE

DESIGN PARAMETERS		CURRENT RTP AND ENGINEERED SAFETY DESIGN RATING	
Heat Transfer (Continued)			
Average Thermal Output, kW/ft		5.69	
Maximum Thermal Output for Normal Operation, kW/ft		13.9	RN 95-022 09-022
Peak Linear Power for Determination of Protection Setpoints, kW/ft		< 22.6	
Fuel Central Temperature			
Peak at Thermal Output Maximum for Maximum Overpower Trip Point, °F		< 4700	
Pressure Drop [3]	Thimble Plug Inserted (TPI)	Thimble Plug Removed (TPR)	
Across Core, psi			
-0% Tube Plugging (552.9°F Inlet Temp)	26.26	23.92	
-10% Tube Plugging (536.7°F Inlet Temp)	26.73	24.35	
Across Vessel, including nozzle, psi			
-0% Tube Plugging (552.9°F Inlet Temp)	44.67	42.34	RN 95-022 09-022
-10% Tube Plugging (536.7°F Inlet Temp)	48.53	43.15	

(1) This limit is associated with the value of FQ = 2.45.

(2) Based on thermal design flow of 277,800 gpm.

(3) From WCAP-16980-P Table 5-1, based on Mechanical Design Flow of 321,300 gpm.

TABLE 4.4-4
COMPARISON OF THINC-IV AND THINC-I PREDICTIONS WITH DATA FROM REPRESENTATIVE WESTINGHOUSE TWO AND THREE LOOP REACTORS

Reactor	Power (MWt)	% Full Power	Measured Inlet Temp (°F)	σ_{rms} (°F) THINC-I	σ(°F) THINC-IV	Improvement (°F) for THINC-IV over THINC-I
Ginna	847	65.1	543.7	1.97	1.83	0.14
	854	65.7	544.9	1.56	1.46	0.10
	857	65.9	543.9	1.97	1.82	0.15
	947	72.9	543.8	1.92	1.74	0.18
	961	74.0	543.7	1.97	1.79	0.18
	1091	83.9	542.5	1.73	1.54	0.19
	1268	97.5	542.0	2.35	2.11	0.24
	1284	98.8	540.2	2.69	2.47	0.22
	1284	98.9	541.0	2.42	2.17	0.25
	1287	99.0	544.4	2.26	1.97	0.29
	1294	99.5	540.8	2.20	1.91	0.29
	1295	99.6	542.0	2.10	1.83	0.27
Robinson	1427.0	65.1	548.0	1.85	1.88	0.03
	1422.6	64.9	549.4	1.39	1.39	0.00
	1529.0	88.0	550.0	2.35	2.34	0.01
	2207.3	100.7	534.0	2.41	2.41	0.00
	2213.9	101.0	533.8	2.52	2.44	0.08

RN 01-113

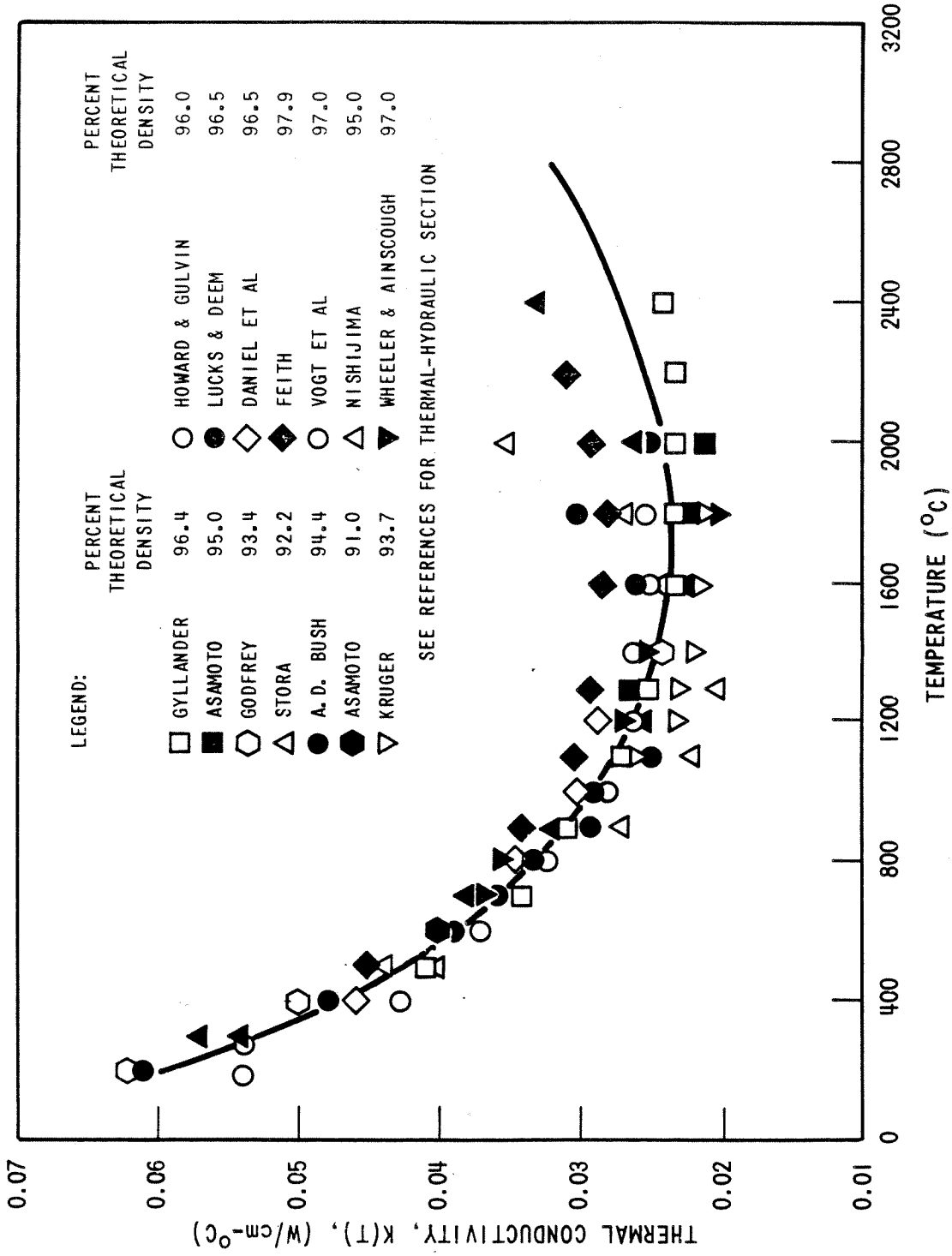

SOUTH CAROLINA ELECTRIC & GAS CO.
VIRGIL C. SUMMER NUCLEAR STATION

Thermal Conductivity of UO_2 (Data Corrected to 95% Theoretical Density)

Figure 4.4-3

Amendment 0
August 1984

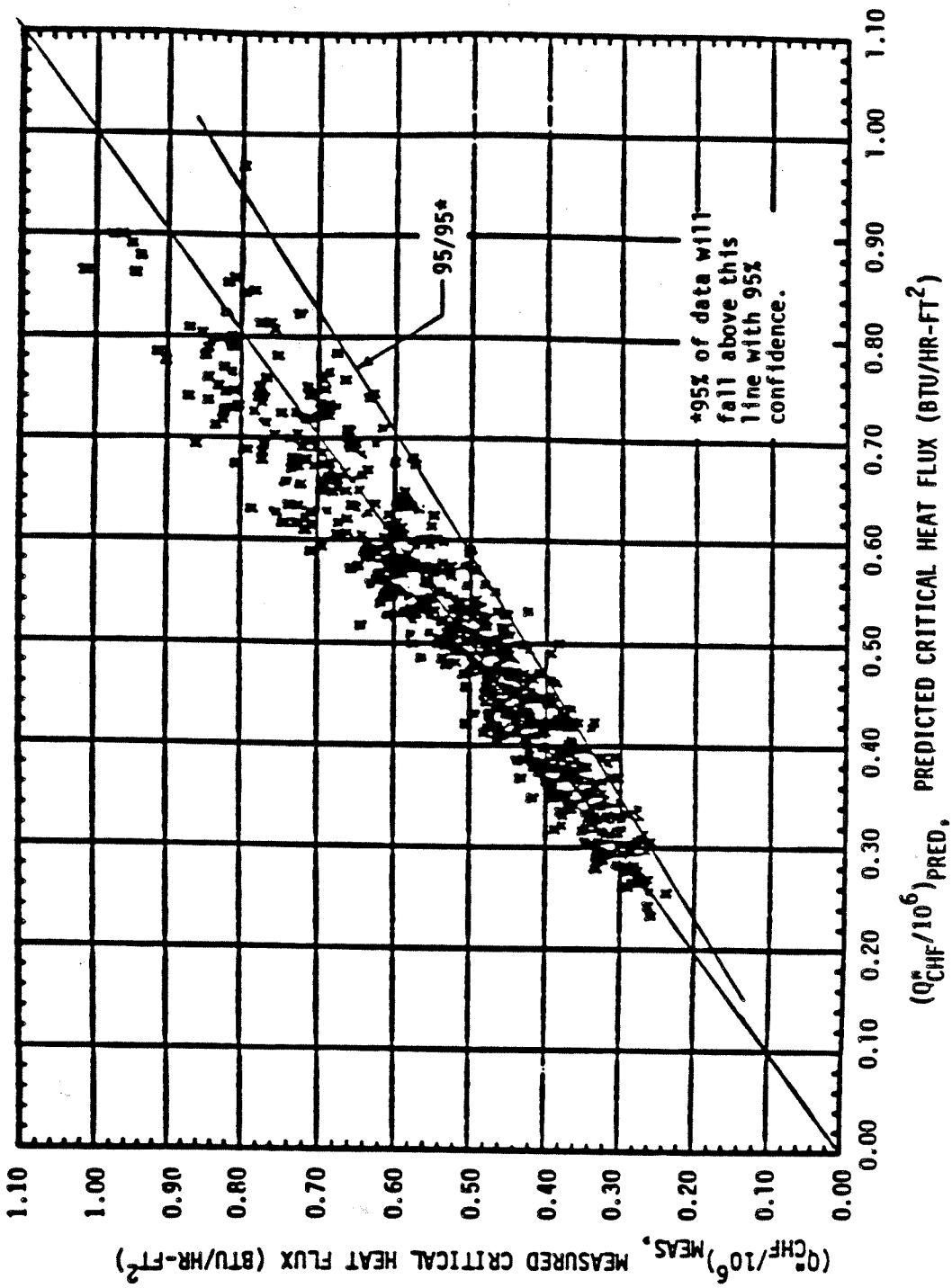

AMENDMENT 6
AUGUST, 1990

SOUTH CAROLINA ELECTRIC & GAS CO.
VIRGIL C. SUMMER NUCLEAR STATION

Measured Versus Predicted Critical Heat Flux - WRB-2 Correlation

Figure 4.4-6

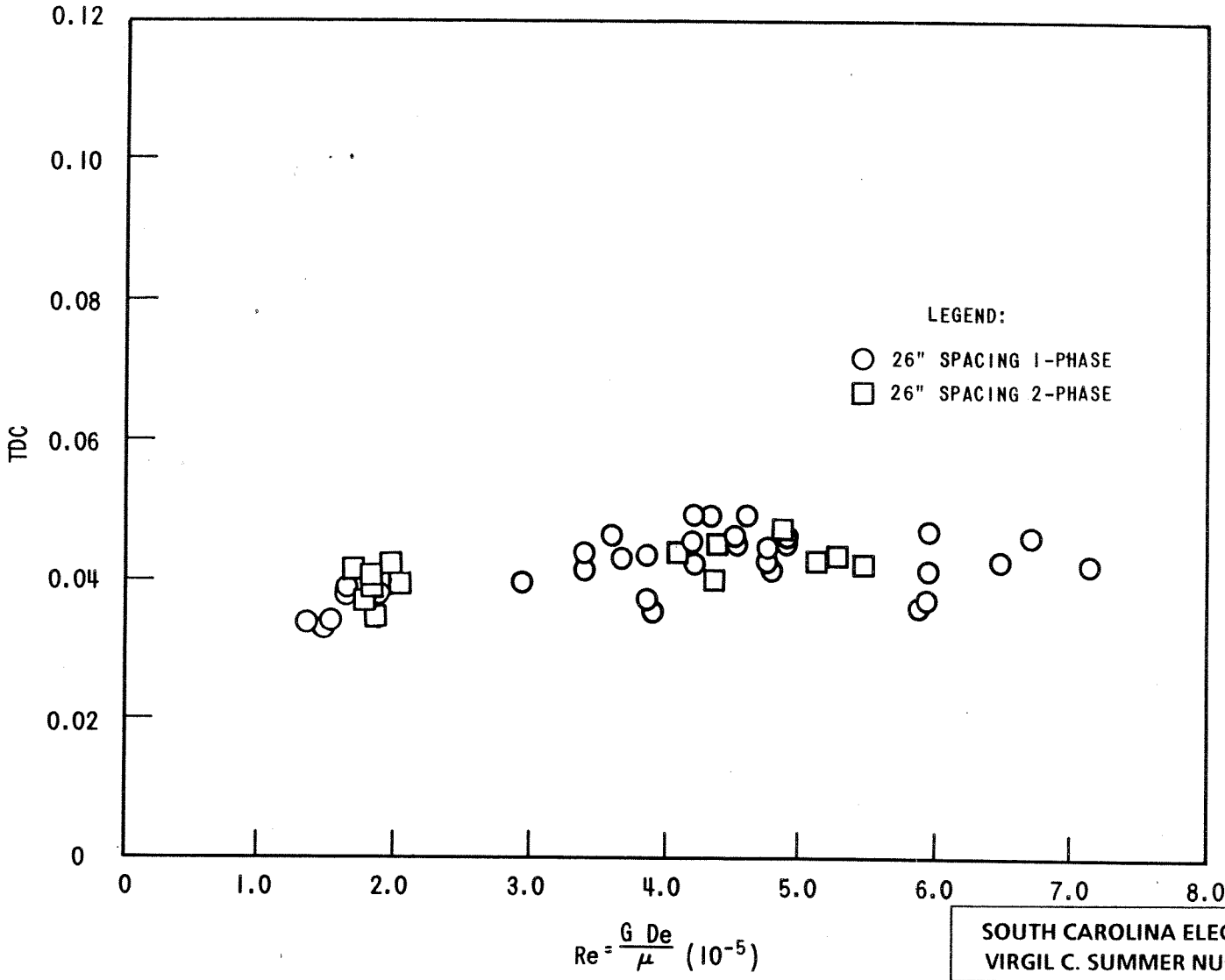

SOUTH CAROLINA ELECTRIC & GAS CO.
VIRGIL C. SUMMER NUCLEAR STATION

TDC versus Reynolds Number for
26" Grid Spacing

Figure 4.4-8

Amendment 0
August 1984

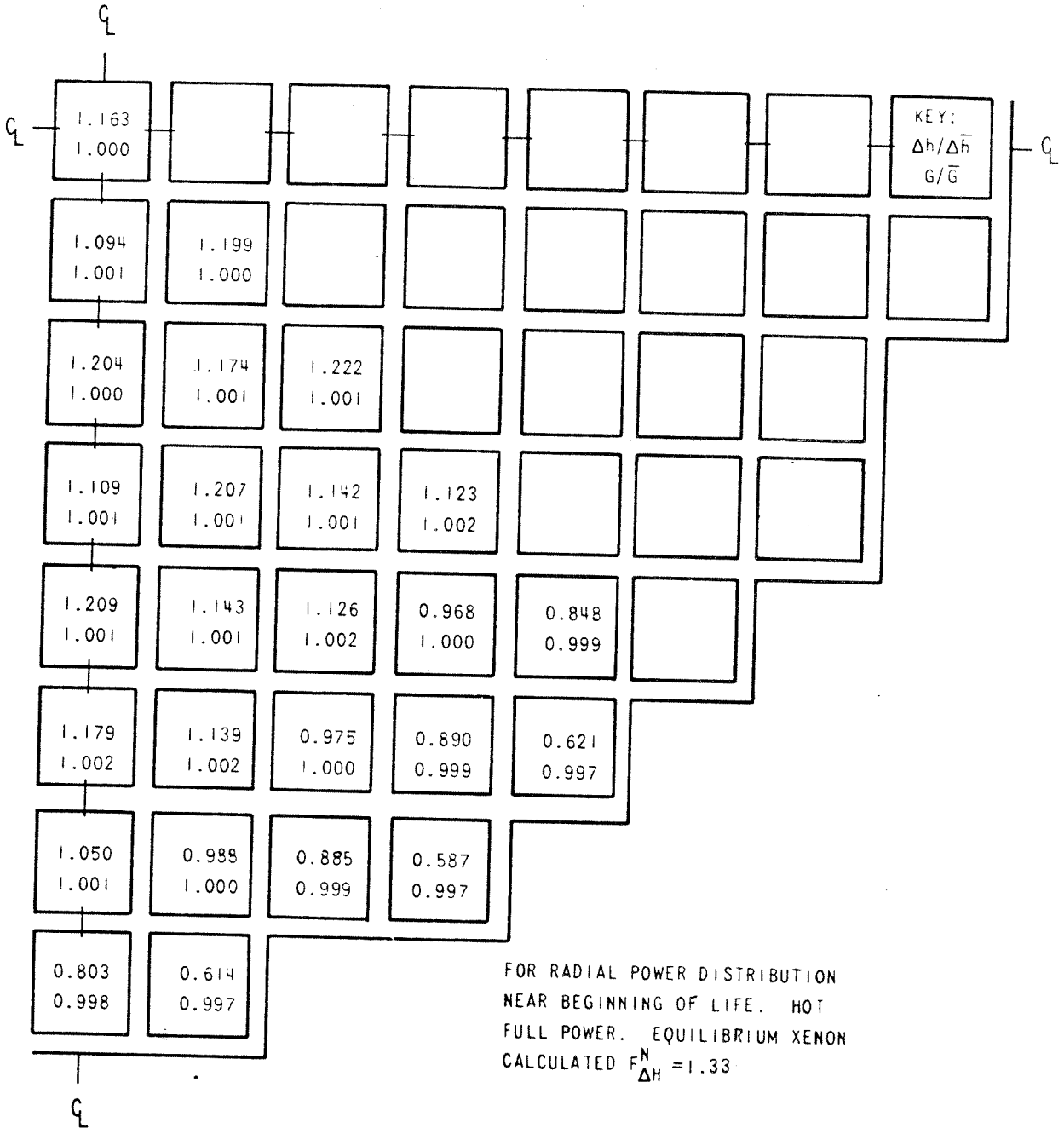

Amendment 0
August 1984

SOUTH CAROLINA ELECTRIC & GAS CO.
VIRGIL C. SUMMER NUCLEAR STATION

Normalized Radial Flow and Enthalpy Distribution at 4 ft. Elevation

Figure 4.4-9

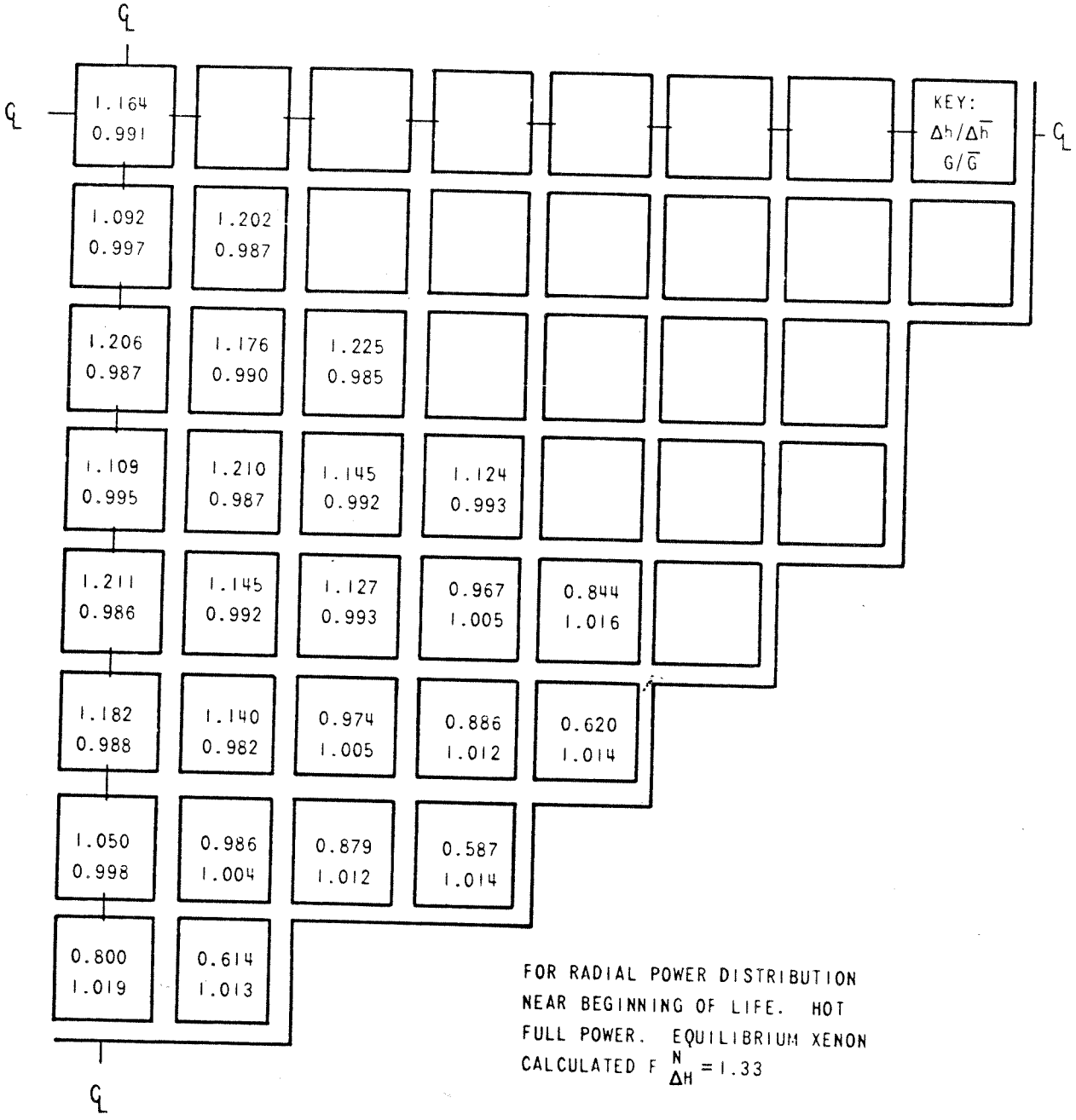

SOUTH CAROLINA ELECTRIC & GAS CO.
VIRGIL C. SUMMER NUCLEAR STATION

Normalized Radial Flow and Enthalpy Distribution at 8 ft. Elevation

Figure 4.4-10

Amendment 0
August 1984

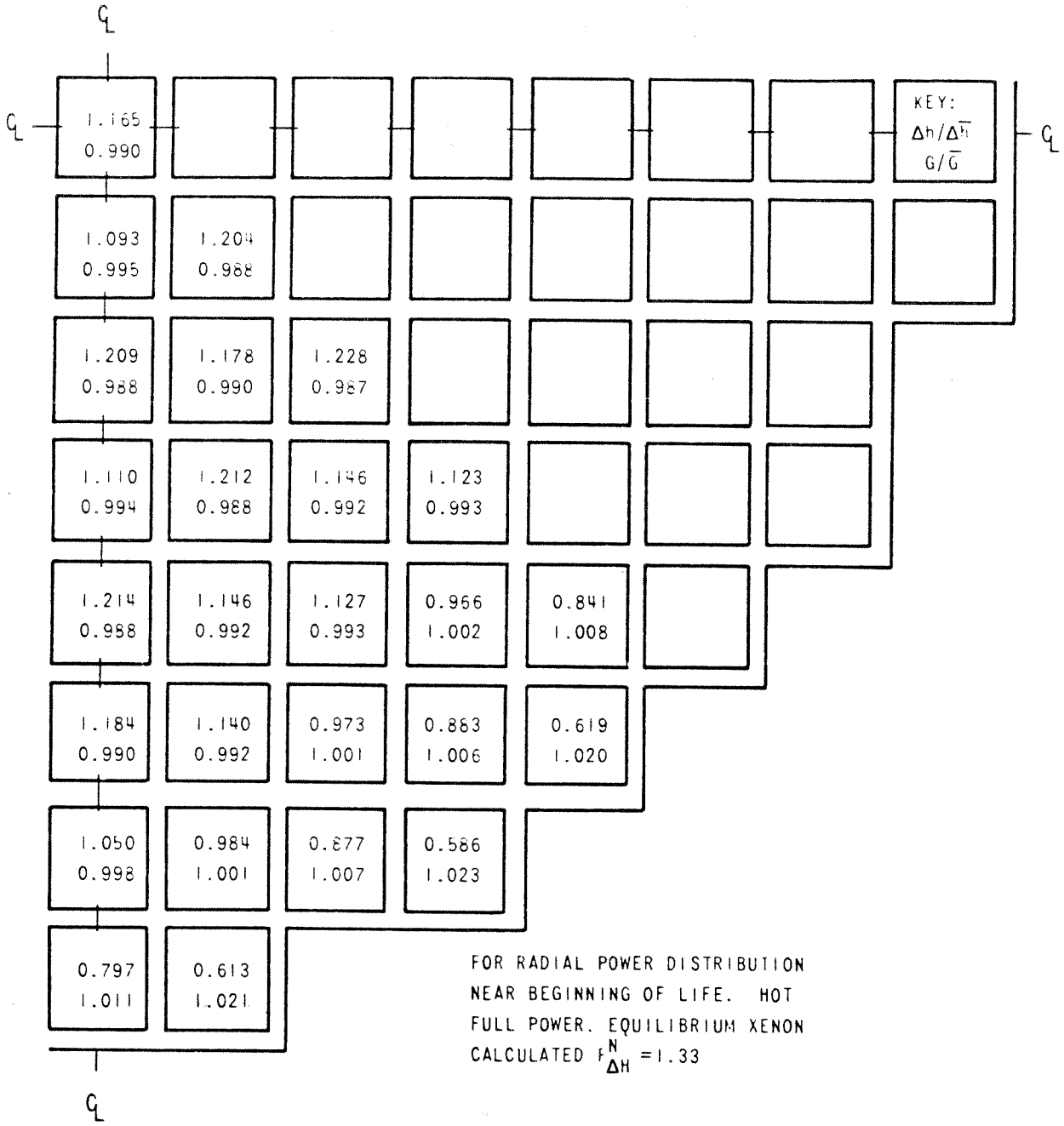

SOUTH CAROLINA ELECTRIC & GAS CO. VIRGIL C. SUMMER NUCLEAR STATION
Normalized Radial Flow and Enthalpy Distribution at 12 ft. Elevation Core Exit Figure 4.4-11

Amendment 0
August 1984

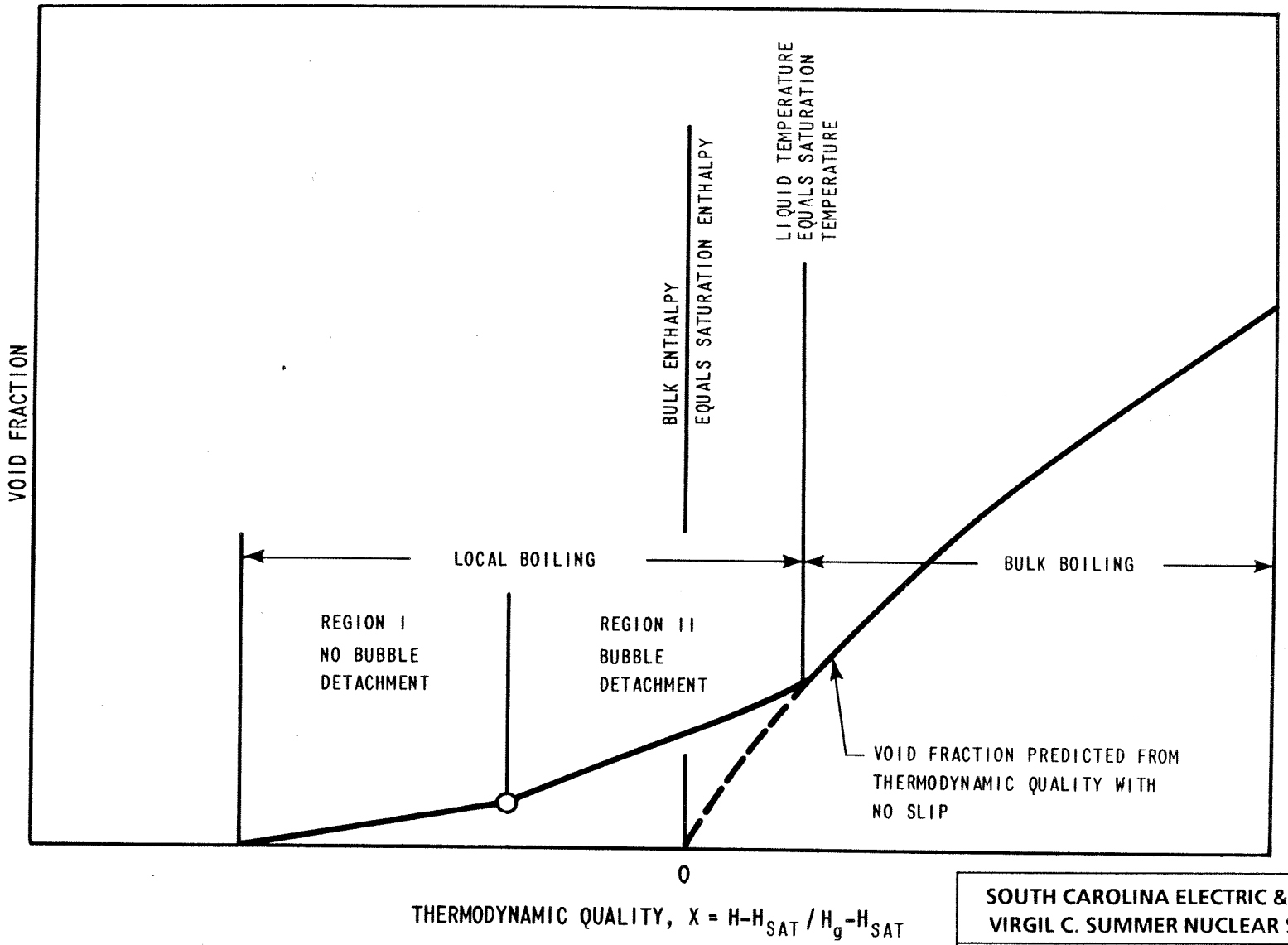

SOUTH CAROLINA ELECTRIC & GAS CO.
VIRGIL C. SUMMER NUCLEAR STATION

Void Fraction versus Thermodynamic Quality $H-H_{SAT}/H_g-H_{SAT}$

Figure 4.4-12

Amendment 0
August 1984

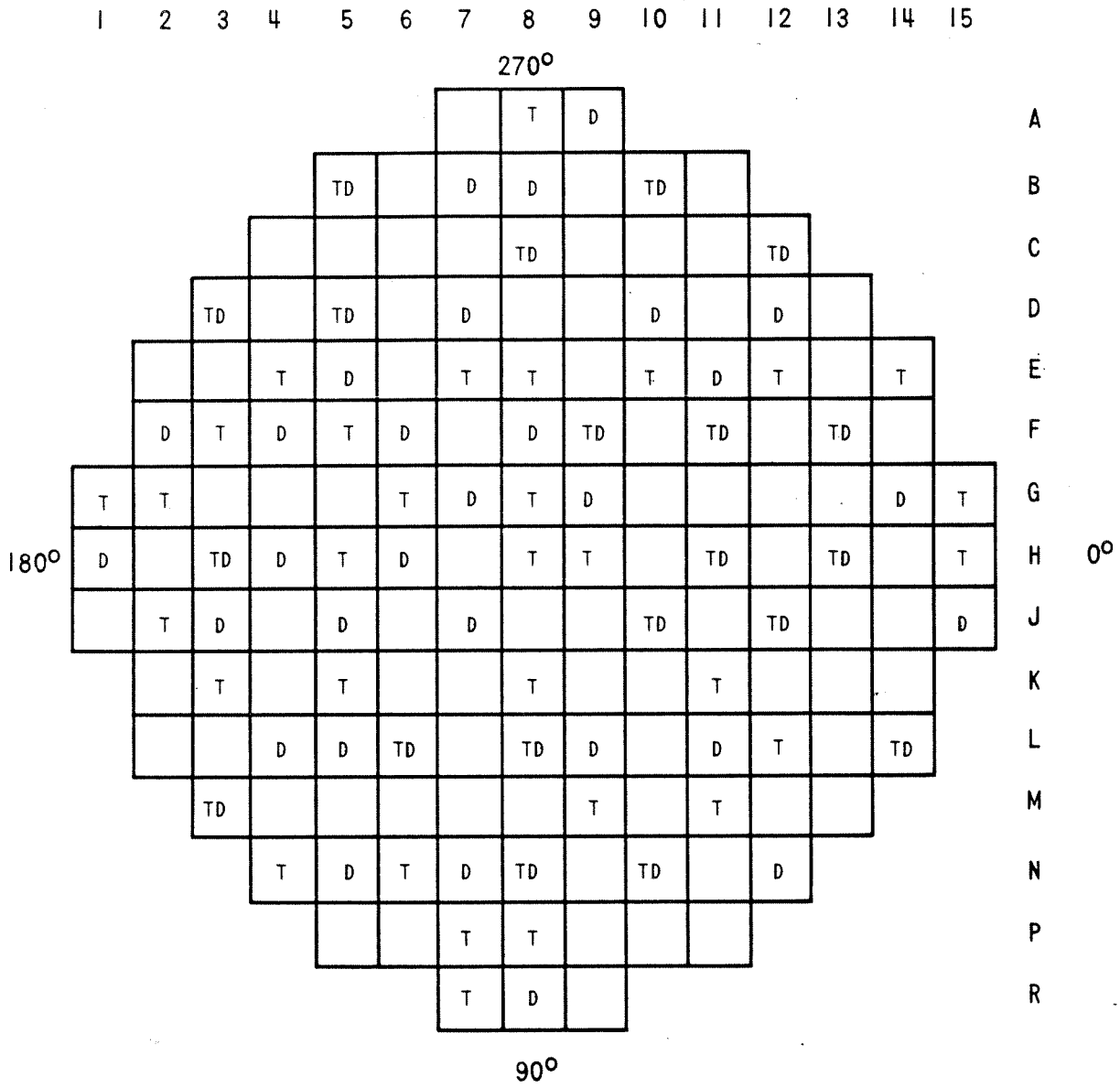

T - THERMOCOUPLE (51)

D - MOVABLE INCORE DETECTOR (50)

Amendment 0
August 1984

SOUTH CAROLINA ELECTRIC & GAS CO.
VIRGIL C. SUMMER NUCLEAR STATION

Distribution of Incore Instrumentation

Figure 4.4-19